Intracellular Delivery of Cancer-Targeting Antibody-Drug Conjugates

Geoffrey Y. Berguig

A dissertation
submitted in partial fulfillment of the
requirements for the degree of

Doctor of Philosophy

University of Washington

2013

Supervisory Committee

Patrick S. Stayton, Chair

Dr. David Hockenbery (GSR)

Dr. Oliver Press

Dr. Suzie Pun

Dr. Peter Senter

Program Authorized to Offer Degree:

Department of Bioengineering

University of Washington

Abstract

Intracellular Delivery of Cancer-Targeting Antibody-Drug Conjugates

Geoffrey Y. Berguig

Chair of the Supervisory Committee:
Professor Patrick S. Stayton
Department of Bioengineering

The use of cancer targeted antibody-drug conjugates aims to reduce the adverse affects of current therapies by selectively seeking and destroying tumor cells. Current systems employ targeted monoclonal antibodies conjugated to chemotoxins which have good cancer cell specificity, but suffer from early decomposition, normal tissue exposure, and limited drug potency in solid tumors. An alternative to chemotherapeutics is the use of proapoptotic peptides that reach the cystosol for action with enhanced specificity and activity in the most chemoresistant cancer cells. **The overall goal of our research is to develop a cancer-targeted intracellular delivery vehicle using monoclonal antibodies for targeting, pH-responsive polymers for endosomal escape, and proapoptotic peptides for cell death.** The ability of pH-responsive polymers to alter the endosomal/lysosomal trafficking pathway of antibodies was evaluated by ratiometric fluorescence and subcellular fractionation studies. A novel diblock copolymer that self-assembles into micelles was developed to address micelle stability, in vivo circulation, and therapeutic activity both in several cancer cell lines, and activity in a tumor-xenograft mouse model.

TABLE OF CONTENTS

LIST OF FIGURES

LIST OF TABLES

ACKNOWLEDGMENTS

This Ph.D. degree would not have been possible without the collaborative research professors at the University of Washington and the Fred Hutchinson Cancer Research Center. My mentor, Patrick Stayton, allowed me to pursue my scientific goals and challenged me every step of the way. In the most trying times, Pat offered just the right amount of support for me to succeed. My co-advisor, Oliver Press, provided invaluable resources and taught me to examine my research from a clinical perspective. Suzie Pun continually welcomed me to her office with unlimited access to her lab. David Hockenbery was directly influential in the selection and characterization of my therapeutic peptide. Peter Senter helped me develop as a scientist with an industry perspective and would invite me to Seattle Genetics for awesome scientific discussion. Anthony Convertine, a leading expert in field of polymer science, has been the most supportive colleague over the past six years. Together, we developed a number of innovative polymer systems which allowed me to constantly sharpen my microscopy technique. Other colleagues who challenged me to excel as a scientist through endless hours of discussion include Corinna Palanca-Wessels, Rob Burke, John Wilson, James Lai, Matt Manganiello, and Jeff Chamberlain, and Salka Keller.

I would also like to acknowledge my parents, Maud and Serge Berguig, for instilling an optimistic outlook and how to be persistent in the face of adversity. As they were not afforded the same opportunities in their lifetime, they insured that I had the appropriate resources and support to achieve the highest level of education.

DEDICATION

To my parents for their unconditional love and support.

Chapter 1

INTRACELLULAR DELIVERY OF CANCER BIOLOGICS

Acquired resistance towards apoptosis is a hallmark of nearly all cancers which can lead to uncontrolled proliferation and chemoresistance[1]. Advances in cancer therapeutics has led to the development of antibody-drug conjugates (ADC) that enhance in vivo targeting and therapeutic potency[2–7]. These conjugates however, are often limited to chemosensitive cancers[8,9]. To address chemoresistance, proapoptotic peptides that target dysregulated apoptotic machinery and induce apoptosis have been developed[10–12]. Their use in clinical application has yet to realized due to a number of extracellular and intracellular delivery barriers. Synthetic polymers that enhance in vivo delivery of biologics and overcome intracellular trafficking barriers through endosomal escape have been employed[13–17]. Combining ADC technology with therapeutic peptides and synthetic polymers could open the door to a new class of intracellular acting biologics with the potential to effect a wider range of cancers.

1.1 Antibody-Targeted Therapeutics

1.1.1 Introduction

Cytotoxic chemo drugs are very effective at killing tumors at the cost of high toxicity in normal tissues[8]. With a low therapeutic index, the toxic and sometimes fatal effects of chemotherapy have spawned the development of targeted cancer drugs. Tumor targeted drugs offer greater efficacy while benefiting from less toxicity[18]. The discovery of tumor ligands overexpressed in and sometimes exclusive to cancer cells has prompted the development of monoclonal antibodies (mAbs) as a moiety for tumor targeting[1]. The first immunoglobulin proteins were murine mAbs generated by Milstein and Kohler[19]. Murine mAbs served as a tool for many clinical studies but their immunogenicity in humans encouraged the synthesis of chimeric, humanized mAbs, beginning in the 1980s[20]. Since then, a number of humanized cancer-targeting mAbs have been developed and approved for clinical use.

1.1.2 Evolution of Radioimmunotherapy

Rituximab, an anti-CD20 antibody for the treatment of non-Hodgkins lymphoma (NHL) was the first antibody approved by the FDA for cancer therapy[21]. Since then, other cancer specific antibodies have been approved, including trastuzumab, an anti-Her2/neu antibody for breast cancer[22]. These treatments benefit from limited adverse effects and immune responses, but as a single agent typically lack the therapeutic potency equivalent to chemotherapy and radiation. Cytotoxic agents, have a low therapeutic index, meaning the dosages required for tumor killing are near those that cause normal tissue damage[23]. Radioimmunoconjugates (RIT), radionuclides conjugated directly to targeted antibodies, offer greater efficacy with less toxicity and increase the therapeutic index[7,24,25]. Rituximab spawned the approval of two

targeted anti-CD20 antibodies conjugated to ^{90}Y (ibritumomab tiuxetan) and ^{131}I (tositumomab)[26,27]. There are also reports using radioiodinated anti-Lym-1, a murine IgG2a monoclonal antibody directed against HLA-DR, in B-cell lymphomas[27]. Antigen expression on the surface of NHL cells often determines the localization ability of the conjugates[28]. The long range gama-emission that occurs during the extended circulation half-life of RIT, results in myelosuppression and radiation exposure to normal organs[29,30].

Myelosuppression limits high dosages of radiolabeled antibodies and has promoted the development of pretargeted radiomimmunotherapies (PRIT)[31]. PRIT involves the injection of antibody-streptavidin (Ab/SA) conjugates that localize to tumors, followed by a biotinylated-clearing agent to remove circulating Ab/SA. Finally, radiolabeled DOTA-biotin, a small tumor penetrating molecule that binds to Ab/SA on the surface of tumors is injected and allowed to complex with Ab/SA bound to the surface of the tumors. Circulating radiolabeled DOTA-biotin is excreted through the urine, limiting the toxic effects associated with standard radiation therapies. In a study comparing the biodistribution of PRIT, targeted CD20, CD22 and DR, Pantelias et al. found a strong correlation between in vitro cell binding capabilities and in vivo tumor targeting[32]. The conjugates with the highest tumor targeting effects were strongly dependent on antigen expression in each cell line. Interestingly, the HD39/SA conjugate targeting CD22 receptors was found to have a 24 hour half-life in BALB/C athymic mice and displayed significantly low background levels in both the blood and kidneys. Of the three conjugates used for PRIT, HD39/SA resulted in the lowest DOTA levels, likely due to its rapid rate of endocytosis[33] preventing binding of DOTA-biotin to the surface of the tumor.

1.1.3 Benefits of Antibody Drug Conjugates

Antibody-drug conjugates (ADCs) have the ability to improve the delivery of potent molecules to tumors that would otherwise be intolerable for prolonged periods of time[6,7,34]. These systems employ monoclonal antibodies conjugated to chemotherapeutic agents and maintain relatively nonimmunogenic properties with a high affinity for antigens overexpressed on cancer cells. The main considerations for the development of ADCs, described by Senter are: the antigen target, localization of ADC to target tissue, fate of ADC once antigen bound, systemic and intracellular stability of ADC linker, and potency of released drug[3]. Disulfide bonds and peptide-based linkers have demonstrated superior activity in vivo, where the addition of steric hindrances around the binding site can improve circulation stability while still promoting reduction or enzymatic degradation within the tumor cells[35–37] Two recently FDA approved ADCs are brentuximab vedotin and trastuzumab emtansine which combine a mAb with a cytotoxic agent through an enzymatically cleavable dipeptide linker[38–42]. Release of the cytotoxic drugs in the cells results in a biological event that leads to apoptosis. A similar approach could also be used to arm ADCs with biomacromolecular drugs (e.g. siRNA, DNA, peptides, and proteins) that require cytosolic delivery in order to exert their therapeutic effect. These systems may offer a safer approach and address some some of the adverse effects associated with ADCs.

1.1.4 Clinical Significance of Anti-CD22 Antibodies

The CD22 receptor has been identified as a useful surface marker for discriminating neoplastic cells from a benign B-cell population[43]. Ligation of CD22 receptors with anti-CD22 mAbs initiates rapid endocytosis followed by trafficking to vesicular compartments, making it an attractive target for ADC technology[33,44,45]. Anti-CD22 has been an exciting potential targeting moiety for targeted therapies[4]. Administration of

the first humanized monoclonal anti-CD22 antibody, epratuzumab, was well tolerated in patients with no dose-limiting toxicity up to 1000 mg/m^2/wk[46]. An extended blood half-life of 23 days indicated that less frequent dosing schedules may be feasible. Combinational therapies involving epratuzumab with chemotherapy could potentially improve it's effectiveness compared standard chemotherapy regimens as has already been demonstrated with rituximab[2,7]. Unconjugated epratuzumab has demonstrated significant therapeutic activity, however delivery was performed at nearly 12 times the dosage of normally delivered ^{90}Y-epratuzumab treatments. Studies using radiolabeled anti-CD22 have shown that estimated dosages do not accurately predict tumor responses, thus the therapeutic efficacy of RIT likely involves other mechanisms for tumor control[27,47]. These findings suggest that targeting of the tumor may also play a role in the magnitude of response. Clinical studies with radiolabeled-ibritumomab tiuxetan and tositumomab, have shown similar tumor responses, showing a consistency that anti-tumor activity is exhibited by many of the B-cell antibodies[25].

1.2 Synthetic Polymers for Intracellular Delivery

1.2.1 Introduction

Endosomal trafficking is the one of the major barriers to the intracellular delivery of biologic drugs[48–51]. Endosomes are responsible for sorting endocytosed material to different organelles within the cell before they are degraded in lysosomes[52,53]. Trafficking from endosomes to lysosomes is associated with a protease rich environment at low pH (4.5) which is unfavorable for biologic drugs. Advanced synthetic polymers have been developed to initiate endosomal escape and cytosolic release of their biologic cargo.

1.2.2 Cationic Polymers for Endosomal Escape

Following receptor-mediated endocytosis, internalized molecules are delivered to acidified, early endosomes (pH 6.6)[54,55]. Components that are not recycled or destined for a distinct cellular compartment are transported to late endosomes (pH 5.8) and eventually lysosomes (pH 4.3) for degradation[56]. Cationic polymers like polyethylenimine (PEI), are thought to promote endosomal escape through what was first described by Behr et al. as the proton-sponge effect[57]. The primary, secondary, and tertiary amino groups on PEI promote endosomal buffering with pKa values ranging from pH 4 to 7. As protons are pumped into endosome to decrease the pH, amino groups become protonated, causing an influx of chloride counter ions, and inducing osmotic swelling and eventual release to the cytosol[58,59]. The polymers can be synthesized in a linear, branched or dendrimeric architecture, however their cytotoxic behavior has made them less advantageous for in vivo delivery[60]. Similar to PEI, a well defined dendrimeric polymer polyamidoamine (PAMAM), is saturated with amino groups (pKa range: 3.9 - 6.9) but exhibits less toxicity than PEI at concentrations up to two orders of magnitude higher[61,62]. Uncharged, hydrophilic polymers like poly(ethylene glycol) (PEG) have been introduced into cationic polymer architectures to improve stability, reduce toxicity and increase serum stability[63].

1.2.3 Mimicking Pathogenic Organisms

Viruses and other pathogens like diphtheria utilize protein coatings on their surface for intracellular delivery of nucleic acids and proteins[64]. At physiological pH, the proteins are in a stealth-like hydrophilic conformation. As pathogens are trafficked to endosomes and lysosomes, a drop in the vesicular pH triggers a conformational change, exposing a hydrophobic membrane-destabilizing domain. The hemagglutinin protein complex found on the influenza virus exhibits a similar response[65,66]. Carboxylate groups on the

peptide are protonated at acidic pH, exposing a hydrophobic coil that forms pores with the endosomal membrane and prompting cytosolic release. Synthetic pH-responsive peptides that undergo a structure change to disrupt endosomal membranes have also been developed, but often suffer from low stability, immunogenicity and minimal escaping activity[50,57,67–69]. The viral delivery phenomenon has inspired the design of synthetic pH-responsive polymers containing alkyl(acrylic acid) monomers that mimic the endosomolytic behavior of pathogens for intracellular delivery[50,58].

1.2.4 pH-Responsive Polymers

One of the first synthetic polymers designed to elicit pH-responsive membrane destabilizing activity was poly(ethylacrylic acid) (PEAA), by Tirrell and coworkers[70–72]. They demonstrated that PEAA could disrupt lipid membranes through a pH-dependent conformational transition. Stayton and Hoffman built on these findings to develop similar carboxyl containing monomers with improved tuneability to pH-responsive, membrane-destabilizing activity[73–76]. An assortment of alky(acrylic acid) containing monomers were synthesized and polymerized to screen for the most membrane-destabilizing in a pH-responsive manner. A red blood cell hemolysis assay was designed to measure the membrane disruptive activity as a function of polymer concentration and buffer pH. The most active of these polymers was poly(propylacrylic acid) (PPAA), which was 15 times more hemolytic than PEAA at pH 6. The pKa of PPAA creates a pH-dependent switch particularly well-tuned for endosomal trafficking[48,73,74,76–78]. In the ionized state, PPAA is hydrophilic and inert. As the polymer is trafficked to endosomal pH (5.5-6.5), a gradual protonation of carboxylic acid residues on each monomer triggers a conformational hydrophobic shift, mediating membrane destabilization. PPAA has been shown to enhance therapeutic efficacy of model proteins both in vitro and in vivo[58,79,80]. PPAA can also enhance the cytoplasmic delivery of macromolecules like antibody complexes to deliver larger proteins[81], or improve the transfection efficiency

of plasmid DNA[82]. PPAA has also modified with cell-penetrating peptides to transport larger biomacromolecules. To improve the activity of PPAA, propylacrylic acidic monomers have also been copolymerized with other hydrophobic monomers[80]

1.2.5 Reversible Addition-Fragmentation Chain Transfer

In order to deliver polymer-protein conjugates for clinical applications they must have well-defined architectures, controlled molecular weights, and high uniformity. Radical living polymerizations like reversible addition-fragmentation chain transfer (RAFT) have been implemented to synthesize telechelic, di-end-functional polymers with low polydispersity, predetermined molecular weights, and a variety of complex architectures[83,84]. RAFT polymerization is similar to free radical polymerization, but the addition of a chain transfer agent suppresses termination and degradative chain transfer reactions. Commercially available thiocarbonylthio compounds have frequently been used as chain transfer agents, and can be tuned to a desired transfer rate[85]. More recently, trithiocarbonate chain transfer agents with defined end groups have been utilized to create homopolymers, block copolymers, and ABA triblock copolymers with controlled molecular weights and narrow polydispersities[86,87]. RAFT provides a clean and precise method for attaching polymers to biomacromolecules for improved in vivo circulation and cell targeting capabilities[88]. End-functional telechelic polymers containing fluorescence labels, pyridyl disulfides (PDS), maleimides, azides and biotin have been synthesized to improve intracellular delivery. These well-defined conjugates maintain uniformity and reproducible biologic activity for clinical applications. Duvall et al. formulated a pyridyl disulfide chain transfer agent for the RAFT synthesis of pH-responsive copolymers with reducible therapeutic peptides[89]. Functional end groups may be introduced into both the R and Z groups of a chain transfer agent, providing heterotelechelic functionality[85,88]. Boyer et al. utilized a bifunctional chain transfer agent to synthesize polymers with biotin and PDS terminal groups[90]. This procedure

allowed for site specific, dual conjugation of bovine serum albumin through a disulfide linkage, and avidin through the biotin functional end. Polymer-protein conjugates with multifunctional architectures are advantageous for drug delivery techniques, allowing for site-specific optimization of polymer drug loading and in vivo targeting[91–93].

1.3 Apoptosis in Cancer

1.3.1 Introduction

In normal cells, intracellular sensors monitor homeostasis and can readily activate the apoptosis pathways once DNA damage, viral infection, growth factor deprivation or signal imbalance are detected[94]. Apoptosis is initiated by a cell-signaling cascade and caspase activation, and often characterized by a loss of cell volume, the disruption of the cell membrane, nuclear and cytoplasmic skeletal breakdown, and chromosomal degradation[95]. An acquired resistance toward apoptosis is common to all types of cancers[9]. Targeting the apoptotic proteins in cancer cells has the potential to improve current cancer therapeutics in even the most highly resistant cancers. Our understanding of the Bcl-2 family and its role in cellular processes has greatly improved over the past 20 years, lending insight into it's role in cancer cell survival. An improved comprehension of the Bcl-2 pathways can pave the way for more specific therapies that specifically target apoptosis in all cancer cells.

1.3.2 BCl-2 Family Members

Apoptosis is a genetically controlled process, dictated by the intracellular ratio of proapoptotic and prosurvival proteins of the Bcl-2 family[96]. Proteins belonging to this family can be divided into multi-domain prosurvival, multi-domain proapoptotic, and BH3-only proapoptotic. The prosurvival proteins include Bcl-2, Bcl-XL, Bcl-2, Mcl-1, and A1 which maintain sequence homology in four domains: BH1, BH2, BH3,

and BH4, and are regulated by transcription factors like NFκB. The multi-domain, proapoptotic proteins BAK and BAX are initiators of apoptosis and share sequence homology in all four domains. The last group are BH3-only proteins regulated by transcription factors in response to cell stress, and can be subdivided into two classes, activators or sensitizers[10,97]. BH3-only activator proteins, BIM and BID can bind to all prosurvival proteins while BH3-only sensitizers PUMA, NOXA, BAD, BIK, BMF, and HRK have more selectively for antiapoptotic proteins (except for PUMA)[12]. The BH3 domain forms an amphipathic alpha-helical structure upon binding to the hydrophobic pocket of prosurvival proteins[98].

1.3.3 Mitochondrial Priming

While the exact mechanism and interplay between the various Bcl-2 family members is under investigation, a widely accepted model is that BAK and BAX mediated apoptosis can only be initiated by the proapoptotic activators BIM and BID, while proapoptotic sensitizers can only displace the proapoptotic by binding to prosurvival members. In a well-designed BH3 profiling study to measure mitochondrial sensitivity, Certo et al. determined that a cell could be in three possible states, unprimed for death, primed for death or dead. Mitochondrial priming was correlated with the interaction of prosurvival and proapoptotic members[97]. Unprimed cells lack expression of activator proteins (BID and BIM) and cannot release cytochrome c in the presence of sensitizers alone. In primed cells, activators are sequestered by prosurvival proteins to inhibit apoptosis. In the dead state, sensitizers free activators from prosurvival proteins and allow them to bind and activate BAK and BAX for apoptosis. Activation of BAK and BAX leads to oligomerization and insertion into the mitochondrial membrane, forming pores in the membrane that causes a loss in membrane potential, and cytochrome c release[99]. Although the exact number of oligomer units formed by BAK and BAX remains unclear, a temporal relationship has been established between oligomerization

and cytochrome c release[100]. Once in the cytosol, cytochrome c recruits APAF-1 and caspase-9 to form the apoptosome complex[101]. The holoenzyme then cleaves and activates caspase-3 to initiate apoptotosis[102]. Within the caspases are the initiator caspases 8, 9, and 10, and executioner caspases 3, 6, and 7, which act downstream of the initiators.

1.3.4 Upregulation of Prosurvival Proteins

Impairment of the apoptotic machinery in cancer cells prevents intracellular sensors from triggering programmed cell death. Upregulation of prosurvival proteins in tumor cells has been linked to radiation and chemotherapeutic resistance[103,104]. 60 cancer cell lines with high expression of Bcl-2, are correlated with chemoresistance to 122 different agents[105]. In normal cells, the P53 tumor suppressor gene upregulates the proapoptotic BAX protein in response to DNA damage or cell-cycle arrest, inducing apoptosis. Mutation of the p53 suppressor gene found in more than 50% of cancers, removes the DNA damage sensor and prevents apoptotic regulation[106]. To overcome these hurdles, a new class of biomimetic peptides derived from the BH3-binding domain act as biologic therapeutics. The first three-dimensional structure of the Bcl-X_L complex bound to the BAK peptide has laid the foundation for the discovery of proapoptotic peptides[105].

1.3.5 Significance of BIM in Cancer Cells

Efficient cell killing is dependent on the ability to neutralize the diverse groups of antiapoptotic members. BID and BIM are the most promiscuous of the proapoptotic BH3-only proteins with the ability to bind to all five prosurvival members and activate apoptosis through BAK and BAX. The BIM protein is expressed in hematopoietic, neuronal, and epithelial cells, localizing to microtubules through binding to the light

chain of the dynein motor complex[12]. BIM levels are modulated via the degradation pathway of proteosomes and are also regulated by FOXO3A in response to growth factor deprivation and endoplasmic reticulum stress[102]. BIM was also found to be crucial for the deletion of T and B cells in the termination of an immune response. In tumor cells, paclitaxel was delivered before and after knockdown of the BIM protein via siRNA and found to be critical for paclitaxel-mediated killing of lymphocyte-tumor cells. In a study by Chen et al. the dissociation constant for the BIM peptide with all five proapoptotic proteins ranged from 0.2 to 4.5 ηM[106]. In a separate study with mitochondria isolated from cancer cells overexpressing Bcl-2, 100 uM of BID or BIM peptides released cytochrome c, while the other BH3-only peptides did not. Although the alpha-helical propensity of each BH3-only peptide varied, no correlation was found with peptide activity or affinity.

1.3.6 TAT-BIM Fusion Peptide

Perturbation of the apoptotic pathway in cancer cells with proapoptotic peptides has the potential to directly induce apoptosis while enhancing sensitization to cytotoxic therapies. The discovery of the BIM peptides ability to efficiently induce apoptosis through all five anti-apoptotic proteins has prompted the development intracellular peptide delivery systems[107]. A peptide containing the HIV-1 derived transduction domain (TAT) was fused to the proapoptotic BIM peptide to demonstrate therapeutic activity in three different cancer cell and in tumor-xenograft bearing mice[108]. In vitro studies performed between 2 and 10 μM, showed that the internalization efficiency of BIM could be increased over 10-fold with the addition of the TAT transduction domain and increased cleaved caspase-3 activity. Interestingly, TAT-BIM was also found to increase sensitization of cancer cells towards radiation but the degree of sensitization was dependent on cell type. In tumor xenograft-bearing mice, TAT-BIM stunted the growth of tumors an in some cases caused shrinkage with no observable

toxicity. The addition of a tumor-targeting modality would have likely improved the modest tumor activity.

1.3.7 Stapled BID and BIM Peptides

BH3 peptides are often tagged with polyarginine tails to facilitate transport across the plasma membrane. In vivo efficacy of the peptides is compromised by the loss of secondary structures and susceptibility to proteolytic degradation[109]. To improve in vivo stability and pharmacological properties, BH3 "stapled" peptides have been generated using a hydrocarbon staple[110,111]. To staple the peptides, non-essential amino acids are replaced with non-natural amino acids containing connectable side chains, creating stabilized alpha-helix structures that are protease resistant and cell permeable with a high binding affinity to prosurvival members. When Walensky et al. constructed the stapled BID (sBID) peptide, they found that the helicity increased from 16% (BID) to 87% (sBID) in solution and that sBID internalized in cells through energy-dependent, hydrophobic interactions[110]. Furthermore, the sBID peptide induced apoptosis in cells after 20 hours at a concentration of 1 μM. Recently, LaBelle and coworkers developed an alpha-helix stapled BIM peptide with similar capabilities to stapled BID[110,112]. The stapled BIM induced apoptosis in resistant hematologic cancers and preferentially affected cancer cells over normal cells. Studies with TAT-BIM and stapled BIM have helped to realize the clinical importance of this peptide for future clinical applications.

1.4 References

[1] D Hanahan and R A Weinberg. The hallmarks of cancer. *Cell*, 100(1):57–70, 2000.

[2] A G Polson, J Calemine-Fenaux, P Chan, W Chang, E Christensen, S Clark, F J de Sauvage, D Eaton, K Elkins, J M Elliott, G Frantz, R N Fuji, A Gray, K Harden, G S Ingle, N M Kljavin, H Koeppen, C Nelson, S Prabhu, H Raab, S Ross, D S Slaga, J-P Stephan, S J Scales, S D Spencer, R Vandlen, B Wranik, S-F Yu, B Zheng, and A Ebens. Antibody-Drug Conjugates for the Treatment of Non-Hodgkin's Lymphoma: Target and Linker-Drug Selection. *Cancer Research*, 69(6):2358–2364, March 2009.

[3] Peter D Senter. Potent antibody drug conjugates for cancer therapy. *Current Opinion in Chemical Biology*, 13(3):235–244, June 2009.

[4] A G Polson, M Williams, A M Gray, R N Fuji, K A Poon, J McBride, H Raab, T Januario, M Go, J Lau, S-F Yu, C Du, F Fuh, C Tan, Y Wu, W-C Liang, S Prabhu, J-P Stephan, J-A Hongo, R C Dere, R Deng, M Cullen, R de Tute, F Bennett, A Rawstron, A Jack, and A Ebens. Anti-CD22-MCC-DM1: an antibody-drug conjugate with a stable linker for the treatment of non-Hodgkin's lymphoma. *Leukemia*, 24(9):1566–1573, July 2010.

[5] Robert M Sharkey and David M Goldenberg. Perspectives on cancer therapy with radiolabeled monoclonal antibodies. *Journal of Nuclear Medicine*, 46(1 suppl):115S–127S, 2005.

[6] B A Teicher. Antibody-drug conjugate targets. *Current cancer drug targets*, 9(8):982–1004, 2009.

[7] Anna M Wu and Peter D Senter. Arming antibodies: prospects and challenges for immunoconjugates. *Nature Biotechnology*, 23(9):1137–1146, September 2005.

[8] Rony Abou-Jawde, Toni Choueiri, Carlos Alemany, and Tarek Mekhail. An overview of targeted treatments in cancer. *Clinical therapeutics*, 25(8):2121–2137, 2003.

[9] W Hu and J J Kavanagh. Anticancer therapy targeting the apoptotic pathway. *The lancet oncology*, 4(12):721–729, 2003.

[10] A Letai, M C Bassik, L D Walensky, M D Sorcinelli, S Weiler, and S J Korsmeyer. Distinct BH3 domains either sensitize or activate mitochondrial apoptosis, serving as prototype cancer therapeutics. *Cancer Cell*, 2(3):183–192, 2002.

[11] Sanjeev Shangary, Christopher L Oliver, Tommy S Tillman, Michael Cascio, and Daniel E Johnson. Sequence and helicity requirements for the proapoptotic activity of Bax BH3 peptides. *Molecular Cancer*, 2004.

[12] E Lomonosova and G Chinnadurai. BH3-only proteins in apoptosis and beyond: an overview. *Oncogene*, 27:S2–S19, December 2008.

[13] Niren Murthy, Jean Campbell, Nelson Fausto, Allan S Hoffman, and Patrick S Stayton. Bioinspired pH-Responsive Polymers for the Intracellular Delivery of Biomolecular Drugs. *Bioconjugate Chemistry*, 14(2):412–419, March 2003.

[14] Amir K Varkouhi, Marije Scholte, Gert Storm, and Hidde J Haisma. Endosomal escape pathways for delivery of biologicals. *Journal of Controlled Release*, 151(3):220–228, May 2011.

[15] Arjen M Funhoff, Cornelus F van Nostrum, Gerben A Koning, Nancy ME Schuurmans-Nieuwenbroek, Daan JA Crommelin, and Wim E Hennink. Endosomal escape of polymeric gene delivery complexes is not always enhanced by polymers buffering at low pH. *Biomacromolecules*, 5(1):32–39, 2004.

[16] S Moffatt, S Wiehle, and R J Cristiano. A multifunctional PEI-based cationic polyplex for enhanced systemic p53-mediated gene therapy. *Gene Therapy*, 13(21):1512–1523, 2006.

[17] Rajan P Kulkarni, Swaroop Mishra, Scott E Fraser, and Mark E Davis. Single Cell Kinetics of Intracellular, Nonviral, Nucleic Acid Delivery Vehicle Acidification and Trafficking. *Bioconjugate Chemistry*, 16(4):986–994, July 2005.

[18] D Schrama and R Reisfeld. Antibody targeted drugs as cancer therapeutics. *Nature Reviews Drug Discovery*, 2006.

[19] G Köhler and C Milstein. Continuous cultures of fused cells secreting antibody of predefined specificity. 1975., March 2005.

[20] Alvin Y Liu, Randy R Robinson, Karl Erik Hellström, E David Murray, C Paul Chang, and Ingegerd Hellström. Chimeric mouse-human IgG1 antibody that can mediate lysis of cancer cells. *Proceedings of the National Academy of Sciences*, 84(10):3439–3443, 1987.

[21] J D Hainsworth. Rituximab as First-Line and Maintenance Therapy for Patients With Indolent Non-Hodgkin's Lymphoma. *Journal of Clinical Oncology*, 20(20):4261–4267, October 2002.

[22] Janice M Reichert, Clark J Rosensweig, Laura B Faden, and Matthew C Dewitz. Monoclonal antibody successes in the clinic. *Nature Biotechnology*, 23(9):1073–1078, 2005.

[23] K J Hamblett. Effects of Drug Loading on the Antitumor Activity of a Monoclonal Antibody Drug Conjugate. *Clinical Cancer Research*, 10(20):7063–7070, October 2004.

[24] K De Santes, D Slamon, S K Anderson, M Shepard, B Fendly, D Maneval, and O Press. Radiolabeled antibody targeting of the HER-2/neu oncoprotein. *Cancer Research*, 52(7):1916–1923, 1992.

[25] Robert M Sharkey and David M Goldenberg. Perspectives on cancer therapy with radiolabeled monoclonal antibodies. *Journal of nuclear medicine : official publication, Society of Nuclear Medicine*, 46 Suppl 1:115S–27S, 2005.

[26] T M Allen. Drug Delivery Systems: Entering the Mainstream. *Science*, 303(5665):1818–1822, March 2004.

[27] Robert M Sharkey, Arnold Brenner, Jack Burton, George Hajjar, Stephen P Toder, Abass Alavi, Alexander Matthies, Donald E Tsai, Stephen J Schuster, and Edward A Stadtmauer. Radioimmunotherapy of non-Hodgkin's lymphoma with 90Y-DOTA humanized anti-CD22 IgG (90Y-Epratuzumab): do tumor targeting and dosimetry predict therapeutic response? *Journal of Nuclear Medicine*, 44(12):2000–2018, 2003.

[28] M Juweid, R M Sharkey, A Markowitz, T Behr, L C Swayne, R Dunn, H J Hansen, J Shevitz, S O Leung, and A D Rubin. Treatment of non-Hodgkin's lymphoma with radiolabeled murine, chimeric, or humanized LL2, an anti-CD22 monoclonal antibody. *Cancer Research*, 55(23 Supplement):5899s–5907s, 1995.

[29] Diane E Milenic, Erik D Brady, and Martin W Brechbiel. Antibody-targeted radiation cancer therapy. *Nature Reviews Drug Discovery*, 3(6):488–499, June 2004.

[30] O W Press, J F Eary, F R Appelbaum, P J Martin, W B Nelp, S Glenn, D R Fisher, B Porter, D C Matthews, and T Gooley. Phase II trial of 131I-B1 (anti-CD20) antibody therapy with autologous stem cell transplantation for relapsed B cell lymphomas. *Lancet*, 346(8971):336–340, August 1995.

[31] J M Pagel, A Pantelias, N Hedin, S Wilbur, L Saganic, Y Lin, D Axworthy, D K Hamlin, D S Wilbur, A K Gopal, and O W Press. Evaluation of CD20, CD22, and HLA-DR Targeting for Radioimmunotherapy of B-Cell Lymphomas. *Cancer Research*, 67(12):5921–5928, June 2007.

[32] A Pantelias, J M Pagel, N Hedin, L Saganic, S Wilbur, D K Hamlin, D S Wilbur, Y Lin, D Stone, D Axworthy, A K Gopal, and O W Press. Comparative biodistributions of pretargeted radioimmunoconjugates targeting CD20, CD22, and DR molecules on human B-cell lymphomas. *Blood*, 109(11):4980–4987, June 2007.

[33] Daming Shan and Oliver W Press. Constitutive endocytosis and degradation of CD22 by human B cells. *The Journal of Immunology*, 154(9):4466–4475, 1995.

[34] Martin C Garnett. Targeted drug conjugates: principles and progress. *Advanced Drug Delivery Reviews*, 53(2):171–216, 2001.

[35] J Yang, H Chen, I R Vlahov, J X Cheng, and P S Low. Evaluation of disulfide reduction during receptor-mediated endocytosis by using FRET imaging. *Proceedings of the National Academy of Sciences*, 103(37):13872–13877, 2006.

[36] Silvia Arpicco, Franco Dosio, Paola Brusa, Paola Crosasso, and Luigi Cattel. New coupling reagents for the preparation of disulfide cross-linked conjugates with increased stability. *Bioconjugate Chemistry*, 8(3):327–337, 1997.

[37] Ben-Quan Shen, Keyang Xu, Luna Liu, Helga Raab, Sunil Bhakta, Margaret Kenrick, Kathryn L Parsons-Reponte, Janet Tien, Shang-Fan Yu, Elaine Mai, Dongwei Li, Jay Tibbitts, Jakub Baudys, Ola M Saad, Suzie J Scales, Paul J McDonald, Philip E Hass, Charles Eigenbrot, Trung Nguyen, Willy A Solis, Reina N Fuji, Kelly M Flagella, Darshana Patel, Susan D Spencer, Leslie A Khawli, Allen Ebens, Wai Lee Wong, Richard Vandlen, Surinder Kaur, Mark X Sliwkowski, Richard H Scheller, Paul Polakis, and Jagath R Junutula. Conjugation site modulates the in vivo stability and therapeutic activity of antibody-drug conjugates. *Nature Biotechnology*, 30(2):184–189, January 2012.

[38] E Oflazoglu, KM Kissler, and EL Sievers. Combination of the antiCD30auristatinE antibodydrug conjugate (SGN35) with chemotherapy improves antitumour activity in Hodgkin lymphoma. *British journal of . . .*, 2008.

[39] S C Alley, X Zhang, N M Okeley, M Anderson, C L Law, P D Senter, and D R Benjamin. The Pharmacologic Basis for Antibody-Auristatin Conjugate Activity. *Journal of Pharmacology and Experimental Therapeutics*, 330(3):932–938, August 2009.

[40] Kelley V Foyil and Nancy L Bartlett. Anti-CD30 Antibodies for Hodgkin Lymphoma. *Current Hematologic Malignancy Reports*, 5(3):140–147, May 2010.

[41] Sandhya Girish, Manish Gupta, Bei Wang, Dan Lu, Ian E Krop, Charles L Vogel, Howard A Burris, III, Patricia M LoRusso, Joo-Hee Yi, Ola Saad, Barbara Tong, Yu-Waye Chu, Scott Holden, and Amita Joshi. Clinical pharmacology of trastuzumab emtansine (T-DM1): an antibody–drug conjugate in development for the treatment of HER2-positive cancer. *Cancer Chemotherapy and Pharmacology*, 69(5):1229–1240, January 2012.

[42] S A Hurvitz, L Dirix, J Kocsis, G V Bianchi, J Lu, J Vinholes, E Guardino, C Song, B Tong, V Ng, Y W Chu, and E A Perez. Phase II Randomized Study of Trastuzumab Emtansine Versus Trastuzumab Plus Docetaxel in Patients With

Human Epidermal Growth Factor Receptor 2-Positive Metastatic Breast Cancer. *Journal of Clinical Oncology*, 31(9):1157–1163, March 2013.

[43] James Huang, Guang Fan, Yanping Zhong, Ken Gatter, Rita Braziel, Gary Gross, and Antony Bakke. Diagnostic Usefulness of Aberrant CD22 Expression in Differentiating Neoplastic Cells of B-Cell Chronic Lymphoproliferative Disorders From Admixed Benign B Cells in Four-Color Multiparameter Flow Cytometry. *American Journal of Clinical Pathology*, 123(6):826–832, April 2005.

[44] Nadia Chaouchi, Aime Vazquez, Pierre Galanaud, and Corinne Leprince. B cell antigen receptor-mediated apoptosis. Importance of accessory molecules CD19 and CD22, and of surface IgM cross-linking. *The Journal of Immunology*, 154(7):3096–3104, 1995.

[45] H Tateno, H Li, M J Schur, N Bovin, P R Crocker, W W Wakarchuk, and J C Paulson. Distinct Endocytic Mechanisms of CD22 (Siglec-2) and Siglec-F Reflect Roles in Cell Signaling and Innate Immunity. *Molecular and Cellular Biology*, 27(16):5699–5710, July 2007.

[46] J P Leonard. Phase I/II Trial of Epratuzumab (Humanized Anti-CD22 Antibody) in Indolent Non-Hodgkin's Lymphoma. *Journal of Clinical Oncology*, 21(16):3051–3059, July 2003.

[47] O Linden. Dose-Fractionated Radioimmunotherapy in Non-Hodgkin's Lymphoma Using DOTA-Conjugated, 90Y-Radiolabeled, Humanized Anti-CD22 Monoclonal Antibody, Epratuzumab. *Clinical Cancer Research*, 11(14):5215–5222, July 2005.

[48] Chantal A Lackey, Oliver W Press, Allan S Hoffman, and Patrick S Stayton. A Biomimetic pH-Responsive Polymer Directs Endosomal Release and Intracellular Delivery of an Endocytosed Antibody Complex. *Bioconjugate Chemistry*, 13(5):996–1001, September 2002.

[49] C Varga. Quantitative Analysis of Synthetic Gene Delivery Vector Design Properties. *Molecular Therapy*, 4(5):438–446, November 2001.

[50] Yong Woo Cho, Jong Duk Kim, and Kinam Park. Polycation gene delivery systems: escape from endosomes to cytosol. *The Journal of pharmacy and pharmacology*, 55(6):721–734, June 2003.

[51] Brian Albarran, Allan S Hoffman, and Patrick S Stayton. Efficient intracellular delivery of a pro-apoptotic peptide with a pH-responsive carrier. *Reactive and Functional Polymers*, 71(3):261–265, March 2011.

[52] Qi Zhong, Cheri S Lazar, Hélène Tronchère, Trey Sato, Timo Meerloo, Michele Yeo, Zhou Songyang, Scott D Emr, and Gordon N Gill. Endosomal localization

and function of sorting nexin 1. *Proceedings of the National Academy of Sciences*, 99(10):6767–6772, 2002.

[53] A Paul Bevan, Paul G Drake, John JM Bergeron, and Barry I Posner. Intracellular signal transduction: the role of endosomes. *Trends in Endocrinology & Metabolism*, 7(1):13–21, 1996.

[54] Qais Al-Awqati. Proton-translocating ATPases. *Annual review of cell biology*, 2(1):179–199, 1986.

[55] B Tycko and F R Maxfield. Rapid acidification of endocytic vesicles containing alpha 2-macroglobulin. *Cell*, 28(3):643–651, March 1982.

[56] Cathrine Nilsson, Katarina Kågedal, Uno Johansson, and Karin Öllinger. Analysis of cytosolic and lysosomal pH in apoptotic cells by flow cytometry. *Methods in cell science*, 25(3-4):185–194, 2004.

[57] Jean-Paul Behr. Gene Transfer with Synthetic Cationic Amphiphiles: Prospects for Gene Therapy. *Bioconjugate Chemistry*, 5(5):382–389, September 1994.

[58] Daniel W Pack, Allan S Hoffman, Suzie Pun, and Patrick S Stayton. Design and development of polymers for gene delivery. *Nature Reviews Drug Discovery*, 4(7):581–593, July 2005.

[59] Akin Akinc, Mini Thomas, Alexander M Klibanov, and Robert Langer. Exploring polyethylenimine-mediated DNA transfection and the proton sponge hypothesis. *The Journal of Gene Medicine*, 7(5):657–663, May 2005.

[60] S-D Li and L Huang. Gene therapy progress and prospects: non-viral gene therapy by systemic delivery. *Gene Therapy*, 13(18):1313–1319, September 2006.

[61] Kris C Wood, Steven R Little, Robert Langer, and Paula T Hammond. A Family of Hierarchically Self-Assembling Linear-Dendritic Hybrid Polymers for Highly Efficient Targeted Gene Delivery. *Angewandte Chemie International Edition*, 44(41):6704–6708, October 2005.

[62] Jean Haensler and Francis C Szoka. Polyamidoamine cascade polymers mediate efficient transfection of cells in culture. *Bioconjugate Chemistry*, 4(5):372–379, September 1993.

[63] E Wagner. Strategies to Improve DNA Polyplexes for in Vivo Gene Transfer: Will "Artificial Viruses" Be the .... *Pharmaceutical Research*, 2004.

[64] Ernst Wagner, Christian Plank, Kurt Zatloukal, Matt Cotten, and Max L Birnstiel. Influenza virus hemagglutinin HA-2 N-terminal fusogenic peptides augment gene transfer by transferrin-polylysine-DNA complexes: toward a

synthetic virus-like gene-transfer vehicle. *Proceedings of the National Academy of Sciences*, 89(17):7934–7938, 1992.

[65] FM Hughson. ScienceDirect - Current Biology : Structural characterization of viral fusion proteins. *Current Biology*, 1995.

[66] D C Wiley and J J Skehel. The structure and function of the hemagglutinin membrane glycoprotein of influenza virus. *Annual review of biochemistry*, 56(1):365–394, 1987.

[67] H BROOKS, B LEBLEU, and E VIVES. Tat peptide-mediated cellular delivery: back to basics. *Advanced Drug Delivery Reviews*, 57(4):559–577, February 2005.

[68] Sandra Veldhoen, Sandra D Laufer, and Tobias Restle. Recent Developments in Peptide-Based Nucleic Acid Delivery. *International Journal of Molecular Sciences*, 9(7):1276–1320, July 2008.

[69] Külliki Saar, Maria Lindgren, Mats Hansen, Emelía Eiríksdóttir, Yang Jiang, Katri Rosenthal-Aizman, Meeri Sassian, and Ülo Langel. Cell-penetrating peptides: A comparative membrane toxicity study. *Analytical Biochemistry*, 345(1):55–65, October 2005.

[70] Jungsoo Kim and David A Tirrell. Synthesis of Well-Defined Poly(2-ethylacrylic acid). *Macromolecules*, 32(3):945–948, February 1999.

[71] J L Thomas and D A Tirrell. Polyelectrolyte-sensitized phospholipid vesicles. *Accounts of chemical research*, 25(8):336–342, 1992.

[72] James L Thomas, Scott W Barton, and David A Tirrell. Membrane solubilization by a hydrophobic polyelectrolyte: surface activity and membrane binding. *Biophysical Journal*, 67(3):1101–1106, 1994.

[73] Chantal A Lackey, Niren Murthy, Oliver W Press, David A Tirrell, Allan S Hoffman, and Patrick S Stayton. Hemolytic Activity of pH-Responsive Polymer-Streptavidin Bioconjugates . *Bioconjugate Chemistry*, 10(3):401–405, May 1999.

[74] Niren Murthy, John R Robichaud, David A Tirrell, Patrick S Stayton, and Allan S Hoffman. The design and synthesis of polymers for eukaryotic membrane disruption. *Journal of Controlled Release*, 61(1):137–143, 1999.

[75] N Murthy, I Chang, P S Stayton, and A Hoffman. pHsensitive hemolysis by random copolymers of alkyl acrylates and acrylic acid. *Macromolecular Symposium*, 172(1):49–56, 2001.

[76] Allan S Hoffman, Patrick S Stayton, Oliver Press, Niren Murthy, Chantal A Lackey, Charles Cheung, Fiona Black, Jean Campbell, Nelson Fausto, and

Themis R Kyriakides. Bioinspired polymers that control intracellular drug delivery. *Biotechnology and Bioprocess Engineering*, 6(4):205–212, 2001.

[77] Rachel A Jones, Charles Y Cheung, Fiona E Black, Jasmine K Zia, Patrick S Stayton, Allan S Hoffman, and Mark R Wilson. Poly (2-alkylacrylic acid) polymers deliver molecules to the cytosol by pH-sensitive disruption of endosomal vesicles. *Biochemical Journal*, 372(Pt 1):65, 2003.

[78] N Murthy, J Campbell, N Fausto, A S Hoffman, and P S Stayton. Design and synthesis of pH-responsive polymeric carriers that target uptake and enhance the intracellular delivery of oligonucleotides. *Journal of Controlled Release*, 89(3):365–374, 2003.

[79] Mohamed E H El-Sayed, Allan S Hoffman, and Patrick S Stayton. Rational design of composition and activity correlations for pH-sensitive and glutathione-reactive polymer therapeutics. *Journal of Controlled Release*, 101(1-3):47–58, January 2005.

[80] Anthony J Convertine, Danielle S W Benoit, Craig L Duvall, Allan S Hoffman, and Patrick S Stayton. Development of a novel endosomolytic diblock copolymer for siRNA delivery. *Journal of Controlled Release*, 133(3):221–229, February 2009.

[81] B Albarran, R To, and P STAYTON. 1111. TAT-Streptavidin: A Novel Drug Delivery Vector for the Intracellular Uptake of Macromolecular Cargo. *Molecular Therapy*, 11:428–428, August 2005.

[82] Charles Y Cheung, Niren Murthy, Patrick S Stayton, and Allan S Hoffman. A pH-Sensitive Polymer That Enhances Cationic Lipid-Mediated Gene Transfer. *Bioconjugate Chemistry*, 12(6):906–910, November 2001.

[83] G Moad, J Chiefari, and BYK Chong. Living free radical polymerization with reversible addition – fragmentation chain transfer (the life of RAFT) - Moad - 2000 - Polymer International - Wiley Online Library. *Polymer*, 2000.

[84] John Chiefari, Y K Bill Chong, Frances Ercole, Julia Krstina, Justine Jeffery, Tam P T Le, Roshan T A Mayadunne, Gordon F Meijs, Catherine L Moad, Graeme Moad, Ezio Rizzardo, and San H Thang. Living Free-Radical Polymerization by Reversible AdditionFragmentation Chain Transfer: The RAFT Process. *Macromolecules*, 31(16):5559–5562, August 1998.

[85] Graeme Moad, Y K Chong, Almar Postma, Ezio Rizzardo, and San H Thang. Advances in RAFT polymerization: the synthesis of polymers with defined end-groups. *Polymer*, 46(19):8458–8468, September 2005.

[86] Anthony J Convertine, Neil Ayres, Charles W Scales, Andrew B Lowe, and

Charles L McCormick. Facile, Controlled, Room-Temperature RAFT Polymerization of N-Isopropylacrylamide . *Biomacromolecules*, 5(4):1177–1180, July 2004.

[87] Roshan T A Mayadunne, Ezio Rizzardo, John Chiefari, Julia Krstina, Graeme Moad, Almar Postma, and San H Thang. Living Polymers by the Use of Trithiocarbonates as Reversible AdditionFragmentation Chain Transfer (RAFT) Agents: ABA Triblock Copolymers by Radical Polymerization in Two Steps. *Macromolecules*, 33(2):243–245, January 2000.

[88] Cyrille Boyer, Volga Bulmus, Thomas P Davis, Vincent Ladmiral, Jingquan Liu, and Sébastien Perrier. Bioapplications of RAFT Polymerization. *Chemical Reviews*, 109(11):5402–5436, November 2009.

[89] Craig L Duvall, Anthony J Convertine, Danielle S W Benoit, Allan S Hoffman, and Patrick S Stayton. Intracellular Delivery of a Proapoptotic Peptide via Conjugation to a RAFT Synthesized Endosomolytic Polymer. *Molecular Pharmaceutics*, 7(2):468–476, April 2010.

[90] Cyrille Boyer, Jingquan Liu, Volga Bulmus, Thomas P Davis, Christopher Barner-Kowollik, and Martina H Stenzel. Direct Synthesis of Well-Defined Heterotelechelic Polymers for Bioconjugations. *Macromolecules*, 41(15):5641–5650, August 2008.

[91] Suzanne Flanary, Allan S Hoffman, and Patrick S Stayton. Antigen Delivery with Poly(Propylacrylic Acid) Conjugation Enhances MHC-1 Presentation and T-Cell Activation. *Bioconjugate Chemistry*, 20(2):241–248, February 2009.

[92] T Sugita, T Yoshikawa, Y Mukai, N Yamanada, S Imai, K Nagano, Y Yoshida, H Shibata, Y Yoshioka, S Nakagawa, H Kamada, S-i Tsunoda, and Y Tsutsumi. Comparative study on transduction and toxicity of protein transduction domains. *British Journal of Pharmacology*, 153(6):1143–1152, January 2009.

[93] J Rinne, B Albarran, J Jylhävä, T O Ihalainen, P Kankaanpää, V P Hytönen, P S Stayton, M S Kulomaa, and M Vihinen-Ranta. Internalization of novel non-viral vector TAT-streptavidin into human cells. *BMC Biotechnology*, 7(1):1, 2007.

[94] Michael D Jacobson, Julia F Burne, and Martin C Raff. Programmed cell death and Bcl-2 protection in the absence of a nucleus. *The EMBO journal*, 13(8):1899, 1994.

[95] Richard J Youle and Andreas Strasser. The BCL-2 protein family: opposing activities that mediate cell death. *Nature Reviews Molecular Cell Biology*, 9(1):47–59, January 2008.

[96] N N Danial. BCL-2 Family Proteins: Critical Checkpoints of Apoptotic Cell Death. *Clinical Cancer Research*, 13(24):7254–7263, December 2007.

[97] Michael Certo, Victoria Del Gaizo Moore, Mari Nishino, Guo Wei, Stanley Korsmeyer, Scott A Armstrong, and Anthony Letai. Mitochondria primed by death signals determine cellular addiction to antiapoptotic BCL-2 family members. *Cancer Cell*, 9(5):351–365, May 2006.

[98] P E Czabotar, P M Colman, and D C S Huang. Bax activation by Bim—[quest]—. *Cell Death and Differentiation*, 16(9):1187–1191, June 2009.

[99] J D Ly, D R Grubb, and A Lawen. The mitochondrial membrane potential ($\Delta\psi$ m) in apoptosis; an update. *Apoptosis*, 8(2):115–128, 2003.

[100] Victoria Del Gaizo Moore and Anthony Letai. BH3 profiling â“ Measuring integrated function of the mitochondrial apoptotic pathway to predict cell fate decisions. *Cancer letters*, pages 1–4, January 2012.

[101] Angel G Martin, Jack Nguyen, James A Wells, and Howard O Fearnhead. Apo cytochrome c inhibits caspases by preventing apoptosome formation. *Biochemical and Biophysical Research Communications*, 319(3):944–950, 2004.

[102] A Sunters. FoxO3a Transcriptional Regulation of Bim Controls Apoptosis in Paclitaxel-treated Breast Cancer Cell Lines. *Journal of Biological Chemistry*, 278(50):49795–49805, October 2003.

[103] Maria Dolores Herman, Tomas Nyman, Martin Welin, Lari Lehtiö, Susanne Flodin, Lionel Trésaugues, Tetyana Kotenyova, Alex Flores, and Pär Nordlund. Completing the family portrait of the anti-apoptotic Bcl-2 proteins: Crystal structure of human Bfl-1 in complex with Bim. *FEBS letters*, 582(25-26):3590–3594, October 2008.

[104] David Karnak and Liang Xu. Chemosensitization of prostate cancer by modulating Bcl-2 family proteins. *Current drug targets*, 11(6):699, 2010.

[105] Sally A Amundson, Timothy G Myers, Dominic Scudiero, Shinichi Kitada, John C Reed, and Albert J Fornace. An informatics approach identifying markers of chemosensitivity in human cancer cell lines. *Cancer Research*, 60(21):6101–6110, 2000.

[106] Lin Chen, Simon N Willis, Andrew Wei, Brian J Smith, Jamie I Fletcher, Mark G Hinds, Peter M Colman, Catherine L Day, Jerry M Adams, and David C S Huang. Differential Targeting of Prosurvival Bcl-2 Proteins by Their BH3-Only Ligands Allows Complementary Apoptotic Function. *Molecular Cell*, 17(3):393–403, February 2005.

[107] Guillaume Lessene, Peter E Czabotar, and Peter M Colman. BCL-2 family

antagonists for cancer therapy. *Nature Reviews Drug Discovery*, 7(12):989–1000, December 2008.

[108] Hiroyuki Kashiwagi, Jonathan E McDunn, Peter S Goedegebuure, Mary C Gaffney, Katherine Chang, Kathryn Trinkaus, David Piwnica-Worms, Richard S Hotchkiss, and William G Hawkins. TAT-Bim Induces Extensive Apoptosis in Cancer Cells. *Annals of Surgical Oncology*, 14(5):1763–1771, January 2007.

[109] G L Verdine and L D Walensky. The Challenge of Drugging Undruggable Targets in Cancer: Lessons Learned from Targeting BCL-2 Family Members. *Clinical Cancer Research*, 13(24):7264–7270, December 2007.

[110] Loren D Walensky, Kenneth Pitter, Joel Morash, Kyoung Joon Oh, Scott Barbuto, Jill Fisher, Eric Smith, Gregory L Verdine, and Stanley J Korsmeyer. A Stapled BID BH3 Helix Directly Binds and Activates BAX. *Molecular Cell*, 24(2):199–210, October 2006.

[111] L D Walensky. Activation of Apoptosis in Vivo by a Hydrocarbon-Stapled BH3 Helix. *Science*, 305(5689):1466–1470, September 2004.

[112] James L LaBelle, Samuel G Katz, Gregory H Bird, Evripidis Gavathiotis, Michelle L Stewart, Chelsea Lawrence, Jill K Fisher, Marina Godes, Kenneth Pitter, Andrew L Kung, and Loren D Walensky. A stapled BIM peptide overcomes apoptotic resistance in hematologic cancers. *Journal of Clinical Investigation*, 122(6):2018–2031, June 2012.

Chapter 2

INTRACELLULAR DELIVERY AND TRAFFICKING DYNAMICS OF A LYMPHOMA-TARGETING ANTIBODY-POLYMER CONJUGATE

Geoffrey Y. Berguig[1], Anthony J. Convertine[1], Julie Shi[1], Maria Corinna Palanca-Wessels[2,3], Craig L. Duvall[1,4], Suzie H. Pun[1], Oliver W. Press[2,3], and Patrick S. Stayton[1*]

1. Department of Bioengineering, University of Washington, Seattle, WA
2. Fred Hutchinson Cancer Research Center, Seattle, WA
3. Department of Medicine, University of Washington, Seattle, WA
4. Current Address: Department of Biomedical Engineering, Vanderbilt University

Ratiometric fluorescence and cellular fractionation studies were employed to characterize the intracellular trafficking dynamics of antibody-poly(propylacrylic acid) (PPAA) conjugates in CD22+ RAMOS-AW cells. The HD39 monoclonal antibody (mAb) directs CD22-dependent, receptor-mediated uptake in human B-cell lymphoma cells, where it is rapidly trafficked to the lysosomal compartment. To characterize the intracellular-release dynamics of the polymer-Ab conjugates, HD39-streptavidin (HD39/SA) was dual-labeled with pH-insensitive Alexa Fluor 488 and pH-sensitive pHrodo fluorophores. The subcellular pH distribution of the HD39/SA-polymer conjugates was quantified as a function of time by live-cell fluorescence microscopy, and the average intracellular pH value experienced by the conjugates was also characterized as a function of time by flow cytometry. PPAA was shown to alter the intracellular trafficking kinetics strongly relative to HD39/SA alone or HD39/SA conjugates with a control polymer, poly(methacryclic acid) (PMAA). Subcellular trafficking studies revealed that after 6 h, only 11% of the HD39/SA-PPAA conjugates had been trafficked to acidic lysosomal compartments with values at or below pH 5.6. In contrast, the average intracellular pH of HD39/SA alone dropped from 6.7 ± 0.2 at 1 h to 5.6 ± 0.5 after 3 h and 4.7 ± 0.6 after 6 h. Conjugation of the control polymer PMAA to HD39/SA showed an average pH drop similar to that of HD39/SA. Subcellular fractionation studies with tritium-labeled HD39/SA demonstrated that after 6 h, 89% of HD39/SA was associated with endosomes (Rab5+) and lysosomes (Lamp2+), while 45% of HD39/SA-PPAA was translocated to the cytosol (lactate dehydrogenase+). These results demonstrate the endosomal-releasing properties of PPAA with antibody-polymer conjugates and detail their intracellular trafficking dynamics and subcellular compartmental distributions over time.

KEYWORDS: intracellular trafficking, endosomal escape, pH-responsive polymer, anti-CD22 antibody, ratiometric fluorescence,

2.1 Introduction

Non-Hodgkin lymphomas are typically treated with chemotherapy regimens[1] in combination with anti-CD20 monoclonal antibodies (mAbs), although their resistance to chemotherapy underscores the need for additional targeted therapeutic strategies.[2–4] Radiolabeled mAbs have also been employed for selective targeting of radioactivity directly to tumor cells[5,6] but eventual relapse in many patients again underscores the need for new therapeutics. Antibody-drug conjugates (ADCs) can improve the delivery of potent molecules to tumor lesions while limiting the toxicities associated with nontargeted chemotoxins.[4,6–9] ADCs constructed with biologic drugs (e.g., siRNA, DNA, peptides, and proteins) that require cytosolic delivery may be directed to a wide variety of oncogenic targets that are otherwise considered "undruggable" by small molecules. However, delivery of these molecules past the endosomal/lysosomal pathway to intracellular microenvironments (i.e., in the cytoplasm) remains a significant challenge. Following receptor-mediated endocytosis, internalized biologic drugs are typically delivered to acidified early endosomes (pH 6.6).[10,11] Biologic contents that are not recycled or destined for a distinct cellular compartment are trafficked to late endosomes (pH 5.8) and eventually lysosomes (pH 4.3) for degradation.[12–14]

Our group has developed synthetic polymers, including poly(propylacrylic acid) (PPAA), that display pH-sensitive, membrane-destabilizing activities that are especially well-tuned for intracellular delivery.[15] Incorporation of PPAA with biologic drugs has demonstrated enhanced therapeutic activity.[13,16–18] The intracellular trafficking kinetics of PPAA conjugates has yet to be evaluated and could help evolve more efficacious drug delivery systems. Fluorescence imaging has been shown to be a powerful tool for following the intracellular trafficking of biomacromolecules. For example, Massignani et al.[19] used subcellular imaging techniques to measure the trafficking kinetics of polymersomes from endocytosis to endosomal trafficking and cytosolic

release. In other studies, Low and co-workers[20,21] employed ratiometric fluorescence techniques to characterize the pH of folate-driven trafficking through endosomes. The intracellular pH was quantified via confocal microscopy of live cells treated with folate modified with pH-sensitive or pHinsensitive fluorophores. Akinc and Langer used a similar methodology to measure the environmental pH of nonviral vectors for DNA delivery; rather than microscopic imaging, the average environmental pH of DNA over a larger population of cells was quantitated by flow cytometry.[22–24]

In this work, quantitative ratiometric fluorescence microscopy was combined with flow cytometry to study the intracellular trafficking dynamics of an anti-CD22-internalizing mAb with an endosomal-releasing polymer (Figure 2.1). CD22 receptor ligation resulted in rapid endocytosis of the mAb followed by lysosomal trafficking. Ratiometric fluorescence studies employing live-cell fluorescence microscopy and flow cytometry were used to quantify the trafficking kinetics of the mAb conjugates. The results were correlated with subcellular fractionation measurements that directly measured quantities of translocated mAb conjugates versus controls.[25,26] These studies provide new mechanistic insight into the activity of endosomal-releasing, pHresponsive polymer carriers.

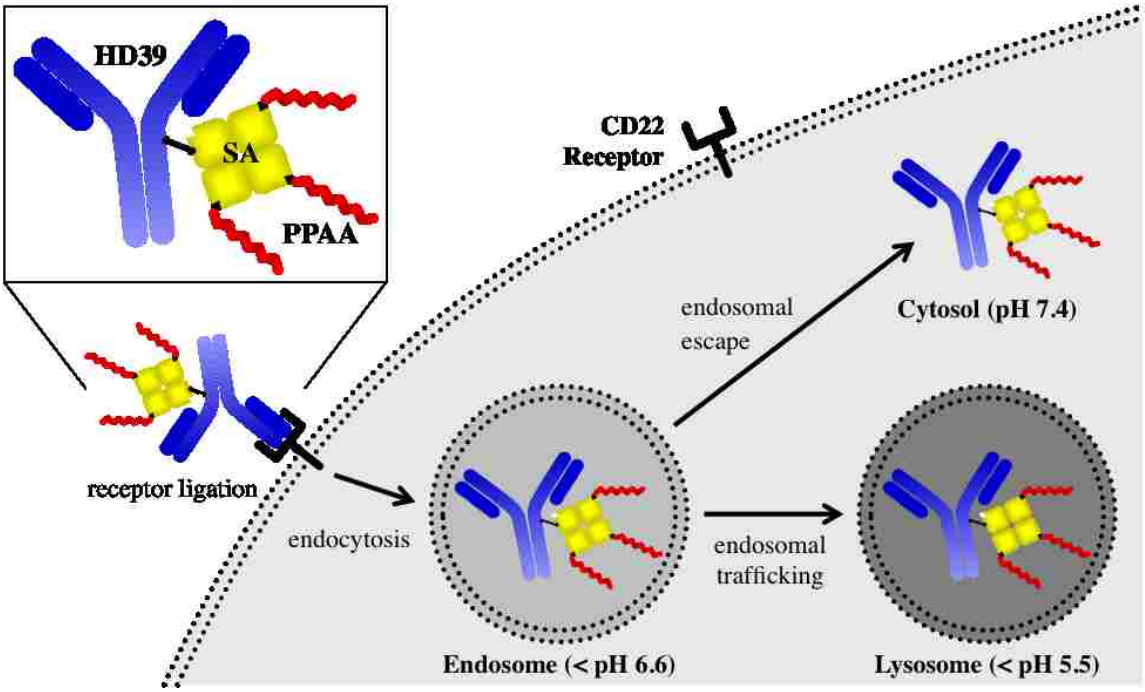

Figure 2.1: Intracellular trafficking of the HD39/SA-PPAA conjugate. Ligation of the anti-CD22 monoclonal antibody (HD39) to CD22 leads to receptor-mediated endocytosis. A portion of the conjugate is trafficked from endosomes to lysosomes while a second fraction is released into the cytosol via endosomal escape mediated by PPAA.

2.2 Experimental Section

2.2.1 Materials

Spectra/Pro molecular porous membrane tubing [molecular weight cutoff (MWCO) = 6000-8000 Da] was purchased from Spectrum Laboratories (Houston, TX). Alexa Fluor 488 carboxylic acid succinimydyl ester (AF488) and pHrodo succinimydyl ester (pHrodo) were purchased from Molecular Probes (Eugene, OR). Bio-Spin 30 chromatography columns prepacked with Bio-Gel P-30 gel in saline/sodium citrate (SSC) buffer [molecular weight limit (MWL) = 40 000 Da; 732-6006 lot 400030949] were purchased from Bio-Rad (Hercules, CA). 2-(4-Hydroxyphenolazo)benzoic acid (HABA) was purchased from Sigma-Aldrich (St. Louis, MO). Proactive biotin-coated microspheres (10.14 μm diameter; CP10N lot 9310) were purchased from Bangs Laboratories (Fishers, IN). Propylacrylic acid (PAA) was synthesized as described previously.[27] Methacrylic acid (MAA) (Sigma-Aldrich) was vacuum-distilled prior to use. [^{3}H]N-Succinimidyl propionate was purchased from American Radiolabeled Chemicals (St. Louis, MO). The HD39 mAb was produced by injecting hybridomas into pristine-primed mice to generate ascites and purified as previously described.[28] HD39 was then conjugated to streptavidin (SA) via a succinimidyl-4-(N-maleimidomethyl)-cyclohexane-1-carboxylate (SMCC) heterobifunctional linker to form covalent chemical conjugates using previously described methods.[29] The purified HD39/SA conjugates contained 1.2 SA per mAb.

2.2.2 Ramos-AW Cell Culture

Ramos-AW cells were obtained from the European Collection of Cell Cultures (ECACC, Salisbury, U.K.). Cell cultures were maintained in log-phase growth in RPMI 1640 medium containing L-glutamine and 25 mM HEPES supplemented with

1% penicillin-streptomycin (GIBCO) and 10% fetal bovine serum (FBS, Invitrogen) at 37 °C and 5% CO2.

2.2.3 Synthesis of Biotinylated Polymers

Radical addition-fragmentation chain transfer (RAFT) polymerizations of PAA and MAA to obtain PPAA and poly(methacryclic acid) (PMAA) were conducted in N,N-dimethylformamide (DMF) and dimethyl sulfoxide (DMSO), respectively, under anhydrous conditions for 24 h at 60 °C using biotin-ECT (ECT = 4-cyano-4-[(ethylsulfanylthiocarbonyl)sulfanyl]pentanoic acid)[30] as the chain-transfer agent (CTA) and azobis(isobutyronitrile) (AIBN) as the radical initiator (Figure 2.2). The initial monomer/CTA and CTA/initiator ratios for the polymerizations of PAA and MAA were $[M]_0/[CTA]_0$ = 150:1 and $[CTA]_0/[I]_0$ = 1:1, respectively. The resultant polymers were isolated by precipitation in diethyl ether. The precipitated polymers were then redissolved in DMF and reprecipitated into ether (X4). The dry polymers were redissolved in DMSO, added to 0.5 M Na_2CO_3 (pH 8.7) at a 10-fold volume dilution, and dialyzed in distilled water (dH2O) using dialysis tubing (MWCO = 6000-8000 Da) to remove monomer and solvent. Gel-permeation chromatography (GPC) was used to determine number-average (M_n) and weight-average (Mw) molecular weights and polydispersities (PDI = M_w/M_n) of PPAA and PMAA using Tosoh SEC TSKGEL α-3000 and α-4000 columns (Tosoh Bioscience, Montgomeryville, PA) connected in series to a 1200 Series liquid chromatography system (Agilent, Santa Clara, CA) and a miniDAWN TREOS three-angle light scattering instrument with an Optilab rEX refractive index detector (Wyatt Technology, Santa Barbara, CA). HPLC-grade DMF containing 0.1 wt % LiBr at 60 °C was used as the mobile phase at a flow rate of 1 mL/min.

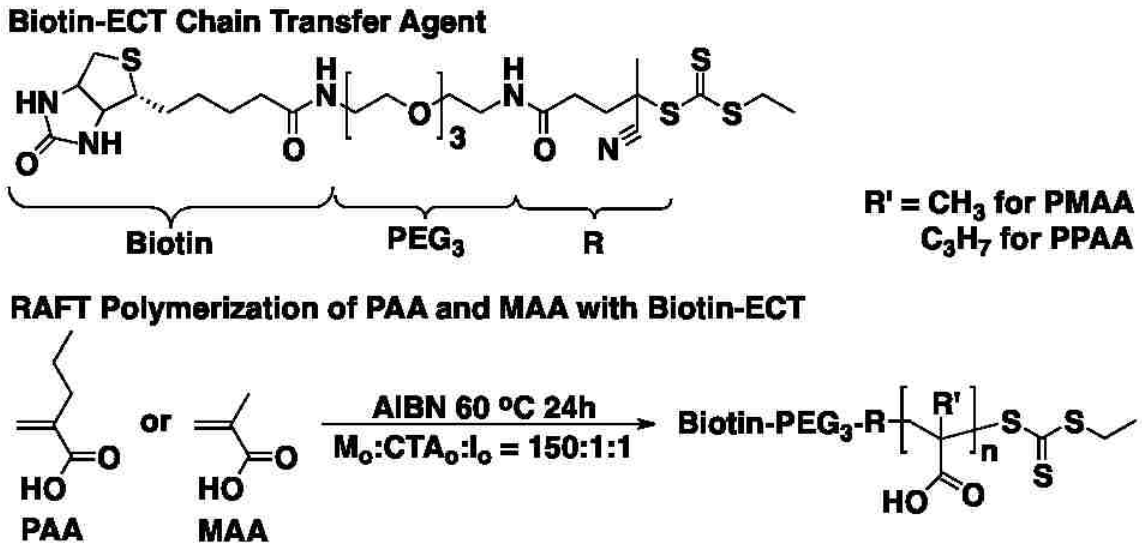

Figure 2.2: (top) Structure of the Biotin-ECT Chain-Transfer Agent and (bottom) RAFT Polymerizations of PAA and MAA. The polymerizations of PAA and MAA were conducted in DMF and DMSO, respectively, under anhydrous conditions for 24 h at 60 °C using biotin-ECT as the CTA and AIBN as the radical initiator. The initial monomer/CTA/initiator ratio for the polymerizations of PAA and MAA was $[M]_o/[CTA]_o/[I]_o = 150:1:1$. The M_n values for the resultant PPAA and PMAA were 10.9 and 10.7 kDa with PDIs of 1.8 and 1.18, respectively.

2.2.4 Antibody-Polymer Conjugation

A HABA binding assay, modified from Green,[31] was used to determine the molar excess of PPAA or PMAA chains needed to achieve four polymer chains per HD39/SA. HABA was dissolved in 10 mM sodium hydroxide buffer (pH 12) at 2.65 mM and added to SA or HD39/SA in sodium phosphate buffer (pH 7.4) at 40-fold molar excess to occupy all biotin-binding sites. Biotin, PPAA, or PMAA in phosphate-buffered saline (PBS) was added to the HABA solution at a range of concentrations. The final SA or HD39/SA solution at 6.6 μM was measured on a plate reader. A biotin standard curve was made to correlate the absorbance at 500 nm (A_{500}) with biotin-binding events and then used to quantify polymer-binding events. To verify complexation of PPAA or PMAA with HD39/SA, a gel retardation assay was performed with 10 μg of streptavidin or 2.56 μg of HD39/SA. Samples were loaded into a Bio-Rad Ready Gel containing 4-15% Tris-HCl using a 5 loading buffer that contained 310 nM Tris HCl, 50% glycerol, and 1 μg/mL of bromphenol blue. The running buffer contained 30 g/L Tris Base, 144 g/L glycine, and 10 g/L SDS in dH2O. Samples were run at a constant 125 V for 1 h and stained using Gel-Code Blue.

2.2.5 Preparation of Dual-Fluorescently Labeled HD39/SA Conjugates

For ratiometric fluorescence studies, HD39/SA was dual-labeled with amine-reactive, pH-insensitive AF488 and pH-sensitive pHrodo. For dual labeling, AF488 and pHrodo were dissolved in DMSO at 1 mg/mL and added to the reaction mixture at a 5-fold molar excess with respect to 6.08 μM HD39/SA in a 0.1 M sodium bicarbonate buffer (pH 8.3). The reaction was performed at room temperature for 1 h with subsequent purification in microspin columns. For 95% recovery of the antibody conjugate with microspin columns, the SSC buffer was removed from the prepacked gel and rinsed with 0.5% bovine serum albumin (BSA) in PBS and 10% acetonitrile in PBS. The spin

columns were then equilibrated with 0.5 mg/mL NaN3 in PBS (pH 7.4). Each rinse consisted of 1.1 mL of buffer volume and centrifugation at 1000 g for 4 min. Dual-labeled HD39/SA was purified from unreacted fluorophore using the pretreated spin columns. The final concentration of HD39/SA and degree of labeling were determined spectrophotometrically by applying absorbance measurements to a formula provided by the manufacturer. Extinction coefficients for HD39/SA (380 000 $M^{-1}cm^{-1}$) and pHrodo (39 600 $M^{-1}cm^{-1}$) were measured experimentally.

2.2.6 Characterization of Ratiometric Fluorescence by Flow Cytometry

The relationship between pH and ratiometric fluorescence of the dual-labeled HD39/SA conjugate was characterized by fluorescence microscopy and flow cytometry. HD39/SA was mixed with biotincoated polystyrene beads and imaged with a fluorescence microscope. Briefly, dual-labeled HD39/SA was incubated at 25 nM with 10^6 beads/mL for 1 h and then aliquoted and washed twice in pH buffers (4.6-7.4). The pH buffers were made by mixing 0.2 M phosphate buffer (monobasic, pH 5.0) with 0.1 M citric acid (pH 4.0) or 0.2 M phosphate buffer (dibasic, pH 8.0). The change in ratiometric fluorescence with pH buffer was measured by flow cytometry and fluorescence microscopy. For flow cytometry, gating was performed with unlabeled beads. For microscopy, beads were added to chamber slides and imaged as described below. The pHrodo/AF488 ratio as a function of pH was analyzed as described below.

2.2.7 Administration of Dual-Labeled Conjugates and pH Calibration

Dual-labeled HD39/SA-PPAA and HD39/SA-PMAA conjugates were formulated as previously described. Samples containing 106 cells/mL in medium were incubated with 25 ηM HD39/SA, HD39/SA-PMAA, or HD39/SA-PPAA for 1 h at 37 °C. The

cells were pelleted; washed with chilled modified PBS containing CaCl2 (0.1 g/L), $MgCl_2$ (0.1 g/L), and 0.5% BSA; and then resuspended in fresh medium at the same concentration and incubated at 37 °C. Untreated cells and cells collected 1, 3, and 6 h after treatment (150,000 cells per sample) were resuspended in 250 μL of modified PBS for flow cytometry or 500 μL for fluorescence microscopy. To develop a pH calibration curve for each time point of the ratiometric studies, cells were incubated in pH-clamping buffers ranging from pH 4.5 to 7.4. The pH-clamping buffers were created by mixing 50 mM MES (pH 6.0) with 50 mM citric acid (pH 4.5) or 50 mM HEPES (pH 7.4) containing KCl (120 mM), NaCl (20 mM), CaCl2 (1 mM), MgCl2 (1 mM), and the ionophores nigericin (10 μM), monensin (1 μM), and valinomycin (10 μM).[32,33] Cells were incubated for 15 min at 4 °C and then analyzed by flow cytometry or fluorescence microscopy.

2.2.8 Flow Cytometry: Acquisition and Analysis

The average intracellular pH exhibited by trafficked HD39/SA conjugates was measured by ratiometric fluorescence using a flow cytometer (Becton Dickinson LSR II Cell Analyzer). Cells were excited at 488 and 532 nm, and fluorescence emission was collected at 510 and 575 nm, respectively. For accurate measurements, cells were gated by forward scattering area (FSC-A) and side scattering as well as FSC height (FSC-H) and FSC width (FSC-W) with 10,000 gated events per sample. Postacquisition analysis of ratiometric fluorescence was performed using FlowJo flow cytometry analysis software (Tree Star, Ashland, Oregon). For each time point, gating of untreated cells was applied to all treatments. For each cell event, the pHrodo signal was divided by the AF488 signal after subtraction of the median autofluorescence from untreated cells to obtain a ratiometric fluorescence value. A pH calibration curve was made to convert ratio values to pH (see Figure 2.7A). pH-clamped cells were analyzed in the same manner, and their median ratio values were plotted against pH. A linear

regression curve was fit to the data and used to convert ratiometric fluorescence values to average intracellular pH.

2.2.9 Fluorescence Microscopy: Acquisition and Analysis

The subcellular compartmental pH distribution of HD39/SA conjugates was measured by ratiometric fluorescence using live-cell microscopy. After treatment, cells were collected and added to Lab-Tek II chambered coverglass slides (NUNC, Rochester, NY), which were placed on a Nikon Ti-E live-cell fluorescence microscope equipped with an environmental control chamber. Cells were imaged with a mercury lamp and a 100 objective using the following filter sets: 480/40 nm (EX) and 535/50 nm (EM) for AF488 and 560/40 nm (EX) and 630/75 nm (EM) for pHrodo (49000 Series, Chroma Technology, Rockingham, VT). Three image stacks per treatment with a minimum of four cells per image were collected for each time point. Image stacks were deconvolved using object-based measurement software (Volocity, PerkinElmer) to remove out-of-focus fluorescence and identify conjugate-containing compartments. For deconvolution, calculated point-spread functions were applied to the green and red channels with 25 iterations to reach a nearly 100% confidence interval. The green and red deconvolved channels were thresholded, and their overlapping voxels were identified as regions of interest (ROIs). All touching voxels within a cell were defined as a compartment, and a ratiometric algorithm was used to measure each compartment's average ratiometric fluorescence from the original green and red channels with background subtraction. Ratios were converted to pH using the pH calibration curves, and the compartmental pH values were plotted as a histogram to evaluate the compartmental pH distribution. Calibration curves were made for other time points by imaging and analyzing pH-clamped cells in the same manner (see Figure 2.7B). The average ratiometric fluorescence of compartments was plotted against pH and fit with a linear regression curve to obtain a relationship between ratiometric fluorescence

and compartmental pH.

2.2.10 Preparation of Tritium-Labeled HD39/SA

For fractionation studies, HD39/SA was radiolabeled with tritium and measured by scintillation counting. HD39/SA (6.2 mg, 2 mg/mL in 50 mM sodium borate, pH 8, 50 mM NaC) was reacted with [3H]N-succinimidyl propionate (1 mCi) for 1 h at 25 °C. A PD-10 desalting column was used for PBS buffer exchange and removal of unreacted radiolabel. Additionally, [3H]HD39/SA was concentrated using an Amicon Ultra-4 centrifugal filter unit with a nominal MWL of 30,000 Da and quantified by A280 measurements. The specific reactivity of [3H]HD39/SA was measured on a scintillation counter with Ultima Gold scintillation fluid (PerkinElmer, Waltham, MA).

2.2.11 Cellular Fractionation

Cytosolic and endosomal/lysosomal fractions containing HD39/SA conjugates were separated by cellular homogenization and fractionation. Briefly, hot antibody was spiked into cold antibody at a molar ratio of 1:2.5 and complexed with PPAA as previously described. A sample containing 3 x 10^7 cells was treated with 25 ηM [3H]HD39/SA or [3H]HD39/SA-PPAA for 1 h pulse and 5 h chase. A 10 μL aliquot of medium containing cells and conjugate was collected at the beginning of the pulse for scintillation counting. After treatment, the cells were washed with cold PBS and TES buffer (1 mM triethanolamine, 1 mM EDTA, 0.25 M sucrose, pH 7.4, and protease inhibitors), resuspended in 1 mL of TES buffer at 4 °C, and homogenized with 15-20 strokes of a syringe with a 26 gauge 5/8 in. needle. After confirmation of 80% cell homogenization, the lysate was centrifuged at 250g for 5 min to sediment nuclei and unbroken cells. A 400 μL aliquot of 20% OptiPrep (Sigma, D1556) was layered under the postnuclear supernatant (PNS), which was then centrifuged for 1 h at 150,000 g

using a swinging bucket rotor (TLS-55) to separate vesicular compartments. Afterward, five fractions (200 μL) were collected from the top of the sample, and 10 μL of each fraction was resuspended in scintillation fluid to measure tritium on a scintillation counter. Untreated cells were also fractionated as described above to analyze the cytosolic, endosomal, and lysosomal content within each fraction. For analysis, fractions were run by sodium dodecyl sulfate polyacrylamide gel electrophoresis (SDS-PAGE) as previously described and transferred to a polyvinylidene fluoride (PVDF) membrane via a conventional protocol using transfer buffer [12 mM Tris-base, 100 mM glycine, 20% MeOH, 1% (w/v) SDS] for 1.5 h at 100 V on ice. The membrane was incubated with blocking buffer (Thermo Scientific, PI-37536) for 1 h at room temperature, washed for 10 min in TBS-T (3), and then incubated with primary antibody (1:2000 dilution in blocking buffer) overnight at 4 °C. Next, the membrane was washed for 10 min in TBS-T (3) and probed with secondary antibody (HRP goat antimouse, 1:100000 dilution in blocking buffer) in blocking buffer for 1 h at room temperature. Finally, the membrane was washed for 10 min in TBS-T (3) and then incubated for 5 min with premixed chemiluminescence substrate (Pierce, West Femto) at room temperature. Excess substrate was drained, and the membrane was developed for 5 min on a Kodak imager (Rochester, NY). Western blotting with anti-Rab5 and anti-Lamp2 antibodies in untreated cells was used to measure endosome and lysosome activity,[34] and a lactate dehydrogenase (LDH) assay (Roche) was used to measure cytosolic activity.

2.3 Results

2.3.1 Polymer Synthesis

Biotin-ECT was employed as the RAFT CTA for the polymerization of PPAA and PMAA, as shown in Scheme 2.2. For both PAA and MAA, the initial monomer/CTA and CTA/initiator ratios were $[M]_o/[CTA]_o = 150{:}1$ and $[CTA]_o/[I]_o = 1{:}1$, respectively. TheMn values for the resultant PPAA and PMAA were 10.9 and 10.7 kDa with PDIs of 1.8 and 1.18, respectively. PMAA was employed as a negative control polymer because of its structural similarity to PPAA but lack of endosomolytic properties.[35,36]

2.3.2 Antibody-Polymer Complexation

A single biotin functional group at the Z terminus of the polymer was incorporated at the time of synthesis for facile conjugation to HD39/SA. Antibody-polymer conjugation through the biotin-streptavidin linkage was measured using the HABA assay (Figure 2.3A). A molar excess of 12 PPAA chains yielded an average of 3.5 polymers bound per SA or HD39/SA. A gel retardation assay was used to verify protein-polymer conjugation, as observed by the disappearance of the free SA band or a shift in the HD39/SA band after polymer conjugation (Figure 2.3B).

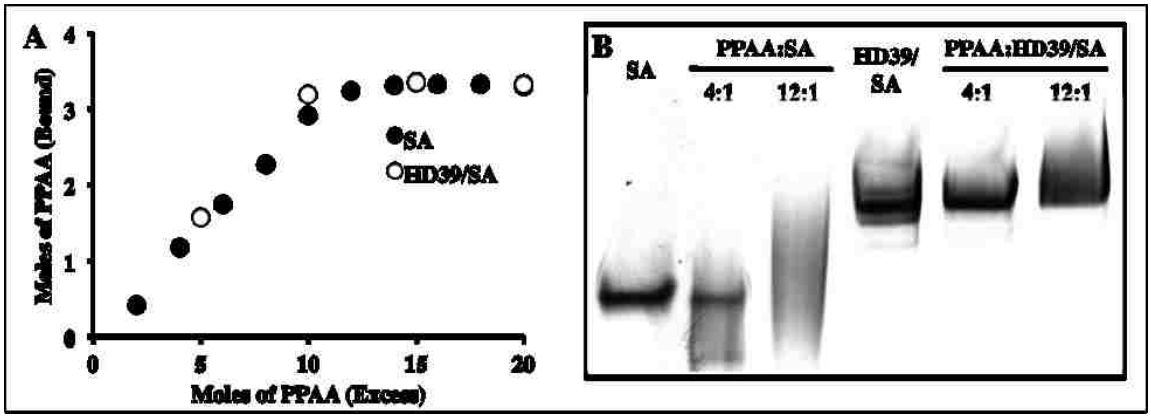

Figure 2.3: The SDS-PAGE gel contains free streptavidin in lane 1 and HD39/SA in lane 4. A molar excess of 4 PPAA to SA or HD39/SA resulted in 1 binding event observed by the protein smear in lanes 2 and 5. The negatively charged polymer attracted the complex closer towards the positive charge during the retardation assay, causing a downward smear. A molar excess of 12 PPAA to SA or HD39/SA resulted in 4 binding events noted in lanes 3 and 6, and a disappearance of the protein band. In the case of SA-PPAA, the complex smears below and above the original band, indicating both charge interactions during gel retardation as well as an increase in the hydrodynamic radius of the SA-PPAA complex. With HD39/SA-PPAA, the increased hydrodynamic radius of the complex is more apparent with an upwards shift in the smear.

2.3.3 Calibration of Ratiometric Fluorescence to a Standard pH Curve

The HD39/SA was dual-labeled with pH-insensitive AF488 and pH-sensitive pHrodo to develop a pH probe for reporting the intracellular pH environment of trafficking protein-polymer conjugates. The dual-labeled HD39/SA conjugate contained 3.2 AF488 and 3.5 pHrodo fluorophores per conjugate (Figure 2.4). To standardize the ratiometric fluorescence as a function of pH, conjugates were incubated with biotinylated polystyrene beads in a range of pH buffers and analyzed by flow cytometry. The fluorescence histograms in Figure 2.5 demonstrate that the AF488 fluorescence was independent of pH but the pHrodo fluorescence was inversely proportional to pH. The plot of the ratio of the pHrodo and AF488 signals as a function of pH (Figure 2.6) demonstrates that the ratiometric fluorescence decreased linearly from pH 5 to 7. These results validate the combination of AF488 and pHrodo for intracellular measurements over a broad but physiologically relevant pH range. Ratiometric fluorescence values measured by fluorescence microscopy and flow cytometry were converted to pH using a pH standard curve made with pH-clamped cells. For each time point, HD39/SA-treated cells were resuspended in a range of clamping buffers from pH 4.5 to 7.4, and the average ratiometric fluorescence value was plotted as a function of pH (Figure 2.7). For the three treatments, ratiometric fluorescence values were converted to compartmental pH (fluorescence microscopy) or average intracellular pH (flow cytometry) using linear regression curves from the pH standard plots.

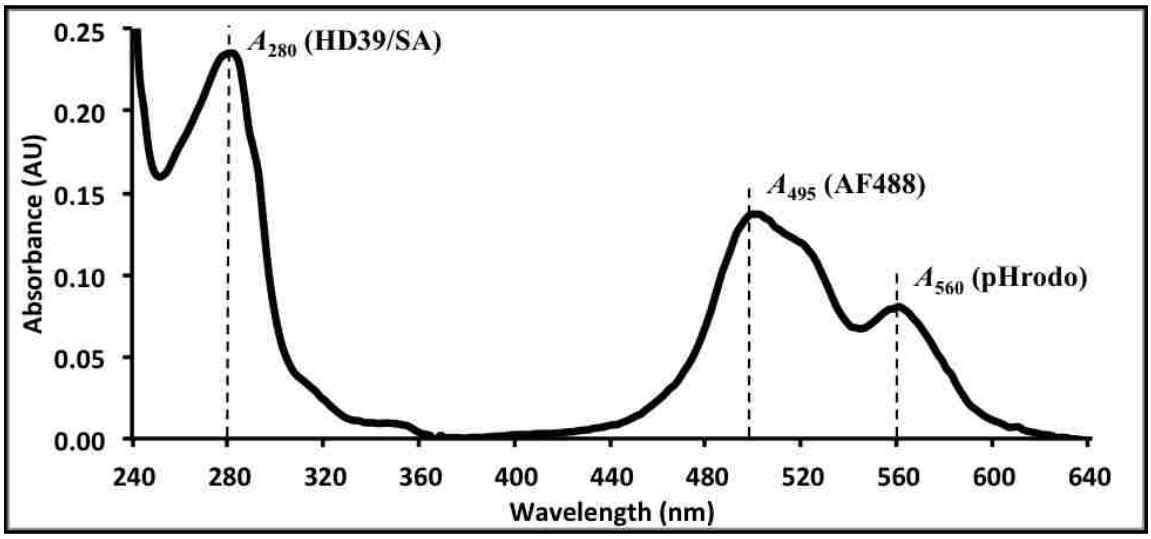

Figure 2.4: The absorbance spectrum of HD39/SA dual-labeled with AF488 and pHrodo. The degree of AF488 and pHrodo labeling was calculated from absorbance maxima at 280 nm for HD39/SA, 495 nm for AF488, and 560 nm for pHrodo. The extinction coefficients were determined experimentally for HD39/SA and pHrodo and from the manufacturer for AF488 (see Methods and Materials).

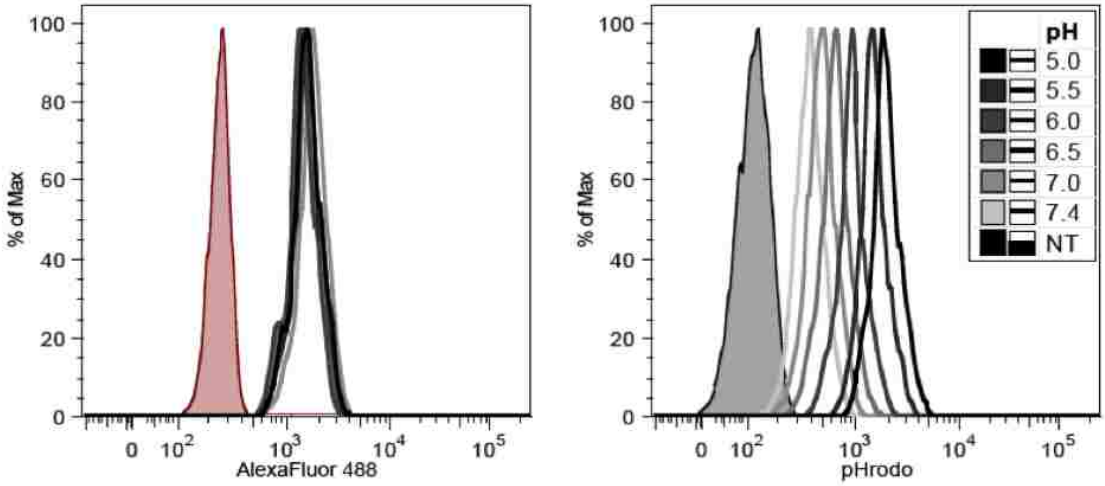

Figure 2.5: The fluorescence intensity of dual-labeled HD39/SA coated polystyrene beads collected by flow cytometry. The pH sensitivity of dual-labeled HD39/SA was measured by incubating polystyrene microspheres coated with dual-labeled HD39/SA in a range of pH buffers. Coated polystyrene beads were then measured by flow cytometry to obtain fluorescence emission histograms for AF488 and pHrodo. The median pHrodo fluorescence was divided by the median AF488 fluorescence to obtain a ratiometric fluorescence value, which was then plotted as a function of pH (see Figure 2.6).

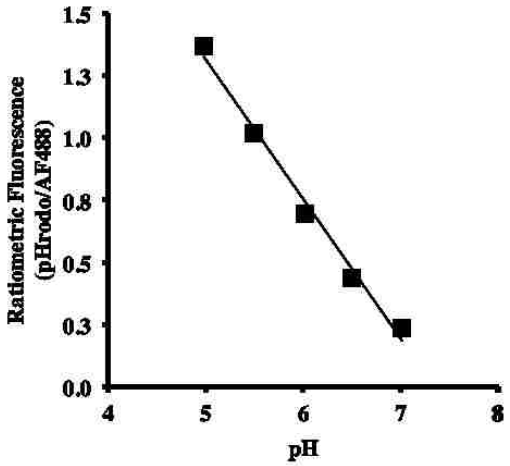

Figure 2.6: The ratiometric fluorescence of dual-labeled HD39/SA is pH-dependent. HD39/SA was dual-labeled with pH-insensitive AF488 and pH-sensitive pHrodo, then coated onto biotinylated-polystyrene beads. HD39/SA-coated beads were resuspended in a range of pH buffers and the AF488 and pHrodo fluorescence intensity was measured at each pH. The median intensity of pHrodo divided by AF488 was defined as ratiometric fluorescence and plotted as a function of pH. A linear regression was fit to the data to demonstrate that the ratiometric fluorescence of the HD39/SA conjugates is pH dependent.

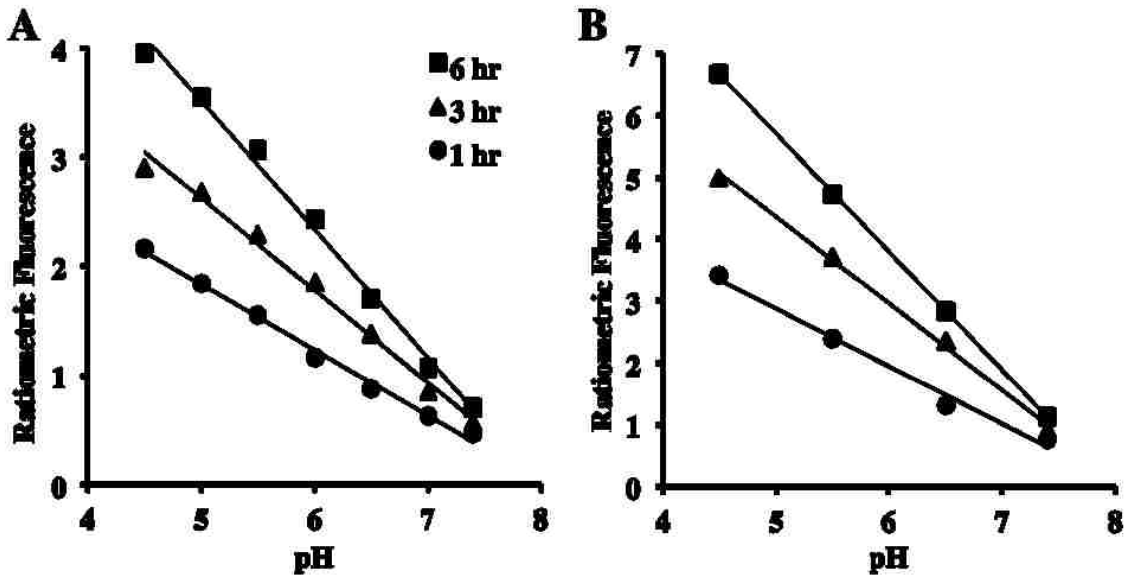

Figure 2.7: Standard pH curves for conversion of ratiometric fluorescence to pH for (A) flow cytometry and (B) fluorescence microscopy obtained using pH-clamping techniques. After 1, 3, and 6 h of treatment with HD39/SA, cells were collected and resuspended in pH-clamping buffers. Ratiometric fluorescence values were then measured by (A) flow cytometry and (B) fluorescence microscopy. The values were plotted as functions of pH (from the pH-clamping buffers), and regression curves were fit to the data sets. The linear equations were applied to the measured ratiometric fluorescence values to obtain the average intracellular pH (flow cytometry) and compartmental pH (fluorescence microscopy) in Figures 2.9- 2.10

2.3.4 Time-Dependent Dynamics of Subcellular Trafficking As Determined by Ratiometric Fluorescence Microscopy

The subcellular pH of HD39/SA-localized compartments was measured by live-cell ratiometric fluorescence microscopy in RAMOS-AW cells, a model B-cell lymphoma cell line that expresses CD22. Representative images of the subcellular compartmental pH are shown in Figure 2.8. The ratiometric fluorescence value for each three-dimensional pixel (called a Voxel) was converted to pH, and a color map was used to visualize the pH of each compartment, as denoted by the legend at the bottom right. The average pH of each compartment in 10-15 cells per treatment was plotted as a histogram in Figure 2.9. After 1 h, the pH of subcellular compartments for all three conjugates ranged from 6.2 to 7.6 (Figure 2.9A). After 3 h, the compartmental pH of HD39/SA and HD39/SA-PMAA ranged broadly from 4.0 to 6.8, indicating endosomal/lysosomal trafficking, whereas 92% of the HD39/SA-PPAA compartments showed pH values between pH 6.4 and 7.6 (Figure 2.9B). After 6 h, 92% of HD39/SA-containing compartments were trafficked below pH 5.6 and 90% of HD39/SA-PMAA-containing compartments were trafficked below pH 6.0; in contrast, HD39/SA-PPAA exhibited a bimodal distribution after 6 h, with 11% of compartments between pH 4.8 and 6.0 and 89% of compartments greater than pH 6.0 (Figure 2.9C). Shown in Figure 2.9D is the fraction of each treatment displaying pH values above those typically encountered in early endosomes as a function of time. After 1 h, 75% of HD39/SA, 53% of HD39/SA-PMAA, and 85% of HD39/SA-PPAA compartments were above pH 6.6. After 3 h, less than 7% of HD39/SA or HD39/SA-PMAA but 72% of HD39/SA-PPAA was still present above pH 6.6. After 6 h, no HD39/SA or HD39/SA-PMAA compartments remained above pH 6.6, but 45% of HD39/SA-PPAA still remained above this threshold. These findings combined with cell fractionation studies (see below) suggest that a significant fraction of HD39/SA-PPAA exists in a combination of early endosomal and cytosolic locations.

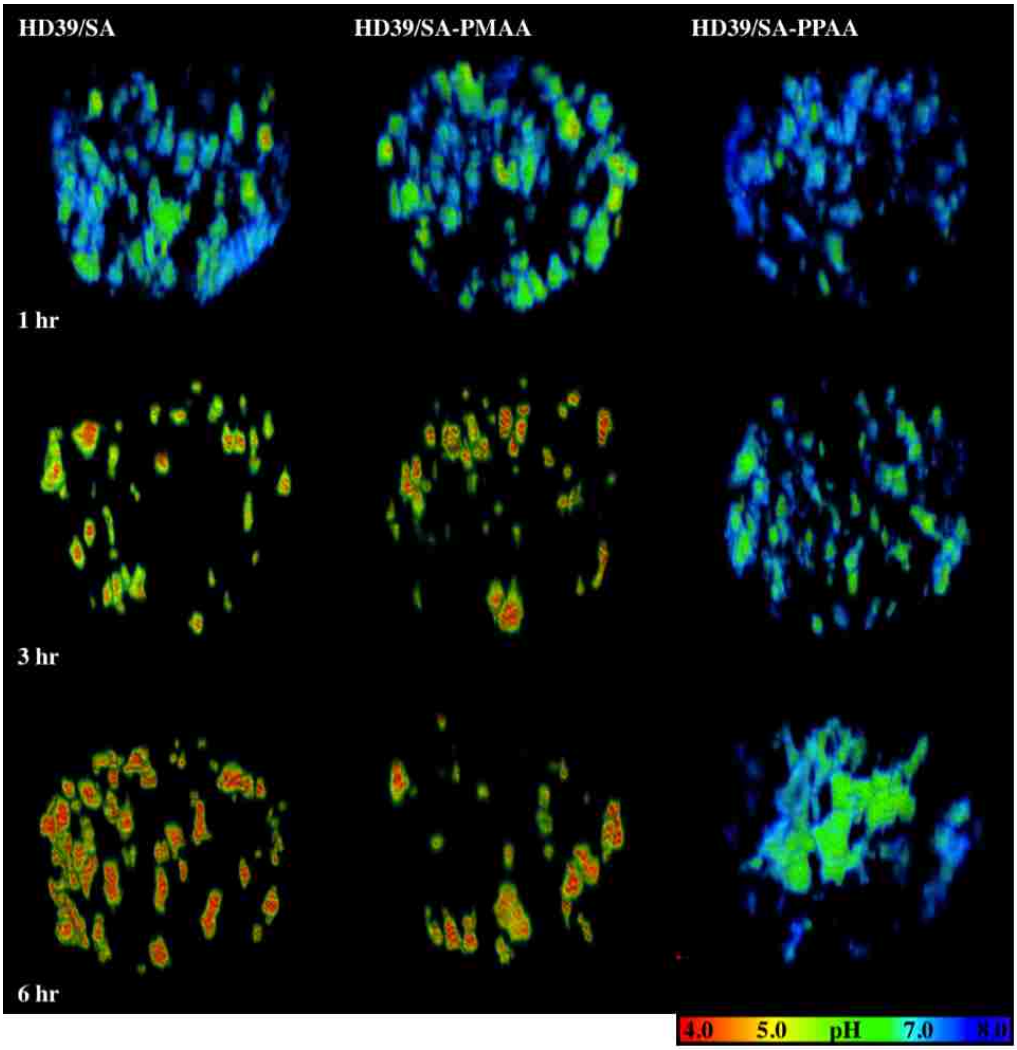

Figure 2.8: RAMOS-AW cells were treated with HD39/SA, HD39/SA-PMAA, or HD39/SA-PPAA for 1 h at 25 nM, washed in PBS, and then resuspended and incubated in fresh medium. At the indicated times, cells were resuspended in PBS and transferred to chamber slides for deconvolution wide-field fluorescence microscopy. Cells were selected by scanning in bright field to avoid fluorescence bias and locate three or more cells per viewing field; 10-15 cells were imaged per treatment, and all were included in morphometric processing. Compartments [defined as touching voxels containing both green (AF488) and red (pHrodo) fluorescence] were identified using Volocity image analysis software. The ratiometric fluorescence of each voxel (defined as the pHrodo signal divided by the AF488 signal) was then converted to pH using the corresponding standard curve made by pH clamping (Figure 2.7B). The pH values of the voxels were converted to a color map defined by the key at the bottom right. Representative cell images for each time point and treatment are shown.

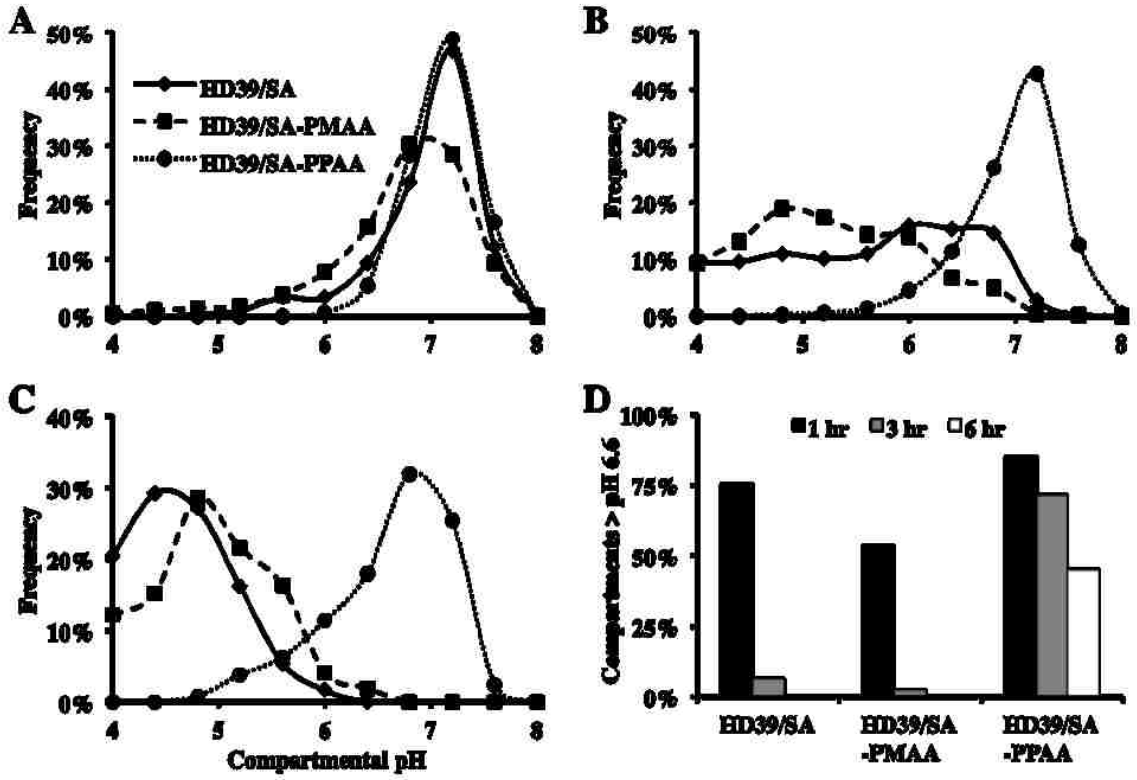

Figure 2.9: RAMOS-AW cells were treated with HD39/SA, HD39/SA-PMAA, or HD39/SA-PPAA at 25 ηM for 1 h, washed in PBS, and then resuspended and incubated in fresh medium. Cells were transferred to chamber slides at indicated time points, and the ratiometric fluorescence (defined as the pHrodo signal divided by the AF488 signal) of subcellular compartments was measured by deconvolution wide-field fluorescence microscopy (see Figure 2.8) and converted to pH using the corresponding standard curve made by pH clamping (Figure 2.7B. Values of the pH of the subcellular compartments (defined as the average pH of the voxels within a compartment) after (A) 1 h, (B) 3 h, and (C) 6 h of trafficking were plotted as histograms. The percentage of subcellular compartments above pH 6.6 at each of these times is shown in (D).

2.3.5 Time-Dependent Trafficking Dynamics Determined by Flow Cytometry.

The time-dependent dynamics of HD39 intracellular trafficking was also evaluated by flow cytometry. The intracellular pH of HD39/SA, HD39/SA-PMAA, and HD39/SA-PPAA averaged over each cell was determined from the ratiometric fluorescence signal measured by flow cytometry over the course of 6 h (Figure 5). After 1 h, the intracellular pH was 6.7 ± 0.2 for HD39/SA, 6.45 ± 0.25 for HD39/SA-PMAA, and 6.75 ± 1.5 for HD39/SA-PPAA. These results are consistent with receptor-±mediated uptake of the conjugates into early endosomal compartments. After 3 h, the intracellular pH dropped to 5.6 ± 0.50 for HD39/SA and 5.45 ± 0.55 for HD39/SA-PMAA, while the HD39/SA-PPAA conjugates had an average intracellular pH of 6.5 ± 0.20. After 6 h the intracellular pH was 4.65 ± 0.55 and 4.9 ± 0.50 for HD39/SA and HD39/SA-PMAA, respectively, characteristic of lysosomal pH. Significantly, the average intracellular pH of the HD39/SA-PPAA conjugates was determined to be 6.25 ± 0.25 with a narrow distribution compared with the other conjugates.

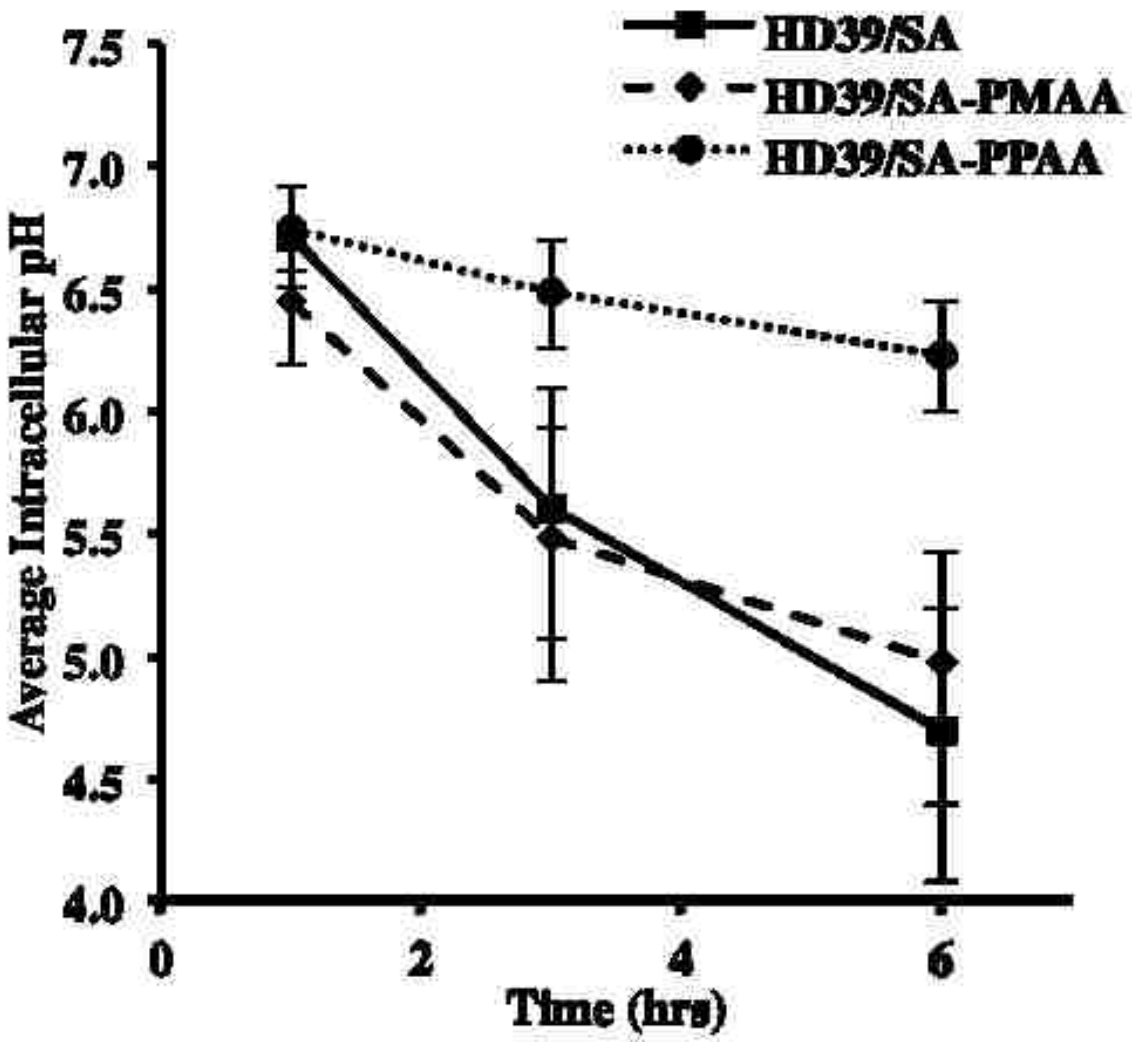

Figure 2.10: RAMOS-AW cells were treated with HD39/SA (dash), HD39/SA-PMAA (solid), or HD39/SA-PPAA (dotted) at 25 ηM for 1 h, washed in PBS, and incubated in fresh medium for up to 6 h. For each time point, 1.5 x 10^5 cells were washed and resuspended in PBS on ice. Ratiometric fluorescence was measured for 10 000 cells per treatment per time point via flow cytometry by dividing the pHrodo fluorescence signal by the AF488 signal. Ratiometric fluorescence was converted to average intracellular pH using the corresponding pH standard curve made by pH clamping (Figure 2.7A). Error bars represent a 50% confidence interval of the total cell population.

2.3.6 Subcellular Fractionation Localization of Antibody-Polymer Conjugates

Cellular fractionation was used to separate cytosolic from vesicular compartments[37] and measure the percent ofradiolabeled HD39/SA conjugates in each fraction. Cytosolic fractions were identified by an assay that measures the cytosolically active enzyme LDH. Vesicular fractions were measured by immunoblotting using anti-Rab5 antibodies to identify endosomes and anti-Lamp2 antibodies to identify late endosomes and lysosomes. Scanned immunoblots were quantified using ImageJ software (NIH) to measure the percentage of Rab5 and Lamp2 activity in each fraction relative to the total signal (Figure 2.11A). LDH (cytosol) was distributed between fractions 1 (25%), 2 (28%), and 3 (32%). Rab5 (endosome) was most active in fractions 3 (38%) and 4 (42%), and Lamp2 activity (late endosome/lysosome) was found in fractions 4 (75%) and 5 (25%) (Figure 2.11B). Fraction 3 was positive for LDH and Rab5 because it was the boundary layer between the supernatant and denser media used to separate the vesicles. The percentage of tritium-labeled HD39/SA and HD39/SA-PPAA in each of the five fractions was quantified, and the results are plotted in Figure 2.11C. HD39/SA was mostly found in three fractions with 8% in fraction 2 (LDH+), 62% in fraction 3 (LDH+, Rab5+), and 20% in fraction 4 (Rab5+, Lamp2+). In contrast, HD39/SA-PPAA was found at the highest level (40%) in the cytosolic fraction 2, with 28% in the mixed fraction 3 (LDH+, Rab5+), and only 22% in fraction 4 (Rab5+, Lamp2+). These results are consistent with the conclusion that PPAA mediates endosomal escape of the HD39 mAb.

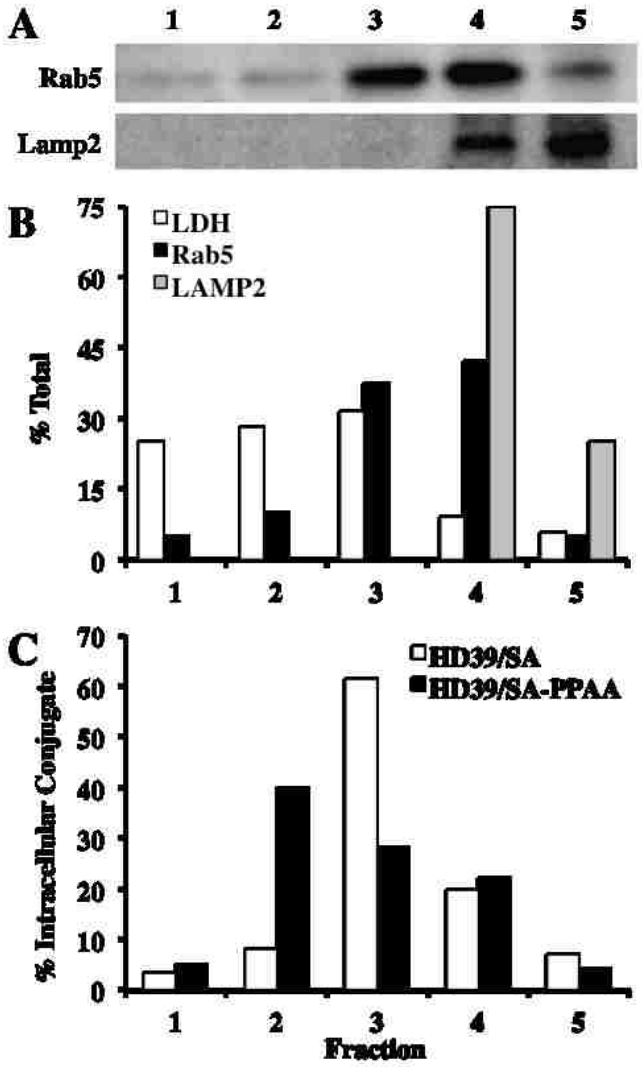

Figure 2.11: Samples containing 30 X 10^6 RAMOS-AW cells were treated with [3H]HD39/SA or [3H]HD39/SA-PPAA at 25 ηM for 1 h, washed with PBS, and then incubated in fresh medium for an additional 5 h. The cells were homogenized with 15-20 needle strokes and separated from the nuclear fractions and nonhomogenized cells. Cytosolic content was separated from vesicular content by ultracentrifugation, and five 200 μL fractions were collected. (A) The untreated cell fractions were separated by SDS-PAGE, transferred to immunoblots, and stained with anti-Rab5 (early and late endosomes) and anti-Lamp2 (late endosome and lysosome) antibodies. (B) ImageJ software was used to measure the antibody signals in each fraction, and an LDH assay was used to measure the cytosolic activity. (C) The amount of HD39/SA or HD39/SA-PPAA in each fraction was measured by radioactivity measurements and plotted as the percentage of total intracellular content.

2.4 Discussion

Bioinformatic studies have proposed that 75-80% of all disease targets reside within the intracellular space.[38] Evading lysosomal trafficking to gain access to intracellular targets remains a delivery challenge for biologic drugs.[39–41] Carriers that provide endosomal-releasing activities are being investigated to address these barriers.[42–44] In the current work, pH-responsive poly-(propylacrylic acid) (PPAA) and the control poly(methacrylic acid) (PMAA) were synthesized with a biotin-functionalized RAFT CTA for complexation with mAb-streptavidin bioconjugates. Ratiometric fluorescence and fractionation studies revealed that PPAA significantly increased the cytosolic transport and altered the natural trafficking fate of HD39/SA out of endosomes and lysosomes. PMAA, a polymer with similar structure but lacking endosomolytic activity, had no significant effect on the HD39/SA trafficking dynamics.

Shan and Press[45] first described the internalization and metabolic degradation of the CD22 receptor when ligated to anti-CD22 and hypothesized that the acidic compartments likely were lysosomes. Anti-CD22 mAb trafficking to endosomal and lysosomal compartments was also confirmed by Carnahan et al.[46] We used ratiometric fluorescence and fractionation techniques to characterize the time-dependent trafficking dynamics and found that HD39/SA was compartmentalized at pH 6.7 at 1 h and trafficked through endosomes to lysosomes between pH 4.0 and 5.2 after 6 h. Incorporation of PPAA had a strong effect on the subcellular pH distribution of HD39/SA over time. By 3 h, the average intracellular pH of HD39/SA-PPAA was 6.5, and 75% of the HD39/SA-PPAA compartments had pH ¿6.6. After 6 h, the average intracellular pH decreased to 6.2, and a bimodal distribution of subcellular compartments with 45% of compartments at pH >6.6 was observed. This bimodality indicates that a fraction of conjugates escape from endosomes while the remainder is eventually trafficked to lysosomes. The use of more potent pH-responsive polymers could increase the

amount of conjugate that escapes from endosomes and improve the cytosolic delivery efficiency.[13,15,16]

Subcellular fractionation studies with radiolabeled mAb-polymer conjugates were used to confirm the interpretation of the pH-trafficking dynamics studies. After 6 h, 89% of HD39/SA was localized within endosome- and lysosome-associated fractions 3-5. Conjugation of PPAA to HD39/SA was shown to increase the mAb-SA quantity in cytosolic fraction 2 by 34%. While HD39/SA and HD39/SA-PPAA were both present in the endosomal and lysosomal fractions, only 27% of the PPAA conjugates were ultimately trafficked to lysosomes (fractions 4 and 5) over the studied time frame. The findings are consistent with previous therapeutic studies showing that PPAA-based polymer-peptide conjugates can escape endosomes and exhibit high cell-killing activity.[47] The quantitative mechanistic information that describes the antibody-polymer trafficking dynamics sheds light onto the fate and distribution of compartmental environments experienced by the mAb. Such information can be used to screen carrier activities and potentially to optimize polymer compositions for endosomal releasing activities and pH profiles.

2.5 Acknowledgements

The authors thank James Lai and Matthew Manganiello for their insightful scientific discussions and experimental support. We are grateful to the NIH (Grants R01EB002991 and 2K12CA076930-11), the Washington State Life Sciences Discovery Fund (Grant 2496490 to the Center for Intracellular Delivery of Biologics), the Lymphoma Research Foundation (Fellowship Award to M.C.P.-W.), and the Wayne D. Kuni and Joan E. Kuni Foundation and the 3725 Fund of the Oregon Community Foundation (Kuni Scholar Award to M.C.P.-W.) for funding this project. G.Y.B. and J.S. are graduate research fellows of the National Science Foundation.

2.6 References

[1] I T Magrath, C Janus, B K Edwards, R Spiegel, E S Jaffe, C W Berard, J Miliauskas, K Morris, and R Barnwell. An effective therapy for both undifferentiated (including Burkitt's) lymphomas and lymphoblastic lymphomas in children and young adults. *Blood*, 63(5):1102–1111, 1984.

[2] J D Hainsworth. Rituximab as First-Line and Maintenance Therapy for Patients With Indolent Non-Hodgkin's Lymphoma. *Journal of Clinical Oncology*, 20(20):4261–4267, October 2002.

[3] J Wang. Cellular Immunotherapy for Follicular Lymphoma Using Genetically Modified CD20-Specific CD8+ Cytotoxic T Lymphocytes. *Molecular Therapy*, 9(4):577–586, April 2004.

[4] A G Polson, J Calemine-Fenaux, P Chan, W Chang, E Christensen, S Clark, F J de Sauvage, D Eaton, K Elkins, J M Elliott, G Frantz, R N Fuji, A Gray, K Harden, G S Ingle, N M Kljavin, H Koeppen, C Nelson, S Prabhu, H Raab, S Ross, D S Slaga, J-P Stephan, S J Scales, S D Spencer, R Vandlen, B Wranik, S-F Yu, B Zheng, and A Ebens. Antibody-Drug Conjugates for the Treatment of Non-Hodgkin's Lymphoma: Target and Linker-Drug Selection. *Cancer Research*, 69(6):2358–2364, March 2009.

[5] K De Santes, D Slamon, S K Anderson, M Shepard, B Fendly, D Maneval, and O Press. Radiolabeled antibody targeting of the HER-2/neu oncoprotein. *Cancer Research*, 52(7):1916–1923, 1992.

[6] Diane E Milenic, Erik D Brady, and Martin W Brechbiel. Antibody-targeted radiation cancer therapy. *Nature Reviews Drug Discovery*, 3(6):488–499, June 2004.

[7] Anna M Wu and Peter D Senter. Arming antibodies: prospects and challenges for immunoconjugates. *Nature Biotechnology*, 23(9):1137–1146, September 2005.

[8] David Schrama, Ralph A Reisfeld, and Jürgen C Becker. Antibody targeted drugs as cancer therapeutics. *Nature Reviews Drug Discovery*, 5(2):147–159, January 2006.

[9] Kelley V Foyil and Nancy L Bartlett. Anti-CD30 Antibodies for Hodgkin Lymphoma. *Current Hematologic Malignancy Reports*, 5(3):140–147, May 2010.

[10] Qais Al-Awqati. Proton-translocating ATPases. *Annual review of cell biology*, 2(1):179–199, 1986.

[11] Benjamin Tycko and Frederick R Maxfield. Rapid acidification of endocytic vesicles containing α 2-macroglobulin. *Cell*, 28(3):643–651, 1982.

[12] Cathrine Nilsson, Katarina Kågedal, Uno Johansson, and Karin Öllinger. Analysis of cytosolic and lysosomal pH in apoptotic cells by flow cytometry. *Methods in cell science*, 25(3-4):185–194, 2004.

[13] Anthony J Convertine, Danielle S W Benoit, Craig L Duvall, Allan S Hoffman, and Patrick S Stayton. Development of a novel endosomolytic diblock copolymer for siRNA delivery. *Journal of Controlled Release*, 133(3):221–229, February 2009.

[14] A Paul Bevan, Paul G Drake, John JM Bergeron, and Barry I Posner. Intracellular signal transduction: the role of endosomes. *Trends in Endocrinology & Metabolism*, 7(1):13–21, 1996.

[15] Chantal A Lackey, Oliver W Press, Allan S Hoffman, and Patrick S Stayton. A Biomimetic pH-Responsive Polymer Directs Endosomal Release and Intracellular Delivery of an Endocytosed Antibody Complex. *Bioconjugate Chemistry*, 13(5):996–1001, September 2002.

[16] Mohamed E H El-Sayed, Allan S Hoffman, and Patrick S Stayton. Rational design of composition and activity correlations for pH-sensitive and glutathione-reactive polymer therapeutics. *Journal of Controlled Release*, 101(1-3):47–58, January 2005.

[17] B Albarran, R To, and P STAYTON. 1111. TAT-Streptavidin: A Novel Drug Delivery Vector for the Intracellular Uptake of Macromolecular Cargo. *Molecular Therapy*, 11:428–428, August 2005.

[18] Daniel W Pack, Allan S Hoffman, Suzie Pun, and Patrick S Stayton. Design and development of polymers for gene delivery. *Nature Reviews Drug Discovery*, 4(7):581–593, July 2005.

[19] Marzia Massignani, Irene Canton, Nisa Patikarnmonthon, Nicholas J Warren, Steven P Armes, Andrew L Lewis, and Giuseppe Battaglia. Cellular delivery of antibodies: effective targeted subcellular imaging and new therapeutic tool. *Nature Proceedings*, 1, 2010.

[20] J Yang, H Chen, I R Vlahov, J X Cheng, and P S Low. Characterization of the pH of Folate Receptor-Containing Endosomes and the Rate of Hydrolysis of Internalized Acid-Labile Folate-Drug Conjugates. *Journal of Pharmacology and Experimental Therapeutics*, 321(2):462–468, January 2007.

[21] R J Lee, S Wang, and P S Low. Measurement of endosome pH following folate

receptor-mediated endocytosis. *Biochimica et Biophysica Acta (BBA)-Molecular Cell Research*, 1312(3):237–242, 1996.

[22] Akin Akinc, Mini Thomas, Alexander M Klibanov, and Robert Langer. Exploring polyethylenimine-mediated DNA transfection and the proton sponge hypothesis. *The Journal of Gene Medicine*, 7(5):657–663, 2005.

[23] Akin Akinc and Robert Langer. Measuring the pH environment of DNA delivered using nonviral vectors: Implications for lysosomal trafficking. *Biotechnology and Bioengineering*, 78(5):503–508, April 2002.

[24] N Bayer, D Schober, E Prchla, R F Murphy, D Blaas, and R Fuchs. Effect of bafilomycin A1 and nocodazole on endocytic transport in HeLa cells: implications for viral uncoating and infection. *Journal of virology*, 72(12):9645–9655, 1998.

[25] F Philipp Seib, Arwyn T Jones, and Ruth Duncan. Establishment of subcellular fractionation techniques to monitor the intracellular fate of polymer therapeutics I. Differential centrifugation fractionation B16F10 cells and use to study the intracellular fate of HPMA copolymer–doxorubicin. *Journal of Drug Targeting*, 14(6):375–390, January 2006.

[26] Maria Manunta, Lorella Izzo, Ruth Duncan, and Arwyn Tomos Jones. Establishment of subcellular fractionation techniques to monitor the intracellular fate of polymer therapeutics II. Identification of endosomal and lysosomal compartments in HepG2 cells combining single-step subcellular fractionation with fluorescent imaging. *Journal of Drug Targeting*, 15(1):37–50, January 2007.

[27] Jungsoo Kim and David A Tirrell. Synthesis of Well-Defined Poly(2-ethylacrylic acid). *Macromolecules*, 32(3):945–948, February 1999.

[28] J M Pagel, A Pantelias, N Hedin, S Wilbur, L Saganic, Y Lin, D Axworthy, D K Hamlin, D S Wilbur, A K Gopal, and O W Press. Evaluation of CD20, CD22, and HLA-DR Targeting for Radioimmunotherapy of B-Cell Lymphomas. *Cancer Research*, 67(12):5921–5928, June 2007.

[29] Mark D Hylarides, Robert W Mallett, and Damon L Meyer. A Robust Method for the Preparation and Purification of Antibody/Streptavidin Conjugates. *Bioconjugate Chemistry*, 12(3):421–427, May 2001.

[30] Maria C Palanca-Wessels, Anthony J Convertine, Richelle Cutler-Strom, Garrett C Booth, Fan Lee, Geoffrey Y Berguig, Patrick S Stayton, and Oliver W Press. Anti-CD22 Antibody Targeting of pH-responsive Micelles Enhances Small Interfering RNA Delivery and Gene Silencing in Lymphoma Cells. *Molecular Therapy*, 19(8):1529–1537, May 2011.

[31] GREEN NM. AVIDIN. 4. STABILITY AT EXTREMES OF PH AND DIS-

SOCIATION INTO SUB-UNITS BY GUANIDINE HYDROCHLORIDE. *The Biochemical journal*, 89:609, 1963.

[32] L L Ng and C Dudley. Intracellular pH clamping of human leucocytes: a technique for determination of cellular buffering power and Na+/H+ antiport characteristics. *Clinical science (London, England: 1979)*, 77(4):417, 1989.

[33] Ludmila V Deriy, Erwin A Gomez, Guangping Zhang, Daniel W Beacham, Jessika A Hopson, Alexander J Gallan, Pavel D Shevchenko, Vytautas P Bindokas, and Deborah J Nelson. Disease-causing mutations in the cystic fibrosis transmembrane conductance regulator determine the functional responses of alveolar macrophages. *Journal of Biological Chemistry*, 284(51):35926–35938, 2009.

[34] L S Chin. Hrs Interacts with Sorting Nexin 1 and Regulates Degradation of Epidermal Growth Factor Receptor. *Journal of Biological Chemistry*, 276(10):7069–7078, December 2000.

[35] Suzanne Flanary, Allan S Hoffman, and Patrick S Stayton. Antigen Delivery with Poly(Propylacrylic Acid) Conjugation Enhances MHC-1 Presentation and T-Cell Activation. *Bioconjugate Chemistry*, 20(2):241–248, February 2009.

[36] Rachel A Jones, Charles Y Cheung, Fiona E Black, Jasmine K Zia, Patrick S Stayton, Allan S Hoffman, and Mark R Wilson. Poly (2-alkylacrylic acid) polymers deliver molecules to the cytosol by pH-sensitive disruption of endosomal vesicles. *Biochemical Journal*, 372(Pt 1):65, 2003.

[37] René Bartz, Haihong Fan, Jingtao Zhang, Nathalie Innocent, Craig Cherrin, Stephen C Beck, Yi Pei, Aaron Momose, Vasant Jadhav, David M Tellers, Fanyu Meng, Louis S Crocker, Laura Sepp Lorenzino, and Stanley F Barnett. Effective siRNA delivery and target mRNA degradation using an amphipathic peptide to facilitate pH-dependent endosomal escape. *Biochemical Journal*, 435(2):475–487, March 2011.

[38] G L Verdine and L D Walensky. The Challenge of Drugging Undruggable Targets in Cancer: Lessons Learned from Targeting BCL-2 Family Members. *Clinical Cancer Research*, 13(24):7264–7270, December 2007.

[39] Amir K Varkouhi, Marije Scholte, Gert Storm, and Hidde J Haisma. Endosomal escape pathways for delivery of biologicals. *Journal of Controlled Release*, 151(3):220–228, May 2011.

[40] Anh-Tuan Dinh, Chinmay Pangarkar, Theo Theofanous, and Samir Mitragotri. Understanding Intracellular Transport Processes Pertinent to Synthetic Gene Delivery via Stochastic Simulations and Sensitivity Analyses. *Biophysical Journal*, 92(3):831–846, February 2007.

[41] Nels C Elde and Harmit S Malik. The evolutionary conundrum of pathogen mimicry. *Nature Reviews Microbiology*, 7(11):787–797, October 2009.

[42] Sharon Y Wong, Jeisa M Pelet, and David Putnam. Polymer systems for gene delivery—Past, present, and future. *Progress in Polymer Science*, 32(8-9):799–837, August 2007.

[43] Steven R Little and Daniel S Kohane. Polymers for intracellular delivery of nucleic acids. *Journal of Materials Chemistry*, 18(8):832, 2008.

[44] Niren Murthy, Jean Campbell, Nelson Fausto, Allan S Hoffman, and Patrick S Stayton. Bioinspired pH-Responsive Polymers for the Intracellular Delivery of Biomolecular Drugs. *Bioconjugate Chemistry*, 14(2):412–419, March 2003.

[45] Daming Shan and Oliver W Press. Constitutive endocytosis and degradation of CD22 by human B cells. *The Journal of Immunology*, 154(9):4466–4475, 1995.

[46] Josette Carnahan, Paul Wang, Richard Kendall, Ching Chen, Sylvia Hu, Tom Boone, Todd Juan, Jane Talvenheimo, Silvia Montestruque, Jilin Sun, Gary Elliott, John Thomas, John Ferbas, Brent Kern, Robert Briddell, John P Leonard, and Alessandra Cesano. Epratuzumab, a Humanized Monoclonal Antibody Targeting CD22. *Clinical Cancer Research*, 2003.

[47] Craig L Duvall, Anthony J Convertine, Danielle S W Benoit, Allan S Hoffman, and Patrick S Stayton. Intracellular Delivery of a Proapoptotic Peptide via Conjugation to a RAFT Synthesized Endosomolytic Polymer. *Molecular Pharmaceutics*, 7(2):468–476, April 2010.

Chapter 3

ANTIBODY-POLYMER CONJUGATES FOR PROAPOPTOTIC PEPTIDE DELIVERY

Antibody-polymer-peptide conjugates were made for intracellular peptide delivery. The platform was composed of an anti-CD22/streptavidin (HD39/SA) conjugate for B-cell targeting with biotinylated polymers for endosomal escape. Biotinylated heterotelechelic polymers were synthesized by reversible addition-fragmentation chain transfer (RAFT) with pendent pyridyl disulfides for peptide conjugation. Low aqueous solubility of the polymer-peptide conjugates led to the development of a second platform using HD39/SA with three biotinylated poly(propylacrylic acid) (PPAA) polymers and one biotinylated BIM peptide with a reducible disulfide linker. The therapeutic potential of conjugates was demonstrated with a cell viability assay in Ramos-AW cells. The pharmacokinetics and biodistribution parameters of dual-radiolabeled conjugates was evaluated in tumor-xenograft mice. With polymer attached, conjugates were cleared from blood within 8 hours. We hypothesized that the anionic polymer was being captured by scavenger receptors found on kupffer cells in the liver. This hypothesis was confirmed by pretreating mice in a second study with scavenger receptor blockers, which increased the circulation half-life of conjugates. Even though liver uptake was blocked with a pretreatment regimen this approach would have little significance in a clinical setting, therefore, a new series of hydrophilic polymers that did not result in scavenger receptor uptake were explored in Chapter 4. These studies helped realize that development of polymer conjugates for intracellular delivery must be done with in vivo consideration and feasibility studies.

3.1 Introduction

Antibody-drug conjugates (ADCs) have the ability to improve the delivery of potent molecules or proteins to tumors in the body[1,2]. General considerations for ADC technology are antigen targeting, endocytosis into targeted cells, release of drug into the cytoplasm, and drug potency. To address these considerations, we have constructed an ADC with a monoclonal antibody (anti-CD22) for targeting and cell uptake, a telechelic, pH-responsive diblock copolymer (biotin-PPAA-b-PDSMA-co-DMA) for endosomal escape with a labile drug linkage, and a therapeutic peptide (BIM) for apoptotic induction. Antibody-drug loading is a key design consideration for cancer therapeutics. Hamblett et al. found that while a higher loading of 8 drugs per antibody had a correlative effect in vitro, medium loading with 4 and low loading with 2, had a better response in vivo with a higher therapeutic index[3]. The ability to control drug loading is an important focus of this chapter which we will explore using a diblock copolymer with multiple PDS groups for conjugating our therapeutic peptide.

RAFT synthesis is a controlled radical polymerization technique used to produce endosomolytic heterotelechelic polymers with pendent functional groups[4–6]. Chain transfer agents (CTA), that control the polymerization process and provide end functionality, have been modified with a number of end groups, such as biotin, to allow for complexation with streptavidin-linked proteins[7,8]. Monomers with pendent functional groups such as pyridyl disulfide (PDS), maleimides, and trifluorophenols can also be incorporated into the polymers for labile or stable linkages with small molecules, peptides, and nucleic acids that require intracellular delivery for activity[9–13]. The diblock copolymer made in this study contained hetero-telechelic functionality, with the ability to bind streptavidin through a biotin-functional CTA and conjugate peptides through PDS-functional monomers. The diblock copolymer also exhibits membrane destabilizing activity at endosomal pH as described in Chapter 2. Conjugated to the

endosomal escaping polymer is the proapoptotic BIM peptide (see Chapter 1). To induce apoptosis, the BIM peptide requires cytosolic delivery, giving rise to the use the pH-responsive membrane destabilizing polymer.

3.2 Experimental Section

3.2.1 Synthesis of biotin-poly[(PPAA)-(PDSMA-DMA)]

RAFT synthesis of biotin-poly(PPAA)-(PDSMA-DMA)] was conducted in DMF, under anhydrous conditions for 24 hours at 60°C using biotin-PPAA as the macroCTA and azobisisobutyronitrile (AIBN) as the radical initiator. The initial monomer to CTA ratios ($[CTA]_o/[M]_o$) initial CTA to initiator ratios ($[CTA]_o/[I]_o$) for the polymerization of the diblock copolymer was 165 to 1 and 16.4 to 1, respectively. The monomer feed ratio for DMA to PDSMA was 9 to 1. The resultant polymer was isolated by precipitation in diethyl ether. The precipitated polymers were then redissolved in DMF and reprecipitated into ether (x 4). The dry polymers were then redissolved in DMSO, added to 0.5 M $Na_2(CO_3)_2$, pH 8.7 at a 10-fold volume dilution, then run through a PD-10 desalting column to remove monomer and solvent and lyophilized.

3.2.1.1 Size-exclusion gel permeation chromatography

Gel permeation chromatography (GPC) was used to determine molecular weight and polydispersity (M_w/M_n, PDI) of the polymer using Tosoh SEC TSK-GEL α-3000 and α-4000 columns (Tosoh Bioscience, Montgomeryville, PA) connected in series to an Agilent 1200 Series Liquid Chromatography System (Santa Clara, CA) and Wyatt Technology miniDAWN TREOS, 3 angle MALS light scattering instrument and Optilab rEX, refractive index detector (Santa Barbara, CA). HPLC-grade DMF containing 0.1 wt.% LiBr at 60°C was used as the mobile phase at a flow rate of 1 mL/min.

3.2.1.2 NMR spectroscopy

1H NMR was performed to measure the diblock copolymer composition. The spectra was recorded on a Bruker AV301 in deuterated water (D_2O) at 25 °C . A deuterium lock (CDCl3, D2O) was used and chemical shifts were determined in ppm from tetramethylsilane (for CDCl3) and 3-(trimethylsilyl)propionic-2,2,3,3-d4 acid, sodium salt (for D2O). Polymer concentration was 7 mg/mL.

3.2.1.3 Quantification of PDS groups on diblock copolymer

The number of functional PDS groups per polymer chain was measured by pyridine-2-thione release in PBS. Polymer and TCEP were brought to a final concentration of 1.25 and 5 mg/mL in PBS, pH 8.0, respectively. The absorbance of the leaving group pyridine-2-thione was measured at 343 nm by spectrophotometry using an extinction coefficient of 8,080 10^{-1} cm^{-1}.

3.2.2 Red blood cell hemolysis assay

pH-dependent membrane disruption of the diblock copolymer was examined by a red blood cell hemolysis assay. Activity of the free polymer was measured in physiologically relevant pH buffers: 7.4, 7.0, 6.6, 6.2, and 5.8. Briefly, whole blood was collected in vacutainer tubes containing EDTA, centrifuged, plasma aspirated and resuspended in 150 mM NaCl to isolate the red blood cells (RBCs). RBCs were resuspended in phosphate buffers at each pH and incubated with polymer (16, 32 and 64 μg/mL) for 1 hour at 37 °C. Hemoglobin release was measured by centrifugation of intact RBCs and measuring the absorbance of the supernatant at 541 ηm.

3.2.3 Characterization of BIM peptide

To measure the extinction coefficient of the BIM peptide, the lyophilized peptide provided by the manufacturer was reconstituted in molecular grade (MG) water, diluted into 4 concentrations and the absorbance of each solution was measured at 280 nm with a spectrophotometer. After plotting the absorbance versus concentration, the slope of the fitted linear curve was determined to be the extinction coefficient. The BIM peptide was also analyzed for purity by HPLC and mass spectrometry.

3.2.4 Formulation of polymer-peptide conjugates

For peptide-polymer conjugations, peptide was dissolved in MG water and incubated with polymer in phosphate buffer, pH 8.0 containing 5 mM EDTA for 18 hours. Conjugation reactions were done at 2:1, 4:1, and 10:1 peptide to polymer molar ratios. Reaction of the pyridyl disulfide with the cysteine on the peptide results in a disulfide linkage and release of pyridine-2-thione which was used to measure conjugation efficiencies by spectrophotometric absorbance at 343 nm. Conjugation of the peptide to the polymer was also verified by SDS-PAGE 16.5% tricine gel. Conjugation reactions were also treated with TCEP prior to running SDS-PAGE to verify peptide cleavage in a reducing environment.

3.2.5 Streptavidin-polymer complexation confirmed by HABA assay

The binding ability of the peptide-bound polymer chains was measured by a HABA Assay (See Chapter 2). The ability to occupy all four biotin-binding pockets with peptide-bound polymer chains was measured.

3.2.6 Purification of free polymer from HD39/SA conjugates

To remove free polymer from HD39/SA conjugate solutions, an Amicon Ultra-0.5mL centrifugal filter with a 100 kDa nominal molecular weight cut off was used. Following manufacture protocol, 500 μL of conjugate solution was added to the filtration device, followed by centrifugation for 10 minutes at 14,000 g. The sample was recovered and analyzed by spectrophotometry to measure polymer depletion and conjugate concentration.

3.2.7 Synthesis of biotinylated BIM peptide

The BIM peptide, MRPEIWIAQELRRIGDEFNAC was ordered from Abgent and synthesized on solid support using standard Fmoc chemistry. A sulfhydryl-reactive biotin agent was reacted with the cysteine at the N-terminus of the peptide to make biotinylated-BIM (btBIM). First, biotin-HPDP (Thermo Scientific, IL) was dissolved in anhydrous DMSO at 10 mg/mL (with heating and vortexing) then mixed with the BIM peptide at a 1:10 molar ratio and reacted overnight at room temperature. DMSO was removed with a high vacuum pump and the reaction mixture was dissolved in 5 mL ddH20. The soluble btBIM was separated by centrifugation, then purified and analyzed by RP-HPLC and MALDI-TOF mass spectrometry.

3.2.8 Synthesis of biotinylated chain transfer agent

The RAFT chain transfer agent (CTA) biotin-PEG-ECT was synthesized as described. 1 g of biotin-PEG-NH3 (Quanta BioDesign) was mixed with NHS-ECT (3 mol eq.) and DIEA (6 mol eq.) using 50 mL DCM for dissolution. The reagents were incubated in a round bottom flask for 18 hours at room temperature under anhydrous conditions then concentrated using a rotary evaporator. The biotin-PEG-ECT product was

purified by flash column chromatography using a DCM/MeOH elution mixture from 10/1 to 9/1. The final product was analyzed by 1H-NMR to confirm purity of the final product.

3.2.9 Synthesis of biotinylated-poly(propylacrylic acid)

RAFT polymerization of PAA was conduced in DMF under anhydrous conditions for 48 hours at 60 °C using the biotin-PEG-ECT as the CTA and AIBN as the radical initiator. The initial monomer to CTA ratio ($[M]_o/[CTA]_o$), and initial CTA to initiator ratios ($[CTA]_o/[I]_o$) for the polymerization of PAA was 150 to 1 and 1 to 1. The resultant polymers were isolated by precipitation in diethyl ether. The precipitated polymers were then redissolved in DMF and precipitated into ether (4X). The dry polymers were redissolved in DMSO, added to 0.5 M $Na_2(CO_3)_2$, pH 9 at a 10-fold volume dilution, desalted using a GE PD10 column to remove monomer and solvent then lyophilized. GPC was used to determine molecular weight and polydispersity. PPAA also characterized for purity by 1H-NMR.

3.2.10 Formulation of antibody-polymer-peptide conjugates

To measure the streptavidin complexation capacity of the btBIM peptide, a HABA assay was conducted as previously described. The streptavidin/HABA solution was mixed with a ratio of biotin to obtain a standard curve, then with btBIM from a 1 to 6 molar excess as previously described. A linear regression curve was fit to the data and binding capacity of btBIM was determined. These steps were repeated to measure the binding capacity of PPAA. A HABA assay was then conducted with HD39/SA to confirm one btBIM bound per HD39/SA followed by saturation with PPAA.

3.2.11 Ramos-AW cell culture

Ramos-AW cells were obtained from the European Collection of Cell Cultures (ECACC, Salisbury, UK). Cell cultures were maintained in log phase growth in RPMI 1640 medium containing L-glutamine, 25 mM HEPES, supplemented with 1% penicillin-streptomycin (GIBCO) and 10% fetal bovine serum (FBS, Invitrogen) at 37°C and 5% CO_2.

3.2.12 Cell viability measured by mTS

An MTS assay was carried out to measure the number of viable cells in culture following the various treatments. For this assay, 40k RAMOS-AW cells per well were seeded in a 96-well round-bottom plate and treated in triplicate with 4 μM HD39/SA-PPAA-btBIM, HD39/SA-PPAA, HD39/SA-btBIM, free btBIM, free PPAA, or staurosporine. After 24 hours, cells were washed with fresh media (2X) then incubated with MTS for 2 hours. Samples were transferred to a flat-bottom 96 well plate and the absorbance at 490 nm was measured on a plate reader. RAMOS-AW viability was normalized to untreated cells.

3.2.13 Synthesis of dual-radiolabeled conjugates

For simultaneous detection of the antibody and peptide in pharmacokinetic and biodistribution studies, a conjugate containing ^{3}H and ^{14}C was prepared. 6.2 mg of HD39/SA at 2 mg/mL in 50 mM sodium borate, pH 8.5, 150 mM NaCl was reacted with 1mCi ^{3}H-N-succinimidyl propionate at 5mCi/mL in DMF for 2 h at 25 °C. PBS buffer exchange and removal of unreacted radiolabel was performed with a PD-10 desalting column. The [^{3}H]HD39/SA solution was concentrated using an Amicon Ultra-4 centrifugal filter unit with 30,000 NMWL. btBIM or BIM peptides were reacted

in 100 μL ddH20 with a 5X molar excess of ^{14}C-acetic anhydride in 5 l dioxane for 30 min. Radiolabeled peptides were lyophilized to remove excess acetic anhydride and acetic acid then resuspended in ddH20 (BIM) or DMF (btBIM). The concentration and specific activity of [^{3}H]HD39/SA, [^{14}C]BIM, and [^{14}C]btBIM was measured by A_{280}— absorbance and scintillation counting with ULTIMA GOLD scintillation fluid. Complexation of one btBIM peptide to per HD39/SA via biotin-streptavidin linkage was confirmed with a HABA assay. After [^{3}H]HD39/SA-[^{14}C]btBIM complexation, trace DMF was removed by centrifugal filtration. The 11kDa PPAA was then added to form the complete [^{3}H]HD39/SA-PPAA-[^{14}C]btBIM conjugate and confirmed by both HABA and scintillation counting.

3.2.14 Optimization of tumor-xenografts mouse model

To optimize tumor growth rates and tumor take rates, RAMOS-AW cells were injected in mice at three concentrations and followed for up to 11 days. For all in vivo studies, BALB/c nu/nu mice (6 to 8 weeks old) were used from Harlan Sprague-Dawley and housed under protocols approved by the FHCRC Institutional Animal Care and Use Committee. To prepare cell suspensions, RAMOS-AW cells were resuspended in PBS at 15, 10, or 5 x 10^{6} cells per 200 μL. In the first study, 2 groups of 5 mice received subcutaneous injections of 15 M cells in the right flank. Tumor measurements were taken with calipers in the x, y, and z direction for up to 10 days. In the second study, 2 groups of 5 mice received 10M cells in the right flank and 5 M cells in the left flank and were followed for 11 days. Tumor growth was plotted as a function of time and data was fit using a logarithmic growth curve.

3.2.15 Pharmacokinetics of dual-radiolabeled conjugates

Mice were injected subcutaneously in the right flank with 10M RAMOS-AW cells and placed on a biotin-free diet (Purina Feed). Tumors were grown for seven days until they reached 50 to 100 mm3. To measure whole blood clearance, 6 mice per treatment each received 1.4 ηmoles of [^{14}C]BIM, [^{3}H]HD39/SA, [^{3}H]HD39/SA-[^{14}C]btBIM, or [^{3}H]HD39/SA-PPAA-[^{14}C]btBIM via tail vein injection. Serial blood samples were drawn in triplicate from the retro-orbital venus plexus using a 10 μL capillary tube at the following time points: 5 m, 15 m, 30 m, 1h, 2 h, 4 h, 8 h, and 24 h. (Exact injection and collection times were collected for each mouse). Blood was transferred to scintillation vials containing 5 mL of ULTIMA GOLD scintillation fluid and sonicated 10 m. ^{3}H and ^{14}C activity in blood was measured by scintillation counting using an automated deconvolution of ^{3}H and ^{14}C signal. Syringe weights were measured before and after injection to calculate the total injection volume and specific activity of each treatment was measured in triplicate from stock solutions. For blood clearance calculations, 80 mL (blood) per kg (mouse) was assumed. Blood concentrations were plotted using GraphPad Prism and fitted to a two-compartmental open model (bi-exponential equation) with $1/y^2$ weighting to account for larger standard deviations at the earliest timepoints. The number of peptides per antibody was calculated by dividing the blood concentration of peptide to antibody.

3.2.16 Biodistribution of dual-radiolabeled conjugates

After 24 hours, mice were weighed, sacrificed and bled. Tumors and normal organs (lung, liver, spleen, stomach, kidney, small intestine, large intestine, muscle) were harvested, weighed and homogenized in 10 mL of ddH20 per gram of tissue. 200 μL of homogenized tissue was transferred to a scintillation vial and 500 uL Solvable (Perkin Elmer) was added. Samples were incubated at 60 ^{o}C overnight until tissues were

solvated. 50 μL of 200 mM EDTA and 200 μL of 30% hydrogen peroxide were added and samples were incubated overnight at room temperature. 25 μL 10N HCl and 10 mL of ULTIMA GOLD scintillation fluid (Perkin Elmer) were added to each sample, then vortexed and incubated overnight at room temperature. Samples were run on a scintillation counter to measure μL and ^{14}C signal and the percent-injected dose per gram (%ID/g) of tissue or blood was calculated. The stability of the peptide was also calculated by plotting the ratio of peptide to antibody in each organ.

3.2.17 Succinylating BSA for scavenger receptor blocking

Succinylated BSA was made according to Takura et al[14]. Briefly, 100 mg of BSA was dissolved at 20 mg/mL in 0.2 M Tris buffer, pH 8.65. Succinic anhydride was dissolved in DMF at 0.9 mg/mL and added to BSA at a molar excess of 0, 120, 240, and 360. Solutions were mixed for 5 hours, purified using a PD-10 column equilibrated with ddH20 then lyophilized. The number of free amines remaining on the succinylated BSA was quantified using an OPA assay. Briefly, BSA was dissolved in PBS at 5 mg/mL then diluted to 0.5 mg/mL to make a standard curve. After adding appropriate reagents, The absorbance at 280 nm was measured and the number of free amines was calculated based on the standard curve. The molecular weight of the succinylated BSA proteins was also measured by aqueous GPC. For in vivo studies, the BSA treated with a 240-fold excess of succinic anhydride was selected.

3.2.18 Pharmacokinetics and biodistribution with scavenger receptor blockers

Mice (3 per group) were pretreated with 50 mg/kg of dextran sulfate, fucoidan, succinylated-BSA or PBS via tail vein injection. One hour after injection of scavenger receptors, dual-radiolabeled HD39/SA-PPAA-btBIM conjugates were injected into mice. Pharmacokinetics and biodistribution were measured as described in the previous

study.

3.2.19 In vivo comparison of PPAA conjugates versus HPMA Micelles

The pharmacokinetics and biodistribution of radiolabeled HD39/SA and BIM peptide was assessed using two polymer systems: PPAA with dextran sulfate pretreatment and the HPMA diblock copolymer. Dextran sulfate was used as a pretreatment to prevent scavenger receptor uptake of the anionic PPAA conjugates. For the pharmacokinetic and biodistribution studies 3 mice received 300 μg of [^{3}H]HD39/SA with PPAA-[^{14}C]BIM, 1 hour after DxSO (50 mg/kg) via tail vein injection. 1 mouse received 300 μg of [^{3}H]HD39/SA with HP-PDB-[^{14}C]BIM via tail vein injection. Analysis was performed as previously described.

3.3 Results and Discussion

3.3.1 Synthesis of poly[(PAA)-(DMA-PDSMA)]

RAFT synthesis of the diblock copolymer is illustrated below in Figure 3.1. PPAA was synthesized using biotin-ECT as the CTA, and AIBN as the radical initiator (see Chapter 2). The resultant polymer was employed as the macro-CTA to synthesize the diblock copolymer. The second block was synthesized by incorporated two monomers; dimethylacrylamide (DMA) and pyridyl disulfide methylacrylate (PDSMA). The target DP of the second block was 165 and the feed ratios were 90% DMA and 10% PDSMA.

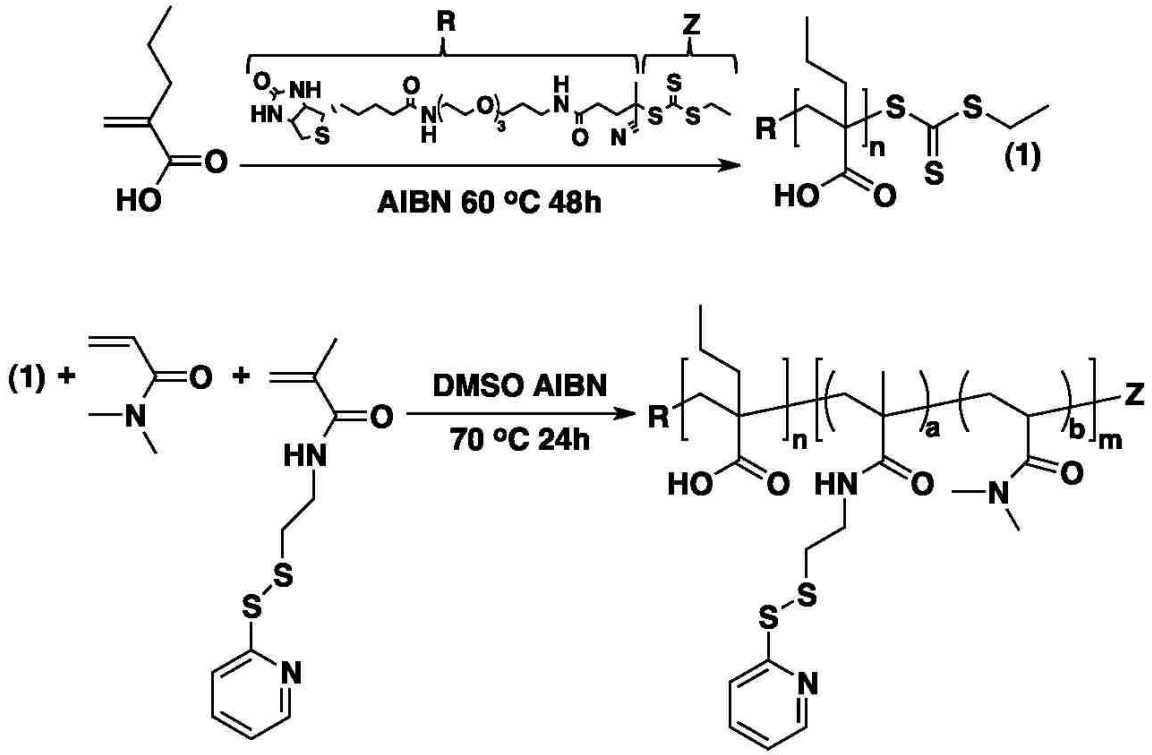

Figure 3.1: RAFT-mediated synthesis of the diblock copolymer containing biotin-poly(propylacrylic acid) (PPAA) with the incorporation of a second block containing hydrophilic dimethylacrylamide (DMA) and the thiol function monomer, pyridyl disulfide methylacrylate (PDSMA)

3.3.2 Characterization of PPAA and diblock copolymer

The macroCTA and diblock copolymer were analyzed by size exclusion chromatography. The refractive index measured for the macroCTA (PPAA) and the diblock copolymer PPAA-b-PDSMA-co-DMA are shown in Figure 3.2. A shift in the chromatogram is observed when the macroCTA is used to polymerize the subsequent diblock copolymer. After calculating dn/dc values for each polymer, the number average molecular weight, Mn, was found to be 18 kDa for PPAA and 35 kDa for diblock copolymer. The polydispersities (PDI) were measured to be 1.7 and 1.8, respectively. The polymerization of sterically hindered, bulky alpha-alkyl substituted acrylic acid monomers is generally difficult and these reactions often exhibit slow polymerization rates and low monomer conversion as demonstrated by Hastings with propylacrylic acid in 1969[?] . Bulky hindered monomers prevent the propagating radical to react with monomer, thus slowing the propagation and termination rates and increasing the polydispersity[?] . For this reason the RAFT polymerization of PPAA was conducted under bulk monomer conditions with a low initial CTA to initiator ratio ([CTA]o/[I]o = 1). These conditions lead to a higher than usual PDI for a controlled radical polymerization however the use of RAFT methodology allows for reasonable control over the molecular weight as well as the incorporation of biotin moieties at the alpha chain terminus.

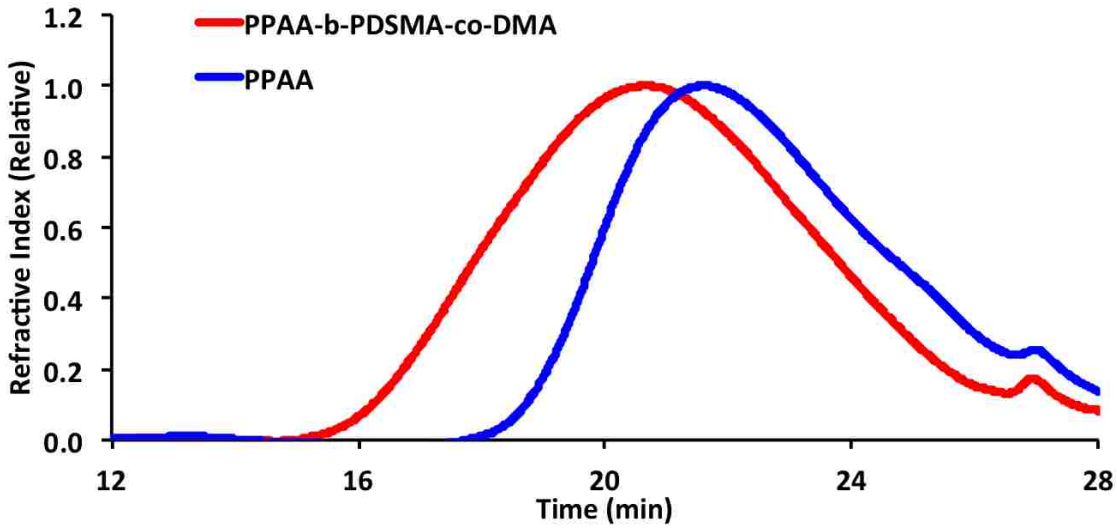

Figure 3.2: A chromatogram of the macro-CTA (PPAA), and the diblock copolymer (PPAA-b-[PDSMA-co-DMA]), measured by refractive index using size exclusion chromatography.

3.3.3 NMR spectroscopy of diblock copolymer

Composition of the diblock copolymer was measured by 1H-NMR using the spectrum in Figure 3.3. After integrating the proton peaks related to PPAA, PDSMA, and DMA, the composition of the second block was determined to be 90% DMA and 10% PDSMA, which was equal to the feed ratio. This composition resulted in a calculated 13 PDS groups per polymer chain.

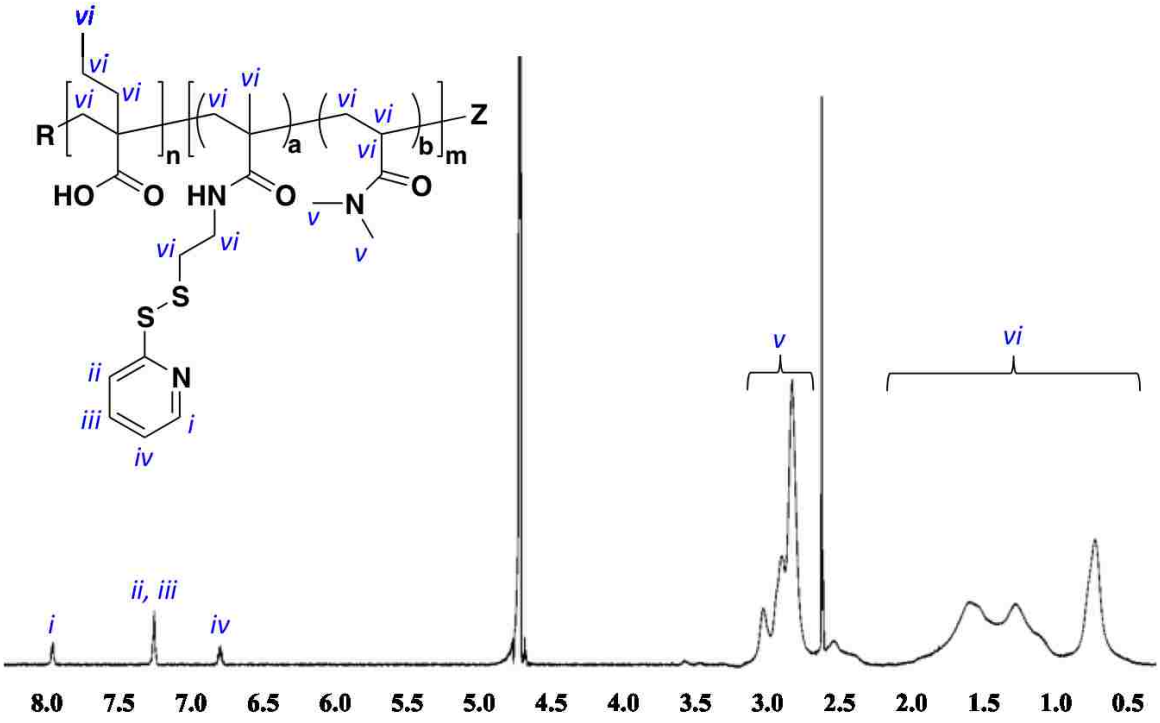

Figure 3.3: The NMR spectrum of the diblock copolymer was used to identify the peaks associated with polymer composition and calculate the conversion of the monomers

3.3.4 Calculating PDS groups on diblock copolymer

The release of pyridine-2-thione from the diblock copolymer after reduction with TCEP was correlated to the number of functional PDS groups per polymer chain. The absorbance peaks for reduced polymer and native polymer are shown in Figure 13. The change in absorbance at the peak maxima (343 ηm) between polymer in the absence and presence of TCEP was used to measure the concentration of pyridine-2-thione, with an extinction coefficient of 8,080 $M^{-1}cm^{-1}$. The average number of PDS groups per polymer chain was found to be 13.7, which is consistent with the PDSMA composition in the polymer measured by NMR in Figure 3.3. For all peptide-polymer conjugations, the number of peptides loaded per polymer remained below the number of PDS groups per chain to ensure a high binding efficiency while limiting the amount of free peptide after conjugation.

3.3.5 Hemolytic activity of diblock copolymer

Endosomal escape is an important functionality for intracellular delivery and has been shown to be correlated with a hemolytic assay. Hemolysis of the diblock was studied to ensure that the addition of the bulky second block did not inhibit the hemolytic activity of PPAA, the macroCTA. The pH responsive activity of both polymers was measured at three concentrations: low (16μg/mL) medium (32μg/mL) and high (48μg/mL). However because the diblock copolymer is nearly double the size of the macroCTA, the medium concentration of the diblock is relatively equivalent to the low concentration of the macroCTA in terms of PPAA concentration. The percent hemolysis at each pH was calculated relative to a 0.1% solution of Triton-X after subtracting the background absorbance at 500 nm and is shown in Figure 3.4. The activity of PPAA was examined at three physiologically relevant pH buffers: pH 7.4 (cytosolic), pH 6.6 (early endosome), and pH 5.8 (late endosome) (Figure 3.4

left). pH-responsive activity was observed for all three concentrations. The lowest concentration of PPAA was non hemolytic at pH 7.4, with 35% hemolysis at pH 6.6 and 100% hemolysis at pH 5.8. At the medium and high concentrations of PPAA, an increase in activity was observed at pH 7.4, with 100% hemolysis at pH 6.6 and 5.8. For the diblock copolymer (Figure 3.4, [right]), five different pH buffers were tested between pH 7.4 and 5.8. At the lowest concentration no significant activity was observed. At the medium concentration, the hemolytic activity reached 50% at pH 6.2 and 5.8. At the highest concentration, the polymer exhibited 20% hemolysis at pH 7.4, reaching 100% at pH 6.6 and below. These data suggest that the diblock copolymer exhibits a desired hemolytic response with minimal activity at physiological pH and high activity at endosomal pH. However, the bulkiness of the second block, polymerized off of PPAA, did inhibit the hemolytic activity of PPAA. Hemolysis of the polymer with peptides bound or complexed with HD39/SA was not evaluated in this study. The addition of antibody-streptavidin, a large protein conjugate on one end of the polymer and multiple peptides on the other end could sterically hinder the polymer and diminished the hemolytic activity. While hemolysis could be correlated with activity, a more quantitative approach would be to perform ratiometric fluorescence microscopy and flow cytometry, as described in Chapter 2.

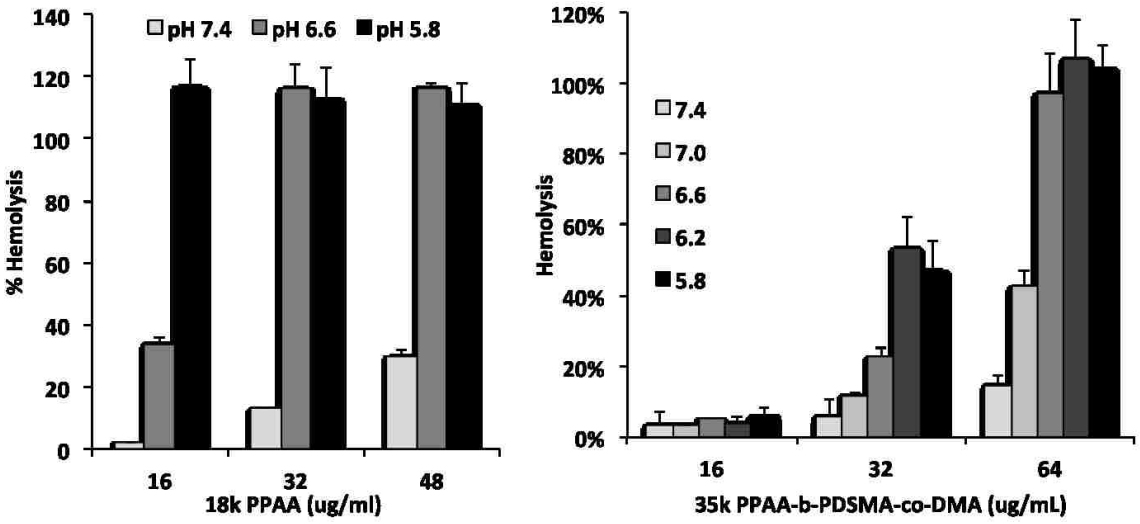

Figure 3.4: Hemolytic activity was normalized to a 0.1% Triton X-100 solution. Data represents the mean of a single experiment performed in triplicate with standard deviation

3.3.6 Streptavidin-polymer complexation

The binding efficiency of the biotinylated diblock copolymer with streptavidin was quantified by a HABA assay. First, a biotin standard curve was made to correlate biotin-binding events with HABA absorbance at 500 nm. Next, the diblock copolymer was added to the streptavidin/HABA solution at increasing concentrations and the change in A_{500} was recorded. Absorbance values were converted to binding events using the biotin standard curve and a graph of molar excess of polymer to biotin binding events was plotted as shown in Figure 3.5. A maximum of 3 polymer-binding events was achieved with a molar excess of 9 polymers per streptavidin. Exceeding this polymer excess resulted in saturation of the biotin binding sites. While the diblock copolymer is a large polymer, a linear relationship exists between polymer concentration and biotin binding events with approximately one binding event per SA for every three polymers in solution.

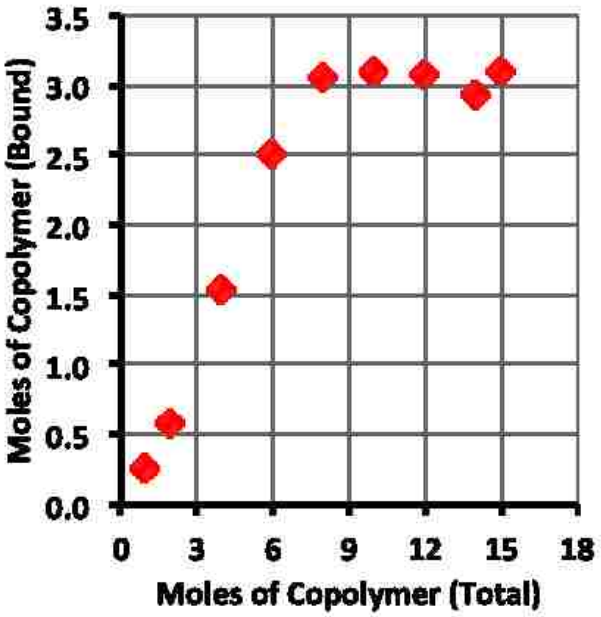

Figure 3.5: A HABA binding curve was used to measure the number of accessible biotin per diblock copolymer and demonstrate saturation of the streptavidin protein with biotinylated polymer

3.3.7 Mass spectroscopy and extinction coefficient of BIM peptide

The 21-amino acid BIM peptide has nearly an equal number of hydrophilic and hydrophobic residues and readily dissolves in both organic and aqueous solutions. The peptide contains a carboxyl-terminus cysteine for disulfide conjugations, has a net charge of -1 at neutral pH, and an isoelectric point at pH 4.7. The hydropathy of the BIM peptide was analyzed using an online innovagen peptide characterization program (Figure 3.6). The purity of the BIM peptide was measured by HPLC and mass spectrometry. Reverse phase HPLC indicated a single peak with high purity. The peptide was measured by mass spectromety as seen in Figure 3.7. The molecular weight determined by mass spec was 2548 Da and also confirmed high purity with a small amount of dimerization. With one tryptophan residue, the concentration of the peptide can be measured at 280 nm. To quantify the molar concentration based on absorbance units, the Beer-Lambert equation can be applied using a known extinction coefficient. To measure the extinction coefficient, the BIM peptide was dissolved at a known concentration and serially diluted into three concentrations. The A_{280} absorbance was plotted against known peptide concentrations and a linear fit was applied to the data set shown in Figure 3.8. The extinction coefficient, determined by the slope of the line was measured to be 4447 $M^{-1}cm^{-1}$.

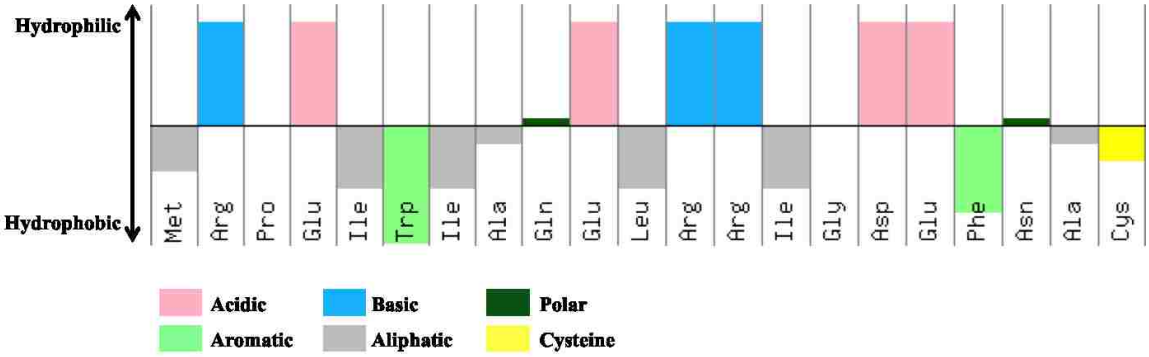

Figure 3.6: Hydropathy plot created online using Innovagen software describes the number of hydrophobic and hydrophilic residues found on the BIM peptide.

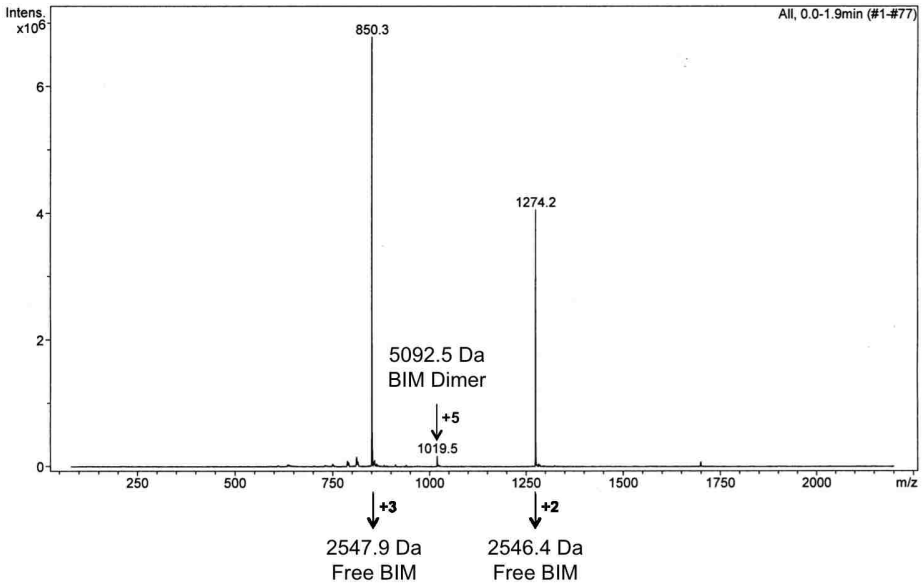

Figure 3.7: Mass spectrometry of the BIM peptide was performed to ensure the correct peptide was delivered from the company with more than 90% purity and little dimerization.

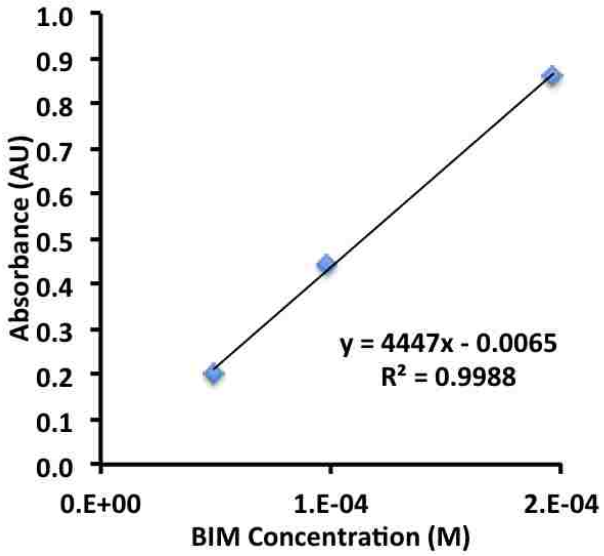

Figure 3.8: The extinction coefficient of the BIM peptide was calculated by plotting the absorbance of the peptide at three concentrations and calculating the slope of a linear regression fit.

3.3.8 Polymer-peptide conjugation and peptide release

The peptide to polymer conjugation efficiency was measured by pyridine-2-thione release at A_{343}. Peptides were incubated overnight at 4, 6, 8 and 10-fold molar excess to polymer and pyridine-2-thione release was measured the next day. The absorbance curves for each polymer-peptide conjugate are displayed in Figure 3.9 (left). The binding efficiency was found to be between 76 and 80% for every peptide loading concentration. These results demonstrate that the peptide binds to the polymer efficiently at all concentrations below the number of accessible sites per polymer chain. Validation of the peptide-polymer conjugation was also measured by running the conjugates on an SDS-PAGE gel. In Figure 3.9 (right), conjugation of the peptide to the polymer is observed by the disappearance of the free peptide band. Furthermore, in the presence of a reducing agent like TCEP, the conjugate smear at the top of the gel disappeared indicating the peptide has been reduced from the polymer via disulfide reduction.

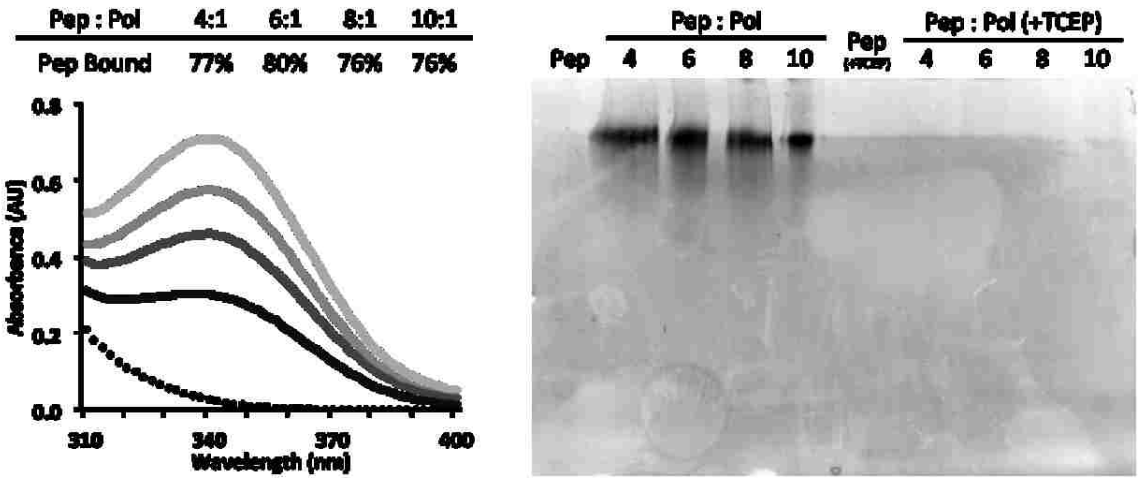

Figure 3.9: The conjugation efficiency of the peptide with the polymer was quantified by pyridine-2-thione release (left). Validation of conjugation and reduction through the disulfide bond was also performed by SDS-PAGE in the presence and absence of a reducing agent TCEP (right).

3.3.9 Conclusions from polymer-peptide conjugations

Although conjugation of the BIM peptide to the diblock copolymer was successful, the peptide-polymer conjugate was very hydrophobic with some turbidity observed in the reaction mixture. This probably occurred because the diblock copolymer has 13 hydrophobic PDSMA monomers per chain which imparts a large hydrophobic effect. Furthermore, multiple peptides per polymer chain increased the hydrophobicity such that the polymer-peptide conjugates could not remain in solution. To overcome the stability issue we explored a different approach by conjugating the BIM peptide directly to HD39/SA via a reducible biotin linker. This would allow for direct complexation to the mAb/SA conjugate while occupying the other three biotin binding sites with PPAA to induced endosomal escape. The next section of this chapter will discuss our approach in developing a unimeric antibody-polymer-peptide conjugate based on the system described in Chapter 2.

3.3.10 Characterization of btBIM by mass spectrometry

In order to complex the BIM peptide directly to the the antibody-streptavidin conjugate, a biotin-hexyl-PDS (Biotin-HPDP) linker was introduced. The BIM peptide was conjugated to the Biotin-HPDP linker in DMSO overnight and the crude product was characterized by mass spec (Figure 3.10) After confirming a high yield of btBIM product (2976 Da), DMSO was evaporated using a high vacuum and the crude product was purified by reverse-phase HPLC. After purification, the purified product was frozen and lyophilized in ddH_20. Mass spec was then used to confirm the purified btBIM product (Figure 3.11) had no remaining Biotiin-HPDP or free BIM peptide.

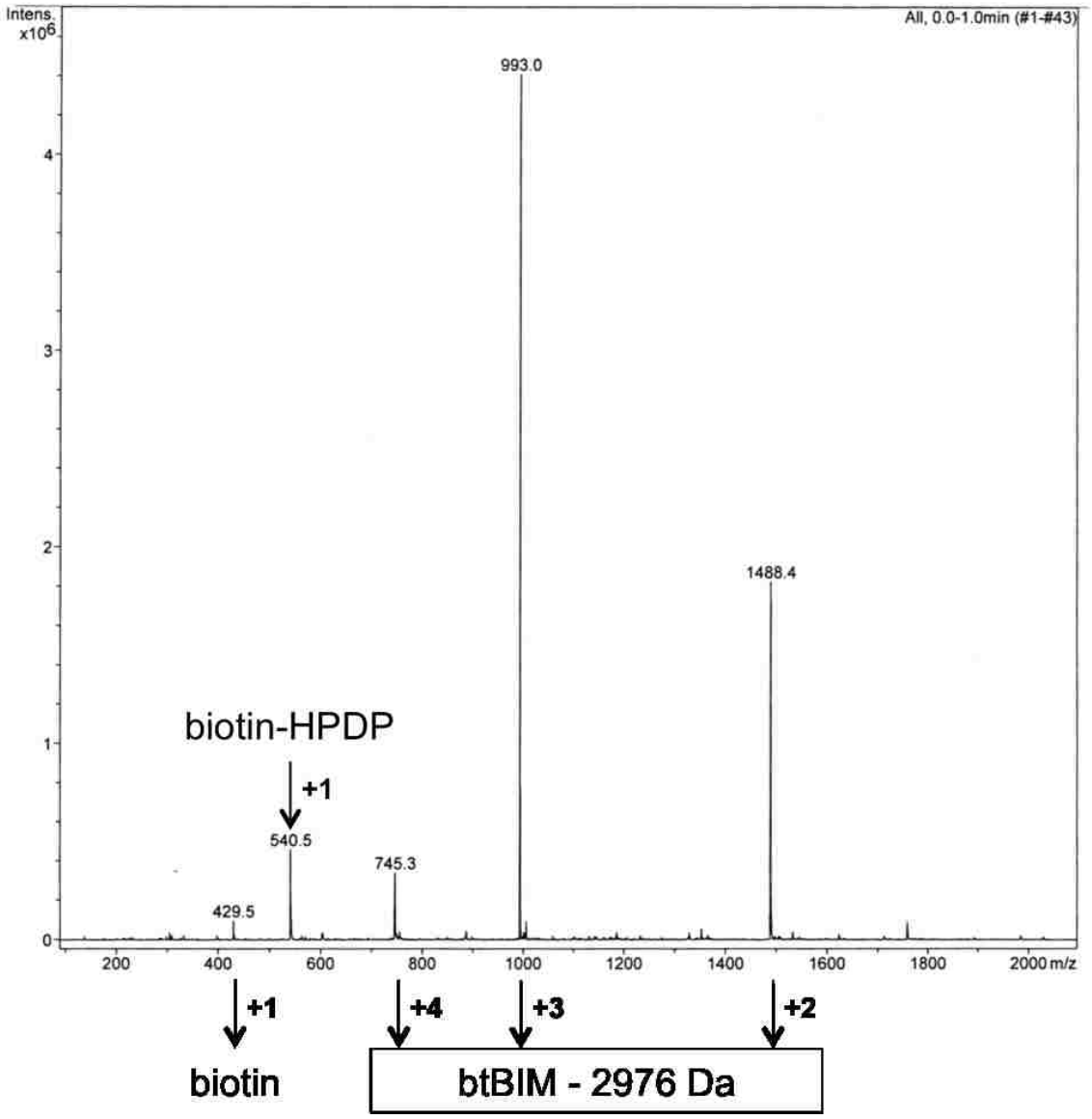

Figure 3.10: The crude btBIM product was analyzed by mass spectrometry to confirm sufficient conjugation. No free peptide was observed in the crude sample suggesting near 100% conjugation with an excess of biotin-HPDP

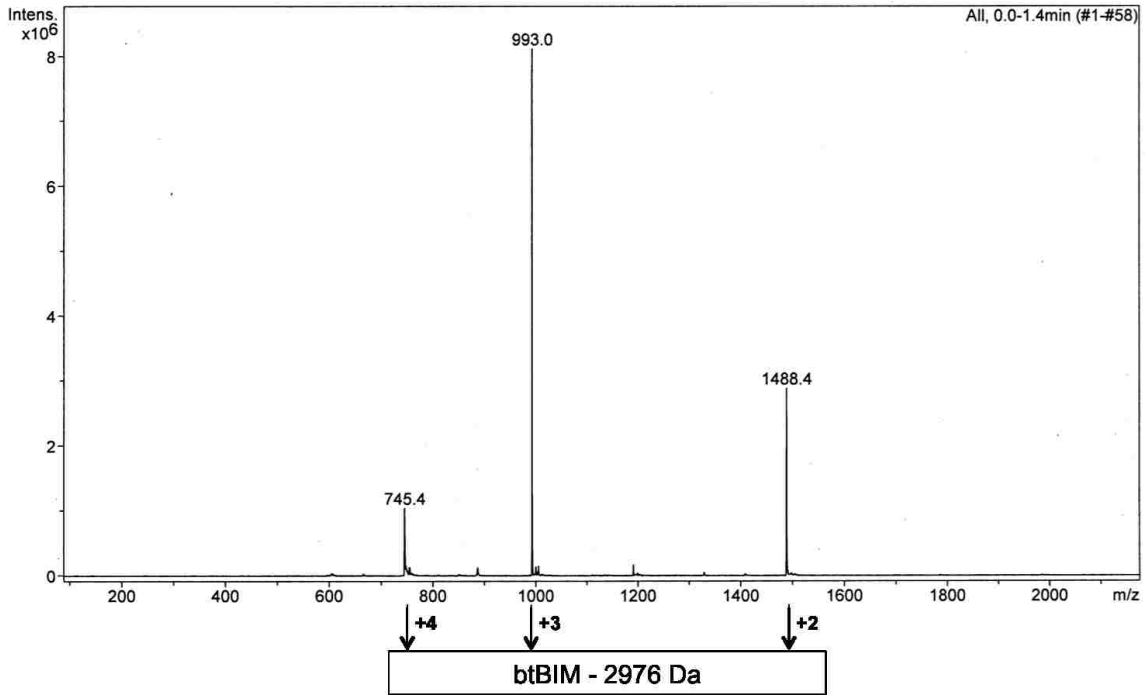

Figure 3.11: The final btBIM product was confirmed by mass spectrometry. The three m/z peaks identified in this spectrum correspond to the +2, +3, and +4 charges associated with the 2976 Da btBIM peptide conjugate

3.3.11 Characterization of btPEG-ECT CTA by NMR

The biotin-PEG_3-ECT chain transfer agent was synthesized and purified using a flash column an increasing gradient of organic solvent. The purified btPEG-ECT product was confirmed by NMR and all the peaks corresponding to protons on the CTA were identified (Figure 3.12). The NMR spectrum helped to confirm the purity of the new CTA using flash column chromatography. In previous versions of synthesizing the biotin-ECT, lower yields were often the result of reacting a one to one molar ratio of biotin to the ECT. With this method, an excess of ECT was reacted to conjugate all the biotin-PEG. This made the process for purification easier because there was no free biotin-PEG left in the solution. After confirming the purity of the new CTA, a subsequent RAFT polymerization was set up for the final PPAA polymer.

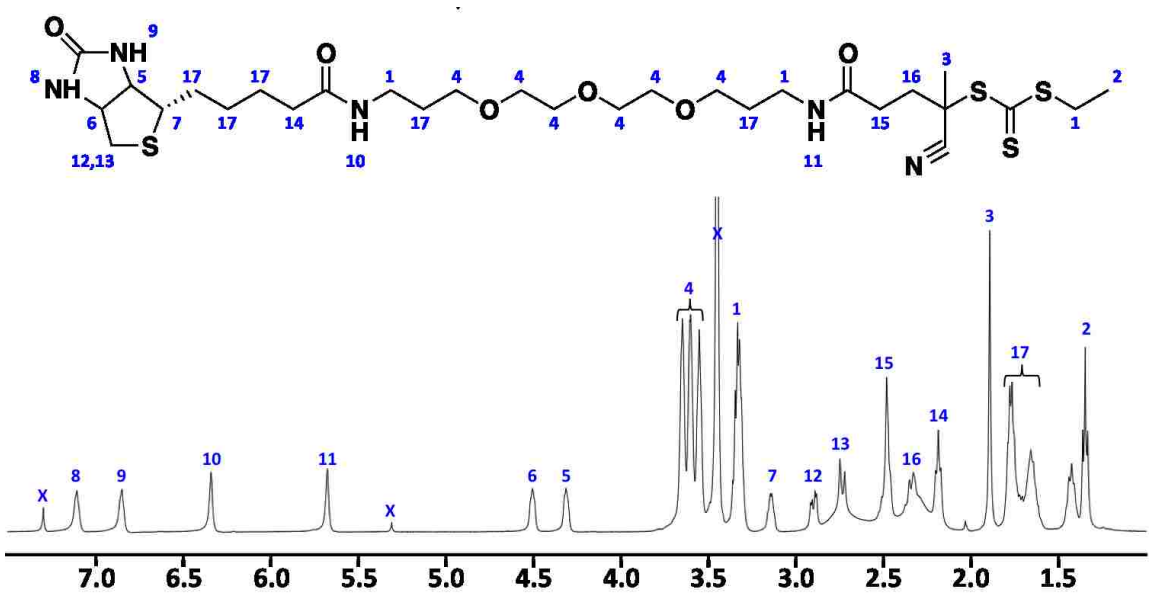

Figure 3.12: NMR spectrum of the btPEG-ECT chain transfer agent following flash column chromatography

3.3.12 Characterization of PPAA by NMR spectroscopy

After purification of the PPAA polymer, analysis by NMR spectroscopy was used to confirm monomer composition, purity and removal of any monomer species (Figure 3.13). All NMR peaks in the spectrum were accounted for in the chemical structure, including the biotinylated chain transfer agent. The carbon backbone of PAA and the propyl pendent group were identified by the large peak spanning between 0.9 to 2.2 ppm.

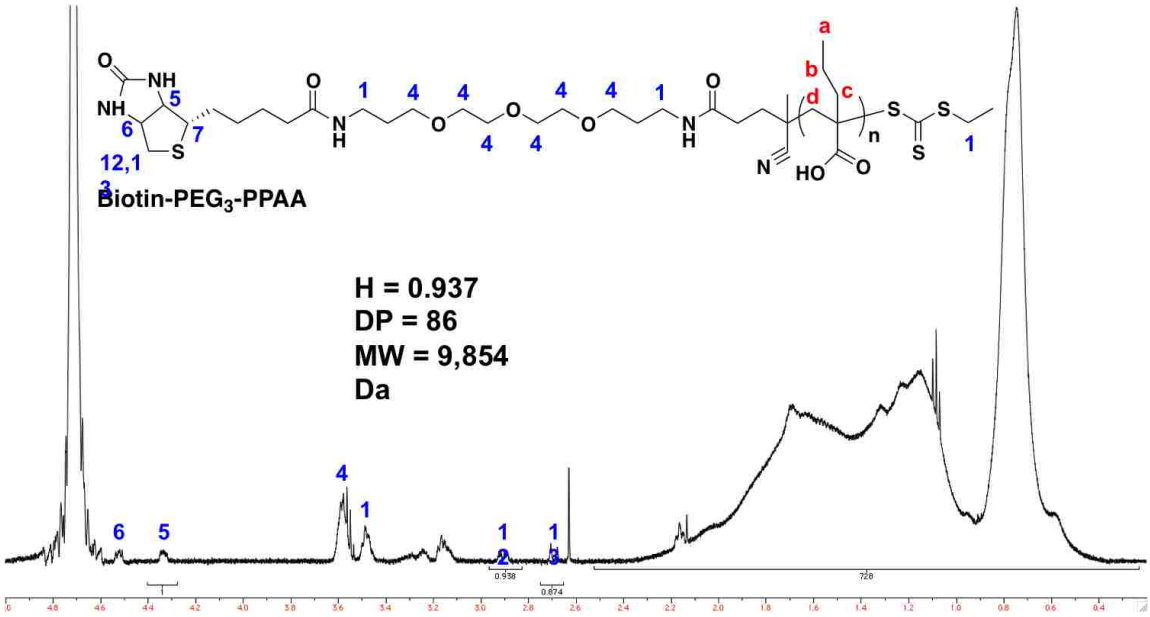

Figure 3.13: NMR spectrum of the btPEG-PPAA polymer

3.3.13 Characterization of PPAA by GPC

The PPAA polymer was also characterized by size-exclusion chromatography via gel permeation chromatography (GPC) (Figure 3.14). Three chromatograms are displayed in the figure collected by light scattering, refractive index, and UV spectrophotometry. The chromatogram indicates a polydisperse polymer always associated with the polymerization of the sterically bulky propylacrylic acid monomer. This polydispersity however is acceptable for RAFT synthesis and so the PPAA polymer was used for all subsequent studies.

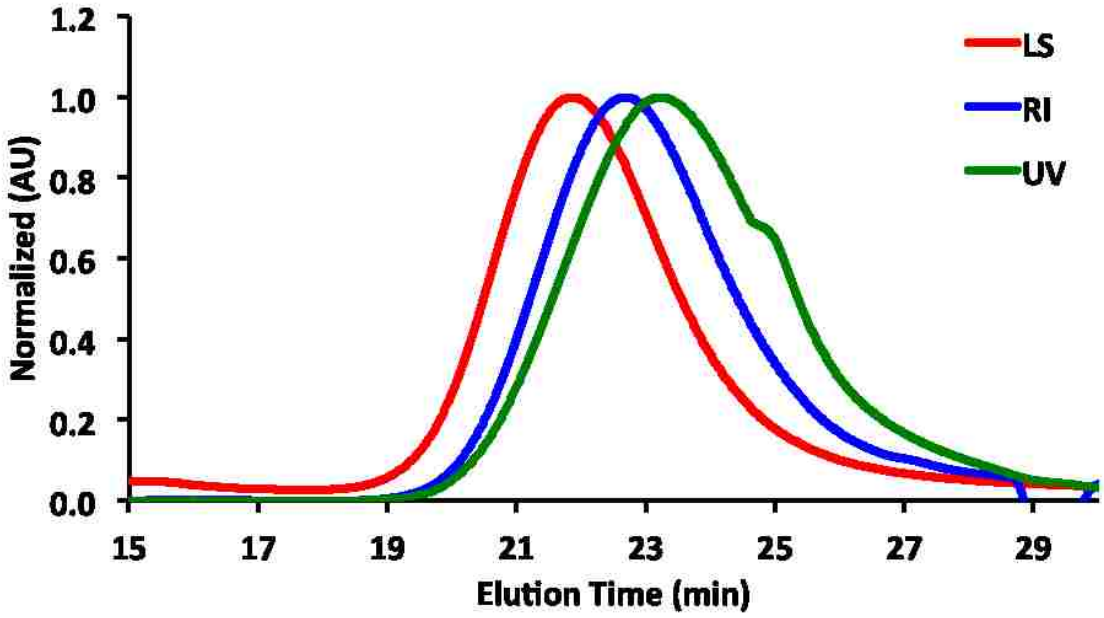

Figure 3.14: GPC chromatogram of btPEG-PPAA polymer following synthesis. The three overlaid chromatograms including light scattering (LI), refractive index (RI), and UV absorbance at 310 nm (UV)

3.3.14 Formulation of HD39/SA-PPAA-BIM conjugates

Conjugation of btBIM and PPAA with streptavidin and HD39/SA through the biotin-streptavidin linkage was quantified by a HABA assay. Using a biotin standard curve, the btBIM binding capacity with streptavidin was quantified (Figure 3.15 Left). btBIM bound to streptavidin with an 82% efficiency and biotin binding was found to increase linearly with concentration. Next the ability of PPAA to bind to streptavidin was quantified and showed a very high binding capacity (Figure 3.15 Right). Saturation of the biotin binding sites on streptavidin with PPAA was observed around 3.5 PPAA chains per streptavidin protein. The ability of HD39/SA to complex both the btBIM peptide and PPAA polymer was also measured (Figure 3.15 Center). In this study, HD39/SA was incubated with an equal molar ratio of btBIM peptide for one hour and binding was confirmed by HABA. Next, PPAA was added sequentially to the HD39/SA-BIM solution and biotin binding was again quantified by HABA absorbance. An excess of 4 PPAA polymers was needed to saturate all biotin binding sites on HD39/SA-BIM conjugates. This protocol was used to formulate the HD39/SA-PPAA-BIM conjugates for all the subsequent therapy studies both in vitro and in vivo.

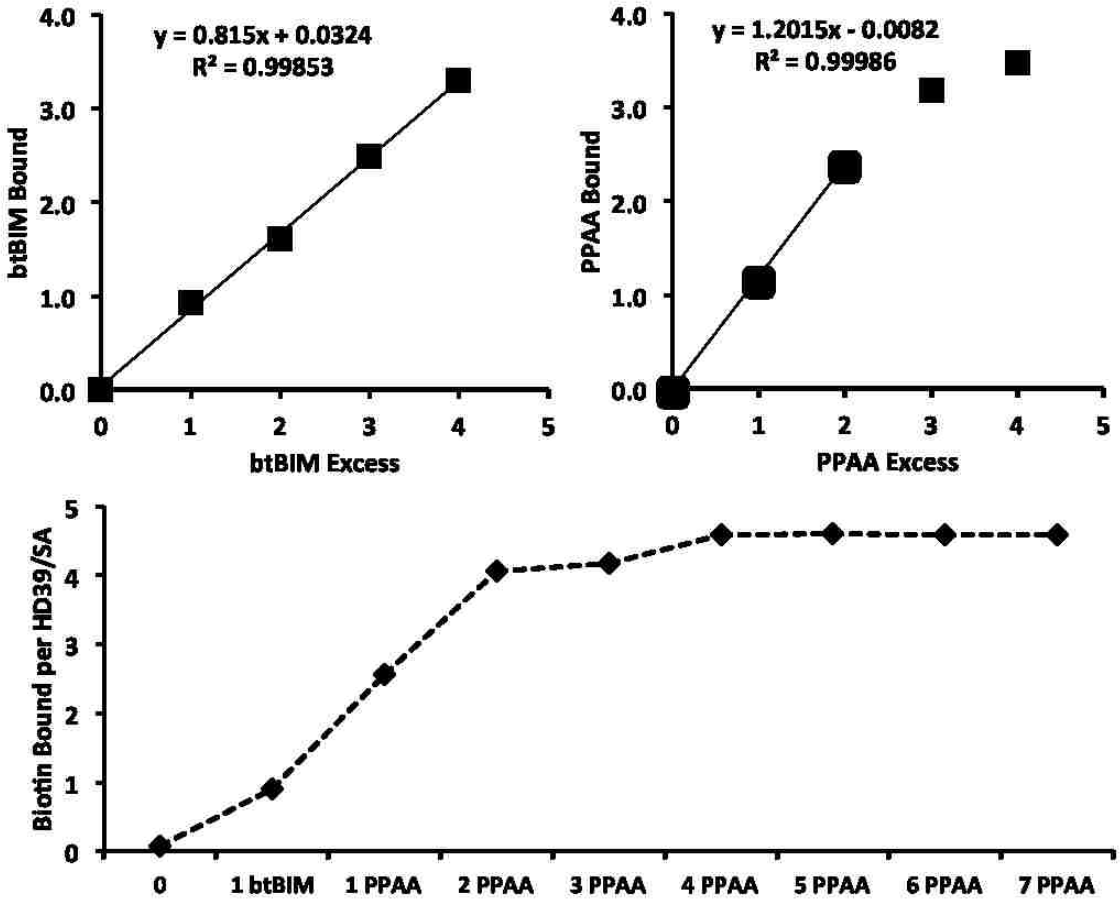

Figure 3.15: A HABA assay was used to confirm the streptavidin complexation ability of btBIM and the biotinylated PPAA. After confirming the binding capacity of each macromolecule, the two were complexed with HD39/SA sequentially until all biotin-binding sites were saturated.

3.3.15 HD39/SA-PPAA-btBIM induces cell death in RAMOS-AW cells

In the following in vitro study, RAMOS-AW cells were treated for 24 hours with staurosporine [5 μM], HD39/SA-PPAA, HD39/SA-btBIM or HD39/SA-PPAA-btBIM with HD39/SA kept at 3.9 μM with one equivalent BIM peptide per conjugate and three PPAA polymers per conjugate. After 24 hours, media was removed from suspension cells by centrifugation and cell viability was measured via MTS. Here we show that while HD39/SA with either BIM or PPAA does not exhibit any activity, the complete conjugate resulted in 40% cell death after 24 hours.

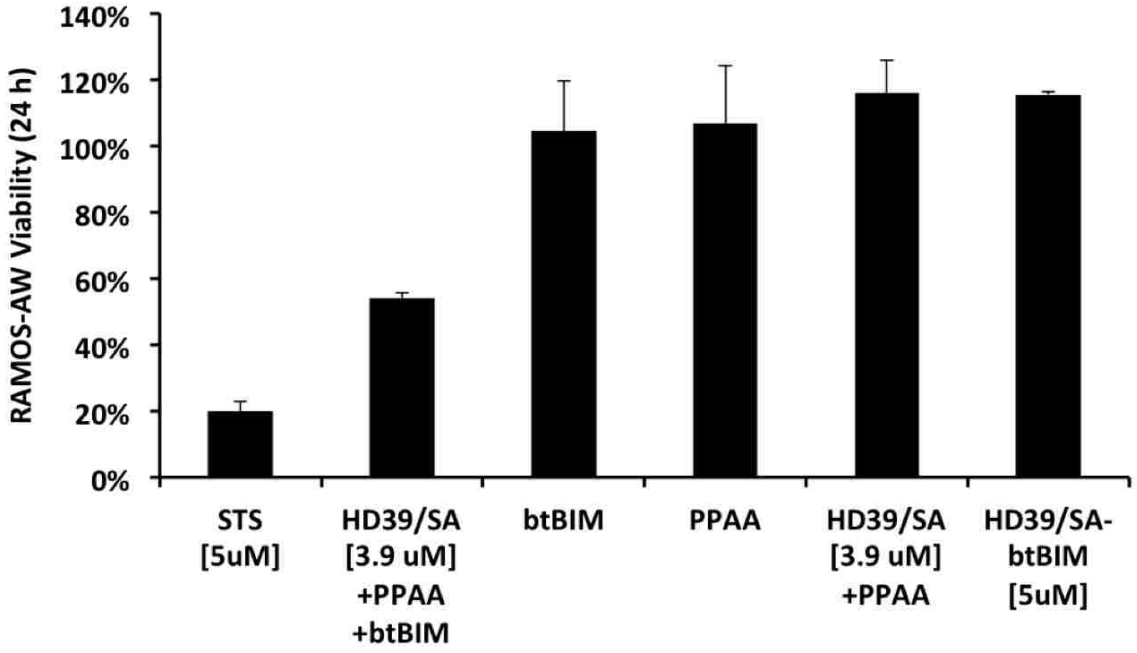

Figure 3.16: RAMOS-AW cells were treated with HD39/SA-PPAA-BIM as well as negative controls and staurosporine as a positive control. RAMOS-AW cell viability was measured after 24 hours of treatment using an MTS assay.

3.3.16 Acetylation of BIM peptide confirmed by mass spectrometry

Before radiolabeling the BIM peptide using ^{14}C-acetic anhydride, a protocol was developed to cap the N-terminus with acetic anhydride. After chemical modification, the peptide was lyophilized to remove free acetic anhydride. The acetylated btBIM peptide was confirmed by mass spectroscopy as shown in Figure 3.17. This reaction yielded 95% efficiency and was then applied to radiolabel BIM and btBIM with ^{14}C-acetic anhydride.

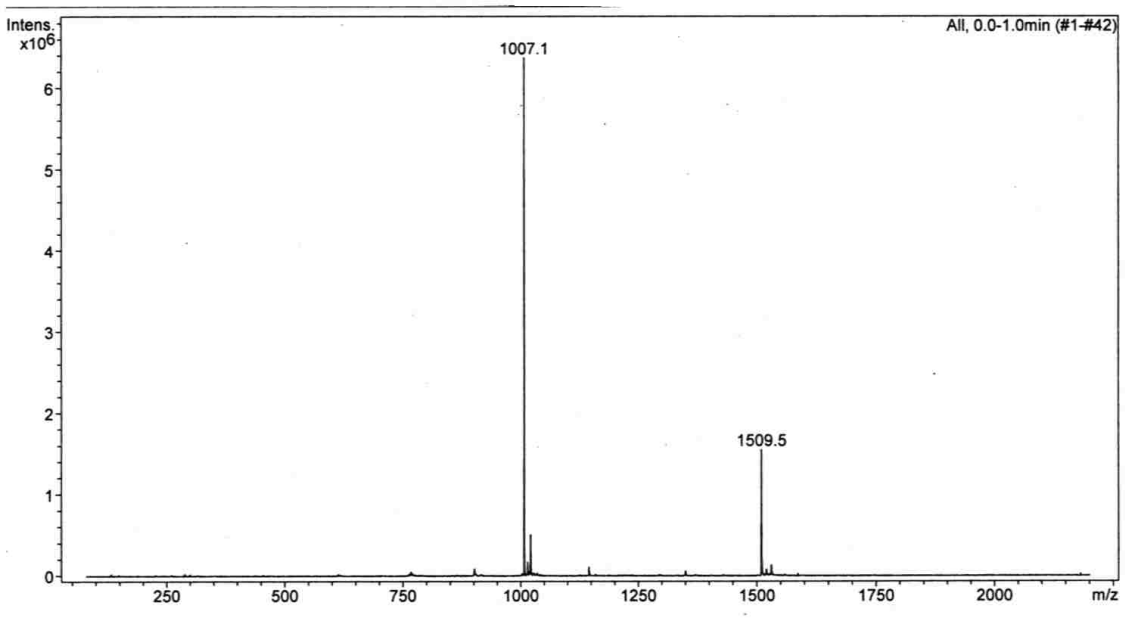

Figure 3.17: To confirm the radiolabeling protocol of btBIM with ^{14}C-acetic anhydride, we reacted btBIM with cold acetic anhydride, then confirmed N-capped acetylation by mass spectroscopy

3.3.17 Radiolabeled HD39/SA and BIM peptide

The HD39/SA conjugate contained 0.92 ^{3}H atoms per HD39/SA with a specific radioactivity of 273 μCi/mg. For in vivo studies, [^{3}H]-HD39/SA was spiked into cold HD39/SA for a final specific radioactivity of 8 μCi/mg. The BIM and btBIM peptides were efficiently labeled using ^{14}C-acetic anhydride via the N-terminus. Because the acetic anhydride is symmetrical, only half of the peptides were conjugated with the radioactive portion and thus contained 0.47 ^{14}C atoms per peptide. The specific radioactivity of the peptides was 7.89 mCi/mg.

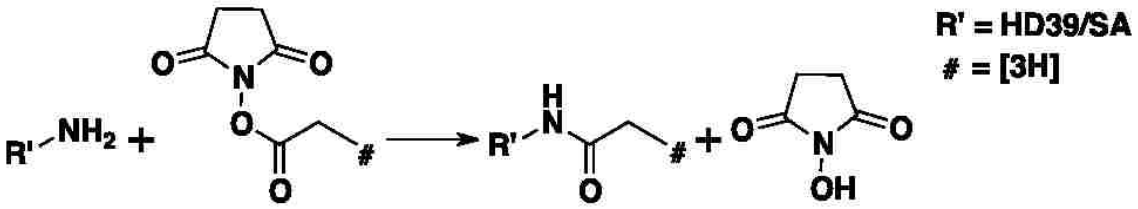

Figure 3.18: HD39/SA was labeled with [^{3}H using [^{3}H]-N-hydroxysuccinimidyl propionate through primary amines to form a stable amide linkage. The final reaction yielded 0.92 [^{3}H] per HD39/SA, with a specific radioactivity of 273 μCi/mg

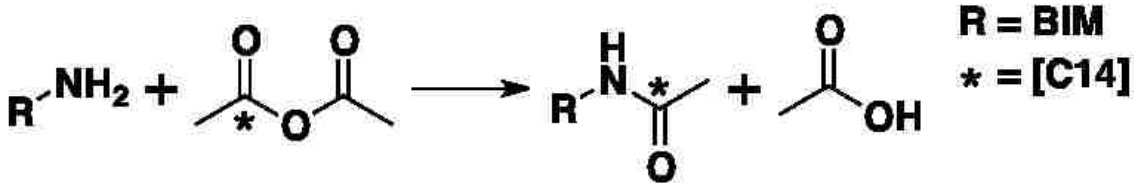

Figure 3.19: BIM peptide was labeled with [^{14}C]-acetic anhydride to acetylate the N-terminus. The final reaction yielded 0.47 [^{14}C] per peptide, with a specific radioactivity of 7,890 μCi/mg

3.3.18 Dual-Radiolabeled HD39/SA-PPAA-BIM Conjugates

Complexation of HD39/SA with [14C]btBIM and PPAA was confirmed with a HABA assay (Figure 3.20). More than 4 biotin-binding sites per HD39/SA were measured with a biotin standard curve because HD39 contains 1.2 streptavidin. First, an excess of 2 [14C]btBIM resulted in 0.8 binding events per HD39/SA. PPAA was then added stepwise until saturation of the remaining biotin binding sites was confirmed. Every 3 PPAA resulted in 1 biotin-binding event until HD39/SA-[14C]btBIM was saturated with 3-4 PPAA. Saturation of all accessible biotin-binding sites was confirmed by the addition of free biotin and no change in HABA signal. These results were also confirmed by scintillation counting. Unbound peptide and trace DMF were removed by spin filtration.

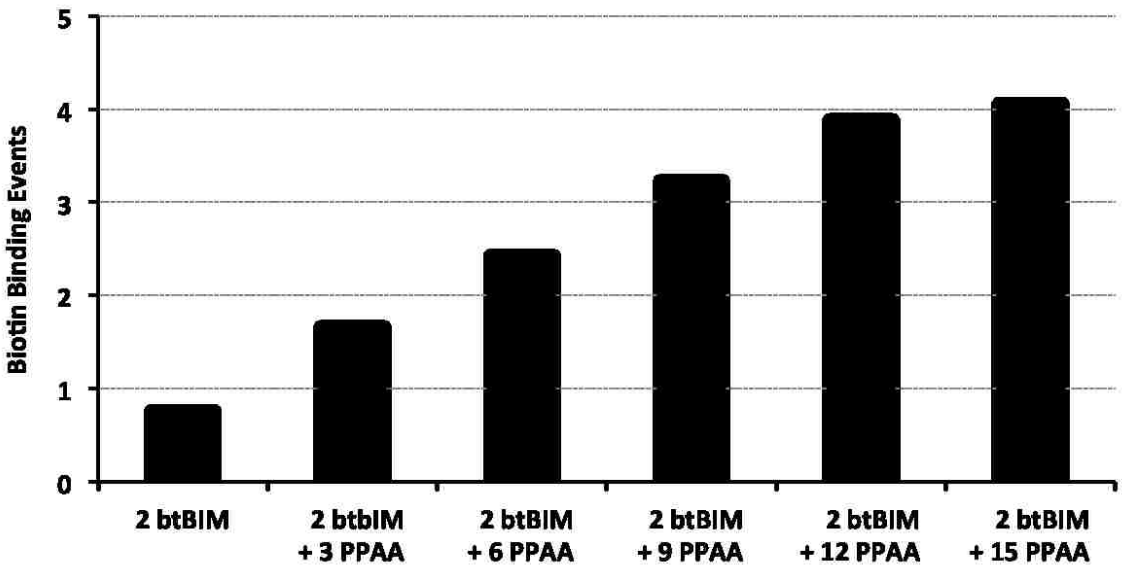

Figure 3.20: Formulation of the HD39/SA-PPAA-[14C]btBIM was confirmed with a HABA assay. First [14C]btBIM was added to saturate one biotin binding site on streptavidin. Next, PPAA was added to saturate the remaining biotin binding on HD39/SA.

3.3.19 Tumor Growth and Take Rate

The optimization parameters for tumor-xenografts are high tumor takes with slow tumor growth (100 mm^3 after 7-10 days). Tumor volume was measured in mice inoculated with 15M, 10M, or 5M RAMOS-AW cells over 11 days (Figure 3.21, Left). The percent of 10 mice bearing tumors for each cell concentration was also plotted in Figure 3.21, Right. 15M cells resulted in a tumor take rate of 100%, however the tumors had grown too large (more than 100 mm^3 by 7 days. Mice injected with 10M cells had a 71% take rate with tumors that were smaller than 100 mm^3 after day 7. 5M cells resulted in a tumor take rate of 50% and the slowest tumor growth. From these studies we concluded that 10M cells per mouse was an optimal cell number for a high tumor take rate and slow tumor growth in the following pharmacokinetic and biodistribution studies.

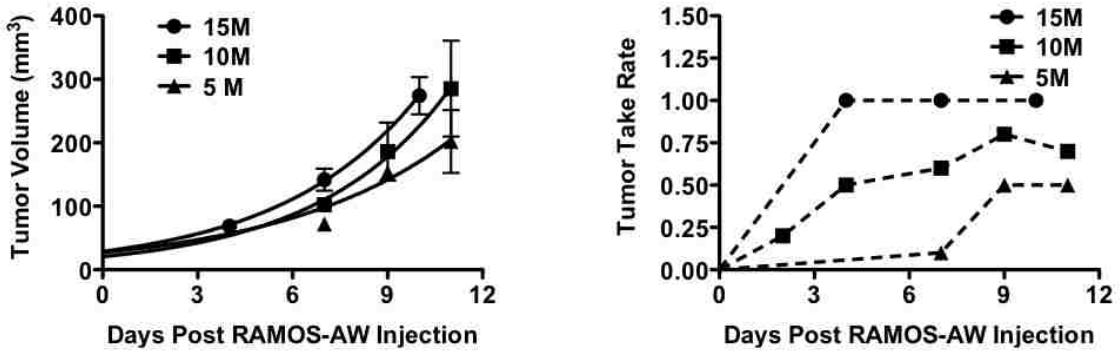

Figure 3.21: Tumor growth and take rate were measured following subcutaneous injection of RAMOS-AW cells in the right flank of BALB/c nude mice. Tumors were measured with calipers in the X, Y, and Z direction. The tumor growth rate from this study was used to select a cell injection concentration and conjugate administration day post cell injection.

3.3.20 Pharmacokinetics of Dual-Radiolabeled Conjugates

Tumor xenografts were formed by subcutaneous injection of 10M RAMOS-AW cells in the right flank of mice. After 7 days, tumors reached a size of 50 to 100 mm^3 and mice were injected with 1.4 nmoles of [^{14}C]BIM, [^{3}H]HD39/SA, [^{3}H]HD39/SA-[^{14}C]btBIM, or [^{3}H]HD39/SA-PPAA-[^{14}C]btBIM. Sequential blood samples were collected in triplicate through the retro orbital vein plexus. ^{3}H and ^{14}C activity were measured on a scintillation counter and the blood concentration level of each radiolabel was calculated and plotted as percent of injected dose (%ID) in Figure 3.22. The concentration of HD39/SA was stable over time and corresponded with previous studies using this antibody streptavidin conjugate. After 24 hours, the blood concentration had plateaued to 20% ID. The free peptide, BIM was cleared from the blood with 4.5% ID after 5 minutes and 1% after 24 hours. The HD39/SA-btBIM conjugates remained together for the first two hours after injection with an HD39/SA and btBIM concentration of 17% of the injected dose. After 2 hours the concentration of peptide in the blood reduced while the antibody concentration remained constant, indicating that the btBIM peptide was being cleaved from the conjugate. After 24 hours, 3% of the peptide and 12% of the antibody remained in the blood. HD39/SA-PPAA-btBIM was cleared from the blood before HD39/SA-btBIM, however the peptide to antibody ratio for HD39/SA-PPAA-btBIM remained the same. This suggests that the peptide linker is more stable with the polymer also bound. After 2 hours, the concentration of peptide and antibody was 9% but after 24 hours had decreased to 2%. The ratio of peptide to antibody in the blood was also calculated to assess peptide stability. For HD39/SA-btBIM, the peptide to antibody ratio rapidly decreased after 2 hours and eventually reached 1:4. For HD39/SA-PPAA-btBIM, the peptide was more stable in the blood and remained at 1:1. These results demonstrate that the BIM is rapidly cleared from the blood but it's bioavailability is increased on HD39/SA conjugate. Furthermore, PPAA on HD93/SA may help to increase the stability of the peptide

linker but also leads to complete clearance after 8 hours.

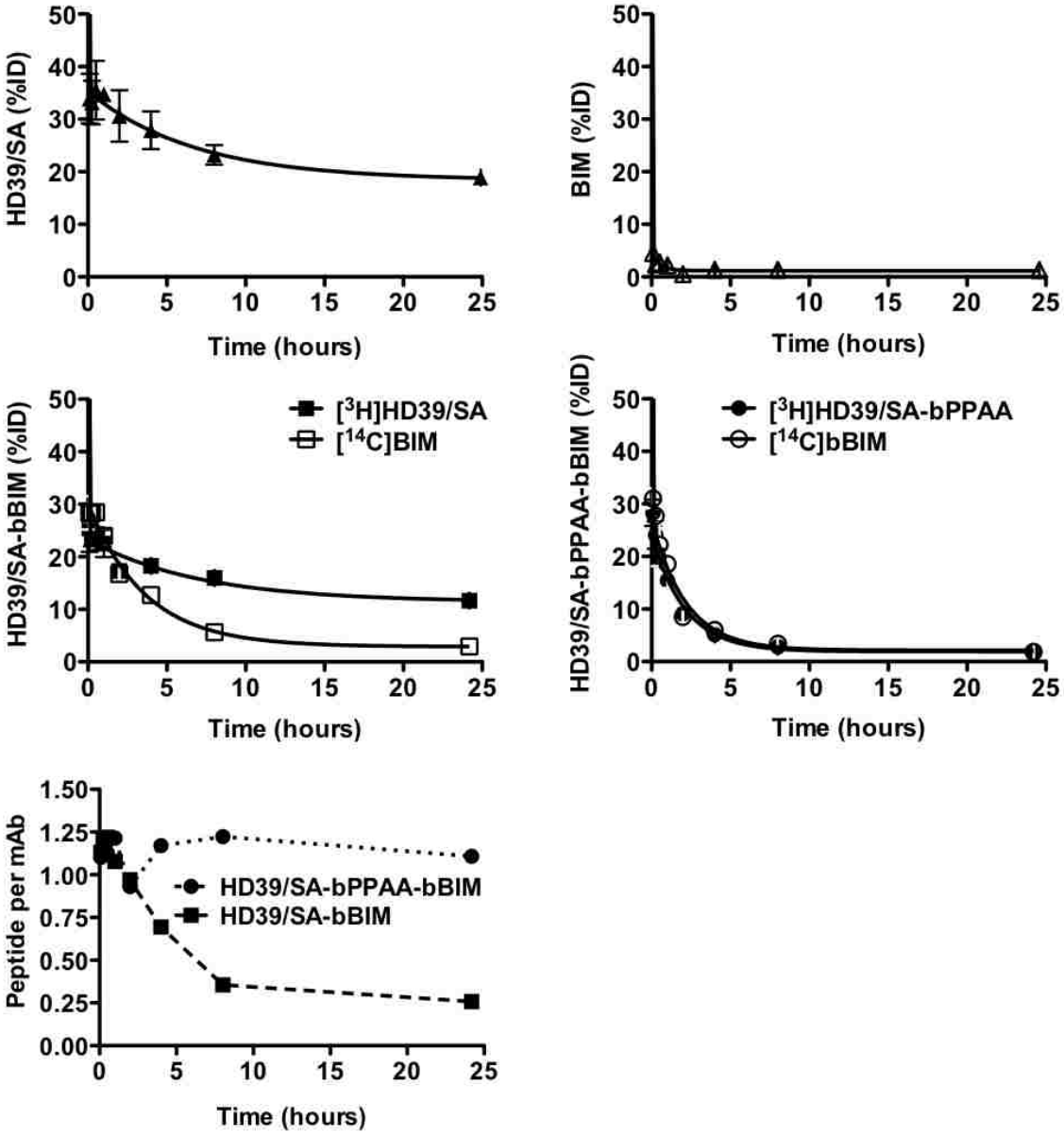

Figure 3.22: The pharmacokinetics of the dual-radiolabeled HD39/SA-PPAA-BIM conjugates was evaluated. The following treatments are HD39/SA (top left), BIM (top right), HD39/SA-BIM (middle left), and HD39/SA-PPAA-BIM (middle right). The ratio of BIM peptide on HD39/SA was compared with and without PPAA (bottom left) over time.

3.3.21 Biodistribution of Dual-Radiolabeled Conjugates

24 hours after injecting radiolabeled conjugates the mice were sacked and tissues processed. The percent of injected per gram (%ID/g) of tissue or blood was calculated and normalized by measuring ^{3}H and ^{14}C signal (below). In the first graph, the %ID/g of antibody was measured for HD39/SA, HD39/SA-BIM, and HD39/SA-PPAA-btBIM. HD39/SA alone was found at more than 10% in the blood and lungs, 5 10% in the liver, spleen and kidneys and 6% in the tumor tissue. This high concentration in the tumor agrees with previous biodistribution studies on the HD39/SA conjugate. For the HD39/SA-btBIM conjugate, the HD39/SA portion was found in all the same tissues as the free conjugate but in lower concentrations. This is likely due to a lower bioavailability in the blood as was demonstrated with the pharmacokinetic study from above. Interestingly, the HD39/SA portion of the HD39/SA-PPAA-btBIM conjugate was found at a lower concentration in all organs except the liver (10%) and spleen (8%). These concentrations are higher than the other two conjugate systems and are likely due to uptake by the scavenger receptor found on kupffer cells in both the liver and spleen. This receptor is known to bind and endocytose anionic polymers and proteins to remove them from the blood as a clearing mechanism. The next plot below describes the %ID/g of the BIM peptide or btBIM on HD39/SA or HD39/SA-PPAA. The free peptide does not appear at a high concentration in any organ likely because it was cleared by the kidney shortly after injection 24 hours before. The only organ with a large amount of btBIM peptide from the HD39/SA conjugate was the liver with 4% ID/g. The peptide concentration in the tumor was below 1% even though it's corresponding antibody was 4%, indicating the antibody only targeted the tumor after most of the peptide had reduced in the blood. The btBIM peptide on the HD39/SA-PPAA conjugate was found at 4% in the liver and 9% in the spleen. These high concentrations further confirm the uptake of the conjugate by kupffer cells found in both organs and the quick removal of the conjugate from the blood. The

peptide to antibody ratio of the two conjugates was also measured in each organ. For HD39/SA-btBIM, the peptide ratio was below 0.5 in all organs except the liver at 0.8. This higher loading ratio indicates the liver had taken the conjugate out of the blood before the peptide had reduced from the antibody. Most significantly however, the peptide ratio on for the HD39/SA-PPAA-btBIM conjugate was near 1 in the spleen, kidney, and stomach, 0.1 in the lung and 0.4 in the tumor. These high ratios further support the hypothesis that the polymer helped to stabilize the peptide in the blood, preventing rapid degradation of the peptide linker. The biodistribution results indicate that 6% of the HD39/SA is targeted to the tumor when normalizing tumor weight. The HD39/SA-PPAA-btBIM conjugate however is depleted from the blood and processed in the liver and spleen, reducing the blood circulation time and tumor targeting effects of the antibody.

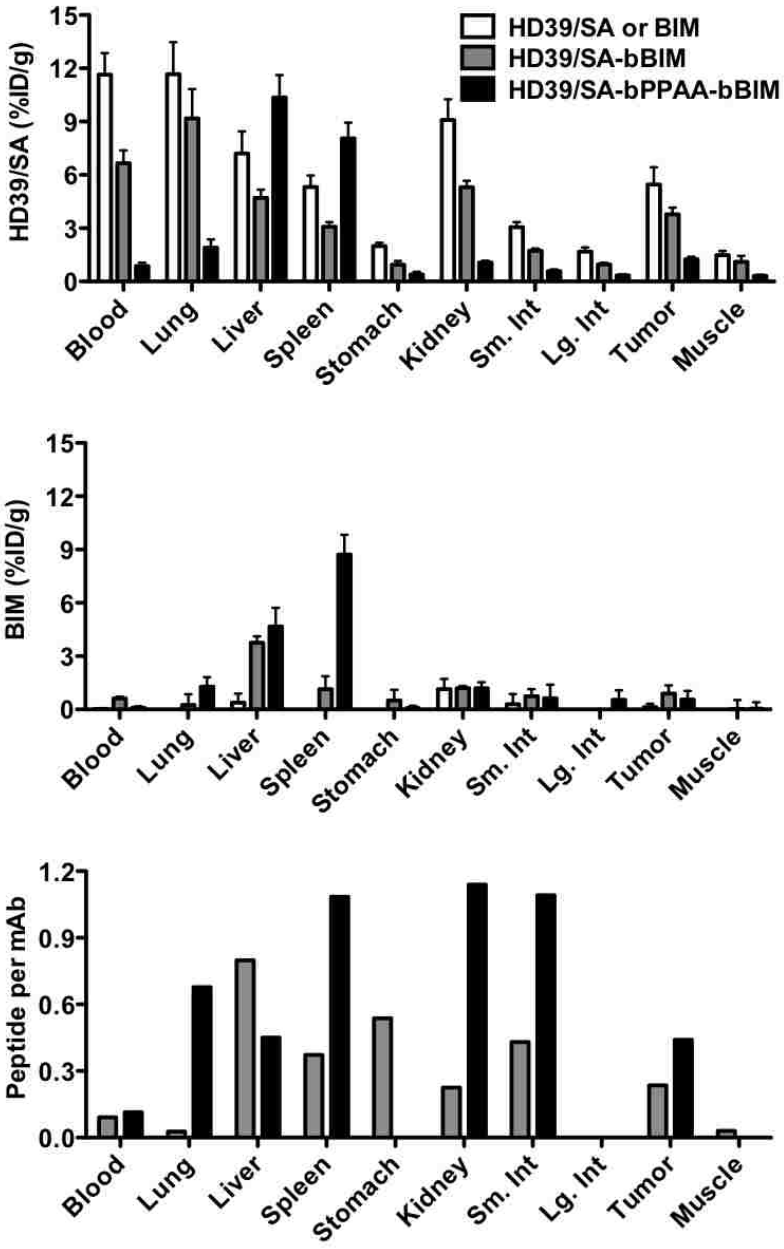

Figure 3.23: The biodistribution of dual-radiolabeled conjugates was evaluated after 24 hours following tail vein administration. HD39/SA and BIM were followed separately using 3H and 14C labeling, respectively. The % injected dose per gram of tissue (%ID/g) was evaluated in the blood, lung, liver, spleen, stomach, kidney, small intestine, large intestine, tumor and muscle. The relative dose of HD39/SA is described in the top plot, BIM in the middle plot and the ratio of Peptide per HD39/SA in the lower plot.

3.3.22 Evaluating the cause of PPAA depletion from the blood

Based on an extensive literature search, we hypothesized that the anionic polymer, PPAA, caused rapid uptake by scavenger receptors on kupffer cells found in the liver and spleen. Other labs that encounter this phenomenon have attempted to reduce scavenger receptor binding through two main mechanisms. The first is to inject or pretreat mice with free polymer 30 minutes prior in order to saturate scavenger receptors. The second and more common approach is to block scavenger receptor binding via blocking agents like fucoidan. Fucoidan is a sulfonated fucose polymer that specifically binds a family of scavenger receptors and is often used to inhibit macrophage binding in vivo. We hypothesized that using fucoidan as a blocking agent would improve the circulation time and increase tumor targeting of the complete conjugate.

Systemic delivery and pharmacokinetic parameters are key obstacles in the design of cancer-targeted conjugates. Conjugates are often unable to reach the active tumor site due to blood clearance by the liver. Scavenger receptors (SR) expressed on kupffer cells (KC) in the liver and spleen have evolved to recognize and endocytose pathogens, apoptotic cells and proteins. The SR also instigates the rapid depletion of anionic macromolecules through a receptor-mediated process. A number of strategies have been developed to prevent blood clearance of drug conjugates via depletion or knockout models and polyanions blocking agents. Gadolinium chloride is a rare earth metal used in animal models to prevent SR binding by eliminating the KCs altogether. For mechanistic studies, KC-depletion by GdCl3 has helped to understand gene delivery mechanisms, liver immunopathology with viral infections and bacterial binding within the liver[15–17]. For clinical therapies, GdCl3 may be more damaging than less invasive than other blocking techniques. Binding competition with polyanions has also been successful as a tool to increase blood circulation while reducing liver uptake. Takakura et al. demonstrated SR targeting with dextran sulfate (DS) at 1 mg/kg and complete

saturation at 100 mg/kg[18]. Coadministration of a model protein with succinylated-BSA (suc-BSA), maleylated-BSA (mal-BSA) or DS (20 mg/kg) resulted in a reduction of hepatic cell uptake by 95, 80, and 75%, respectively. Kawabata et al. used these same polyanions to alter the fate of negatively charged plasmid DNA. On its own, pDNA was quickly removed from the blood by the liver[19]. In competition, polyanions administered at 20 mg/kg 1 minute before pDNA increased plasma concentration and decreased liver uptake. Of the 5 macromolecules, DS was the most effective blocker, followed by mal-BSA and suc-BSA. Other sulfate-modified polysaccharides have been discovered from nature and used for SR inihibition. Fucoidan, a sulfate-modified polysaccharide has shown good SR blocking against a number of peptides and polymers.

It has been well established that strongly anionic macromolecules are recognized and rapidly endocytosed by scavenger receptors (SRs) found on kupffer cells in the liver. Blocking SRs with anionic macromolecules has been shown to prolong circulation and increase plasma concentrations of macromolecules and chemotherapeutic drugs in vivo. Biodistribution measurements show that pretreatment with DxSO results in a greater amount of antibody in the blood and a reduction in the liver and spleen. Fucoidan also resulted in a slight increase in the blood and a decrease in the liver but no effects in the spleen. DxSO and fucoidan appeared to also increase tumor concentration above PBS and Suc-BSA. For the future studies, DxSO will be selected as the optimal receptor blocker for therapeutic studies.

3.3.23 Succinylated-BSA

A series of succinylated BSA proteins were made for scavenger receptor blocking. An excess of 120, 240, and 360 succinic anhydrides were reacted with BSA and the number of free amines remaining on the protein were quantified with an OPA assay (Figure 3.24). An excess of 120, 240, and 360 succinc anhydrides reduced the number

of free amines from 60 to 30, 20, 20, respectively. The molecular weight of the succinylated BSA proteins was quantified using aqueous size exclusion chromatography. The experimental and theoretical molecular weights are shown in Table 3.1. These results confirm that the BSA proteins were modified and resulted in larger molecular weights. A decrease in the Suc120-BSA could be an artifact of running aqueous GPC. BSA tends to be a sticky protein especially when running through aqueous columns and small changes in the elution run from each batch could have resulted in a skew in the molecular weight down to 63,000 (experimental) in place of 69,000 (theoretical).

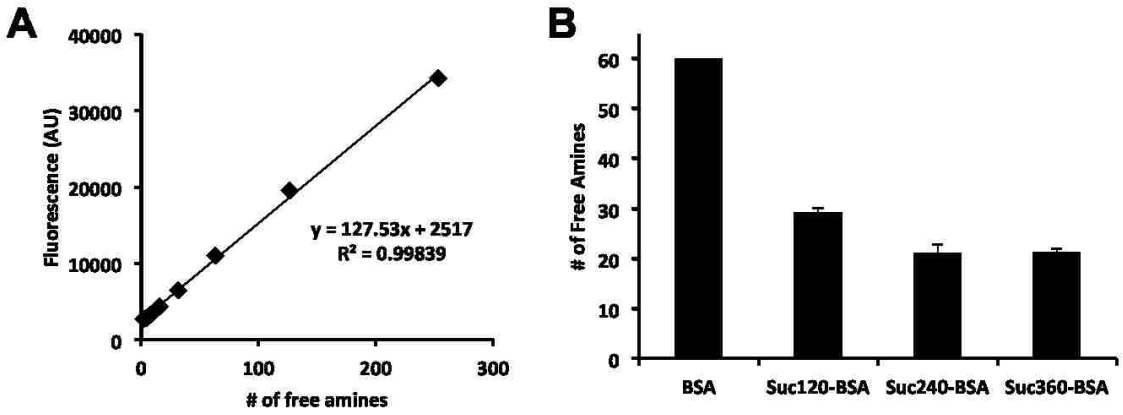

Figure 3.24: The number of free amines following succinylation of BSA with an excess of 120, 240, and 360 succinic anhydrides was confirmed with an OPA assay. (A) A standard curve demonstrates the linearity between free amines and fluorescence intensity. (B) The number of free amines after succinylation was quantified for each reaction.

	M_n (Theoretical)	M_n (Experimental)
BSA	66,500	67.1
Suc120-BSA	69,600	63,000
Suc240-BSA	70,400	69,600
Suc360-BSA	70,400	74,000

Table 3.1: The theoretical molecular weight was calculated based on the number of free amines after the reaction of BSA with succinc anhydride. Experimental molecular weight was measured on an aqueous gel-permeation chromatography system.

3.3.24 Pharmacokinetics of conjugates with scavenger receptor blockers

The pharmacokinetics of the dual-radiolabeled HD39/SA-PPAA-btBIM conjugates was evaluated over 8 hours post tail vein injection using a pretreatment of several different scavenger receptor blockers (50 mg/kg) and PBS alone (Figure 3.25). The dual-radiolabeled conjugates had a [3H] label on HD39/SA, and [14C] label on the btBIM peptide. In the first graph we see that the complete conjugate is cleared from the blood over the same 8 hours time time course as previously demonstrated. With 500 kDa dextran sulfate (DxSO), the conjugates remained in the blood at approximately 40% of the injected dose for the first 4 hours and then a decrease to 30% after 8 hours. Similarly, the btBIM and HD39/SA signal remained relatively close. Using fucoidan, an algae extract, the bioavailability was 50% of the injected dose after 1 hour, then eventually decreased down to 15% after 8 hours. With the succinylated-BSA (Suc-BSA) the conjugates had a high bioavailability at 50% for the first hour but eventually dropped to 10% after 8 hours. The comparison of the three scavenger receptor blockers demonstrated that DxSO exhibited the best block capability to increase the bioavailability of the conjugates. DxSO is known to saturate scavenger receptors upon in vivo administration and therefore the hypothesis that the conjugates are cleared by scavenger receptor binding to PPAA has been supported.

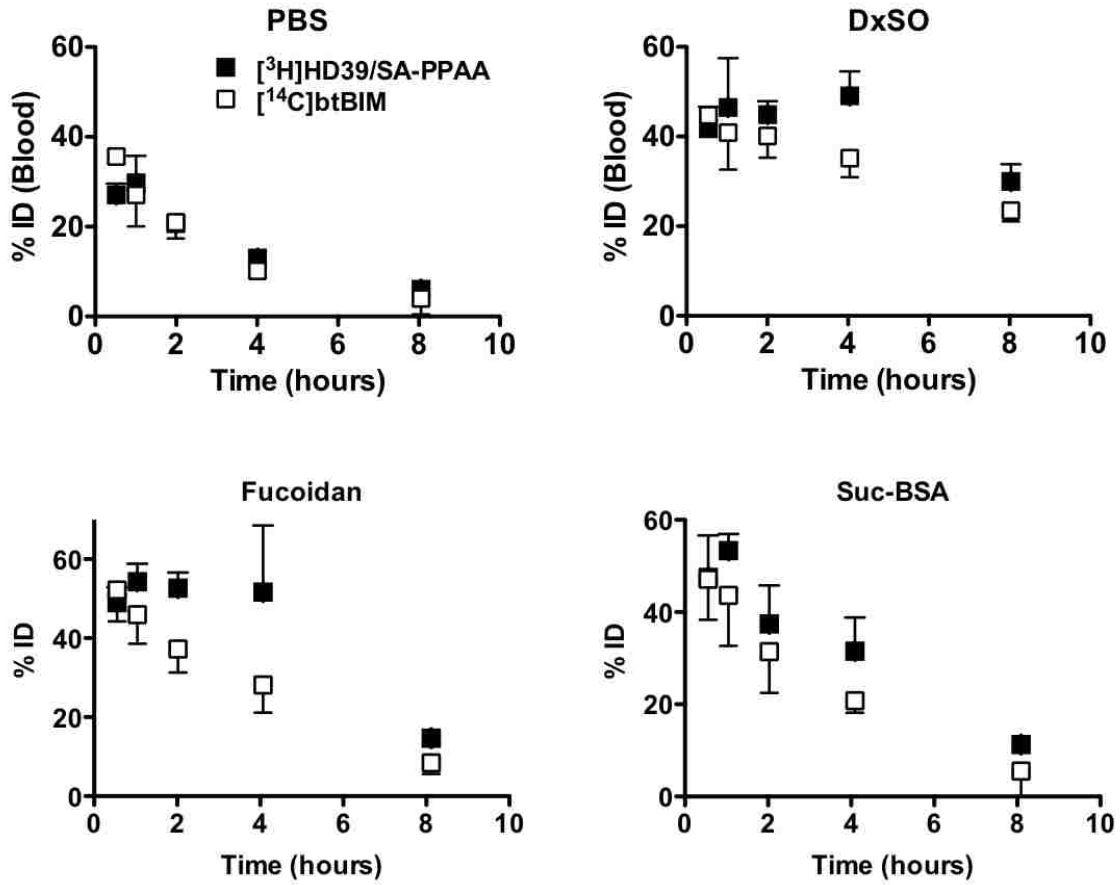

Figure 3.25: The pharmacokinetics or bioavailability of the conjugates was monitored over 8 hours following pretreatment with three different scavenger receptor blockers: dextran sulfate (DxSO), fucoidan, and succinylated-BSA (Suc-BSA), administered 30 minutes prior to conjugates via tail vein injection. Black squares represent the signal measured by [3H]HD39/SA ad white squares represent the signal measured by [14C]btBIM.

3.3.25 Biodistribution of conjugates with scavenger receptor blockers

Biodistribution of the conjugates in the blood, liver, spleen, and tumor were assessed by harvesting tissues and measuring the amount of [3H] and [C14] per gram of tissue (Figure 3.26). As was observed in the four groups by pharmacokinetics, the percent of conjugate in the blood was highest with DxSO pretreatment at 14% ID/g. All other pretreatments including PBS resulted in 5% ID/g after 8 hours. The DxSO group was also lowest in the liver but PBS exhibited the highest percentage. This result was expected considering each of the scavenger receptor blockers was designed to saturate the kupffer cells in the liver to an extent. In the spleen, the DxSO and SucBSA groups were lowest at 12% relative to PBS at 15%. In the tumor, the highest percentage of conjugate was experienced by fucoidan pretreatment at 2% ID/g.

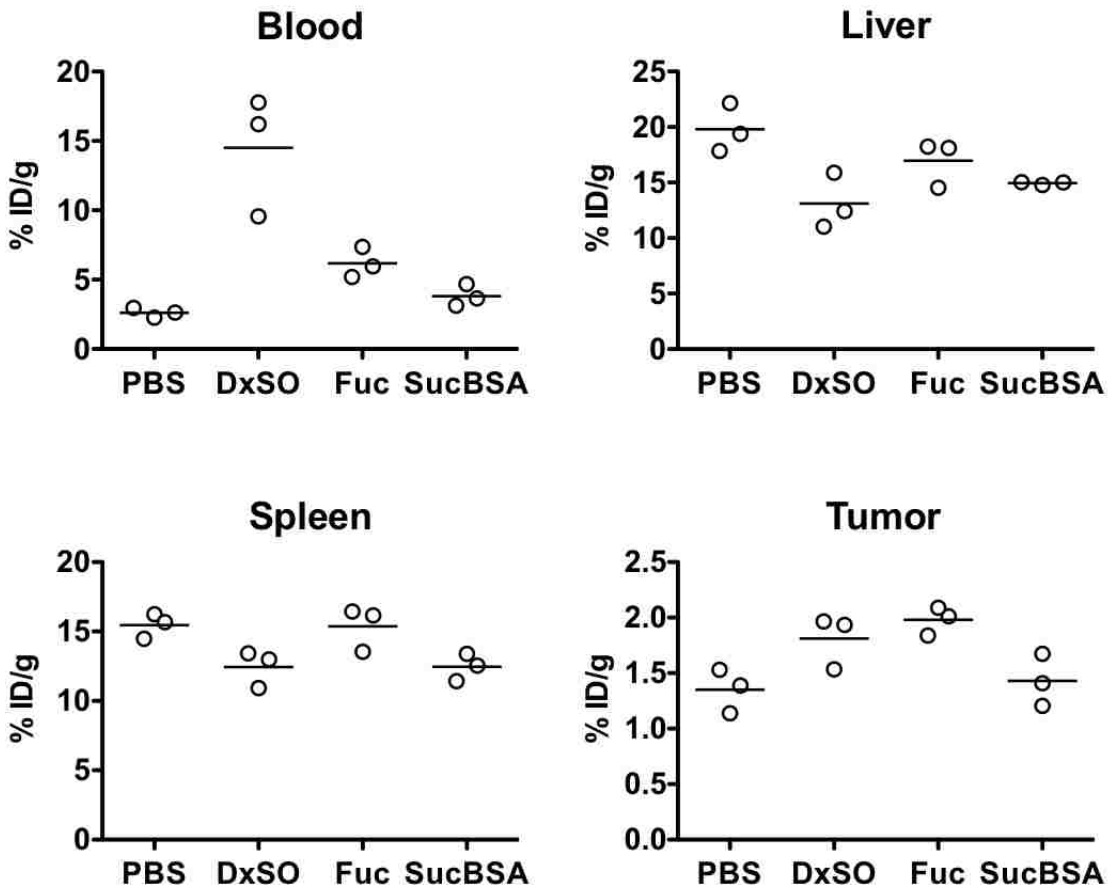

Figure 3.26: Biodistribution of the conjugates was quantified in the blood, liver, spleen, and tumor. The horizontal lines in each plot represent the mean collected from three mice per group. The y-axis denotes the percent injected dose per gram of tissue (%ID/g).

3.3.26 In Vivo Comparison of PPAA versus HPMA conjugates

After demonstrating that HD39/SA-PPAA-BIM was depleted from the blood by scavenger receptors in the liver, we determined if we could increase tumor targeting of the conjugate using the scavenger receptor blocker DxSO. Additionally, we wanted to use a second polymer biotin-HPMA-co-PDSMA-b-PDB (HP-PDB) with a neutral corona and biotin on the hydrophilic end to increase circulation of the antibody without a scavenger receptor blocker.

The pharmacokinetics of the two conjugate systems was measured over 24 hours (Figure 3.27). These results demonstrate that the HPMA diblock copolymer improves the blood half-life of [^{3}H]HD39/SA compared to PPAA with the DxSO pretreatment. After 24 hours, 40% of the HD39/SA-HPMA injected dose (ID) remained in the blood, while 20% ID of the HD39/SA-PPAA remained in the blood. The [^{3}H]HD39/SA-[^{14}C]BIM conjugates were initially made for another in vivo study and had been purified and stored at 4 oC for over a month. Over this time, if the BIM linker partially degraded a fraction of the peptide could have been free in solution. This phenomenon could explain why 40% of the peptide in both conjugates had cleared in the first 30 minutes. Nonetheless, 3 PPAA chains appeared to better protect the peptide linker from degradation compared with one HPMA polymer. There was a faster decrease in the blood concentration and peptide to mAb ratio. The diblock copolymer was designed to conjugate peptides directly to the polymer through functional PDS groups in the polymer, but this approach was not used for the sake of comparing the PPAA polymers to the neutral corona of HPMA. Future work may include the BIM peptide conjugated directly to the polymer through disulfide bonds.

A comparison of the biodistribution of the two polymer conjugates after 24 hours shows that in the blood, HPMA conjugates are at 15 %ID/g while PPAA conjugates are at 10 % ID/g (Figure 3.27). The use of DxSO significantly changed the biodistribution

of PPAA conjugates. The concentration in the blood increased from 1 to 10 %ID/g, concentration in the liver decreased from 11 to 5 %ID/g and the spleen decreased from 8 to 4 %ID/g. The concentration of HPMA conjugates in the liver and spleen was approximately the same as PPAA suggesting that the neutrality of the HPMA diblock copolymer does not promote scavenger receptor uptake. Finally, tumor targeted increased with the HPMA conjugates, with 1.3 %ID/g of PPAA conjugates and 2.4 %ID/g of HPMA conjugates in the tumor.

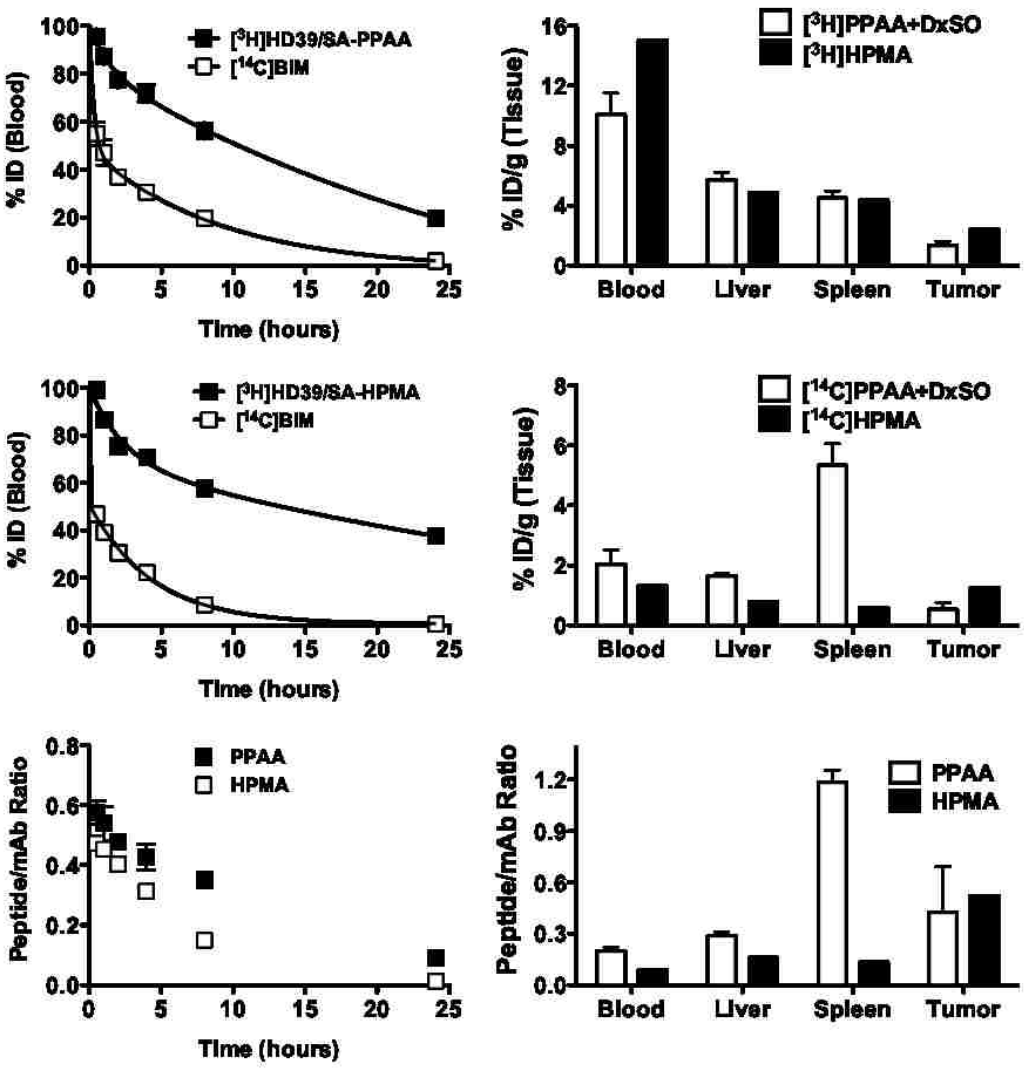

Figure 3.27: The pharmacokinetics and biodistribution of HD39/SA-PPAA-BIM with DxSO pretreatment was compared to a HD39/SA-HPMA-BIM conjugate where HPMA is a diblock composed of biotin-poly[(HPMA-PDSMA)-b-(PAA-DMAEMA-BMA)]. Blood circulation was measured for over 24 hours while tissues including blood, liver, spleen, and tumor were measured to calculate the %ID/g of tissue.

3.4 Conclusion

In this chapter, we explored the development of a unimeric antibody-polymer-peptide conjugate. Initially we synthesized a biotinylated diblock copolymer with an endosomolytic block consisting of PAA and a peptide conjugating block with pendent PDS groups that would complex with the antibody-streptavidin conjugate characterized in Chapter 2. After assembling the conjugates we found that the polymer was not hydrophilic enough to support multiple BIM peptides without crashing out of solution, therefore we pursued an alternative system. Using the HD39/SA-PPAA conjugates we developed in Chapter 2, we modified the BIM peptide with a biotin linker using a reducible disulfide bond. The biotinylated peptide was then complexed with HD39/SA at a 1:1 molar ratio and the remaining biotin binding sites were occupied by the PPAA polymer. This system was somewhat complex to assemble consistently and often the in vitro results were inconsistent, but because we achieved in vitro activity with the proapoptotic peptide on the HD39/SA-PPAA conjugates we pursued these conjugates in vivo. The pharmacokinetics and biodistribution studies revealed that although the disulfide linked peptide was stable in the presence of PPAA polymer chains, the PPAA caused the conjugates to be rapidly cleared from the blood by scavenger receptors found in the liver. To overcome this effect, we used scavenger receptor blockers described in the literature to saturate the receptors and increase the circulation time of the conjugates. While this method did improve the circulation there was little clinical significance this technique. Comparing PPAA conjugates to a more hydrophilic, neutral micelle, we found that the micelles out performed PPAA both in circulation and low distribution to organs. Development of this micelle carrier is described in further detail in Chapter 4.

3.5 References

[1] A G Polson, J Calemine-Fenaux, P Chan, W Chang, E Christensen, S Clark, F J de Sauvage, D Eaton, K Elkins, J M Elliott, G Frantz, R N Fuji, A Gray, K Harden, G S Ingle, N M Kljavin, H Koeppen, C Nelson, S Prabhu, H Raab, S Ross, D S Slaga, J-P Stephan, S J Scales, S D Spencer, R Vandlen, B Wranik, S-F Yu, B Zheng, and A Ebens. Antibody-Drug Conjugates for the Treatment of Non-Hodgkin's Lymphoma: Target and Linker-Drug Selection. *Cancer Research*, 69(6):2358–2364, March 2009.

[2] Peter D Senter. Potent antibody drug conjugates for cancer therapy. *Current Opinion in Chemical Biology*, 13(3):235–244, June 2009.

[3] K J Hamblett. Effects of Drug Loading on the Antitumor Activity of a Monoclonal Antibody Drug Conjugate. *Clinical Cancer Research*, 10(20):7063–7070, October 2004.

[4] Cyrille Boyer, Volga Bulmus, Thomas P Davis, Vincent Ladmiral, Jingquan Liu, and Sébastien Perrier. Bioapplications of RAFT Polymerization. *Chemical Reviews*, 109(11):5402–5436, November 2009.

[5] Cyrille Boyer, Jingquan Liu, Volga Bulmus, Thomas P Davis, Christopher Barner-Kowollik, and Martina H Stenzel. Direct Synthesis of Well-Defined Heterotelechelic Polymers for Bioconjugations. *Macromolecules*, 41(15):5641–5650, August 2008.

[6] Peter J Roth, Kerstin T Wiss, Rudolf Zentel, and Patrick Theato. Synthesis of Reactive Telechelic Polymers Based on Pentafluorophenyl Esters. *Macromolecules*, 41(22):8513–8519, November 2008.

[7] Geoffrey Y Berguig, Anthony J Convertine, Julie Shi, Maria Corinna Palanca-Wessels, Craig L Duvall, Suzie H Pun, Oliver W Press, and Patrick S Stayton. Intracellular Delivery and Trafficking Dynamics of a Lymphoma-Targeting Antibody–Polymer Conjugate. *Molecular Pharmaceutics*, 9(12):3506–3514, 2012.

[8] Maria C Palanca-Wessels, Anthony J Convertine, Richelle Cutler-Strom, Garrett C Booth, Fan Lee, Geoffrey Y Berguig, Patrick S Stayton, and Oliver W Press. Anti-CD22 Antibody Targeting of pH-responsive Micelles Enhances Small Interfering RNA Delivery and Gene Silencing in Lymphoma Cells. *Molecular Therapy*, 19(8):1529–1537, May 2011.

[9] Suzanne Flanary, Allan S Hoffman, and Patrick S Stayton. Antigen Delivery with Poly(Propylacrylic Acid) Conjugation Enhances MHC-1 Presentation and T-Cell Activation. *Bioconjugate Chemistry*, 20(2):241–248, February 2009.

[10] Suzanne Foster, Craig L Duvall, Emily F Crownover, Allan S Hoffman, and Patrick S Stayton. Intracellular Delivery of a Protein Antigen with an Endosomal-Releasing Polymer Enhances CD8 T-Cell Production and Prophylactic Vaccine Efficacy. *Bioconjugate Chemistry*, 21(12):2205–2212, December 2010.

[11] David Putnam. Polymers for gene delivery across length scales. *Nature materials*, 5(6):439–451, 2006.

[12] Daniel W Pack, Allan S Hoffman, Suzie Pun, and Patrick S Stayton. Design and development of polymers for gene delivery. *Nature Reviews Drug Discovery*, 4(7):581–593, July 2005.

[13] Craig L Duvall, Anthony J Convertine, Danielle S W Benoit, Allan S Hoffman, and Patrick S Stayton. Intracellular Delivery of a Proapoptotic Peptide via Conjugation to a RAFT Synthesized Endosomolytic Polymer. *Molecular Pharmaceutics*, 7(2):468–476, April 2010.

[14] Takakura Yoshinobu, Fujita Takuya, Furitsu Hisao, Nishikawa Makiya, Sezaki Hitoshi, and Hashida Mitsuru. Pharmacokinetics of succinylated proteins and dextran sulfate in mice: Implications for hepatic targeting of protein drugs by direct succinylation via scavenger receptors. *International Journal of Pharmaceutics*, 105(1):19–29, 1994.

[15] Naoki Kobayashi, Takeshi Kuramoto, Kiyoshi Yamaoka, Mitsuru Hashida, and Yoshinobu Takakura. Hepatic uptake and gene expression mechanisms following intravenous administration of plasmid DNA by conventional and hydrodynamics-based procedures. *Journal of Pharmacology and Experimental Therapeutics*, 297(3):853–860, 2001.

[16] Giovanni Sitia, Matteo Iannacone, Roberto Aiolfi, Masanori Isogawa, Nico van Rooijen, Cristina Scozzesi, Marco E Bianchi, Ulrich H von Andrian, Francis V Chisari, and Luca G Guidotti. Kupffer Cells Hasten Resolution of Liver Immunopathology in Mouse Models of Viral Hepatitis. *PLoS Pathogens*, 7(6):e1002061, June 2011.

[17] S Moein Moghimi, A Christy Hunter, and J Clifford Murray. Long-circulating and target-specific nanoparticles: theory to practice. *Pharmacological reviews*, 53(2):283–318, 2001.

[18] Yoshinobu Takakura, Ram I Mahato, and Mitsuru Hashida. Extravasation of macromolecules. *Advanced Drug Delivery Reviews*, 34(1):93–108, 1998.

[19] K Kawabata, Y Takakura, and M Hashida. The fate of plasmid DNA after intravenous injection in mice: involvement of scavenger receptors in its hepatic uptake. *Pharmaceutical Research*, 12(6):825–830, 1995.

Chapter 4

EVOLUTION OF POLYMER MICELLE CONJUGATES FOR ANTIBODY-TARGETED PEPTIDE DELIVERY

In the previous chapters, we developed an antibody-polymer-peptide conjugate for the intracellular delivery of proapoptotic peptides. Rapid blood clearance of the conjugates caused by binding to scavenger receptors led us to explore new polymer architectures in the form of micelles (20 η). A series of diblock copolymers were developed that could self-assemble into micelles with a hydrophilic shell and a hydrophobic core. The hydrophilic shell provided micelle stability with peptide- and antibody-loading modalities. The membrane destabilizing hydrophobic core exhibited endosomal escaping properties for intracellular delivery. Micelles were optimized for peptide-loading, antibody-targeting, and in vivo safety.

4.1 Introduction

The first diblock copolymers develop in this chapter were based on work by Convertine et al.[1,2]. for the intracellular delivery of siRNA. The first block (HP), contained the hydrophilic monomer hydroxypropyl methacrylate (HPMA) to impart micelle stability[3–5] and pyridyldisulfide methacrylate (PDSMA) for peptide conjugation[6–8]. The endosomol releasing segment (PDB) was a tercopolymer with propylacrylic acid (PAA), dimethylaminoethyl methacrylate (DMAEMA), and butyl methacrylate (BMA). PAA and DMAEMA are pH-sensing monomers with a pKa below physiological pH (7.4). At endosomal pH (6.6) the two monomers are protonated causing the polymer to undergoe a phase transition from self-assembled micelles to unimers. BMA is a hydrophobic monomer thought to interact with and disrupt the lipid bilayer of endosomes. While HP-PDB diblock copolymers have demonstrated good activity with siRNA, no peptide activity was achieved. The polymer concentrations required for peptide delivery exceed for those for siRNA, resulting in high polymer toxicity in B-cell lymphoma, ovarian and breast cancer Furthermore, the micelles stability was also compromised with high peptide loading.

To improve peptide-loaded micelle stability, reduce toxicity, and increase the circulation half-life of conjugates, a new series of diblock copolymers were formulated based on a poly(ethylene glycol) methyacrylate (PEGMA)-containing hydrophilic block. PEG polymers have demonstrated good safety profiles in humans and are approved by the food and drug administration[9–12]. Coating proteins and nanoparticles with PEG polymers has been proven to increase circulation times. Higher PEG densities, in the form of PEG brushes have also shown reduced toxicity due to steric hindrances and low permeability[13,14]. To maximize the desired effects of PEG in the diblock copolymer, we selected a PEGMA monomer with 19 ethylene glycol repeat units (M_n = 950 Da). Homopolymerization via using reversible additions-fragmentation chain

transfer (RAFT), resulted in a 15-mer repeat with a molecular weight up to 15,000 Da. Densely packed monomers were hypothesized to exhibit similar properties to a PEG brush as previously described.

The PEGMA homopolymer was used a macro chain transfer agent (CTA) for the synthesis of a PEGMA-PDB diblock copolymer. We aimed to increase micelle stability and reduce toxicity by replacing the HPMA monomer with PEGMA. Unfortunately, PEGMA also reduced the hemolytic activity of the PDB block. Low hemolysis is usually correlated with poor endosomal escaping properties. To increase endosomolytic activity of the micelles, the PDB block was replaced with diethylaminoethyl methacrylate (DEAEMA) and butyl methacrylate (BMA). Manganiello et al. previously studied the activity of these monomers and their feed ratios for plasmid delivery[15,16]. The "EB" block, as it was termed, with a feed ratio of 60:40 (DEAEMA:BMA) was found to be most active with minimal toxicity. For our studies, the PEGMA macroCTA was employed for the synthesis of PEGMA-EB diblock copolymers. A series of polymers were made by varying the degree of polymerization for the EB block and studying it's effects on micelle stability, hemolytic activity, in vitro toxicity, and maximum tolerated dose in a mouse model.

4.2 Experimental Section

4.2.1 Solid phase synthesis of BIM and BIM/LE peptides

Peptides were synthesized using Fmoc solid phase synthesis at a 0.1 mmole quantity. BIM and BIM-L62E (BIM/LE) peptides were synthesized on an arg preloaded NovaSyn resin (EMD Millipore) using the following sequences:

BIM NH2-CMRPEIWIAQELRRIGDEFNAYYARR-OH

BIM/LE NH2-CMRPEIWIAQEERRIGDEFNAYYARR-OH

Upon completion of peptide synthesis, peptide-loaded resin was rinsed sequentially with N-methyl-2-pyrrolidone, dimethylformamide, dichloromethane, and methanol, dried under vacuum, then cleaved and deprotected with a solution containing 9.4 mL trifluoroacetic acid, 250 μL dH20, 250 μL ethanedithiol, and 100 μL triisopropylsilane. Following resin filtration, crude peptide was precipitated into cold ether/hexane (60/40), dissolved in ddH20 containing TCEP then purified by reverse-phase high performance liquid chromatography on a Jupiter 5um C18 300 column (Phenomenex). HPLC purified peptides were confirmed by ion trap mass spectrometry.

4.2.2 Cytochrome c release induced by BIM peptide

The ability of BIM and BIM/LE to induce cytochrome c release from isolated mitochondria was confirmed by an ELISA assay. Ramos cells (5 x 108) were grown in 3-tier culture flasks, transferred to tubes, washed with PBS and equilibrated with 5 mL of homogenization buffer (0.25 M sucrose, 1 mM EGTA, 10 mM HEPES/NaOH, 0.5% BSA, pH 7.4) for 5 minutes at 4°C. Cells were then homogenized under high nitrogen pressure using a sealed steel container for 10 min at 400 psi, 4°C. Disruption of cell membranes was confirmed with Trypan blue under a microscope. Cells were collected

and centrifuged for 10 min at 750 g in 15 mL round bottom tubes (BD (35)2059). After lipids were removed from the surface, the supernatant was transferred to a new vial and centrifuged for 12 minutes at 12,000 g, 4°C. The mitochondria pellet was resuspended in 500 uL of wash buffer (0.25 M sucrose, 1 mM EDTA, 10 mM Tris/HCl, pH 7.4, supplemented with protease inhibitor (Roche Complete minitablets) and placed on ice. Next, a BCA assay was performed to measure total protein. 15 μL of mitochondria solution was collected and added to 15 uL of 0.6% SDS, then heated for 10 minutes at 95°C. 10 μL of BSA at 0, 0.5, 1, 1.5, and 2 mg/mL and 5 uL 0.9% SDS was added to a 96 well plate and 4, 10, an 15 μL of mitochondria/SDS solution was added to the plate and equilibrated with dH20. 100 μL of bichonic acid/copper(III) sulfate (50/1) was added to each well and incubated for 50 minutes at 37°C. The BSA standards were used to make a standard curve and measure the total protein in the mitochondria solution. Finally, peptides in DMSO (1 mM) were incubated with 50 ug of mitochondria in 100 μL of experimental buffer (125 mM KCl, 10 mM Tris-MOPS [pH 7.4], 5 mM glutamate, 2.5 mM malate, 1 mM KPO4, 10 μM EGTA-Tris, pH 7.4) for 35 minutes at 37°C. Solutions were then centrifuged at 13,000 rpm for 10 minutes, 4°C, and supernatant was collected for Western Blot analysis.

4.2.3 Gel-permeation chromatography

Gel-permeation chromatography (GPC) was used to determine number average (Mn) molecular weight and polydispersity (PDI) of the polymers using Tosoh SEC TSK GEL α-3000 (X2) and α-4000 (X1) columns (Tosoh Bioscience, Montgomeryville, PA) connected in series to a 1200 Series liquid chromatography system (Agilent, Santa Clara, CA) and a miniDAWN TREOS three-angle light scattering instrument with an Optilab TrEX refractive index detector (Wyatt Technology, Santa Barbara, CA). HPLC-grade DMF containing 0.1 wt% LiBr at 60°C was used as the mobile phase at a flow rate of 1 mL/min. Reverse-phase high performance liquid chromatography

(RP-HPLC) was used to measure monomer conversions for each macroCTA using aliquots collected at To and Tx.

4.2.4 Synthesis of poly(HPMA-PDSMA) macroCTA

The multifunctional HPMA-PDSMA diblock copolymer was synthesized as a macro chain transfer agent (macroCTA). The polymerization was conducted with an initial molar ratio of HPMA to PDSMA at 9:1. HPMA was dissolved in ultrapure water (5.87 g). Biotinylated 4-cyano-4-(ethylsulfanylthiocarbonyl)sulfanylvpentanoic acid (biotin-ECT) was dissolved in ethanol. The initiator solution was prepared by dissolving V70 in ethanol. PDSMA was dissolved in ethanol. Ethanol solutions were combined and added to the aqueous HPMA solution in a 25 mL round-bottom flask. The final solvent ratio was 2:1, water to ethanol. The solution was purged with nitrogen for 30 min on ice and allowed to react at 70°C for 4 h. The resultant polymer was isolated by repeated precipitation from ethanol into an excess of ether. The polymer was rinsed after final precipitation with pentane to remove excess ether and dried overnight in a vacuum oven. The macroCTA was characterized by SEC to be 14,700 g/mol with a PDI of 1.07 from the measured dn/dc of 0.091. 1H NMR was used to determine the composition of 87% HPMA and 13% PDSMA by evaluating the peak at 3.9 ppm and aromatic peaks at resonances between 7 and 8.5 ppm for HPMA and PDSMA, respectively.

4.2.5 Synthesis of poly[(HPMA-PDSMA)-b-(PAA-DMAEMA-BMA)]

Poly[(HPMA-PDSMA)-b-(PAA-DMAEMA-BMA)] was prepared by adding the poly-(HPMA-co-PDSMA) macroCTA (0.638 g, 43.3 μmol) to a solution of BMA (0.861 g, 6.06 mmol), DMAEMA (0.715 g, 4.55 mmol), and PAA (0.519 g, 4.55 mmol) (40:30:30 mol %) in dimethylformamide (DMF) (5.076 g) such that the final solvent concentration

was 65% by weight. The initial macroCTA to V70 initiator (5.3 mg, 17.3 ?mol) ratio ($[macroCTA]_o/[I]_o$) and initial monomer to macroCTA ([M]o/[macroCTA]o) were 2.5:1 and 350:1, respectively. The polymerization solution was purged with nitrogen for 30 min before being allowed to react at 30°C for 24 h. The final polymers were isolated by precipitation from ethanol into a 50-fold excess of pentane/ether (3:1 v/v). The polymer precipitant was rinsed with neat pentane and dried under vacuum overnight. The polymer was dissolved in deionized water and further purified by passing them through PD10 desalting columns. The final dry polymer was obtained via lyophilization. The diblock copolymer was characterized by SEC to be 35 000 g/mol with a PDI of 1.80 from the measured dn/dc of 0.081. 1H NMR was used to determine the composition of the second block.

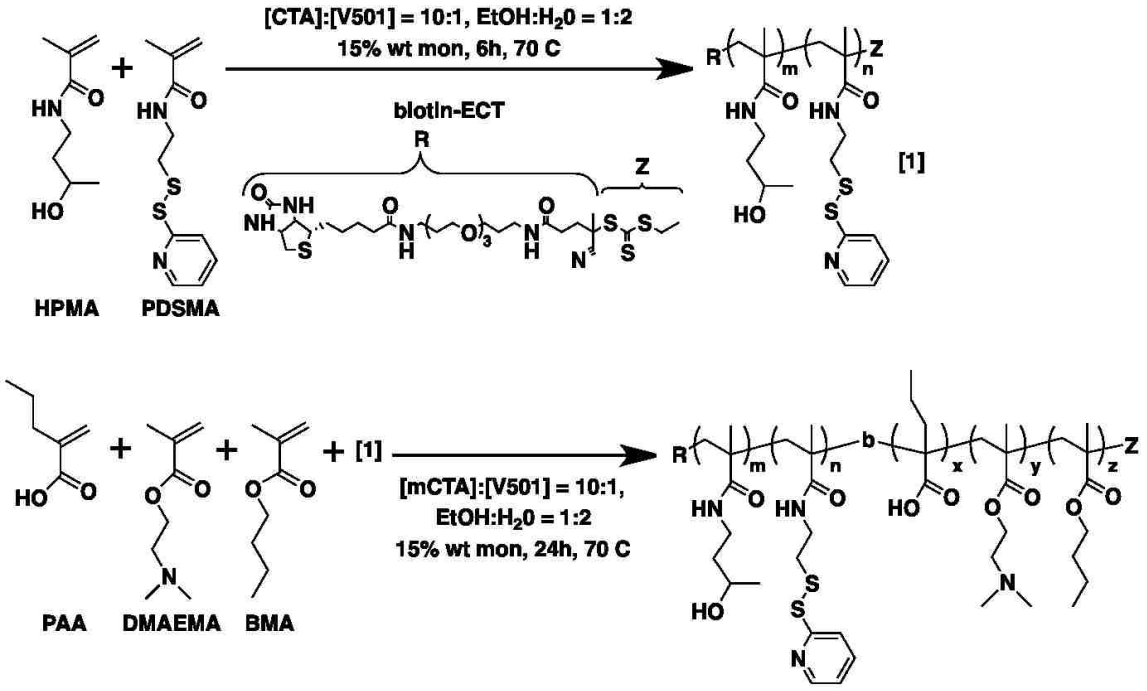

Figure 4.1: The HPMA-PDSMA macroCTA was first synthesized by RAFT using the biotin-ECT chain transfer agent and the initiator V501. After purification, the macroCTA was subsequently polymerized with PAA, DMAEMA, and BMA to form a diblock copolymer.

4.2.6 Synthesis of poly(PEGMA)

A series of Poly(polyethylene glycol methacrylate) polymers were synthesized via RAFT to serve as macroCTAs for subsequent polymerizations. In the reaction Azobis-(4-cyanopentanoic acid) (ABCVA) was used as the initiator and 4-cyanopentanoic acid dithiobenzoate (CTP) as the chain transfer agent (CTA), with 20 wt% monomer in dimethylacetamide. The initial monomer ($[M]_o$) to CTA ($[CTA]_o$) to initiator ($[I]_o$) ratios for the three polymers was 25:1:0.2 or 50:1:0.2. Solutions were vortexed in 20 mL scintillation vials, transferred to septa-sealed 10 mL round bottom flasks, purged under N_2 for 30 minutes, and transferred to a preheated water bath at 70°C for various time points. The resultant polymers were isolated by precipitation in diethyl ether. The precipitated polymers were then dissolved in acetone and precipitated into diethyl ether (x6). The dried polymers were analyzed by 1H NMR to assess purity and gel-permeation chromatography (GPC) was used to determine number average (M_n) molecular weight and polydispersity (PDI) of the polymers.

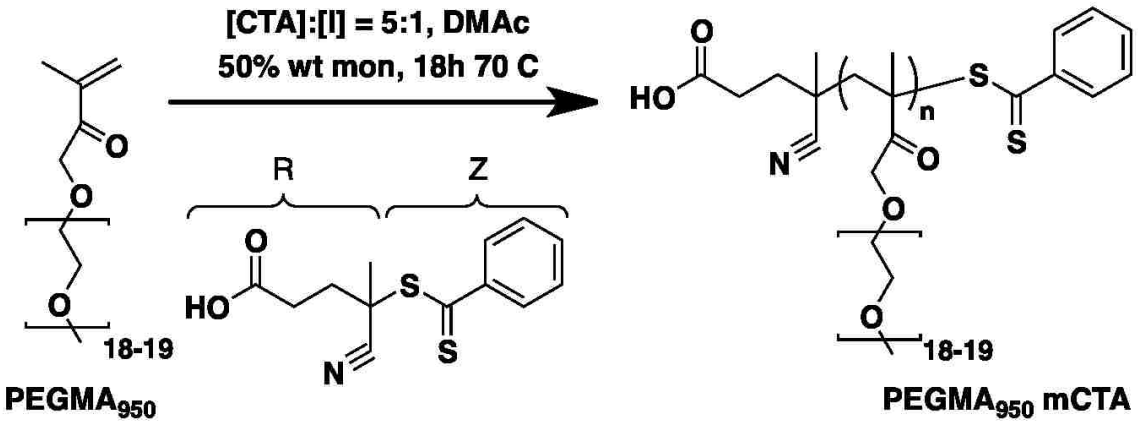

Figure 4.2: RAFT polymerization was used to synthesize a macroCTA composed of Polyethylene glycol methacrylate (950 Da) ($PEGMA_{950}$) as the monomer, V501 as the initiator, and dimethylacetamide as the solvent.

4.2.7 Synthesis of poly[(PEGMA)-(PAA-DMAEMA-BMA)]

Poly[(PEGMA)-b-(PAA-DMAEMA-BMA)] was prepared by adding the poly-(PEGMA) macroCTA to a solution of BMA (0.166 g, 1.17 mmol), DMAEMA (0.137 g, 876 μmol), and PAA (0.100 g, 876 μmol) (40:30:30 mol %) in dioxane such that the final solvent concentration was 50% by weight. The initial macroCTA to V501 initiator (5.3 mg, 17.3 ?mol) ratio ([macroCTA]o/[I]o) and initial monomer to macroCTA ([M]o/[macroCTA]o) were 5:1 and 300:1, 200:1, or 100:1, respectively. The polymerization solutions were purged with nitrogen for 30 min before being allowed to react at 70°C for 24 h. The final polymers were isolated by precipitation from dioxane into a 10X excess of diethyl ether. The polymer precipitant was rinsed with diethyl ether and dried under vacuum overnight. The polymer was dissolved in deionized water and further purified by passing them through PD10 desalting columns. The final dry polymer was obtained via lyophilization. The diblock copolymer was characterized by SEC and 1H NMR to determine composition of the second block.

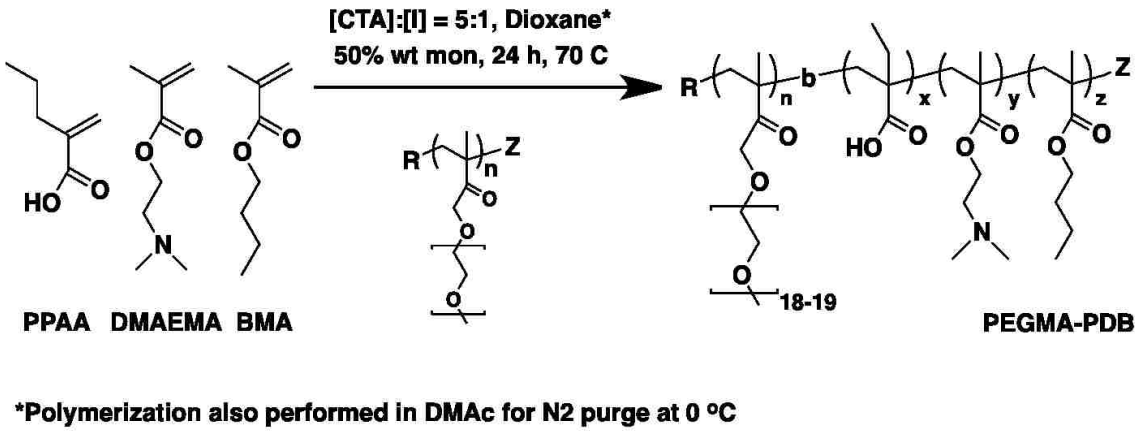

Figure 4.3: The PEGMA polymer synthesized in the previous step was used as the RAFT macroCTA while propylacrylic acid, dimethylethyl methacrylate, and butyl methacrylate were used as the monomers to form a statistical copolymer second block for endosomolytic activity.

4.2.8 Synthesis of poly[(PEGMA)-b-(DEAEMA-BMA)]

Poly[(PEGMA)-b-(DEAEMA-BMA)] was prepared by adding the poly(PEGMA) macroCTA to a solution of DEAEMA and BMA (60:40 mol %) in dimethylacetamide (DMAc) such that the final solvent concentration was 50% by weight. The initial macroCTA to V501 initiator (5.3 mg, 17.3 μmol) ratio ($[\text{macroCTA}]_o/[\text{I}]_o$) and initial monomer to macroCTA ([M]o/[macroCTA]o) were 5:1 and 50:1, 100:1, 150:1, 200:1, or 300:1, respectively. The polymerization solutions were purged with nitrogen for 30 min before being allowed to react at 70°C for 24 h. The final polymers were isolated by precipitation from dioxane into a 10X excess of petroleum ether. The polymer precipitant was rinsed with petroleum ether and dried under vacuum overnight. The polymer was dissolved in deionized water and further purified by lyophilization. The diblock copolymer was characterized by SEC and 1H NMR to determine composition of the second block.

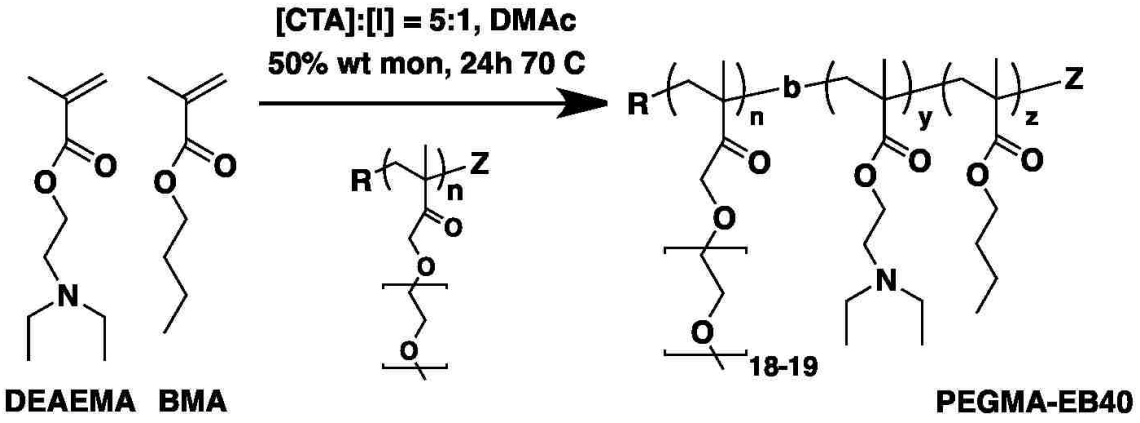

Figure 4.4: The PEGMA polymer synthesized in the first step was used as the RAFT macroCTA while diethyl methyl methacrylate and butyl methacrylate were used as the monomers to form a statistical copolymer second block for endosomolytic activity.

4.2.9 Monomer conversion by HPLC

Determination of monomer conversion by 1H-NMR was inconclusive because the vinyl resonances of the two methacrylate-based comonomers could not be distinguished. To measure monomer conversion we developed a new method using reverse-phase high-performance liquid chromatography (RP-HPLC). RP-HPLC was performed using a Finnigan Surveyor LC Pump Plus with UV-Vis Detector and a 250 mm Vydac 218TP C18 5μ column (Part 218TP52). 10 uL of the polymer reaction were collected before (T_o) and after (T_x) polymerization, then diluted 500x in a solution of hexafluoro-2-propanol (50%), methanol (25%), ddH_2O (25%), and trifluoroacetic acid (TFA 0.1%). With a 20 μL sample loop on a manual injector, samples were injected and run using ddH20 (0.1% TFA) as the aqueous phase and acetonitrile (0.1% TFA) as the organic phase. A gradient was set from 5% to 95% acetonitrile over 12 minutes and UV absorbance was measured at 220 nm to observe the vinyl species in each monomer. The percent monomer conversion was measured by integrating the absorbance peak to find the area under the curve (AUC) and the following equation $(1\text{-}(AUC_{TX}/AUC_{TO})\times 100)$.

4.2.10 Preparation of micelles in aqueous buffer

To prepare polymer micelles in aqueous buffer, dried polymer was weighed into 1.5 mL eppindorf tubes then dissolved with ethanol at 100 mg/mL. After vigorous mixing by vortexing and sonication, polymers were diluted 10X with DPBS (GIBCO) and vortexed. Ethanol was removed by spin filtration with an Amicon Ultra-4 3k MWCO centrifugation filter (EMD Milipore). Polymer concentration was analyzed by UV spec using an absorbance maxima at 290 nm before and after centrifugation to determine the final concentration.

4.2.11 Particle sizing

Particle sizes of polymers were measured by dynamic light scattering (DLS) using a Malvern Zetasizer Nano ZS. Lyophilized polymers were prepared as previously described then diluted to 0.5 mg/mL into phosphate buffer, pH 7.4. Polymers were filtered with a 400 ηm Milipore hydrophilic PTFE filter prior to measurement.

4.2.12 Red blood cell hemolysis assay

pH-dependent membrane disruption of the diblock copolymers was examined by a red blood cell hemolysis assay. Activity of the free polymer was measured in physiologically relevant pH buffers: 7.4, 7.0, 6.6, 6.2, and 5.8. Briefly, whole blood was collected in vacutainer tubes containing EDTA, centrifuged, plasma aspirated and resuspended in 150 mM NaCl to isolate the red blood cells (RBCs). RBCs were resuspended in phosphate buffers at each pH and incubated with polymer (5, 10, 20, and 40 μg/mL) for 1 hour at 37°C. Hemoglobin release was measured by centrifugation of intact RBCs and absorbance of the supernatant was measured at 541 *eta*m.

4.2.13 Cytotoxic profile of polymers in vitro

To measure the toxicity of the diblock copolymers, Ramos-AW cells were plated in 96-well plates with 25,000 cells per well and SKBR3 cells were seeded in 96-well plates with 6,000 cells per well the night before. Cells were treated with various concentrations of polymer for 1, 2 or 3 days. At the initiated time point, cell culture media was replaced and 20 μL of MTS reagent was added to each well. The conversion of MTS to formazan in metabolically active cells was measured by 490 ηm absorbance on a plate reader. The percent viable cells was normalized to untreated cells after subtracted background MTS absorbance.

4.2.14 In vivo toxicity of PEGMA-EB40 polymers

To determine the maximum tolerated dose (MTD) of the PEGMA-EB40 polymers, three polymers were selected from the series, DP 50, 100, and 200 and injected into nude BALBc mice via tail vein injection. Micelles were formulated in DPBS as previously described. For a 200 uL injection in the tail vein at 60, 90, and 120 mg/kg in 0.02 kg mice, polymers were prepared at 6, 9, and 12 mg/mL. Polymers were injected sequentially from 60 to 120 mg/kg with one injection per mouse. Mice were monitored for 1 hour post injection for any signs of discomfort or toxicity. After 1, 3, 5 and 10 days, 250 μ of blood was drawn via retro orbital eye bleed and body weight was monitored. Blood was collected into 1 mL Heparin-coated vacutainers, centrifuged at 1,500 at 4°C to separate plasma from serum. The supernatant containing serum was collected, and centrifuged in 1.5 mL eppindorf tubes at 1,500 rpm at 4°C, then transferred to new tubes, kept on ice and submitted for pick up by Phoenix Central Laboratories for blood enzyme analysis.

4.3 Results and Discussion

4.3.1 Cytochrome c release

Cytochome c release induced by the BIM peptide was confirmed by Western blot using mitochondria isolated from Ramos-AW cells. One day before study, cells were either left untreated or treated with staurosporine (0.1 μM) to observed a synergistic effect. Mitochondria isolated from cells were treated with varying concentrations of BIM peptide. After 30 minutes, mitochondria were pelleted and separated from supernatant. The amount of cytochrome c released into the supernatant was measured by a Western blot (Figure 4.5). For each concentration the mitochondria pellet (mito) and supernatant (sup) was analyzed. With BIM peptide alone, we observed complete release of cytochrome c down to 1 μM, and approximately 25% release at 0.1 μM. For STS treated cells, an increase in cytochrome c was observed to nearly 50% at the lowest concentration indicating a synergistic effect. Dose dependent cytochrome c release of the BIM peptide indicates that the newly synthesized sequence is able to activate cytochrome c release from Ramos-AW cells.

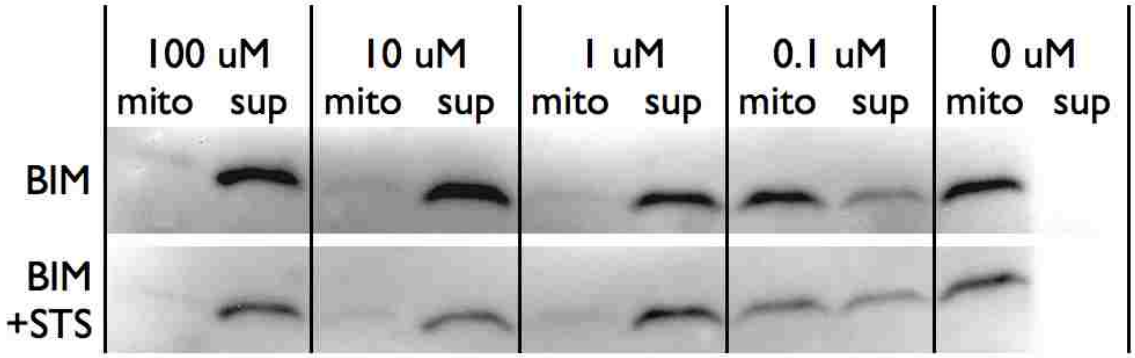

Figure 4.5: Cytochrome C release was measured in mitochondria isolated from Ramos-AW cells. Cells were treated with or without staurosporine (STS) at 0.1 μM for 24 hours prior to isolating mitochondria. Peptide was incubated with mitochondria for 30 minutes and the amount of cytochrome c found in the mitochondria pellet (mito) or supernatant (sup) was measured by Western blot.

4.3.2 Diblock copolymers for peptide and antibody loading

Below is a chemical representation of the diblock copolymer synthesized by RAFT polymerization. The biotin functional end group allows for facile complexation to an antibody/streptavidin conjugate through the most stable non covalent-interaction, biotin-streptavidin. Additionally, the pyridyl disulfide monomer PDMSA incorporated into the first block of the micelle allows for conjugation of the cysteine functional BIM peptide through a cleavable disulfide bond. This is the basis for the diblock copolymer, micelle formulation in order to deliver antibody-targeted polymer-peptide conjugates to the intracellular cytosolic compartment of a cell for therapeutic action.

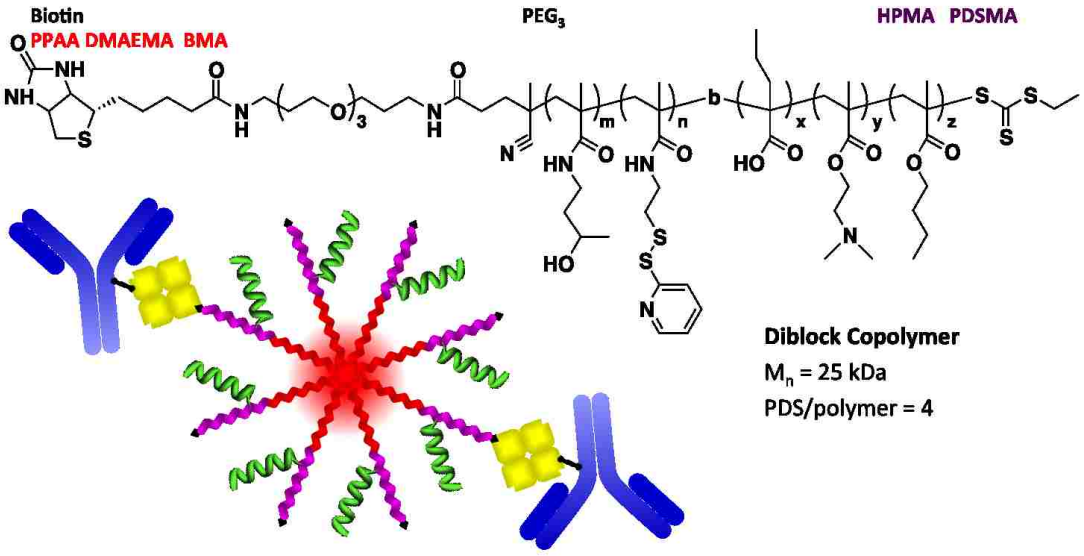

Figure 4.6: The chemical structure of HP-PDB is drawn with a cartoon representation of the polymer micelle with peptide and antibody/streptavidin loading.

4.3.3 Characterization of poly[(HPMA-PDSMA)-b-(PAA-DMAEMA-BMA)]

Upon synthesis and purification of the macroCTA and then the diblock copolymer, both polymers were analyzed by gel-permeation chromatography to measure the number average molecular weight (M_n), weight average molecular weight (M_w), and polydispersity (PDI = M_n/M_w). Figure 4.7 represents the chromatogram of both the macroCTA (btPEG-HP) and the diblock copolymer (btPEG-HP-PDB) measured by the refractive index detector. The first peak in blue represents the macroCTA which is unimodal with a low polydispersity of 1.15. Addition of the second block causes a shift in the molecular weight indicated by a curve shift to the left and a broader distribution and a polydispersity of 1.82. The broad distribution yields a higher PDI which is caused by the low hand off of propylacrylic acid (PAA) during polymerization. The sterically hindered PAA monomer decreases the rate of hand off to the next monomer during RAFT polymerization which we believe causes an uneven distribution and increased polydispersity. Nonetheless, the polymerization of the macroCTA and subsequent second block was successful by RAFT.

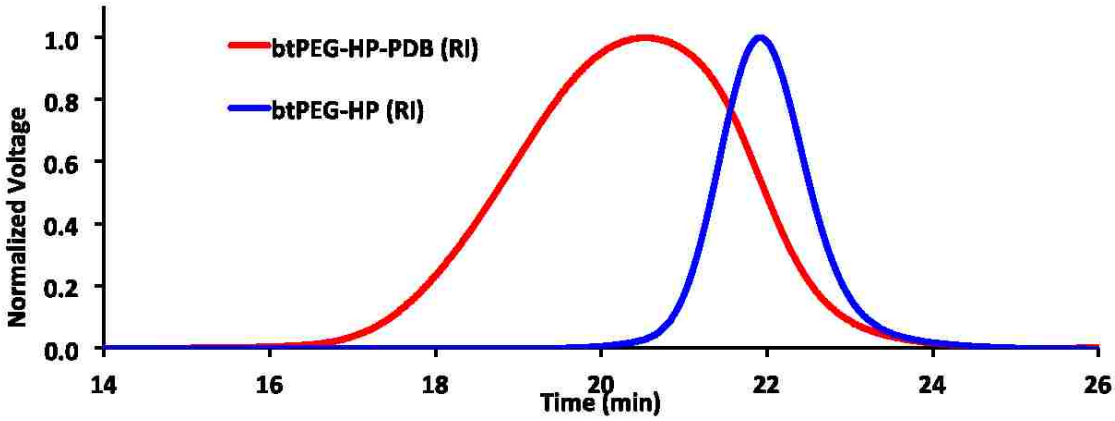

Figure 4.7: Size exclusion chromatography using gel-permeation was used to monitor the molecular weight and polydispersity of the macroCTA and diblock copolymer shown in blue and red, respectively.

To quantify the monomer composition of the macroCTA made from the biotinECT and ECT chain transfer agent, 1H-NMR was performed on both macroCTAs. A comparison of both NMR spectrums reveal consistent monomer peaks associated with HPMA and PDSMA (Figure 4.8). Integration of these peaks was then used to determine the percent of PDSMA monomer in the macroCTAs. For the macroCTA without biotin, the PDSMA concentration was 6.1% of the polymer and for the biotin-containing macroCTA, PDSMA was found to be 6% of the polymer composition.

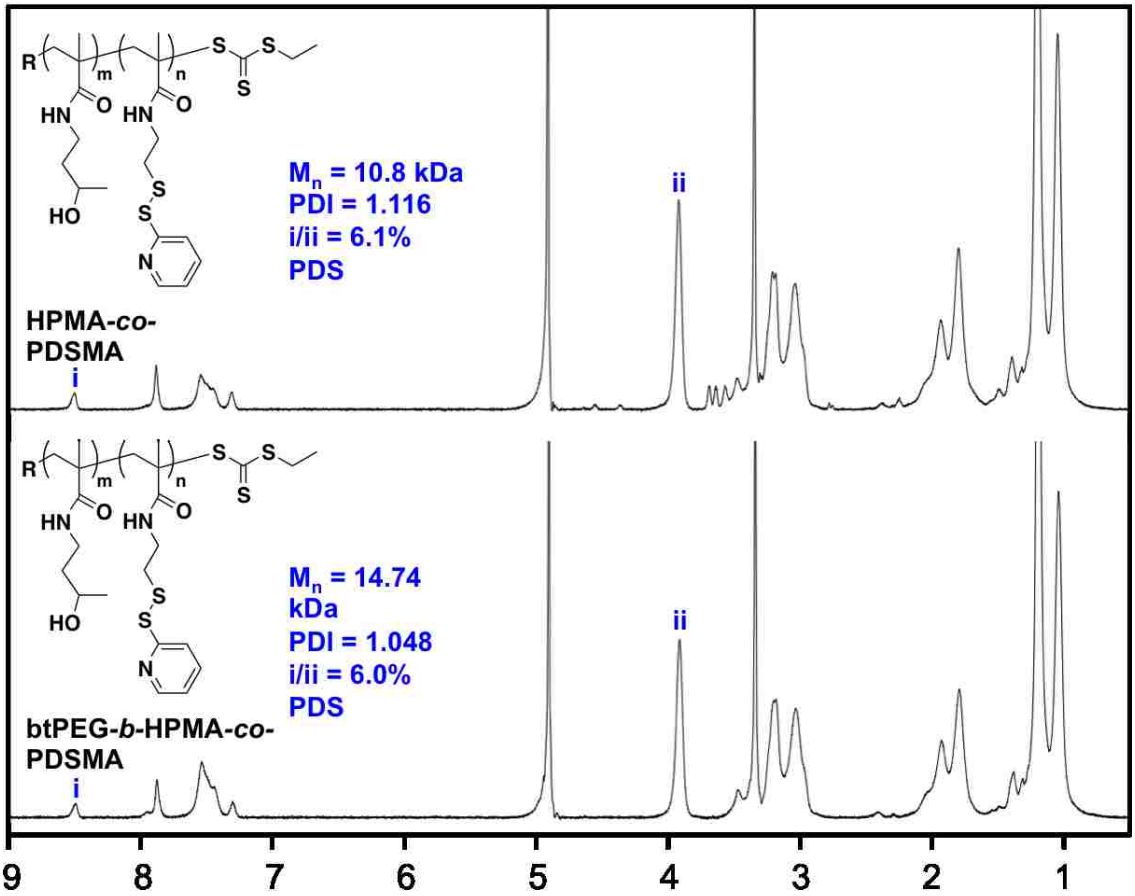

Figure 4.8: Two macroCTAs are analyzed by NMR spectroscopy. The top is HPMA-PDSMA using ECT as the chain transfer agent (CTA). The spectrum below is HPMA-PDSMA using a biotin-CTA for antibody/streptavidin conjugation. The composition and percent of PDS groups in each polymer is quantified by taking the ratio of respective peaks.

The complete polymer poly[(HPMA-PDSMA)-b-(PAA-DMAEMA-BMA)] was analyzed by 1H-NMR following purification by precipitation in diethyl ether and PD10 filtration. All relevant proton peaks associated with HPMA, PDSMA, DMAEMA, and BMA were identified in the clean NMR spectrum (Figure 4.9). By integrating these peaks and subtracting from the back bone peak up field, the monomer composition within the second block was determined to be 13:25:62 for PAA:DMAEMA:BMA, respectively.

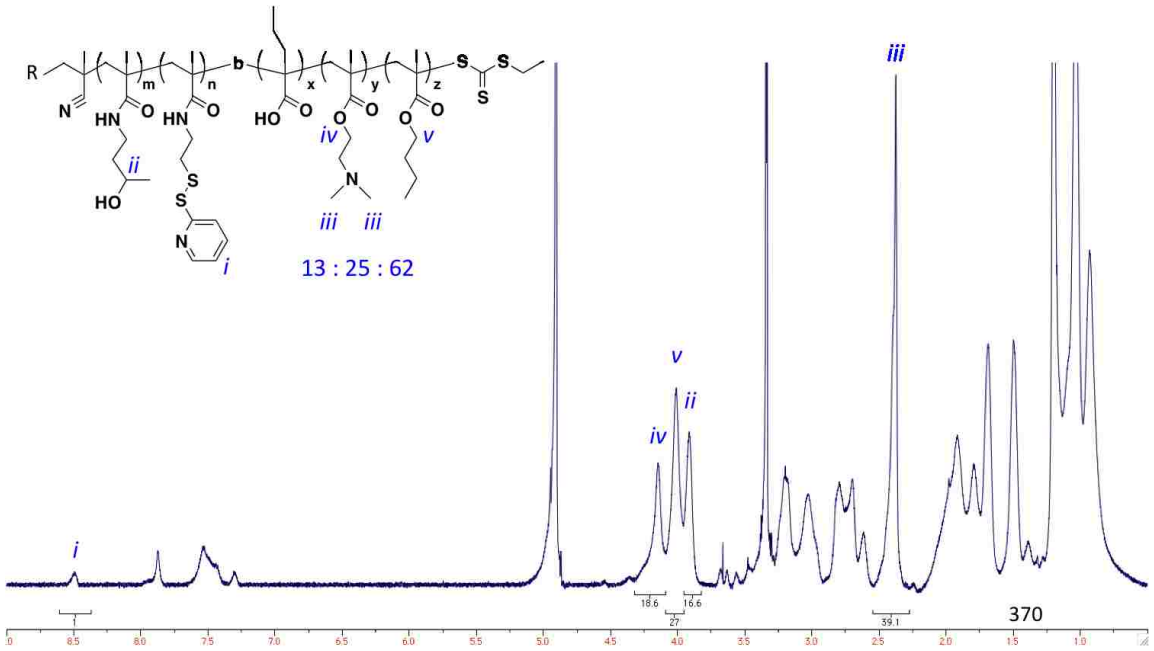

Figure 4.9: An NMR spectrum of the complete diblock copolymer poly([HPMA-PDSMA]-b-[PAA-DMAEMA-BMA]) is shown above. All peaks pertaining to the each monomer are identified in the spectrum. Purity and monomer composition are also verified.

The theoretical and experimental monomer composition for the macroCTA and diblock copolymer poly([HPMA-PDSMA]-b-[PAA-DMAEMA-BMA]) was tabulated in Table 4.1. The theoretical composition represents the feed ratio of each monomer for the polymerization and the experimental composition represents the values determined by 1H-NMR. With a target degree of polymerization (DP) of 150, the macroCTA reached 68% monomer conversation with a DP of 102. Furthermore, the feed ratio of PDSMA and HPMA were 7.5% and 92.5% respectively, while the resultant composition was 6% and 94%. There is close agreement between the feed ratio and actual composition demonstrating the control of monomer composition through RAFT synthesis. In the subsequent synthesis of the second block, PAA, DMAEAMA, and BMA were incorporated at a feed ratio of 30%, 30%, and 40%, respectively. The final composition of the three monomers was 13%, 25%, and 62%, respectively. The low reactivity ratio of PAA caused by the steric hindrance from the propyl group generally yields a low monomer composition. Because the ratio of cationic monomer, DMAEMA, was twice more than the anionic monomer, PAA, the second block was slightly cationic. There was also a higher percentage of the hydrophobic monomer, BMA, then was desired. The overall monomer conversion was 41.9%.

	DP	PDSMA Ratio	HPMA Ratio	Mn (kDa)	PDI	Conv (%)	DP	PPAA Ratio	DMAEMA Ratio	BMA Ratio	M_n (kDa)	PDI	Conv (%)
btPEG-HP theoretical	150	7.5%	92.5%	22.7	-	100	-	-	-	-	-	-	-
btPEG-HP experimental	102	6%	94%	15.4	-	67.8	-	-	-	-	-	-	-
btPEG-HP-PDB theoretical	-	-	-	-	-	-	350	30	30	40	48.4	-	100
btPEG-HP-PDB experimental	-	-	-	-	-	-	147	13	25	62	20.3	-	41.9

Table 4.1: The following table describes the experimental and theoretical monomer composition of the HP macroCTA and HP-PDB diblock copolymer determined by NMR spectroscopy and GPC

4.3.4 Hemolytic activity of poly([HPMA-PDSMA]-[PAA-DMAEMA-BMA])

The diblock copolymer was designed to form stable micelles at physiological pH, with a hydrophilic corona to impart stability of the peptide and an endosomolytic second block that remains in the core at physiological pH. Upon acidification in endosomes and lysosomes, the diblock copolymer changes confirmation from micellar to unimeric. The PAA and DMAEMA monomers are protonated, exposing BMA causing endosomolytic activity. To measure this response, the polymer was incubated with isolated red blood cells in different pH buffers. At acidic pH, the polymers causes red blood cell lysis, or hemolysis, releasing hemoglobin into the buffer. After centrifugation, the amount of hemoglobin is measured in the supernatant and calculated relative to red blood cells treated with 1% TritonX. In this study, the polymers were incubated with red blood cells at 5, 10 and 20 μg/mL for one hour and the amount of hemolysis was measured after 1 hour at 37°C (Figure 4.10). At all three concentrations, no hemolytic activity was observed at pH 7.4 and 7.0. At pH 6.6, 30% hemolysis was observed at the highest concentration. The hemolytic activity peaked at pH 6.2, with 90% at 20 μg/mL and less activity at pH 5.8. The hemolytic profile observed here was not the most desirable because ideally we would like the polymers to escape endosomes as soon as they are internalized. At lower pH, protein cargo can be degraded by proteases and other enzymes. Ideally the polymers would not exhibit any activity at physiological pH, but a sharp increase at pH 7.0 or 6.6.

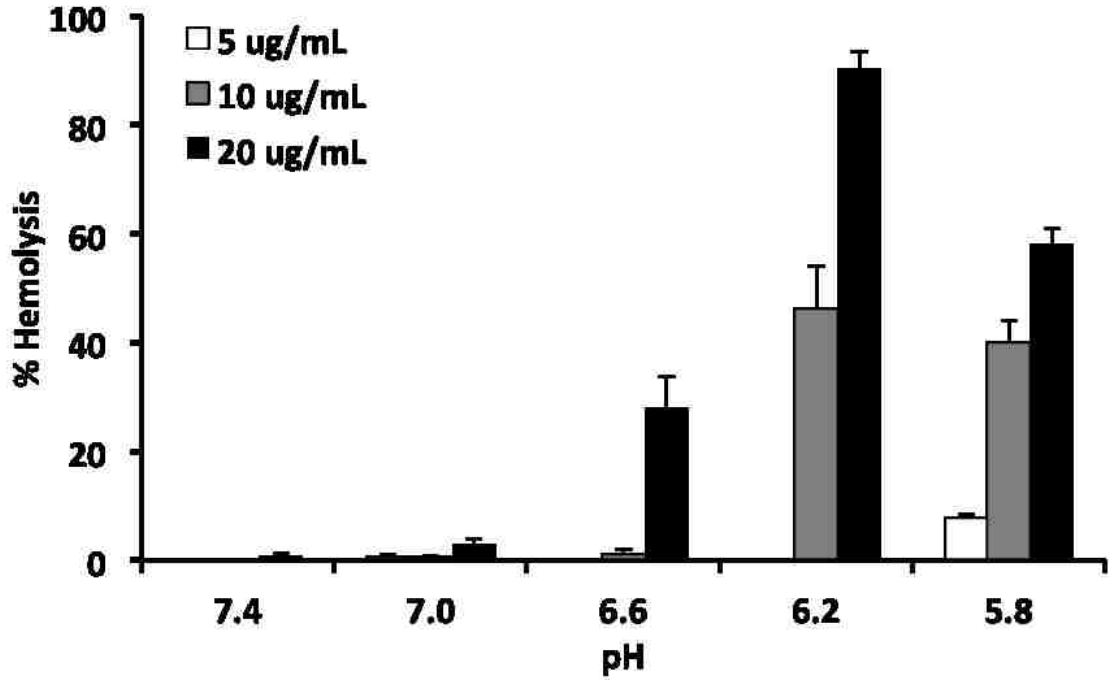

Figure 4.10: The ability of HP-PDB to lyse red blood cells was confirmed by a hemolysis assay. Polymer was incubated with isolated red blood cells and diluted into different pH buffers. The percent release of hemoglobin relative to TritonX positive control is plotted. The polymer was incubated with red blood cells at 5, 10, and 20 ug/mL for 1 hour. Supernatant was isolated and absorbance was measured on a plate reader at 500 nm.

4.3.5 Characterization of polymer-peptide conjugates

After characterizing the intrinsic properties of the polymer alone, the ability of the polymer to conjugate to the BIM peptide was confirmed in Figure 4.11 . In phosphate buffer, the polymer was reacted with the BIM peptide at three ratios: 4:1, 2:1, and 1:1, polymer to peptide. After allowing the free cysteine on the peptide to react with the PDS groups on the polymer overnight, the diameter of the polymer-peptide nano particles was measured by dynamic light scattering (Figure 4.11 (upper left)). At all three ratios, the number average diameter ranged from 18 to 25 ηm with no statistical difference at any polymer to peptide ratio. Next, the reactivity of the peptide to the PDS groups was verified by the release of PDS and conversion to 2-mercaptopyridine which absorbs at 343 ηm (Figure 4.11 (upper right)). The peptide conjugation efficiency ranged from 95% for the 4:1 ratio down to 82% for the 1:1 ratio. The ability of the biotinylated polymer to conjugate to streptavidin with various peptide loading ratios was measured using a HABA assay (Figure 4.11 (lower left)). Conjugation to streptavidin through the biotin linkage was not affected by peptide loading. At all three peptide loading ratios, an excess of one polymer to streptavidin resulted in 0.66 biotin binding events. All the numerical values from the three studies are tabulated in Figure 4.11 (lower right).

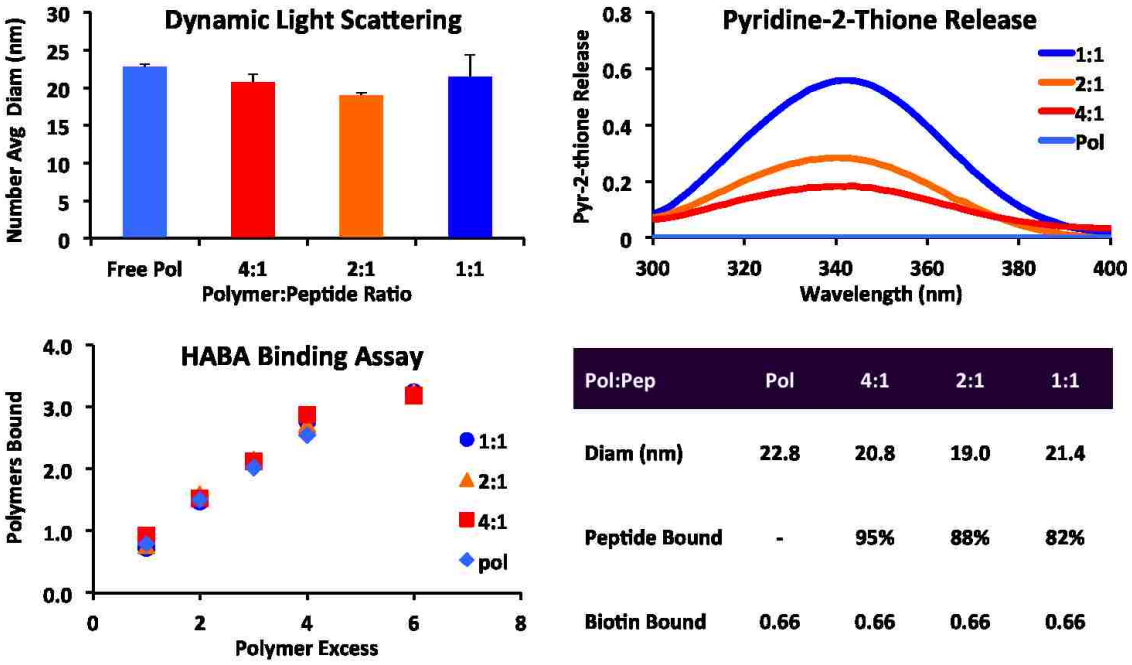

Pol:Pep	Pol	4:1	2:1	1:1
Diam (nm)	22.8	20.8	19.0	21.4
Peptide Bound	-	95%	88%	82%
Biotin Bound	0.66	0.66	0.66	0.66

Figure 4.11: The ability of HP-PDB to conjugate to peptides and bind to streptavidin was characterized. First the BIM peptide was conjugated to the polymer with increasing molar ratios 4:1, 2:1, and 1:1 Polymer:Peptide. Dynamic light scattering was used to measure the number average diameter and confirm that peptide loading did not effect the size of the micelles. Next, peptide conjugation was measured by the release of pyridyl disulfide and conversion to 2-mercaptopyridine which can be measured by absorbance measurements. Finally the ability of the peptide-polymer conjugates to bind to streptavidin was confirmed using a HABA assay. The resultant peptide conjugation efficiency and biotin binding events were plotted in the table at the bottom right.

4.3.6 Toxicity profile of poly([HPMA-PDSMA]-[PAA-DMAEMA-BMA])

The toxicity of the diblock copolymer was measured in vitro. Polymer micelles were formed in phosphate buffer and incubated with RAMOS-AW cells for up to six hours from 100 to 500 μg/mL (Figure 4.12). After six hours, the cells were pelleted and washed, then MTS was added for 2 hours and viability was measured by measuring the absorbance at 490 nm. Unfortunately, this polymer was very toxic at even low polymer dosages. From 300 to 500 μg/mL, there was 0% cell viability after only 6 hours. The concentrations required for peptide delivery were too toxic with poly([HPMA-PDSMA]-[PAA-DMAEMA-BMA]). The realization of this toxicity led us to explore alternative polymer designs that are more hydrophilic and biologically compatible.

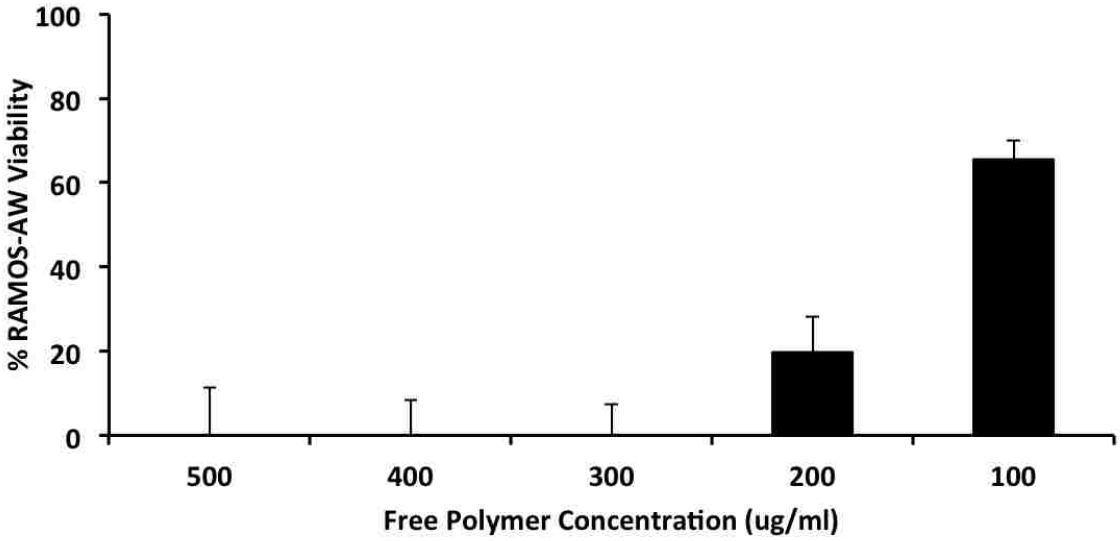

Figure 4.12: The cytotoxicity of HP-PDB was measured in Ramos-AW cells. Cells were incubated with polymer from 100 to 500 ug/mL for up to 6 hours and cell viability was measured by MTS. HP-PDB was determined to be very toxic to Ramos-AW cells.

4.3.7 Characterization of poly(PEGMA) macroCTAs

A series of poly($PEGMA_{950}$) macroCTAs were synthesized via RAFT by varying the degree of polymerization (DP) from 25 to 50 and reaction time from 5 to 18 hours. After the reaction, the polymers were precipitated in diethyl ether to remove unreacted monomer and the purified polymers were analyzed by gel-permeation chromatography. Figure 4.13 represents an overlay for each macroCTA chromatogram. An increase in reaction time resulted in an increase in molecular weight noted by the shift to the left. The macroCTA with a DP of 50 was much larger and had a high polydispersity indicated by the larger distribution. Table 4.2 shows the incubation time and DP for each macroCTA as well as the number average molecular weight (M_n) and polydispersity (PDI). The molecular weight increased from 8,400 Da at 5 hours to 13,800 Da at 12 hours and 15,700 Da after 18 hours. All the measured PDIs were between 1.04 and 1.08. The macroCTA made with a DP = 50, was 34,900 Da with a higher PDI at 1.21. Because of the high polydispersity at DP = 50, we decided to use a DP = 25 for subsequent studies with a reaction time of 12 hours.

Polymer	Time (h)	Target DP	M_n (g/mol)	PDI
PEGMA	18	50	34,900	1.21
PEGMA	18	25	15,700	1.08
PEGMA	12	25	13,800	1.08
PEGMA	5	25	8,400	1.04

Table 4.2: The target degree of polymerization (DP), reaction time, M_n, and PDI for each $PEGMA_{950}$ is described in the following table

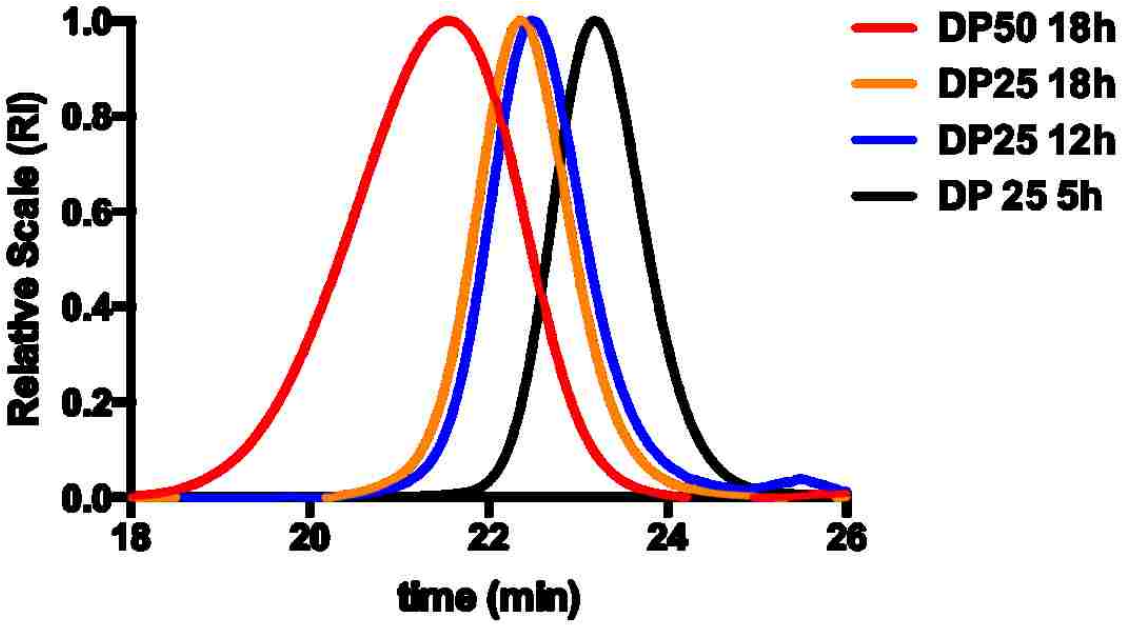

Figure 4.13: A series of $PEGMA_{950}$ polymers were synthesized by varying both reaction time and degree of polymerization $[mon]_o/[CTA]_o$. The purified PEGMA polymers were analyzed by size exclusion chromatography to measure the molecular weight (M_n) and polydispersity (M_w/M_n)

The poly(PEGMA) macroCTAs were characterized by 1H-NMR to confirm their composition and purity (Figure 4.14). All protons associated with carbons atoms on the CTP chain transfer agent were identified by 1H-NMR. Furthermore, the protons associated with the ethylene repeats as well as the methyl group on the end were also identified by 1H-NMR. 1H-NMR was also used to ensure no vinyl peaks are present which would be associated with unreacted monomer.

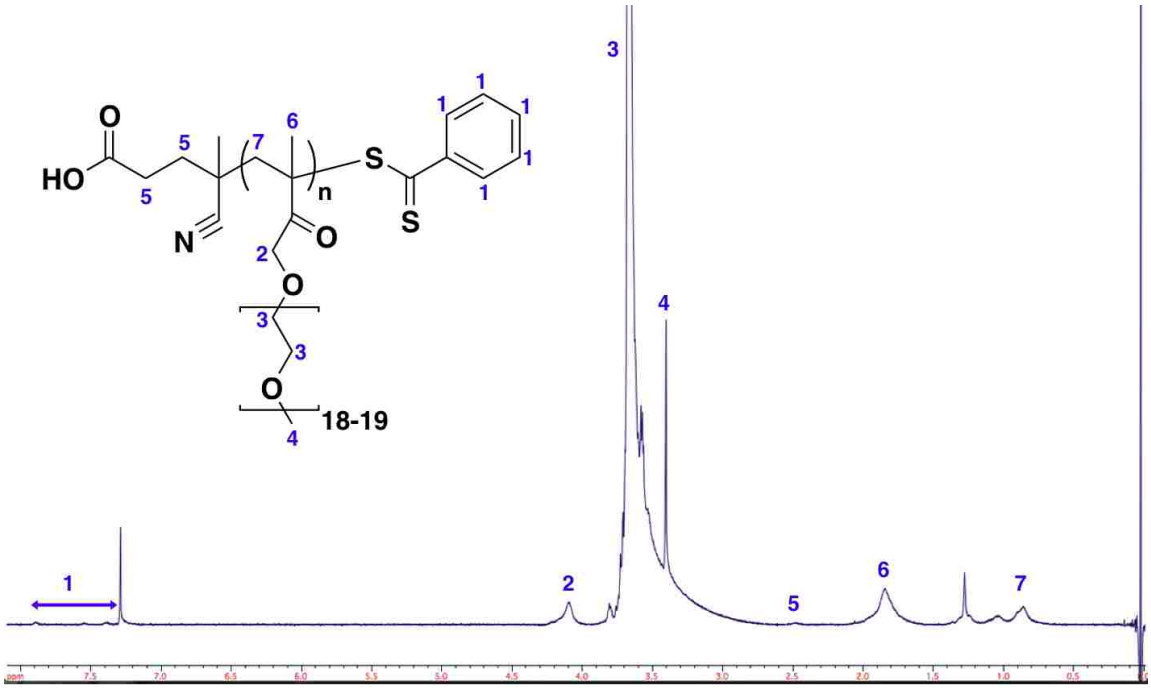

Figure 4.14: The $PEGMA_{950}$ polymer was analyzed by NMR to confirm purity and determine the actual monomer conversion. All protons on the polymer were accounted for by NMR spectroscopy.

4.3.8 Characterization of poly([PEGMA]-[PAA-DMAEMA-BMA]) Polymers

A series of diblock copolymers were synthesized using the PEGMA macroCTA (15,700 Da) made in the previous study. The second block containing the PDB formulation, was synthesized using a target degree of polymerization of 100, 200, and 300. A chromatogram collected by gel-permeation chromatography (GPC) is shown in Figure 4.15. In this figure is an overlay for all the diblock copolymers made in this series as well as the macroCTA. A clear shift to larger molecular weights is seen in the chromatogram indicating successful polymerization of the subsequent second block. The molecular weight of the first and second block, polydisersity, and block ratios were also determined by GPC and given in Table 4.3. An increase in the target DP resulted in and increase in the second block length and increased the ratio of the second to first block from 0.55 up to 1.24. Furthermore, the PDI remained relatively low but increased from 1.14 up to 1.26 with a DP of 300. The length of the second block correlated linearly with DP as is often the case when using RAFT synthesis for controlled polymerizations.

Polymer	Target DP	M_n 1st Block (g/mol)	M_n 2nd Block (g/mol)	M_n Total (g/mol)	PDI	Ratio
PEGMA-PDB	100	15,700	8,700	24,400	1.14	0.55
PEGMA-PDB	200	15,700	13,900	29,600	1.16	0.89
PEGMA-PDB	200*	15,700	15,900	31,600	1.23	1.01
PEGMA-PDB	300	15,700	19,500	35,200	1.26	1.24

Table 4.3: The target DP, M_n of the first and second block, PDI and ratio of second block to first block are all described in the following table for each polymer.

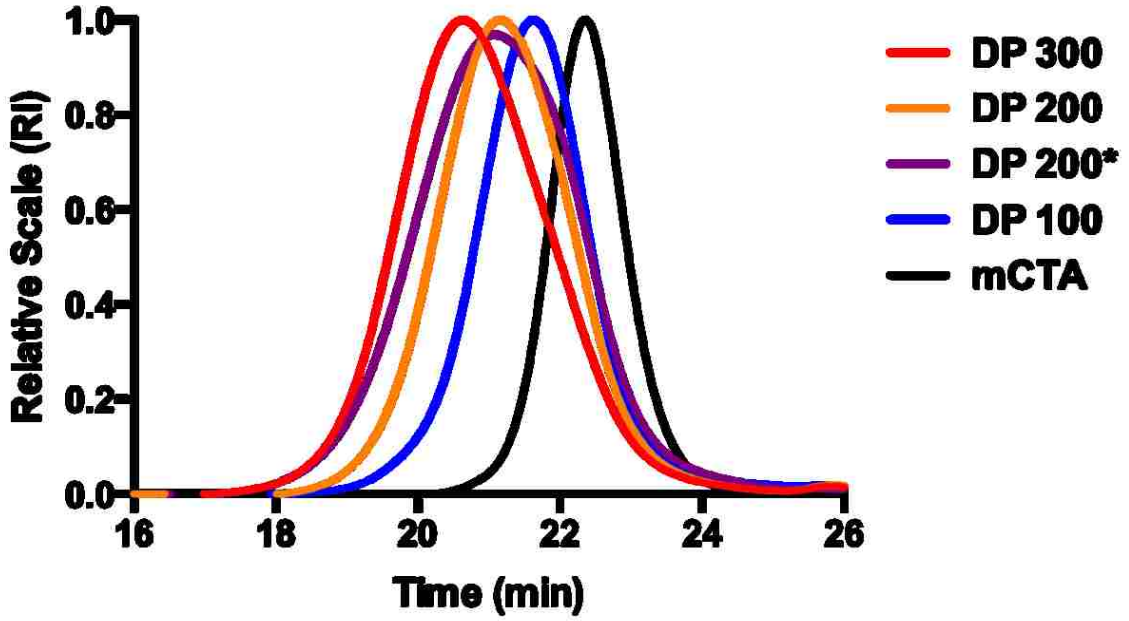

Figure 4.15: Size exclusion chromatography was performed on the PEGMA-PDB diblock copolymer series. PEGMA-PDB was synthesized by RAFT using a degree of polymerization of 100, 200 and 300. All three polymers, including DP200 synthesized in dimethylacetamide denoted by (*), and the macroCTA are plotted in the figure and represented by a shift from the macroCTA.

The PEGMA-PDB polymer series was also characterized by 1H-NMR to confirm purity and obtain data on monomer composition (Figure 4.16). The NMR spectrum of the diblock copolymer synthesized with a target DP of 200 demonstrated a clean spectrum with no monomer impurities. All proton peaks found in the spectrum were quantified and accounted for on the diblock copolymer. Overlap of the backbone peak downfield however, make it somewhat difficult to characterize the exact monomer composition of the second block.

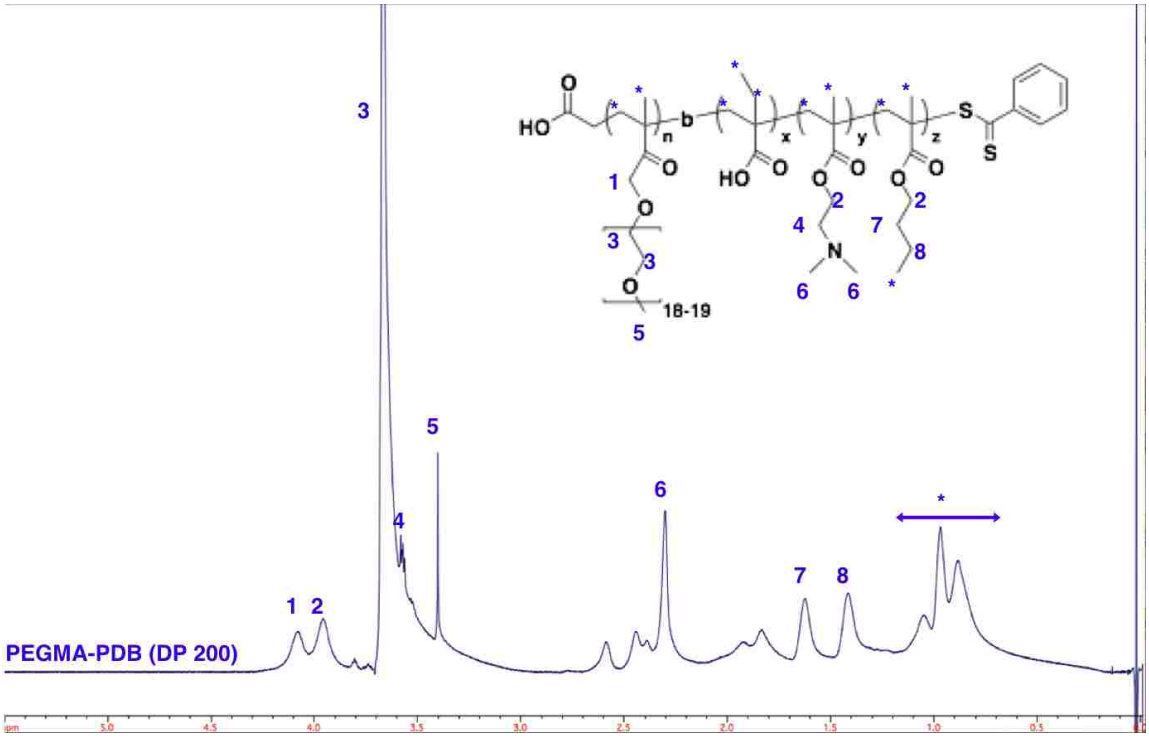

Figure 4.16: The PEGMA-PDB polymer series was also confirmed by NMR spectroscopy. Observance of the three monomers in the second block confirm the presence of the second block as well as monomer composition within the diblock copolymer. All relevant proton peaks in the NMR spectrum were accounted for on the diblock copolymer.

To form micelles with the PEGMA-PDB polymers, unimers were first formed by dissolved dried polymers in ethanol at 100 mg/mL. The polymer solution was then diluted into phosphate buffer at 10 mg/mL and mixed by vortexing. Polymers were then diluted to 0.5 mg/mL in phosphate buffer, sterile filtered and analyzed by dynamic light scattering to obtain particle size. The number mean diameter was measured for all four PEGMA-PDB polymers and ranged from 8 to 15 ηm. A low polydispersity indicates fairly uniform particles with no large increase in size with increasing DP.

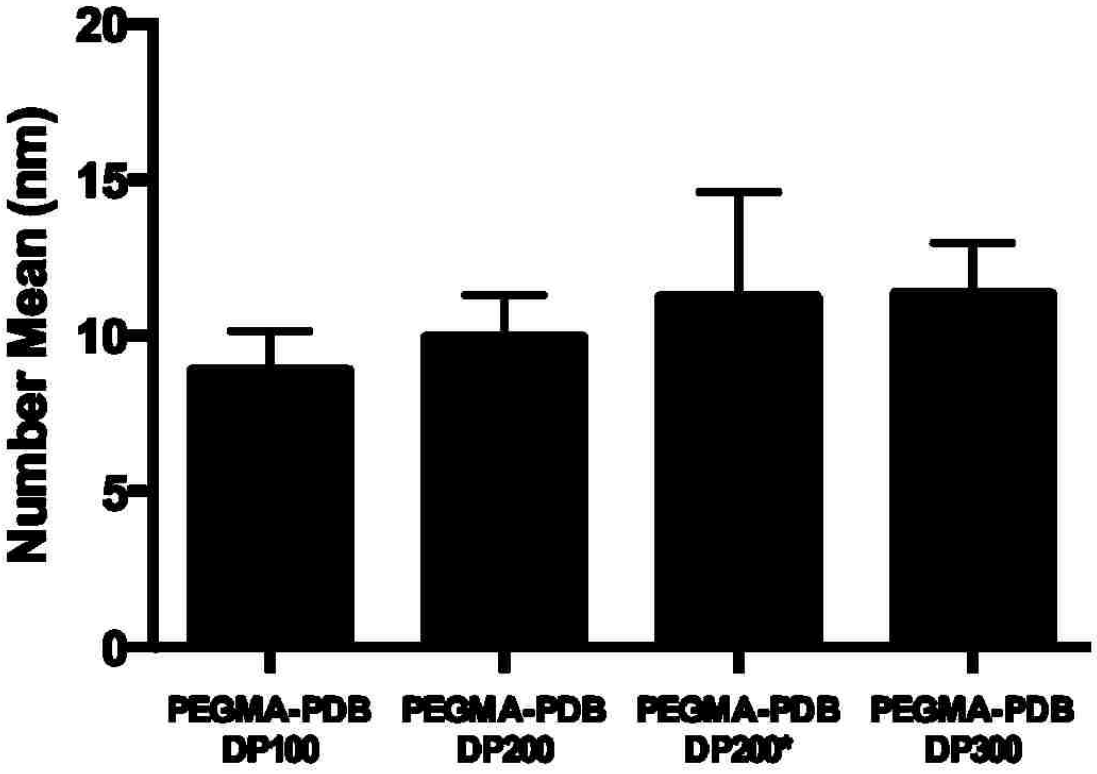

Figure 4.17: Dynamic light scattering was used for each PEGMA-PDB polymer to determine the number mean diameter in nanometers. All polymers exhibited similar diameters irrespective of DP.

4.3.9 Hemolytic activity of poly([PEGMA]-[PAA-DMAEMA-BMA])

The hemolytic activity of the PEGMA-PDB polymers as a function of pH and degree of polymerization (DP) was measured in (Figure 4.18). The PEGMA-PDB polymer series was incubated with red blood cells in different pH buffers at several concentrations. The percent hemoglobin release from red blood cells was measured relative to a 0.1% TritonX control. The percent hemolysis appeared to increase with higher DP polymers however the total relative levels were very low. This was very concerning considering PDB containing polymers usually have higher activity. One possible reason for this low hemolytic activity is a low incorporation of PAA monomer which helps to trigger the membrane lytic response. A second possibility is that the PEGMA macro CTA is so bulky and sterically hindered that the second block never gets a chance to interact with the hydrophobic membrane of the red blood cells. Another concern with this polymer series is that the hemolytic activity only appears to increase below pH 6.6. If the polymer only become endosomolytic below this pH, the endosomes could have matured to late endosomes which contain a number of enzymes and proteases that could degrade the biologic cargo, in this case peptide. Ideally, the polymer would escape endosomes much earlier in the maturation at high pH. This would likely give the cargo the best chance to stay in tact before reaching the cytosol.

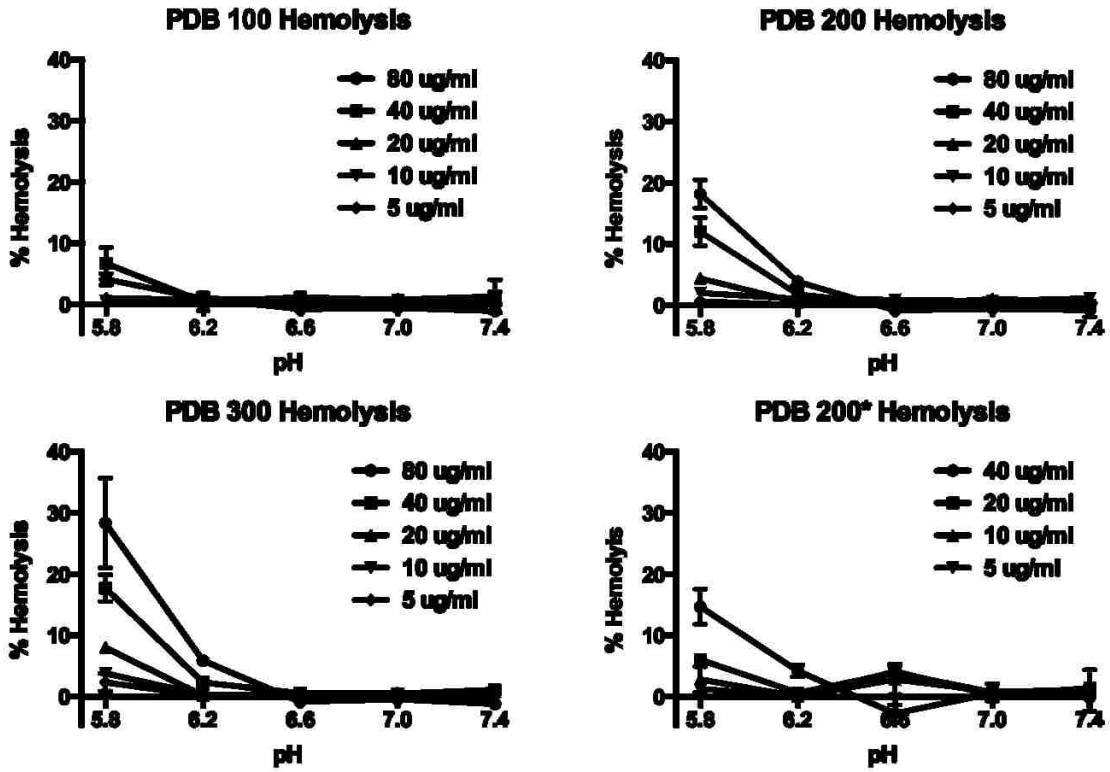

Figure 4.18: The hemolytic activity of each polymer was measured using a red blood cell hemolysis assay. In this assay, polymers were incubated with isolated red blood cells in different pH for one hour. The concentration of hemoglobin released from the red blood cells was isolated and measured on a plate reader using an absorbance measurement at 500 ηm. Polymers were incubated with red blood cells at a range of 5 to 80 μg/mL.

4.3.10 Cytotoxicity of poly([PEGMA]-[PAA-DMAEMA-BMA])

After characterizing the PEGMA-PDB polymer series and observing the hemolytic response, the polymers were analyzed for cytotoxicity in Ramos-AW and SKBR3 cells (Figure 4.19). Cells were treated in 96 well plates for up to 1 day at concentrations varying from 0.1 to 1 mg/mL. MTS was used to measure the percent viability relative to the untreated controls. A clear trend in toxicity is observed with increasing the degree of polymerization in Ramos-AW cells. In SKBR3 cells however, no toxicity was observed for any of the polymers up to 1 mg/mL. This is a significant finding as most of the pH responsive polymers we make in our lab exhibit some toxicity in adherent cell lines at these concentrations. Because of the low hemolytic activity even at 80 μg/mL, we decided to explore a new second block that could be more active than PDB and has already shown good activity when delivering plasmid DNA.

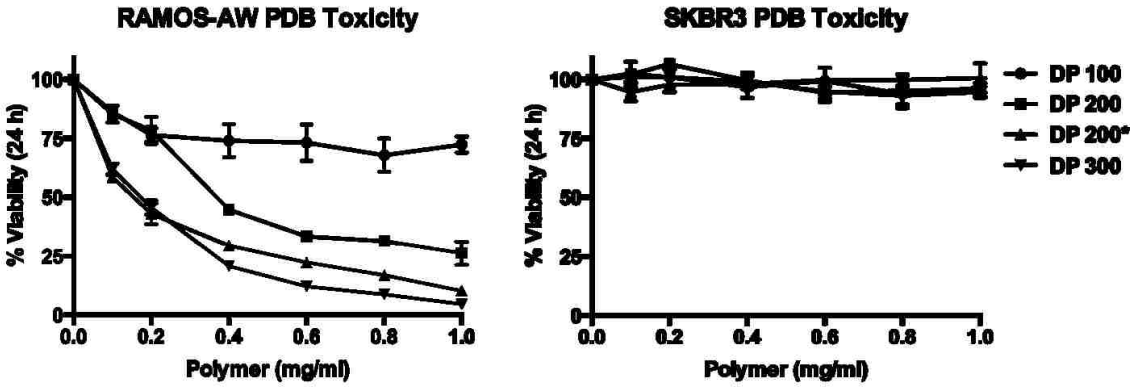

Figure 4.19: Cytotoxicity of the PEGMA-PDB polymer series was measured in Ramos-AW and SKBR3 cells. Cells were incubated with various concentrations of each polymer for 24 hours and cell viability was measured using an MTS assay. Cells were treated in triplicate.

4.3.11 Characterization of poly([PEGMA]-[DEAEMA-BMA])

The next series polymers made by RAFT also included the 15,700 Da PEGMA polymer as the macroCTA. The endosomal-releasing second block however, was composed of two monomers: diethylaminoethyl methacrylate (DEAEMA) and butyl methacrylate (BMA) at a 60 to 40 molar feed ratio, respectively. Protonation of the DEAEMA monomer at endosomal pH helps to promote micelle destabilization and exposure of the hydrophobic BMA to destabilize endosomal membranes. The ratio of 60 to 40 was selected based on previous finding by Manganiello et al.[15]. A series of PEGMA-EB40 polymers were synthesized by RAFT polymerization with varying degrees of polymerization (DP): 50, 100, 150, 200, and 300. The chromatograms for each polymer, collected by GPC are displayed in Figure 4.20 along with the PEGMA macro CTA. A clear shift to the right is observed for increasing DP, signifying higher molecular weight. The molecular weight of the first and second block as well as polydispersity were measured by GPC. While a clear shift to higher molecular weights is observed by GPC, there is also the appearance of a larger coupling peak as the DP increases. This coupling peak could be due to dead chain ends formed during the synthesis of the macroCTA or caused by RAFT synthesis of the second block. Optimization of the RAFT synthesis of the first and second block could also be performed to eliminate the formation of the coupling peak however will not be considered in the scope of this thesis.

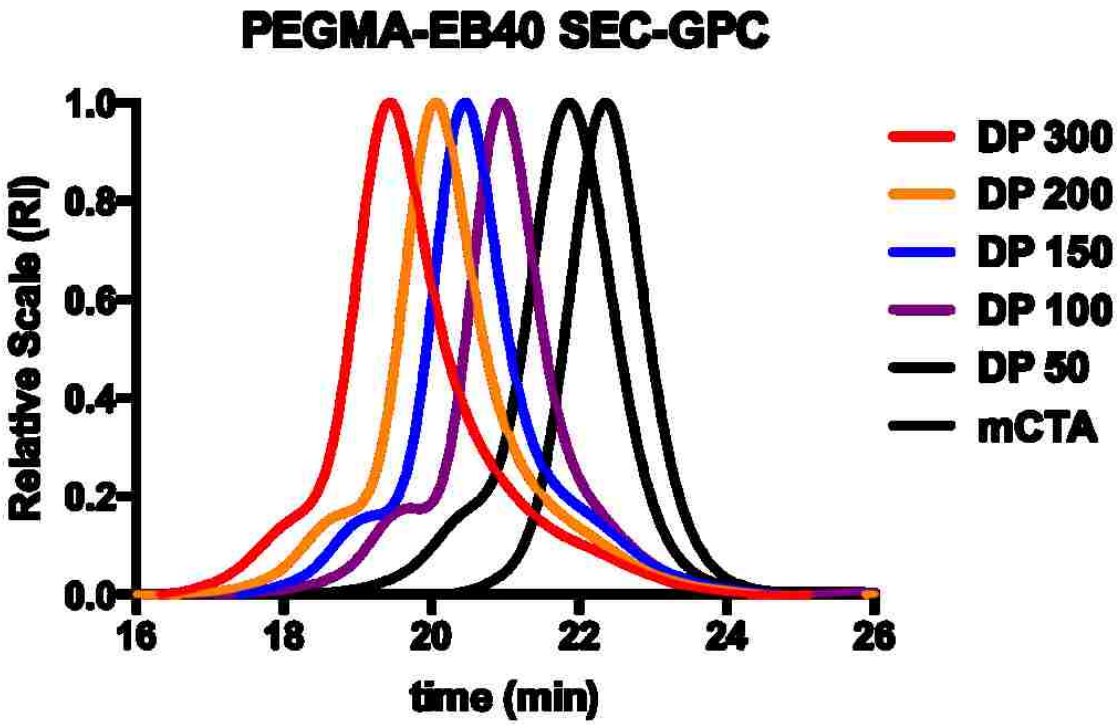

Figure 4.20: Size exclusion chromatography was performed on the PEGMA-EB40 polymer series. The chromatograms include the PEGMA macroCTA and the diblock copolymers ranging in DP from 50 to 300, noted by a shift to higher molecular weight.

Table 4.4 lists the theoretical and experimental molecular weights, monomer conversion, PDI, and block ratios determined by GPC and HPLC. We observed a linear increase in the second block length with an increase in the DP. The controlled polymerization of the second block via RAFT yielded very close ratios of DEAEMA and BMA relative to the feed ratios. The conversions were all very high around 90% and the theoretical molecular weights determined by HPLC were all in very close agreement with the experimental molecular weights determined by GPC. Additionally, the PDI of all the polymers was relatively low (less than 1.2). Good control of the block lengths and block ratios via RAFT were also demonstrated. It is thought that the block ratio is a crucial part to optimizing activity of the polymer carrier as the ratio of the second to first block helps determine how active the polymer is at endosomal escape. The activity of each carrier was also characterized by hemolysis as will be described later in this chapter.

Pol #	$\frac{[M]_o}{[CTA]_o}$	$\frac{[CTA]_o}{[I]_o}$	t (h)	DEAEMA (% feed)	BMA (% feed)	DEAEMA (% conv)	BMA (% conv)	mCTA (g/mol)	M_n, Th (g/mol)	M_n, Exp (g/mol)	PDI	Ratio
1	50	5	24	60	40	65	83	15,700	22,500	21,400	1.12	0.4
2	100	5	24	60	40	89	93	15,700	31,200	32,900	1.15	1.1
3	150	5	24	60	40	88	92	15,700	39,200	41,300	1.14	1.6
4	200	5	24	60	40	91	94	15,700	46,900	46,800	1.19	2.0
5	300	5	24	60	40	86	89	15,700	59,900	68,600	1.13	3.4

Table 4.4: The following table describes the feed and conversion ratios of each monomer in the PEGMA-EB40 diblock polymerization using the same macroCTA. Monomer conversion was measured by HPLC using t_o and t_x samples. The theoretical and experimental molecular weights determined from HPLC and GPC are also given, with PDI and block ratios.

The PEGMA-EB40 polymer series was also characterized by 1H-NMR (Figure 4.21). All the relevant proton peaks have been assigned to each of the monomers and the NMR spectrum demonstrates a clean polymer without monomer impurities. Additionally, monomer conversion was also measured by integrating the peaks associated with DEAEMA and BMA and found to be very similar to the monomer conversion determined by HPLC.

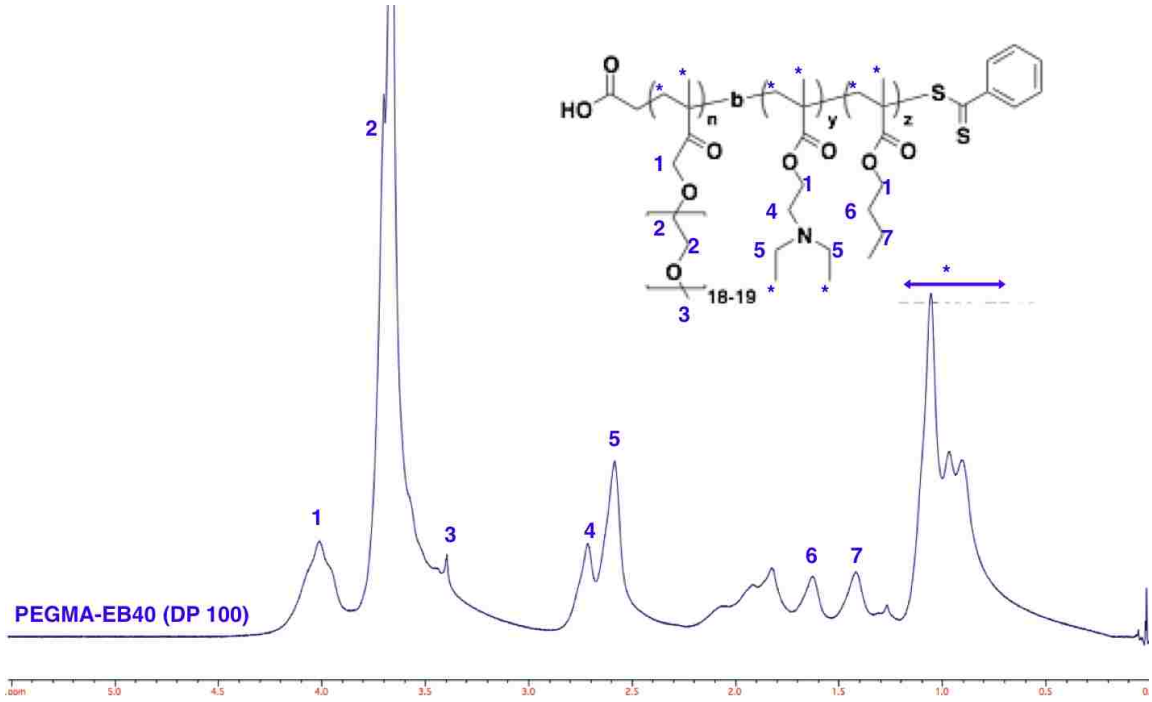

Figure 4.21: NMR spectroscopy was performed for the PEGMA-EB40 polymer series. The following is the NMR spectrum for PEGMA-EB40 DP 100. The first and second block are confirmed by NMR with good purity and conversion. NMR spectroscopy was used to determine the theoretical molecular weight.

Particle sizing of the PEGMA-EB40 polymer series was performed for a selection of the polymers (Figure 4.22). DP 50, 100, and 200 were analyzed by dynamic light scattering to determine the number average diameter. With a DP of 50 and a block ratio of 0.4, the polymers didn't appear to form micelles, likely because there was not enough hydrophobic block to impart the formation of micelles. The DP 100 and 200 polymers were able to form micelles that were 20 and 25 ηm in diameter, respectively.

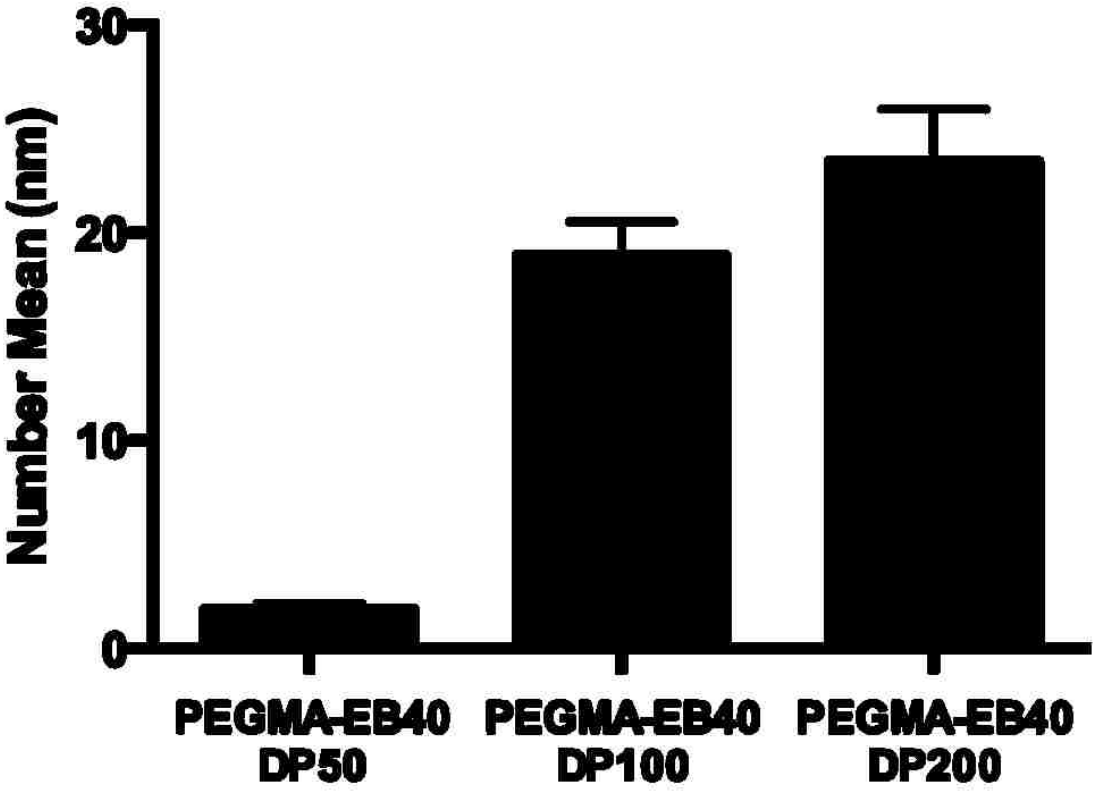

Figure 4.22: Dynamic light scattering for three polymer from the PEGMA-EB40 polymer series are shown. The number mean diameter was measured for DP 50, 100, and 200. Polymers at 0.5 mg/mL were measured in PBS following passage through a 0.4 μm syringe filter.

4.3.12 Hemolytic activity of poly([PEGMA]-[DEAEMA-BMA])

The hemolytic activity of the PEGMA-EB40 polymer series was also explored in Figure 4.23. While the DP 50 polymer did not exhibit any hemolytic activity, the DP 100, 200, and 300 were all extremely active. DP 100 and 200 exhibited a sharp increase in hemolysis below pH 7.0, while DP 300 was active below pH 7.4. Interestingly, the PEGMA-EB40 polymers were much more active than the PEGMA-PDB polymers. For the DP 200 and 300, 100% hemolysis was achieved with only 10 μg/mL which is very high relative to the other pH-responsive polymers that have been previously synthesized. From the hemolytic profile it appears that having a DP above 100 would be ideal for the best endosomolytic activity. Hemolysis activity has been linked with in vitro activity for siRNA delivery as described by Convertine et al.[1]. The DP 300 polymer however, was only slightly soluble during the formulation process and exhibits very high hemolysis close to physiological pH, making it a low contender for peptide delivery. This polymer if delivered to cells would likely cause high cytotoxicity.

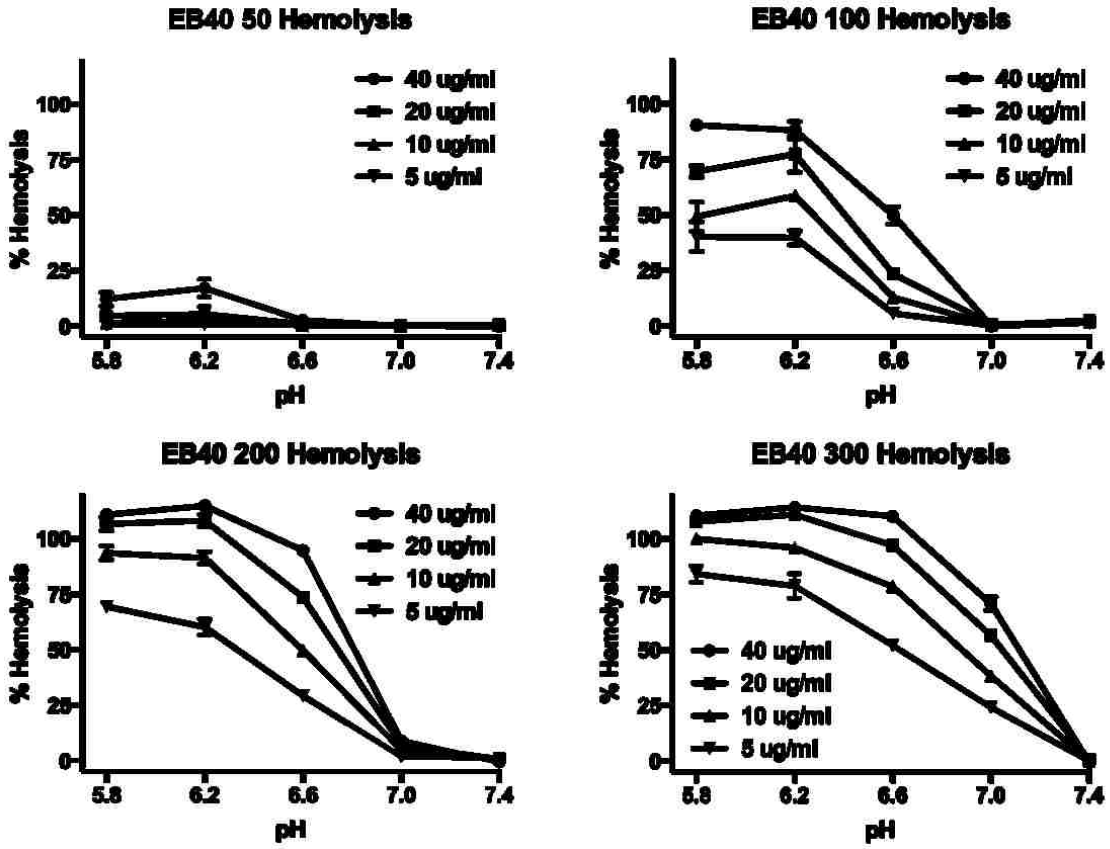

Figure 4.23: The hemolytic activity of each PEGMA-EB40 polymer was studied. PEGMA-EB40 DP 50, 100, 200, and 300 were incubated with red blood cells for 1 hour at various concentrations. The percent release of hemoglobin was measured relative to TritonX 1% positive control. The dependency of hemolysis on pH was confirmed by incubating polymers with red blood cells in various pH buffers ranging from ph 5.8 to pH 7.4. All samples and treatments were analyzed in quadruplicate.

4.3.13 In vitro toxicity of poly([PEGMA]-[DEAEMA-BMA])

The in vitro toxicity of the PEGMA-EB40 polymers was assessed in Ramos-AW and SKBR3 cells after 24 hours (Figure 4.24). Polymers were incubated with cells at various concentrations from 0.1 to 1 mg/mL and cell viability was measured by MTS. The polymer toxicity was higher than expected in the Ramos-AW suspension cells, however, polymer toxicity is often higher in suspension cells as we have seen with previous results. In the adherent SKBR3 cells, no toxicity was observed with the DP 100 polymer. The DP 200 did exhibit higher toxicity however at the concentration that will be administered with the peptide (300 μg/mL or less) SKBR3 cells were 75% viable. For this reason we will select a polymer with a DP below 200 and above 100 for peptide delivery.

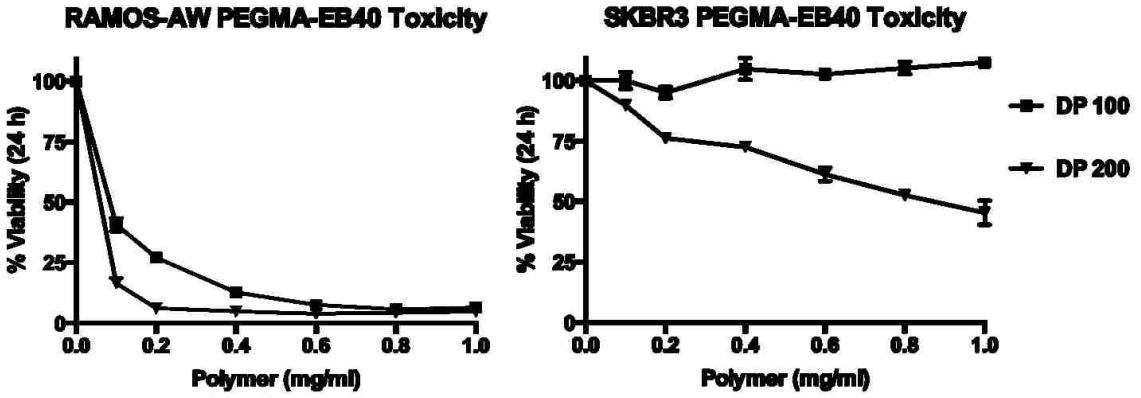

Figure 4.24: The cytotoxicity of each polymer was measured in Ramos-AW and SKBR3 cells. PEGMA-EB40 DP 100 and 200 were incubated with cells for unto 24 hours at various concentrations. Cell viability was measured by MTS using triplicate samples in a 96 well plate.

4.3.14 In vivo toxicity of Poly([PEGMA]-[DEAEMA-BMA])

The maximum tolerated dose of the PEGMA-EB40 polymers was assessed following tail vein injection in nude mice. Because this was the first time we injected a diblock copolymer with this formulation, we do did not know the therapeutic window and used a parameter matrix. PEGMA-EB40 polymers DP 50, 100, and 200 were injected sequentially at 60, 90, and 120 mg/kg with each mouse receiving a single injection. 250 μL of blood was collected via retro orbital bleeds and mice were weighed on days 1, 3, 5, and 14. Serum was isolated from red blood cells and processed by Phoenix Central Laboratories to analyze blood enzyme levels. Glucose, amylase and lipase enzymes were measured for pancreas toxicity; AST, ALT, and total bilirubin were measured for liver toxicity; creatinine for kidney toxicity; and creatine kinase for muscle toxicity (Figure 4.25). As a negative control, one untreated mouse was used for baseline measurements of each enzyme. All mice maintained their body weights after 5 days and throughout the two weeks of observations. All enzyme levels remained near baseline, 5 days post injection except for some of the polymers at the highest dosage (120 mg/kg). Slightly elevated glucose, creatinine, and lipase levels were observed at the highest concentration but these levels returned to baseline 2 weeks after treatment. One consideration for this study is that all treatments were performed on a sample size of one. This was done to determine if any of the polymers would be lethal at the concentrations administered. Because no obvious toxicity was reported in the time span of 2 weeks we continued to investigate the PEGMA-EB40 polymer formulation for future peptide delivery studies.

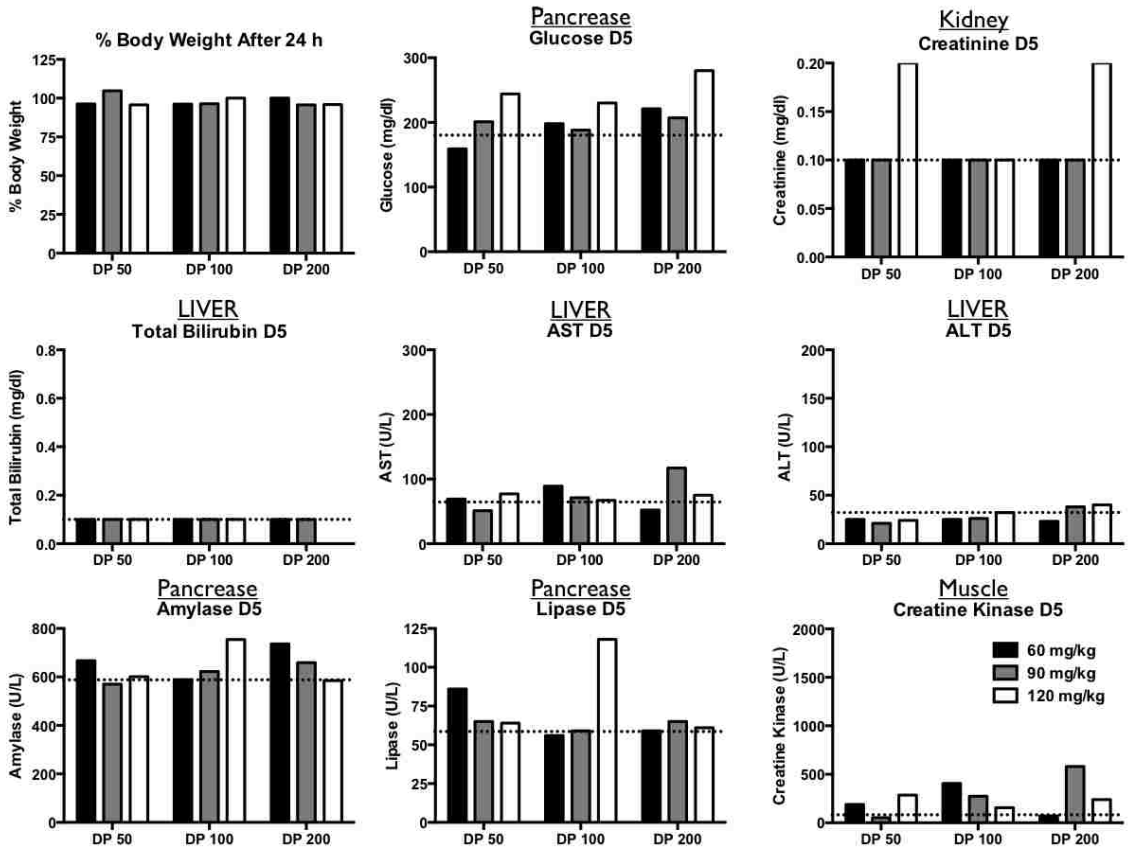

Figure 4.25: The toxicity of the PEGMA-EB40 polymer series was measured in vivo. PEGMA-EB40 DP 50, 100 and 200 were administered in nude mice via tail vein injection at 60, 90 and 120 mg/kg. 200 uL of blood was collected from mice via retrorbital eye bleeds, purified and submitted to Phoenix Laboratories for analysis. Enzyme activity levels for the pancreas, kidney, liver, and muscle are compared to a control untreated mouse (dotted line). Enyzme activity was monitored for up to 13 days but the plot above represents activity after 5 days.

4.4 Conclusions

In this chapter, optimization of a diblock copolymer formulation led us to discover a novel diblock copolymer with high hemolytic activity and a safe in vivo profile. The unique feature of this polymer design is the 950 Da PEGMA monomer that forms a PEG-like brush on the shell of the micelle. Our hypothesis was that a large PEGMA monomer on the micelle shell would impart a good in vitro/vivo safety profile. Based on this initial data, the PEGMA block combined with EB forms stable micelles with a good hemolysis profile as well. In the next chapter we will expand on the PEGMA-EB design to include peptide- and antibody-loading capabilities for targeted intracellular delivery.

4.5 References

[1] Anthony J Convertine, Danielle S W Benoit, Craig L Duvall, Allan S Hoffman, and Patrick S Stayton. Development of a novel endosomolytic diblock copolymer for siRNA delivery. *Journal of Controlled Release*, 133(3):221–229, February 2009.

[2] Brittany B Lundy, Anthony Convertine, Martina Miteva, and Patrick S Stayton. Neutral Polymeric Micelles for RNA Delivery. *Bioconjugate Chemistry*, 24(3):398–407, March 2013.

[3] E H Leduc. HYDROXYPROPYL METHACRYLATE, A NEW WATER-MISCIBLE EMBEDDING MEDIUM FOR ELECTRON MICROSCOPY. *The Journal of cell biology*, 26(1):137–155, July 1965.

[4] G Liu, C K Smith, N Hu, and J Tao. Formation and Properties of Polystyrene-block-poly(2-hydroxyethyl methacrylate) Micelles - Macromolecules (ACS Publications). *Macromolecules*, 1996.

[5] A B Lowe and C L McCormick. Homogeneous Controlled Free Radical Polymerization in Aqueous Media. *Australian Journal of Chemistry*, 55(7):367, 2002.

[6] Cyrille Boyer, Jingquan Liu, Lingjiun Wong, Michael Tippett, Volga Bulmus, and Thomas P Davis. Stability and utility of pyridyl disulfide functionality in RAFT and conventional radical polymerizations. *Journal of Polymer Science Part A: Polymer Chemistry*, 46(21):7207–7224, November 2008.

[7] Cyrille Boyer, Jingquan Liu, Volga Bulmus, Thomas P Davis, Christopher Barner-Kowollik, and Martina H Stenzel. Direct Synthesis of Well-Defined Heterotelechelic Polymers for Bioconjugations. *Macromolecules*, 41(15):5641–5650, August 2008.

[8] V Bulmus. A new pH-responsive and glutathione-reactive, endosomal membrane-disruptive polymeric carrier for intracellular delivery of biomolecular drugs. *Journal of Controlled Release*, 93(2):105–120, December 2003.

[9] Hidenori Otsuka, Yukio Nagasaki, and Kazunori Kataoka. PEGylated nanoparticles for biological and pharmaceutical applications. *Advanced Drug Delivery Reviews*, 64:246–255, December 2012.

[10] Chris Oerlemans, Wouter Bult, Mariska Bos, Gert Storm, J Frank W Nijsen, and Wim E Hennink. Polymeric Micelles in Anticancer Therapy: Targeting, Imaging and Triggered Release. *Pharmaceutical Research*, 27(12):2569–2589, August 2010.

[11] Frank Alexis, Eric Pridgen, Linda K Molnar, and Omid C Farokhzad. Factors

Affecting the Clearance and Biodistribution of Polymeric Nanoparticles. *Molecular Pharmaceutics*, 5(4):505–515, August 2008.

[12] Michelle R Longmire, Mikako Ogawa, Peter L Choyke, and Hisataka Kobayashi. Biologically Optimized Nanosized Molecules and Particles: More than Just Size. *Bioconjugate Chemistry*, 22(6):993–1000, June 2011.

[13] Andrew A Brown, Neelam S Khan, Lorenz Steinbock, and Wilhelm T S Huck. Synthesis of oligo(ethylene glycol) methacrylate polymer brushes. *European Polymer Journal*, 41(8):1757–1765, August 2005.

[14] Hidenori Otsuka, Yukio Nagasaki, and Kazunori Kataoka. Self-assembly of poly(ethylene glycol)-based block copolymers for biomedical applications. *Current Opinion in Colloid & Interface Science*, 6(1):3–10, February 2001.

[15] Matthew J Manganiello, Connie Cheng, Anthony J Convertine, James D Bryers, and Patrick S Stayton. Diblock copolymers with tunable pH transitions for gene delivery. *Biomaterials*, 33(7):2301–2309, March 2012.

[16] Connie Cheng, Anthony J Convertine, Patrick S Stayton, and James D Bryers. Multifunctional triblock copolymers for intracellular messenger RNA delivery. *Biomaterials*, 33(28):6868–6876, October 2012.

Chapter 5

ANTIBODY-MICELLE CONJUGATES FOR PROAPOPTOTIC PEPTIDE DELIVERY

A rationally designed diblock copolymer was synthesized by RAFT for the intracellular delivery of a proapoptotic peptide. The diblock copolymer was composed of three monomers in the first block: polyethylene glycol methacrylate (PEGMA 950 or 300 Da), biotin-hydroxyethyl methacrylate (bioHEMA), and pyridyl disulfide methacrylate (PyrSMA), and two monomers in the second block: diethylaminoethyl methacrylate (DEAEMA) and butyl methacrylate (BMA). The hydrophilicity of the first block and hydrophobicity of the second block caused the polymer to self-assemble into compact micelles (20 ηm). The proapoptotic BIM peptide was modified with a cysteine and conjugated through a reducible disulfide bond. The micelle-peptide conjugates were then loaded with antibody/streptavidin conjugate through the bioHEMA monomer using anti-CD22/SA for B-cell targeting and anti-Her2neu/SA for ovarian cancer cell targeting. The effect of antibody-targeting and proapoptotic activity were quantified in Ramos and SKOV3 cells. A Ramos tumor-xenograft model was used to study the pharmacokinetic and biodistribution parameters of dual-radiolabeled conjugates. Early tumor activity was also measured by histology and immunohistochemistry with cleaved caspase 3 and Ki67 markers.

5.1 Introduction

Dysregulated apoptotic machinery is a hallmark of cancer leading to apoptosis inhibition, uncontrolled proliferation, and chemoresistance[1]. In cancer cells, the balance of proapoptotic and prosurvival proteins is tipped toward overexpression of the prosurvival B-cell lymphoma 2 (Bcl-2) proteins. Increased Bcl-2 expression has been linked with poor prognosis and a diminishing response to chemo and radiation treatment[2,3]. Patients with cancers near the apoptotic threshold, known as mitochondrial priming, exhibit c better clinical response to chemotoxins[4]. In patients with multiple myeloma, AML, ALL, and ovarian cancer, mitochondrial priming consistently correlated with better clinical outcomes to chemotherapy. Targeting Bcl-2 proteins in unprimed cancer cells has the potential to decrease the apoptotic threshold and increase sensitivity to chemotherapeutics in highly resistant cancer cells.

Small molecules derived from the Bcl-2 homology 3 (BH3) domain, elicit apoptotic activity by binding Bcl-2 proteins and displacing the activators BAK and BAX to initiate apoptosis.[5]. BH3-mimetics like ABT-737 and ABT-263, which specifically target Bcl-2, Bcl-X_L, and Bcl-w, have shown promising clinical outcomes as a single agent or in combination with chemo drugs[6–8]. One of the set backs to these small molecules is that they only target a specific subset of cancers that don't have increased Mcl-1 and BFL1 expression. To affect a broader range of cancers, BH3-mimetic peptides have been developed. One of the most promiscuous peptides, BIM, exhibits a high binding affinity (K_D = 1-5 nM) to all five Bcl-2 proteins (including Mcl-1 and BFL1). BH3 profiling by Letai and Certo showed that BIM peptides can induce cytochrome c release in primed and unprimed mitochondria isolated from different cancer lines[9,10]. When fused to the polycationic HIV-1 derived TAT peptide, TAT-BIM could penetrate and induce apoptosis in cancer cells[11]. Recently, LaBelle and coworkers introduced a hydrocarbon "staple" in the BIM peptide to improve stability, protease-

resistance, and cell-permeability[12,13]. Stapled BIM induced apoptosis in resistant hematologic cancers and preferentially affected cancer cells over normal cells. Studies with TAT-BIM and stapled BIM have highlighted the clinical importance of BIM but effective in vivo delivery of therapeutic peptides has not yet been addressed.

Antibody-drug conjugates (ADC), designed to target cancer cells and deliver small molecules that would otherwise be too toxic on their own have become a clinical success[14–18]. A similar ADC platform may be harnessed for delivering biologics like the BIM peptide. Unfortunately, receptor-mediated endocytosis of ADCs results in endosomal/lysosomal trafficking and degradation by proteases at low pH. To overcome this trafficking barrier, proteins and nucleic acids have been delivered using pH-responsive polymers for endosomal escape and cytosolic release[19–22]. These polymers undergo a phase transition from a hydrophilic state at physiological pH (7.4) to a hydrophobic and membrane disruptive state at endosomal pH ($\leq$ 6.6). Polymers used in this application often self-assemble into particles known as micelles with a hydrophilic core, and hydrophilic corona. Reversible addition-fragmentation chain transfer (RAFT) synthesis allows for the development of well-tuned heterotelechelic diblock copolymers with endosomal-releasing capabilities. Manganiello et al. demonstrated that the copolymerization of diethylaminoethyl methacrylate (DEAEMA) with butylmethacrylate (BMA) by RAFT could be tuned for endosomal escape and intracellular delivery of plasmid DNA[23]. A hydrophilic block like poly(ethylene glycol) on the corona of the micelle could provide steric stabilization with "stealth-like" properties to minimize protein adsorption and increase blood circulation[24–30]. The incorporation of functional and/or reactive monomers (e.g. pyridyl disulfides, maleimides, and biotin) facilitate the integration of targeting and therapeutic elements into the copolymer[31–36].

In the following work, RAFT was employed for the synthesis of a multifunctional diblock copolymer with antibody-targeting capabilities and proapoptotic peptide delivery in SKOV3 ovarian cells and Ramos B-cell lymphoma cells. The hydrophilic

first block is composed of three different monomers: polyethylene glycol methacrylate 950 (O950) or 300 Da (O300), pyridyldisulfide methacrylate (PyrSMA), and biotin-hydroxyethyl methacrylate (bioHEMA). The first block was designed to promote micelle stability in vivo, a labile peptide bond, and complexation of an antibody/streptavidin conjugate. The hydrophobic second block is composed of DEAEMA and BMA and was designed for endosomal escape. In vivo parameters such as maximum tolerated dose and blood toxicity were studied to optimize formulation parameters and polymer block lengths. The proapoptotic activity of the BIM peptide on the antibody-micelle conjugate was demonstrated in SKOV3 and Ramos cells. In vivo activity of the conjugates was evaluated in a Ramos tumor-xenograft mouse model and measured by cleaved caspase 3 and Ki67 activity. The pharmacokinetics and biodistribution of the [^{3}H]antibody-micelle-[^{14}C]peptide conjugates was also studied.

5.2 Experimental Methods

5.2.1 Fmoc solid phase peptide synthesis

Peptides were synthesized using Fmoc solid phase synthesis at a 0.1 mmole quantity. BIM and BIM-L62E (BIM/LE) were synthesized from trityl-cys preloaded NovaPEG resin (EMD Millipore) using the following sequences:

BIM = NH2-CMRPEIWIAQELRRIGDEFNAYYARR-OH

BIM/LE = NH2-CMRPEIWIAQEERRIGDEFNAYYARR-OH

After synthesis, resin was rinsed sequentially with N-methyl-2-pyrrolidone, dimethylformamide, dichloromethane, and methanol, dried under vacuum, then cleaved and deprotected with a solution containing 9.4 mL trifluoroacetic acid, 250 μL dH20, 250 μL ethanedithiol, and 100 μL triisopropylsilane. Following resin filtration, crude peptide was precipitated into cold ether/hexane (60/40), dissolved in ddH20 containing TCEP then purified by reverse-phase high performance liquid chromatography on a Jupiter 5μm C18 300 column (Phenomenex). HPLC purified peptides were confirmed by ion trap mass spectrometry.

5.2.2 Cytochrome c release from isolated mitochondria

The potential for BIM and BIM/LE to induce cytochrome c release from isolated mitochondria was measured with an ELISA assay. Ramos and Ramos-AW cells (500 x 10^6) were grown in 3-tier culture flasks, washed with PBS and equilibrated in 5 mL of homogenization buffer (0.25 M sucrose, 1 mM EGTA, 10 mM HEPES/NaOH, 0.5% BSA, pH 7.4) for 5 minutes at 4°C. Cells were homogenized under high nitrogen pressure in a steel container for 10 min at 400 psi, 4°C. Disruption of cell membranes was confirmed with Trypan blue under a microscope. Cells were collected and centrifuged

for 10 minutes at 750 g in 15 mL round bottom tubes (BD (35)2059). After lipids were removed from the surface, the supernatant was transferred to a new vial and centrifuged for 12 minutes at 12,000 g, 4°C. The mitochondria pellet was resuspended in 500 μL of wash buffer (0.25 M sucrose, 1 mM EDTA, 10 mM Tris/HCl, pH 7.4, supplemented with protease inhibitor (Roche Complete minitablets) and placed on ice. Next, a BCA assay was performed to measure total protein. 15 μL of mitochondira solution was collected and added to 15 μL of 0.6% SDS, then heated for 10 minutes at 95°C. 10 μL of BSA at 0, 0.5, 1, 1.5, and 2 mg/mL and 5 μL 0.9% SDS was added to a 96 well plate and 4, 10, an 15 μL of mitochondria/SDS solution was added to the plate and equilibrated with dH20. 100 μL of bichonic acid/copper(III) sulfate (50/1) was added to each well and incubated for 50 minutes at 37°C. The BSA standards were used to make a standard curve and measure the total protein in the mitochondria solution. Finally, peptides in DMSO (1 mM) were incubated with 50 ug of mitochondria in 100 uL of experimental buffer (125 mM KCl, 10 mM Tris-MOPS [pH 7.4], 5 mM glutamate, 2.5 mM malate, 1 mM KPO4, 10 uM EGTA-Tris, pH 7.4) for 35 minutes at 37°C. Solutions were then centrifuged at 13,000 rpm for 10 minutes, 4°C, and supernatant was collected for measurement using a Cytochrome c ELISA kit.

5.2.3 Synthesis of PyrSMA monomer

Mono-2-(methacryloxy)ethyl succinate)(SMA, 8.9 g, 0.0387 mol) was dissolved in 300 mL chloroform in a 500 mL round-bottomed flask. To this solution N-hydroxy succinimide (NHS, 4.89 g, 0.0425 mol) was added and stirred for 30 min under nitrogen environment. This solution was cooled to 0°C in an ice bath and the reaction mixture was further stirred for 30 min. N,N-dicyclohexyl carbodimide (DCC, 9. 57 g, 0.0464 mol) and a catalytic amount of 4-(dimethylamino)pyridine (66 mg) were added and the solution was stirred for 1 h at 0°C. The reaction was further continued for 22

h at room temperature under nitrogen environment. After reaction, a large white precipitated powder of dicyclohexyl urea was filtered off twice. A solution of 2-(pyridyl dithiol)-ethylamine hydrochloride (1.0 g, 0.0045 mol) and Et3N (1.13 g, 0.0112 mol) was cooled to 0°C in an ice bath and stirred for 30 min. Previously synthesized NHS-activated SMA solution in chloroform (65 mL chloroform solution 2.2 g, 0.0067 mol) was then added dropwise for 1 h. The reaction mixture was stirred overnight (16 h) at room temperature and transferred to a separating funnel followed by washing three times with H2O (150 mL). The organic extracts were finally washed with brine and dried over Na_2SO_4, filtered, and concentrated in vacuo to afford a crude oil which was purified by column chromatography [SiO2, EtOAc/ hexane 3:1] to obtain 1.62 g pure product (yield=60.5%). 1H NMR CDCl3; MS(ESI) m/z calcd for $C_{17}H_{22}N_2O_5S_2$ M+ 421.5, found 421.2.

5.2.4 Synthesis of bioHEMA monomer

To make biotin monomer, the small molecule biotin was conjugated to hydroxyethyl methacrylate through an ester bond. First, 1 gram of biotin was dissolved in 30 mL of dimethylacetamide. A 2-fold molar excess of hydroxyethylmethacrylate (HEMA), N,N-diisopropylcarbodiimide (DIC), and 4-dimethylaminopyridine (DMAP) were dissolved in the biotin solution and reacted overnight at 4°C. The reacted product was filtered to remove dicyclohexylurea (DCU) by-product, then precipitated in cold diethylether (4X) to remove DMAP. Finally the product was dissolved in dimethylsulfoxide and precipitated in 0.5 M NaOH to remove free biotin. The pellet was washed with ddH_2O and the final product was lyophilized into a dry powder. The purity of the bioHEMA monomer was confirmed by 1H-NMR and mass spectrometry.

5.2.5 RAFT synthesis of multifunctional PEGMA macroCTAs

Two copolymers were synthesized via RAFT using Azobis(4-cyanopentanoic acid) (ABCVA) as the initiator, 4-cyanopentanoic acid dithiobenzoate (CTP) as the chain transfer agent (CTA), with 20 wt% monomer in dimethysulfoxide (Figure 5.1). The initial monomer ($[M]_o$) to CTA ($[CTA]_o$) to initiator ($[I]_o$) ratios for the two polymers was 25:1:0.1. Both reaction solution contained a feed ratio of 10% pyridyl disulfide methacrylate (PyrSMA), 10% bioHEMA, and either 80% polyethylene glycol methacrylate 950 Da (O950) or 300 Da (O300) (Scheme 1). Individual polymerization solutions were vortexed in 20 mL scintillation vials, transferred to septa-sealed 10 mL round bottom flasks, purged under N2 for 30 minutes, and transferred to a preheated water bath at 70°C for 14 h. The resultant polymers were isolated by precipitation in diethyl ether. The precipitated polymers were then dissolved in acetone and precipitated into diethyl ether (x6). The dried polymers were analyzed by 1H NMR to assess purity and gel-permeation chromatography (GPC) was used to determine number average (Mn) molecular weight and polydispersity (PDI) of the polymers using Tosoh SEC TSK GEL α-3000 and α-4000 columns (Tosoh Bioscience, Montgomeryville, PA) connected in series to a 1200 Series liquid chromatography system (Agilent, Santa Clara, CA) and a miniDAWN TREOS three-angle light scattering instrument with an Optilab TrEX refractive index detector (Wyatt Technology, Santa Barbara, CA). HPLC-grade DMF containing 0.1 wt% LiBr at 60°C was used as the mobile phase at a flow rate of 1 mL/min. Reverse-phase high performance liquid chromatography (RP-HPLC) was used to measure monomer conversions for each macroCTA using aliquots collected at T_o and T_x.

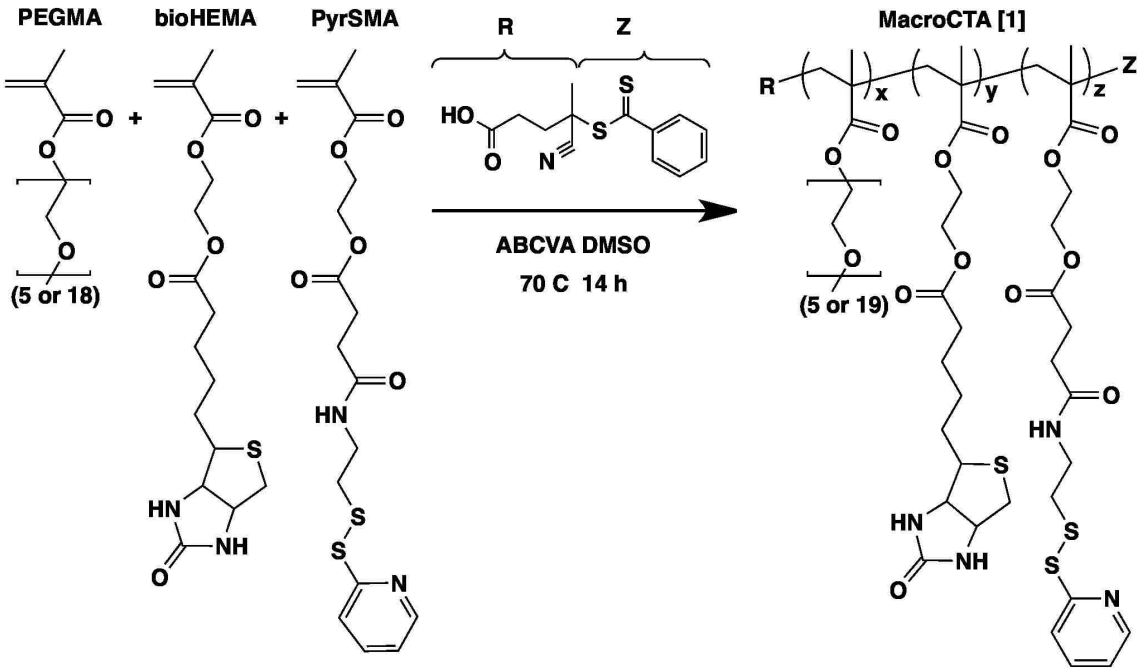

Figure 5.1: RAFT synthesis was used to make two macro chain transfer agents (CTA) with ABCVA as the radical initiator and dithiobenzoate as the chain transfer agent (CTA). Three monomers were incorporated into the macroCTAs: poly(ethylene glycol) methacrylate (PEGMA 300 or 950 Da), biotin-hydroxyethyl methacrylate (bioHEMA), and pyridyl disulfide methacrylate (PyrSMA).

5.2.6 RAFT synthesis of diblock copolymers with PEGMA macroCTAs

O950 and O300 polymers were isolated from the previous synthesis and used as the macroCTA for RAFT copolymerization with Azobis(4-cyanopentanoic acid) (ABCVA) as the initiator, 4-cyanopentanoic acid dithiobenzoate (CTP) as the chain transfer agent (CTA), 50 wt % monomer in 1,4-dioxane (Figure 5.2). The initial monomer ($[M]_o$) to macroCTA ($[mCTA]_o$) to initiator ($[I]_o$) ratios for both polymers was 125:1:0.2. The two polymer solutions contained a monomer feed of 60% diethylaminoethyl methacrylate (DEAEMA) and 40% butyl methacrylate (BMA). Individual polymerization solutions were vortexed in 20 mL scintillation vials, transferred to septa-sealed 5 mL round bottom flasks, purged under N_2 for 20 minutes, and transferred to a preheated water bath at 70°C for 8 h. The resultant polymers were isolated by precipitation in petroleum ether. The precipitated polymers were then redissolved in acetone and reprecipitated into petroleum ether (x5). The dried diblock copolymers were analyzed by 1H NMR, GPC and RP-HPLC as previously described.

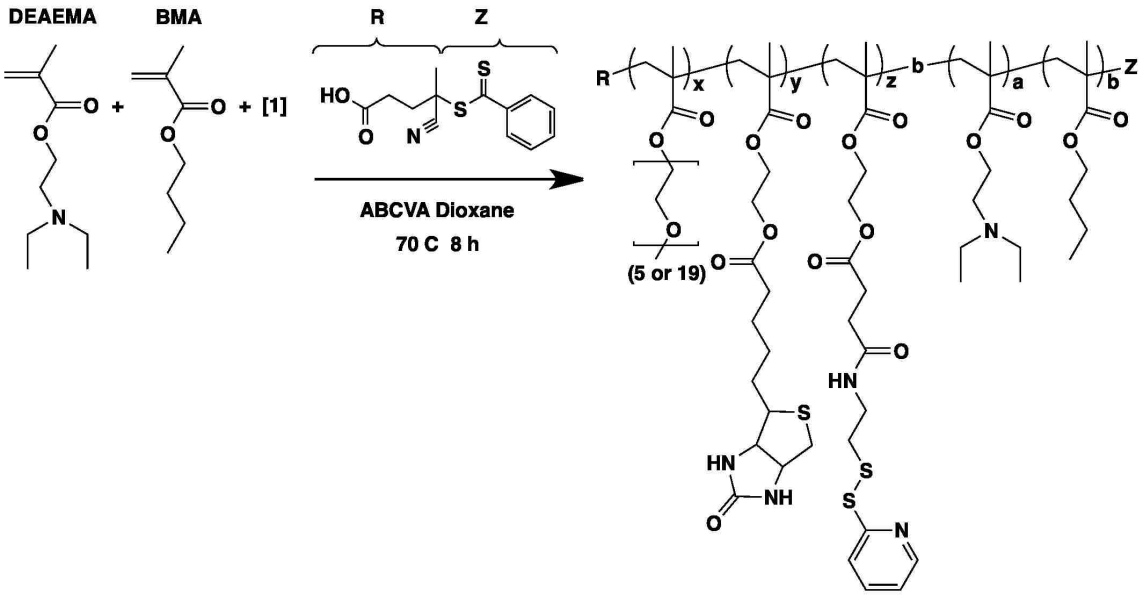

Figure 5.2: RAFT synthesis was used to make two diblock copolymers by incorporating the multifunctional O950 and O300 polymers as the macroCTAs with ABVCA as the radical initiator. To make the second block, the monomer feed ratio was 60% diethylaminoethyl methacrylate (DEAEMA) and 40% butyl methacrylate (BMA).

5.2.7 Formulation of peptide-loaded micelles

Polymeric micelles were conjugated to peptides via disulfide exchange. First, polymers were dissolved as unimers in ethanol (100 mg/mL) then diluted 10-fold into DPBS, pH 7.4 to spontaneously form micelles. Ethanol content was reduced to less than 0.01% using Amicon-4 Ultra 3k MWCO spin columns (EMD Millipore) and the polymer concentration was verified by 290 ηm absorbance. The number of pyridyl disulfde (PDS) groups per polymer chain was quantified by reducing PDS groups on the polymeric micelles with an excess of Bond Breaker TCEP solution (Pierce). Conversion of PDS to 2-mercaptopyridine results in a colorimetric change quantified by a 343 nm absorbance with an extinction coefficient of 8,080 $M^{-1}cm^{-1}$. Next, BIM or BIM/LE were dissolved in anhydrous dimethylsulfoxide (30 mM), added to the polymer solutions and mixed vigorously by vortexing then reacted overnight at room temperature. In the final reaction mixture, the polymer concentration was 500 μM with a 1.25 molar excess of peptide which resulted in one peptide bound per polymer chain. Disulfide conjugation was monitored via PDS release and the formation of 2-mercaptopyridine. Reduction of the disulfide bond in the presence of glutathione was confirmed by HPLC purification. The formation of micelles and the number average diameter before and after peptide loading was measured by dynamic light scattering following filtration through a 0.45 μm syringe filter with a polymer concentration of 0.5 mg/mL. The ability of the biotin-containing polymer micelles to complex with streptavidin and antibody/streptavidin conjugates was quantified using a HABA assay as previously describedBerguig:2012vz.

5.2.8 Cell culture

SKOV3 and Ramos cells were obtained from the American Type Culture Collection (ATCC, Mannassas, VA). Cells were maintained in log-phase growth at 37°C and 5%

CO_2 and grown in RPMI 1640 medium supplemented with L-glutamine and 25 mM HEPES supplemented with 1% penicillin-streptomycin (GIBCO) and 10% fetal bovine serum (FBS, GIBCO).

5.2.9 Antibody-mediated uptake of polymer-peptide conjugates

To study the effect of antibody targeting on the polymeric micelles, fluorescently-labeled peptide was conjugated and measured within the cells by flow cytometry. To make the fluorescent peptide, a 4-fold molar excess of Rhodamine Red-X, succinimidyl ester was reacted with the N-terminal amine of the BIM peptide in anhydrous DMSO with diethylethanolamine (DIEA). After 4 hours, Rhodamine-labeled BIM (RhoBIM) peptide was purified by RP-HPLC and the final product was confirmed by mass spectrometry. For uptake studies, RhoBIM was conjugated to the polymer micelles as previously described. Anti-Her2neu/SA conjugates were loaded on the peptide-polymer conjugates at various ratios for one hour prior to cell treatment. SKOV3 cells were seeded at 1.5 x 10^5 cells per well in 6-well plates one day before and Ramos cells were seeded at 3.0 x 10^5 cells per well on the day of the study. Cells were treated in triplicate with fluorescent conjugates for 1, 2, and 4 hours at a 50 μM peptide dose. After the indicated incubation times, cells were washed with PBS containing 2% BSA and 0.1% Trypan blue to quench extracellular fluorescence. The median fluorescence intensity of treated cells was measured by flow cytometry. Cells were excited at 532 ηm and fluorescence emission was collected at 575 ηm. To accurately measure fluorescence, cells were gated by forward scattering area (FSC-A) and side scattering as well as FSC height (FSC-H) and FSC width (FSC-W) with 10,000 gated events per sample. Post-acquisition analysis was performed with FlowJo flow cytometry software (Tree Star, Ashland, Oregon). Gating of untreated cells was applied to each cell type and time point and autofluorescence from untreated cells was subtracted from each treatment.

5.2.10 Cell viability measured by MTS

Peptide conjugates were formulated as previously described. SKBR3 and SKOV3 cells were seeded in 96 well plates, 6 x 10^3 cells per well and allowed to adhere overnight. Ramos cells were seeded in 96 well round bottom plates at 50 x 10^3 cells per well. In triplicate, peptide conjugates were added to each well at various concentrations with at a final volume of 100 μL including media. Cell viability was measured after 1 and 2 days of incubation with conjugates after washing with fresh media. 20 μL of CellTiter 96 Aqueous One Solution Cell Proliferation Assay (MTS Promega) was added to 100 μL of media and allowed to react for up to 2 hours. After significant conversion of MTS to formazan was observed, 100 μL of the MTS/media solution was transferred to a new 96 well plate and the absorbance at 490 ηm was measured on a plate reader (Tecan)

5.2.11 Radiolabeling HD39/SA and BIM with [3H] and [14C]

Conjugates were dual-radiolabeled with 3H and 14C in order to follow the antibody and peptide in vivo. First, 6.2 mg of HD39/SA at 2 mg/mL in buffer containing 50 mM sodium borate, 150 mM NaCl, pH 8.5, was reacted with 1 mCi 3H-N-succinimidyl propionate (American Radiolabeled Chemicals, Inc.) at 5 mCi/mL in DMF for 2 hours at 25°C. Unreacted radiolabel was removed using a PD-10 desalting column equilibrated with PBS. The final [3H]HD39/SA product was concentrated using an Amicon Ultra-4 centrifugal filter unit with 30,000 NMWL and the final concentration was measured by A_{280}. The 10 mg of BIM peptide was dissolved in DMSO containing an excess of N,N-diisopropylethylamine. A 5X molar excess of 14C-acetic anhydride in 1 mL of toluene was reacted with the BIM peptide for 30 minutes. Radiolabeled peptides were precipitated in ether to remove excess radiolabel and acetic acid. The concentration and specific activity of [^{3}H]HD39/SA and [^{14}C]BIM was measured

by A_{280} absorbance and scintillation counting with ULTIMA GOLD scintillation fluid.

5.2.12 Pharmacokinetics of dual-radiolabeled conjugates

For all in vivo studies, BALB/c nu/nu mice (6 to 8 weeks old) were used from Harian Sprague-Dawley and house under protocols approved by the FHCRC Institutional Animal Care and Use Committee. To prepare cell suspensions, Ramos cells were resuspended 10 x 106 cells per 200 μL PBS. Mice were injected subcutaneously in the right flank with 10 x 10^6 Ramos cells and placed on a biotin-free diet (Purina Feed). Tumors were allowed to grow for seven days until they reached 50 to 100 mm^3. To measure whole blood clearance, 6 mice per treatment each received 1.4 nmoles of [3H]HD39/SA with or without 14 ηmoles of Polymer-[14C]BIM conjugates via tail vein injection. Serial blood samples were drawn in triplicate from the retro-orbital venus plexus using a 10 uL capillary tube at the following timepoints: 5 m, 15 m, 30 m, 1 h, 2 h, 4 h, 8 h, and 24 h. (Exact injection and collection times were collected for each mouse). Blood was immediately transferred to scintillation vials containing 500 uL of Solvable (Perkin Elmer). 5 mL of ULTIMA GOLD scintillation fluid was added and sonicated for 10 minutes. 3H and 14C activity in the blood was measured by scintillation counting using an automated deconvolution of radioactive signal. Syringe weights were measured before and after injection to calculate the total injection volume. Specific radioactivity for each treatment was measured in triplicate from stock solutions. For blood clearance calculations, 80 mL (blood) per kg (mouse) was assumed. Blood concentrations were plotted using GraphPad Prism and plotted to a two-compartmental open model (bi-exponential equation) with 1/y2 weighting to account for larger standard deviations at the earliest time points. The number of peptides per antibody/streptavidin conjugate was calculated by dividing the peptide to antibody/streptavidin concentration.

5.2.13 Biodistribution of Dual-Radiolabeled Conjugates

After 24 hours, mice were weighed, sacrificed and blood by heart stick. Tumors, lung, liver, spleen, stomach, kidney, small intestine, large intestine, and muscle were harvested, weighed, and homogenized in 10 mL of ddH_2O per gram of tissue. 200 μL of homogenized tissue was transferred to a scintillation vial and 500 μL of Solvable was added. Samples were incubated at 60 oC overnight until tissues were solvated. 50 uL of 200 mM EDTA and 200 μL of 30% hydrogen peroxide were added and samples were incubated overnight at room temperature. 25 uL 10N HCl and 10 mL of ULTIMA GOLD scintillation fluid were added to each sample, vortexed, then incubated overnight at room temperature. Samples were run on a scintillation counter to measure ^{3}H and ^{14}C signal and the percent-injected dose per gram (%ID/g) of tissue or blood was calculated. The stability of the peptide bound to the polymer was calculated by plotting of peptide to antibody for each organ.

5.2.14 Cleaved Caspase 3 Activity in Tumor Xenografts

Xenograft tumors were formed as previously described. Seven days after inoculation mice were injected via tail vein in groups of 5 with HD39/SA, HD39/SA-Polymer, HD39/SA-Polymer-BIM or Polymer-BIM at a dose of 15 mg/kg (HD39/SA), 275 mg/kg (O950) or 159 mg/kg (O300), and 16 mg/kg (BIM). The molar ratio of HD39/SA to Polymer to BIM was 1:90:90. Three days following treatment, mice were sacrificed and blood was collected via heart stick. Tumor, liver, lung, and kidney were harvested and prepared for formalin fixing. Lungs were perfused with formalin, kidneys bisected longitudinally, and liver cut into two sections containing the median lobe and left median lobe. Sections were placed into cassettes, soaked in formalin for 3 days than submitted to pathology for processing.

5.3 Results and Discussion

5.3.1 Cytochrome c release confirms BIM not BIM/LE activity

To test the activity of the BIM and control BIM/LE peptides, a cytochrome C release study was performed (Figure 5.3). Mitchondria isolated from Ramos cells, a B-cell lymphoma line were incubated with either BIM or BIM/LE at 1, 0.1, or 0.01 μM for 30 minutes. This would allow sufficient time to bing all Bcl-2 proteins and release activator proteins, Bak and Bax, which were previously sequestered by the Bcl-2 family proteins. Release of Bak and Bax would allow for homodimerization, insertion into mitochondrial membrane, mitochondria depolarization and cytochrome c release. After incubation with the peptides, mitochondria were isolated from the supernatant by centrifugation and the percent cytochrome c released from mitochondria was measured using an ELISA assay. 100% release was based on mitochondria treated with 0.1% TritonX. As is seen from the figure μM BIM but not BIM/LE caused 100% cytochrome c release. The effects were also dose dependent with 0.1 μM and 0.01 μM yielding 80% and 50%, respectively. The single point mutation in BIM/LE however, was enough to inhibit the binding activity of the BIM peptide. These results indicate that the BIM peptide sequence is critical to induce cytochrome c release in Ramos cells and that BIM/LE will serve as a good negative control peptide for the polymer carrier. The next challenge will be to deliver significant quantities of this peptide intracellularly to induce apoptosis in vitro and possibly in vivo.

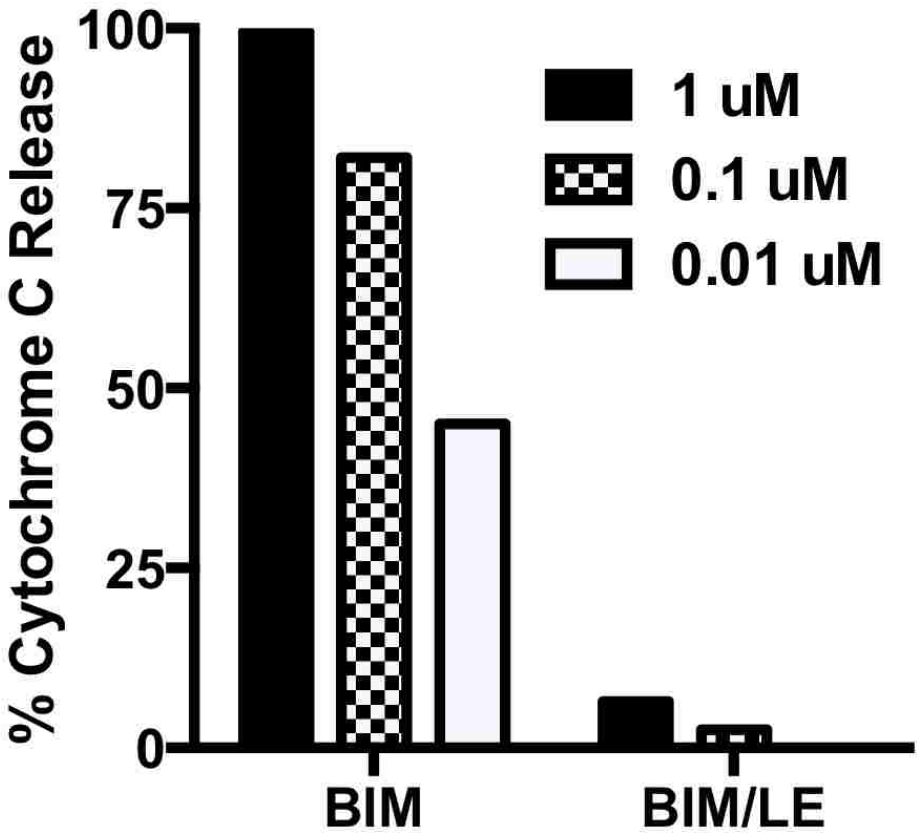

Figure 5.3: Mitochondria isolated from Ramos cells were treated for 30 minutes with BIM or control BIM/LE peptide. Cytochrome C release induced by the BIM peptide was quantified with an ELISA assay on the supernatant. The control BIM/LE peptide with a leucine to glutamic acid mutation did not exhibit any considerable release.

5.3.2 Optimization of poly[(PEGMA)-(DEAEMA-BMA)]

A series of diblock copolymers were synthesized by RAFT to identify a good target degree of polymerization (DP) and block ratios for the hydrophilic and endosomolytic blocks. The scheme for RAFT synthesis of the first and second block are given in Figure 5.4. The polyethylene glycol methacrylate 950 ($PEGMA_{950}$) monomer with 19 repeat units was homopolymerized using a target DP of 25. After purification, the polymer was then used as a macro chain transfer agent (CTA) for the copolymerization of DEAEMA and BMA (EB) at a monomer feed ratio of 60 to 40, respectively. A series of diblock copolymers (PEGMA950-EB40) were synthesized with a target DP of 50, 100, 150, 200, and 300 in order to study correlate the effects on particle size and hemolytic activity. Gel-permeation chromatography was used to measure the number average molecular weight (M_n) of the polymer series. An overlay of the chromatograms is shown in Figure 5.5A. Some polymer coupling is seen on the left edge for each peak which often occurs when using the CTP as the CTA. The theoretical (HPLC) and experimental (GPC) molecular weight is plotted against the target DP in Figure 5.5B. A linear relationship exists between the target DP and molecular weight of O950-EB as is commonly seen with living polymerizations by RAFT. Furthermore RAFT provides good control of molecular weights with low polydispersities (PDI) less than 1.1. Particle size for the polymer the DP 50, 100, and 200 polymers in phosphate buffer was measured by dynamic light scattering (DLS) as seen in Figure 5.5C. Interestingly, the DP 50 polymer was unable to form particles, while DP 100 and 200 had a number average diameter of 19 and 23 nm, respectively. The phenomenon seen with the DP 50 polymer is likely due to the short chain length of the EB block which may not impart enough hydrophobicity to form micellar structures. The sterically bulky PEGMA first block is very hydrophilic and therefore requires a larger second block (DP 100 or more) to form stable particles. The potential for each polymer in the series to exhibit membrane destabilizing activity in a pH dependent manner was studied with

a hemolysis assay as shown in Figure 5.5D. The polymers incubated at 20 μg/mL with red blood cells exhibited distinct activities with respect to their DP. The first polymer, DP 50, did not exhibit any hemolytic activity which further demonstrates that a small hydrophobic second block not only prevents the formation of particles but also makes it inactive for hemolysis. The DP 100 polymer exhibited some hemolytic activity at pH 6.2 and below, reaching up to 60%. The DP 200 polymer exhibited higher activity starting at pH 6.6 and below, reaching 100%. The DP 300 polymer exhibited the highest activity starting at pH 7.0 and below and also reaching 100%. Based on these results, we decided to target a DP between 100 and 200 to achieve stable particles with membrane destabilizing activity around endosomal pH 6.6

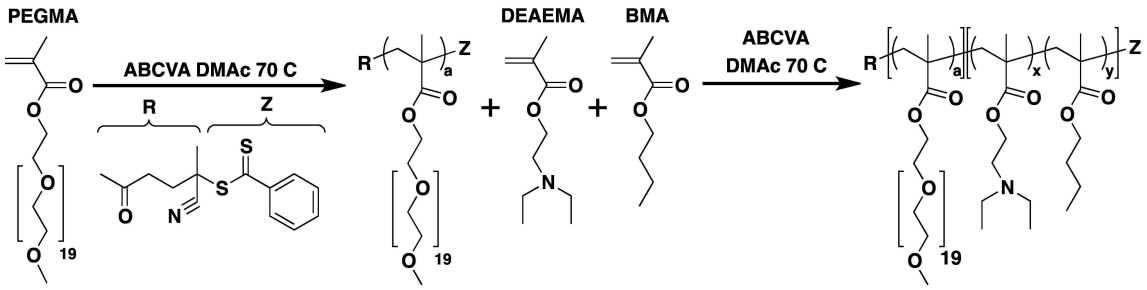

Figure 5.4: The RAFT synthesis of the Poly(PEGMA) and Poly[(PEGMA)-(DEAEMA-BMA)] (PEGMA950-EB40) diblock copolymers was performed under nitrogen using ABCVA as the initiator, CTP as the chain transfer agent, and dimethylacetamide (DMAc) as the solvent at 70°C.

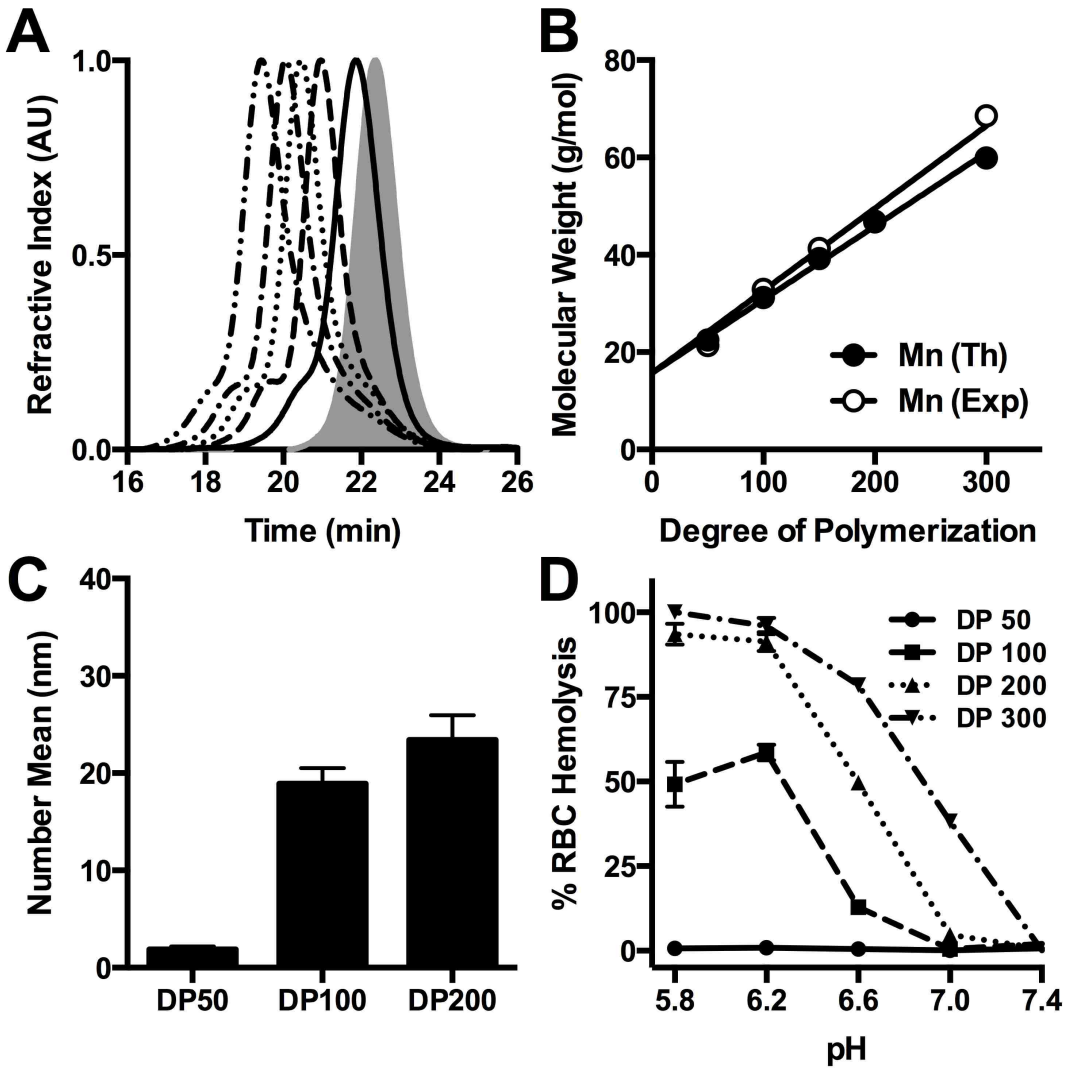

Figure 5.5: The PEGMA950-EB40 polymer series was analyzed by gel-permeations chromatography (A) to determineM_n. A plot of target DP versus experimental and theoretical molecular weight determined by GPC and HPLC, respectively is also shown (B). Thea ability to form micelles in phosphate buffer and the number average diameter was measured by dynamic light scattering (C). The hemolytic activity of each polymer as a function of pH was also measured (D).

5.3.3 Characterization of PyrSMA monomer by NMR

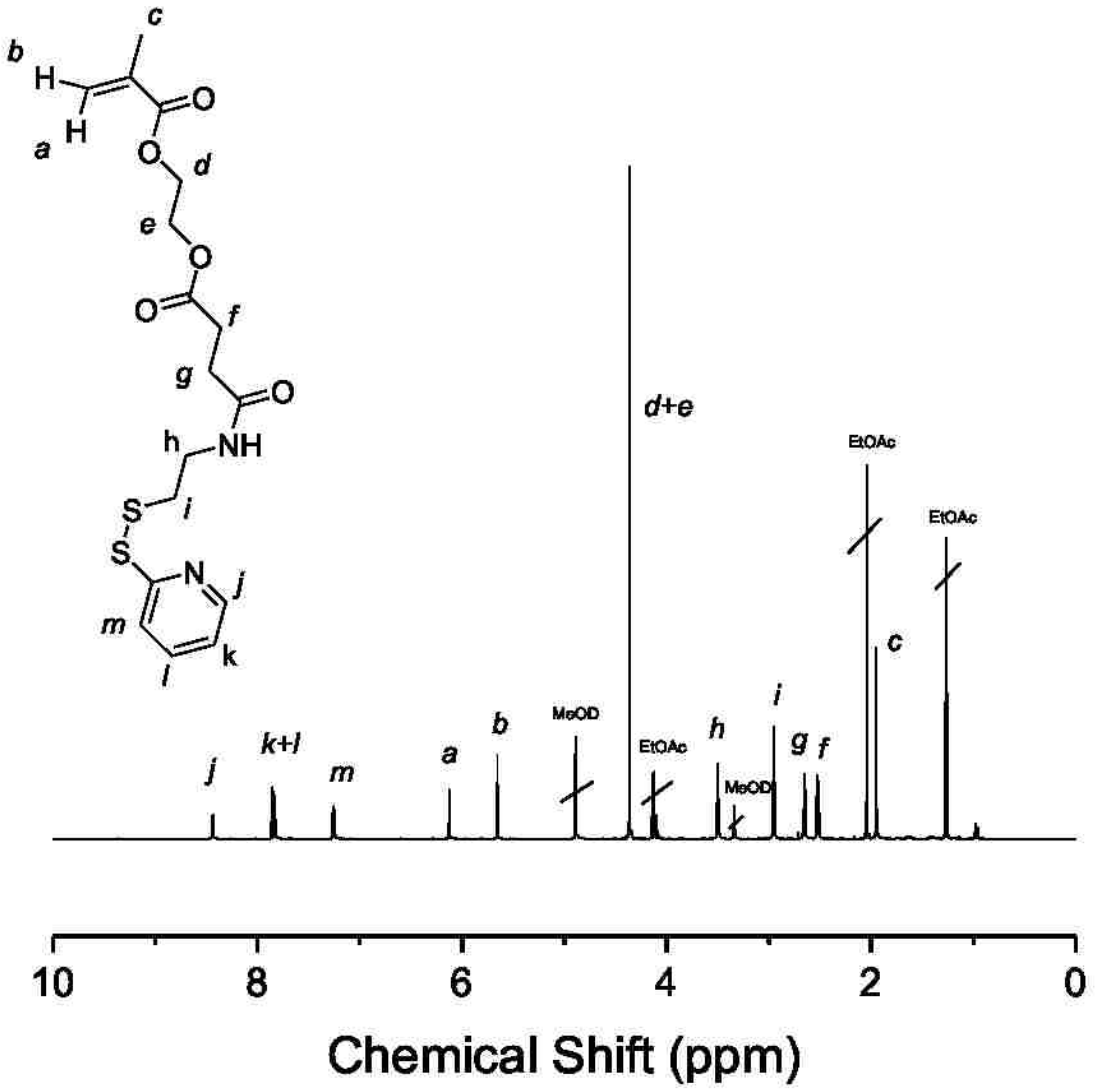

Figure 5.6: 1H-NMR was performed on the PyrSMA monomer to confirm purity of the final product. All the proton peaks on the NMR spectrum were accounted for in the monomer and assigned letters as seen in the figure.

5.3.4 Synthesis of poly[(PEGMA-PyrSMA-bioHEMA)-(DEAEMA-BMA)]

The multifunctional diblock copolymer poly[(PEGMA-PyrSMA-bioHMEA)-(DEAEMA-BMA)] termed "O950" was synthesized to incorporate several components for successful intracellular peptide delivery (Figure 5.7). The first monomer PEGMA is 950 Da with 19 ethylene oxide repeating units. This monomer serves as the bulk of the hydrophilic block, promoting aqueous solubility with peptide and antibody loading and biocompatibility for in vitro and in vivo application. This sterically bulky methacrylate monomer is longer than most monomers used in RAFT synthesis but it's reactivity and polymerization capabilities have been optimized in previous formulations. The next methacrylate monomer, bioHEMA allows for facile complexation with cancer-targeting monoclonal antibodies that has been previously conjugated to streptavidin. Incorporation of the bioHEMA monomer in the hydrophilic block allows for easy complexation while the polymer is assembled in a micelle structure. The last methacrylate monomer PyrSMA, contains a pyridyl disulfide end group for disulfide conjugation to the cysteine modified BIM peptide. Again, this monomer was incorporated in the hydrophilic block to allow for easy conjugation of the BIM peptide while the polymer is aggregated in the micelle state. It was also thought that incorporation of the PDS containing monomer between the bulky PEGMA monomers would allow for some steric hindrances and protect the peptide from reduction in the blood prior to arriving at the tumor site. After synthesis and purification of the hydrophilic block, the polymer was employed as the macro chain transfer agent (macroCTA) for the synthesis of the second block. The 60:40 feed ratio for the DEAEMA and BMA monomers was previously optimized by Anthony Convertine and coworkers[23,30]. The optimized ratio helps the unimeric polymers form micelles in aqueous solutions, while taking advantage of the pH-tranisition from DEAEMA upon acidification in endosomes and the hydrophilic residue of BMA for membrane interactive properties. Together these monomers have demonstrated the delivery and intracellular release of microRNA and

plasmid DNA in living cells. Varying this feed ratio too high or twoo low above the 60:40 feed ratio often results in micelle instability, an undesirably charged micelle core, or no pH-transition. The phase transition of the polymer micelles into unimers triggered by acidic pH is a key component of this polymer design. The micelles should remain stable and inactive while circulating in the body but undergo a phase transition endosomolytic, or membrane disruptive upon endocytosis and exposure to the acidic endosomes. This allows for the release of the biological cargo, in this case peptide, into the cytosol for therapeutic action.

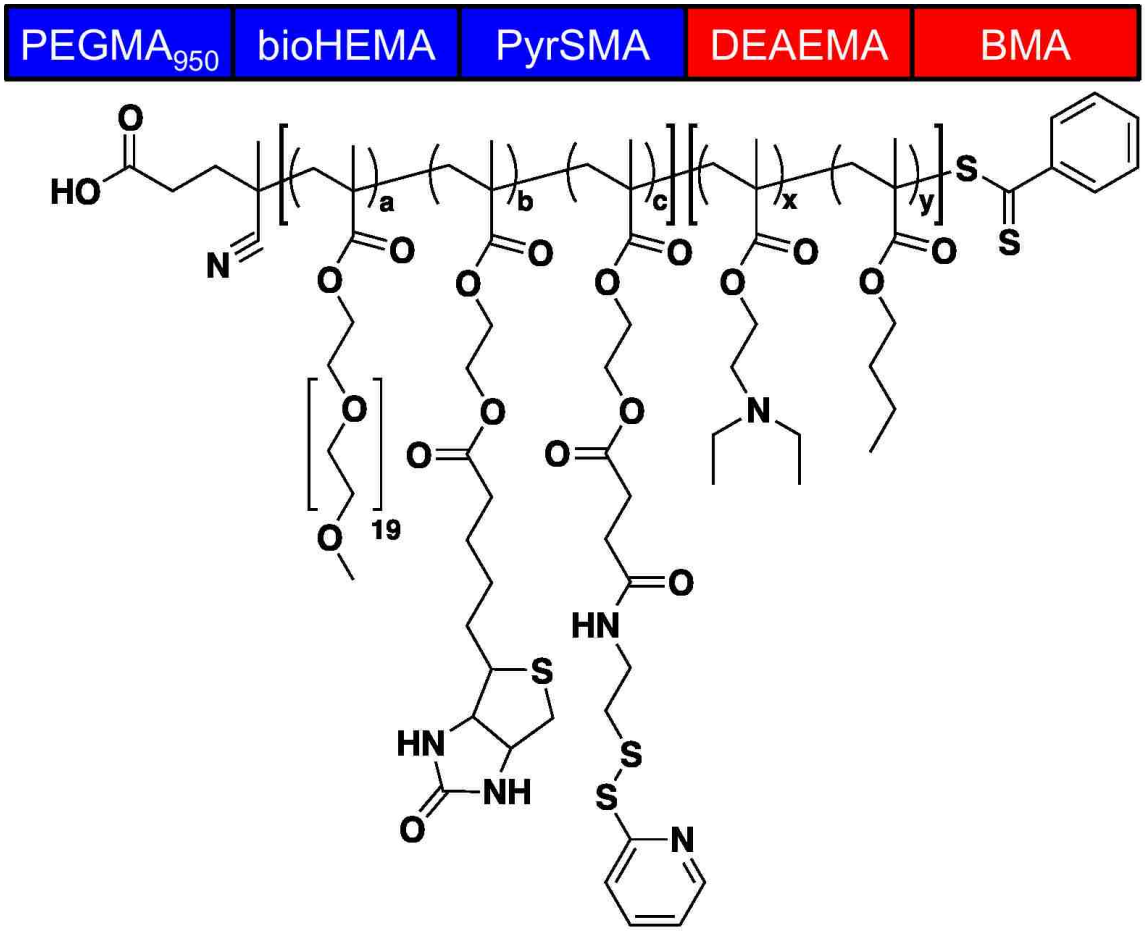

Figure 5.7: The diblock copolymer poly[(PEGMA-PyrSMA-bioHEMA)-(DEAEMA-BMA)] (O950) was synthesized by RAFT with a multifunctional hydrophilic first block containing $PEGMA_{950}$ for in vivo biocompatibility, a biotin-containing monomer (bioHEMA) for antibody/streptavidin complexation and a PDS-containing monomer (PyrSMA) for disulfide conjugation to a cysteine containing peptide. The second block contains the DEAEMA monomer which undergoes a pH-dependent phase transition and the BMA monomer for hydrophobic interactions with membrane disruption.

5.3.5 Gel-permeation chromatography with O950 polymer

Gel-permeation chromatography (GPC) was utilized to determine the M_n and PDI of the macroCTA and the diblock copolymer. Figure 5.8 provides the chromatograms measured by light scattering (left), refractive index (center), and UV Absorbance (right). In each chromatogram both the macroCTA (solid line) and diblock copolymer (dotted line) are displayed. A clear shift from the first and second polymer is noted indicating good synthesis of the second block to a larger molecular weight. A larger peak coupling is seen in the light scattering signal more so than the other two chromatograms due to the sensitivity to larger species by light scattering. Slight coupling was observed in the RI and UV signal and was estimated to be around 5% of the total peak. A characterization table for each polymer is shown in Table 5.8. The first block was made using a DP of 50 with a CTA to Initiator ratio $[CTA]_o:[I]_o$ = 10 and a reaction time of 24 hours. The feed ratio for this polymer was 90:5:5 [PEGMA:PyrSMA:bioHEMA]. For the second block, a DP of 300 was used with a $[CTA]_o:[I]_o = 5$, and a reaction time of 8 hours. In previous studies, a longer reaction time was used however this resulted in significant loss of the functional PDS groups on the PyrSMA monomer. The % monomer conversion for DEAEMA and BMA were calculated to be 29 and 32, respectively. The reactivity ratio for these two monomers was determined to be nearly 1 indicating that the feed ratio is preserved in the monomer conversion during polymerization. The PDI for this polymer was calculated to be 1.17 with an M_n = 38,000 Da.

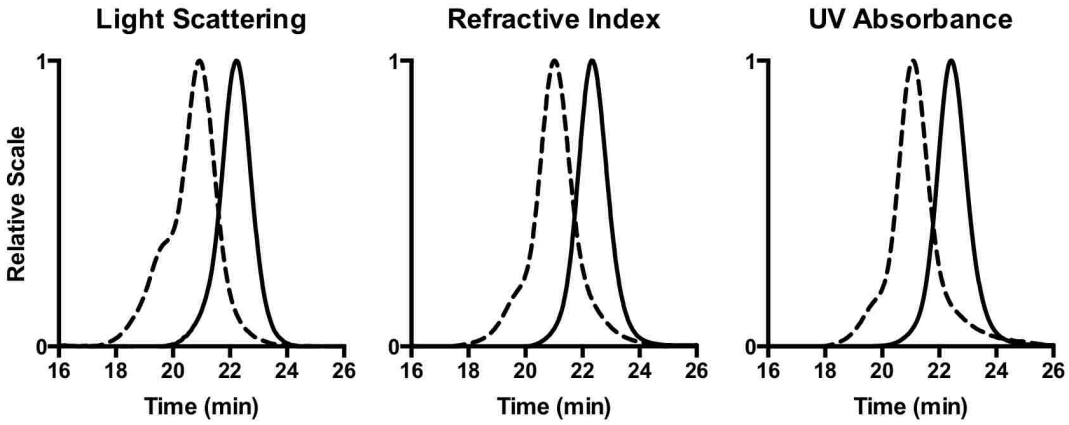

Figure 5.8: Size exclusion chromatography was used to measure the M_n of the macroCTA and diblock copolymer and determine the PDI of each. The O950-EB polymer was run on a gel-permeation chromatography instrument equipped with three detectors: three-angle light scattering(LS), refractive index (RI), and UV spectrophotometry. The RI and LS detectors were used to calculate M_n and PDI.

Poly(O950-PyrSMA-bioHEMA)

Polymer	$\frac{[M]_o}{[CTA]_o}$	$\frac{[CTA]_o}{[I]_o}$	t (h)	PEGMA (% feed)	PyrSMA (% feed)	BioHEMA (% feed)	PEGMA (% conv)	PyrSMA (% conv)	BioHEMA (% conv)	M_n Th (g/mol)	M_n Exp (g/mol)	PDI
PPB	50	10	24	90	5	5	-	18,000	-	-	18,000	1.06

Poly[(O950-PyrSMA-bioHEMA)-(DEAEMA-BMA)]

Polymer	$\frac{[M]_o}{[CTA]_o}$	$\frac{[CTA]_o}{[I]_o}$	t (h)	DEAEMA (% feed)	BMA (% feed)	DEAEMA (% conv)	BMA (% conv)	mCTA (g/mol)	M_n Th (g/mol)	M_n Exp (g/mol)	PDI	Ratio
PPB-EB40	300	5	8	60	40	29	32	18,000	33,130	38,000	1.17	1.11

Table 5.1: The O950 macroCTA and diblock copolymer were characterized by GPC to determine molecular weight and polydispersity. Monomer conversion for the second block was measured by HPLC purification. Monomer conversion and feed ratios are also given in the following table.

5.3.6 Quantification of PDS release and peptide conjugation

The number of PDS groups per polymer was quantified by first reducing with a 10X molar excess of TCEP then measuring the conversion of pyridyldisulfide to 2-mercaptopyridine which absorbs at 343 ηm (Figure 5.9A). As a blank, polymer at the same concentration without TCEP was used. Using the Beer-Lambert's law with an extinction coefficient of 8,080 $M^{-1}cm^{-1}$, we determined there to be 1.9 PDS groups per polymer chain. Next we reacted the BIM peptide at various concentrations with a fixed concentration of polymer to form a disulfide linkage and measured PDS release (Figure 5.9B). The conjugation efficiency at all peptide to polymer ratios (1:2, 1:1, 2:1, and 4:1) was 60%, except for the highest ratio because all PDS groups were saturated on the polymer. Furthermore, no solutions crashed out upon adding the peptide suggesting the micelles were stable even with up to 1-2 peptides per polymer. With the previous HPMA-based micelles, this had been a concern because too much peptide on the polymers often caused precipitation and crashing out of the micelles. The PEGMA-based polymer carriers are more stable in aqueous solution with peptide bound. These peptide loading ratios for the O950-BIM conjugates were further characterized in the subsequent studies.

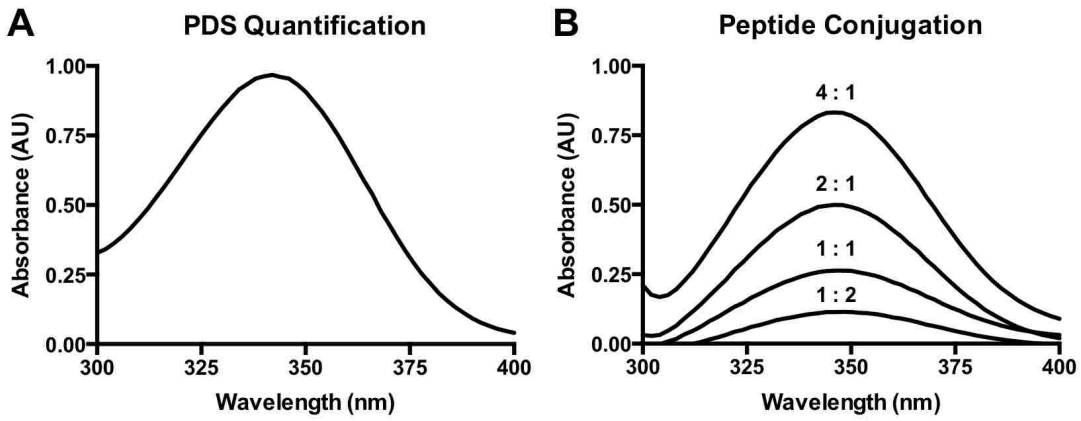

Figure 5.9: The number of PDS groups per O950 polymer chain was measured to be 1.9. (left). Polymer in phosphate buffer was reduced with an excess of TCEP and the conversion of PDS to 2-mercaptopyridine was quantified by A_{343} absorbance. Conjugation of the BIM peptide to the polymer was also quantified by PDS release with a peptide to polymer ratio of 1:2, 1:1, 2:1, and 4:1 (right). The conjugation efficiency of BIM to O950 was determine to be approximately 60%.

5.3.7 Hemolytic activity of O950 and O950-BIM conjugates

The ability of the O950 polymer and O950-BIM conjugates to lyse red blood cells (hemolysis) in a pH-dependent manner was studied (Figure 5.10). O950 polymer (5, 10, 20, 40 μg/mL) was incubated with red blood cells for one hour at 37°C and the amount of hemoglobin released by lysed red blood cells was quantified (Figure 5.10A). The O950 polymer exhibited good hemolytic activity in a concentration dependent manner with good activity at only 5 μg/mL. At all concentrations the polymer did not exhibit any hemolytic activity until below pH 7.0. This is advantageous for in vivo application because the polymer must remain nontoxic and inert at or near physiological pH. Good activity at pH 6.6 is preferred since this is the pH of early endosomes, a point at which endosomal escape would be preferred. Next the hemolytic activity of the O950-BIM was assessed for each peptide loading ratio at 20 μg/mL (Figure 5.10B). The O950-BIM conjugates exhibited a similar hemolysis profile to O950 indicating that the peptide-loading did not have any effect on the polymers pH-responsive activity. Furthermore, all peptide loading ratios (1:2, 1:1, 2:1, and 4:1 [BIM:O950] exhibited the same hemolysis profile which suggests that the pH-responsive activity of the second block is unaffected by the peptide, even with 1.9 peptides per polymer. A good hemolysis profile is not a direct indication of the potential intracellular activity however, good hemolytic activity is often linked with positive intracellular delivery of siRNA, peptides, and plasmid DNA.

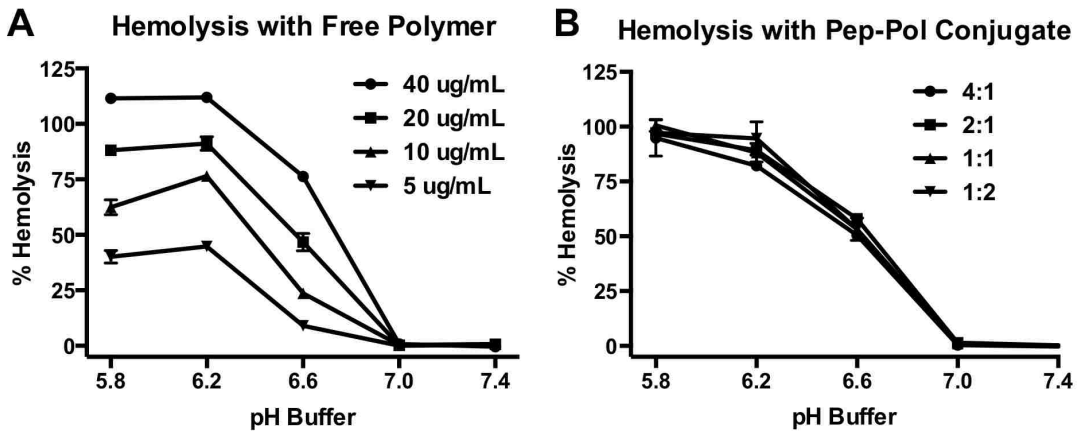

Figure 5.10: The hemolytic activity of O950 was quantified at 5, 10, 20, and 40 μg/mL from pH 5.8 to 7.4 (left). For all concentrations, the polymer was inactive at pH 7.0 and above. Furthermore, the O950-BIM conjugates did not appear to effect the hemolytic activity of the polymer for any of the peptide loading ratio (right).

5.3.8 Particle sizing for O950 and O950-BIM conjugates

The number average diameter of the O950 and O950-BIM micelles in phosphate buffer was quantified using dynamic light scattering (Figure 5.11). First the O950 was suspended in phosphate buffer to form micelles, then diluted into a range of pH buffer (pH 5.8, 6.2, 6.6, 7.0, and 7.4) (Figure 5.11A). DLS was performed with polymer in each buffer at 0.5 mg/mL. At pH 7.4 and 7.0, micelles were measured to be approximately 20 ηm. At pH 6.6 and below, the micelles fell apart and the polymer exhibited a unimeric confirmation. Interestingly, the pH transition from 7.0 to 6.6 yielded a unimeric confirmation. In the hemolysis study, this same pH transition caused the polymers to go from a nonactive state to hemolytic. The phase transition of O950 is likely between pH 6.6 and 7.0. Next the particle sizes of the O950-BIM conjugates for each peptide loading ratio was also measured at pH 7.4. For peptide loading ratios between 0 and 2:1, the micelles maintained the same particle sizes. At the 4:1 ratio however, larger particles were observed with an average size of 70 ηm. These results indicate that the micelle sizes remain stable up to 1 peptide per polymer (2:1). For future in vitro and in vivo studies we will likely form O950-BIM conjugates such that each polymer chain is bound to a single peptide. This would allow for maximum peptide (drug) loading without affecting micelle stability or activity, determined by DLS and hemolysis, respectively.

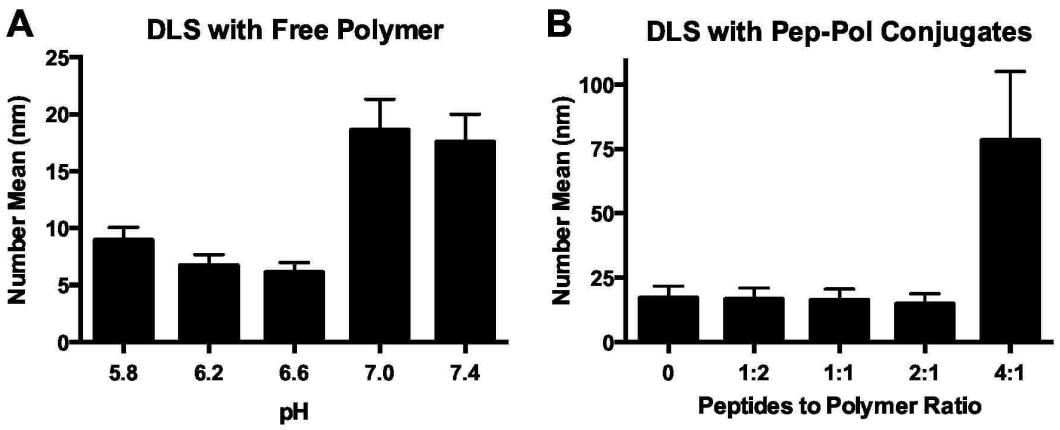

Figure 5.11: Dynamic light scattering was used to measure the number average diameter of the polymer micelles in a range of pH buffer (left). A decrease below pH 7.0 shows a drop in the diameter from 20 ηm to 5 indicating the phase transition to unimers. Peptide loading did not effect particle sizes except at the highest peptide loading ratio of 4:1. Polymers were analyzed in phosphate buffer at 0.5 mg/mL after filtering samples through a 0.4 μm syringe filter. All samples were analyzed in triplicate.

5.3.9 Streptavidin binding to O950 and O950-BIM

The ability of the biotin-containing O950 polymer to bind to streptavidin through the very stable, non-covalent interaction was quantified by a HABA assay (Figure 5.12). In this study, O950 and O950-BIM conjugates (1:2, 1:1, 2:1, and 4:1 [BIM:O950]) were incubated a molar excess of 2, 3, and 4 with streptavidin and the displacement of HABA measured by absorbance at 500 ηm was quantified. A standard curve made with a known concentration of biotin was utilized to convert absorbance values to biotin binding events. The O950 polymer alone exhibited a linear binding curve with a biotin binding capacity of 1 biotin for every 2 polymers. This indicates that there is 0.5 biotin monomers accessible for every polymer chain. In the case of the O950-BIM conjugates, a similar streptavidin binding capacity was observed, albeit slightly decreased. This indicates that even with peptide loaded on the first block, the O950-BIM conjugates can still actively bind to streptavidin. This is an important observation because in order to make use of the antibody-streptavidin conjugates for cell targeted, the O950-BIM conjugates must be able to bind to the streptavidin protein and remain stable in solution.

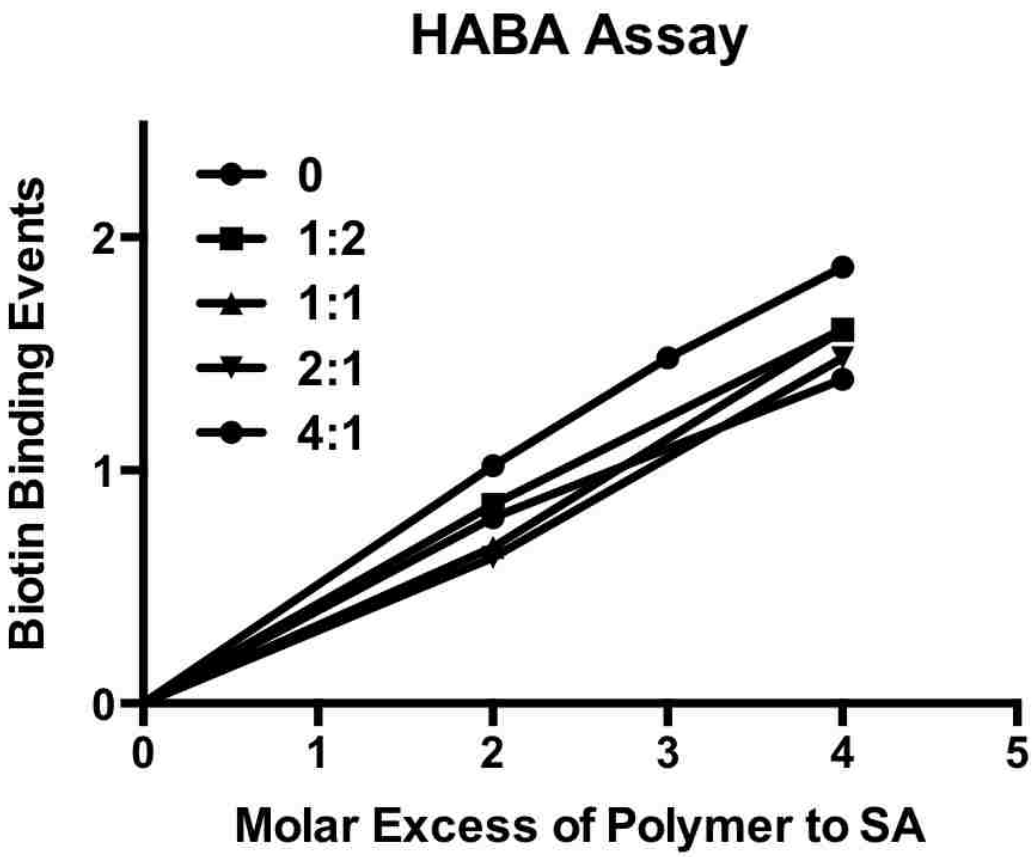

Figure 5.12: A HABA binding assay was performed to confirm the accessibility of the biotin monomer in the O950 polymer. Complexation with streptavidin confirmed that an excess of 2 polymers was required for a single biotin binding event. Furthermore, O950-BIM conjugates exhibited similar biotin binding efficiencies as the free polymer with only a slight decrease in activity.

5.3.10 Antibody mediated uptake of O950-fluorescent BIM conjugates

To determine whether the anti-Her2/streptavidin (Her2/SA) conjugates could enhance uptake of O950-BIM, cells were treated with Her2/SA-O950-BIM modified with a Rhodamine fluorophore on the BIM peptide. One hour after incubation, extracellular fluorescence was quenched with Trypan Blue and mean fluorescence intensity within cells was quantified by flow cytometry (Figure 5.13). Her2/SA-O950-BIM conjugates were made with varying Her2/SA to O950-BIM ratios at 1:8, 1:4, and 1:2, however cells were treated with equal concentrations of O950-BIM. Compared to the untargeted O950-BIM conjugates, 1 antibody per 8 polymer chains doubled the MFI from 3200 to 7000. With twice as much antibody, or 1 antibody per 4 polymers, the MFI increased to 8000 but with 1 antibody per 2 polymers chains the MFI remained at 8000. These results suggest that Her2/SA helps to increase the amount of O950-BIM uptake in SKOV3 cells however the amount taken up is likely limited to the amount of free Her2 receptors on the cells surface. This is demonstrated at the higher antibody ratios. The MFI from 1:4 and 1:2 did not vary most likely because all Her2 receptors had been saturated. Increased incubation time with cells would likely result in greater differences between O950-BIM and the Her2/SA-O950-BIM conjugates, as the Her2 receptors would have more time to recycle and express on the cell surface.

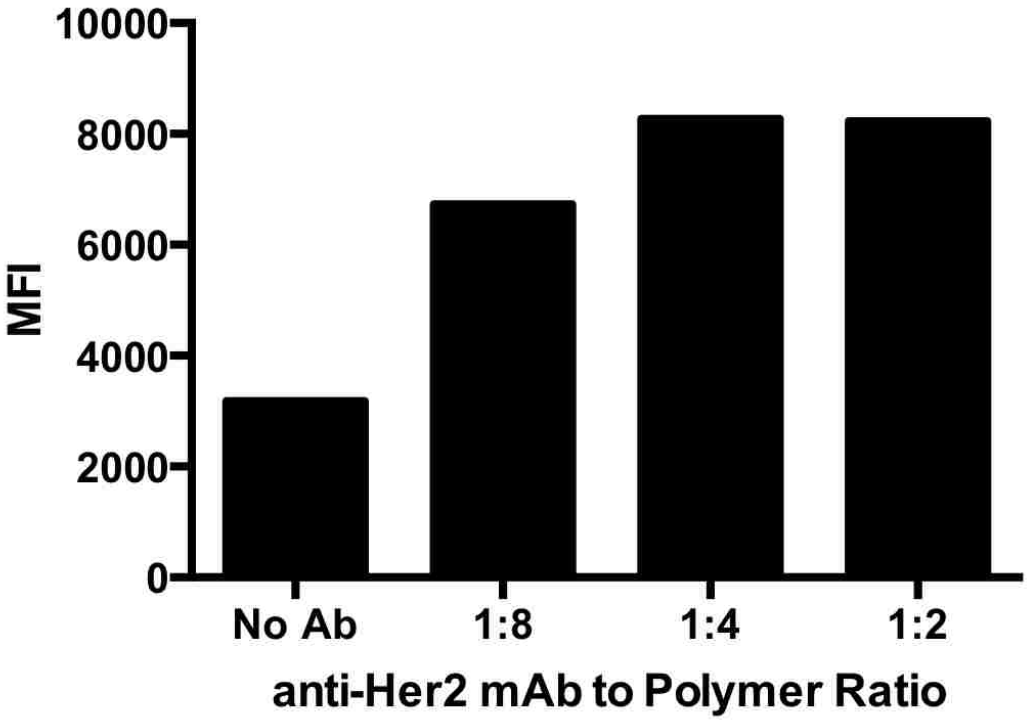

Figure 5.13: Fluorescently-labeled BIM peptide was conjugated to O950 at a 1:1 molar ratio. O950-BIM was then complexed with anti-Her2/SA conjugates at various ratios (1:8, 1:4, and 1:2 [mAb:Pol] and incubated with SKOV3 cells at a peptide concentration of 1 μM. After 1 hour, cells were trypsanized, washed with FACS buffer (0.1% Trypan blue, 2% BSA in PBS) and the mean fluorescence intensity was measured by flow cytometry.

5.3.11 Maximum tolerated dose study with O950 polymer

To determine the maximum tolerated dose of the O950 polymer in mice, the polymer was administered via tail vein at 120, 160, 200, and 240 mg/kg (n = 1). Blood was collected on day 1, 3, and 5 to measure toxicity through blood enzyme levels. Figure 5.14 shows the blood toxicity 3 days after administration using markers for pancreas, liver, kidney, and muscle. Although this study was performed with a single mouse at each dosage level, no trends were observed between dosage and blood toxicity levels. Glucose, amylase, total bilirubin, and creatinine were all at normal levels. Lipase, AST, ALT, and creatine kinase had some aberrant levels but none of these increased levels were related to polymer dose. Furthermore, the maximum tolerated dose of O950 was not realized in this study suggesting that the administration dose for O950 could likely be increased. For all future in vivo studies, the O950 polymer will be administered at 240 mg/kg to conserve on polymer usage, while administering a significant dose for peptide delivery. With one peptide per polymer this would equate to 15-20 mg/kg of BIM peptide.

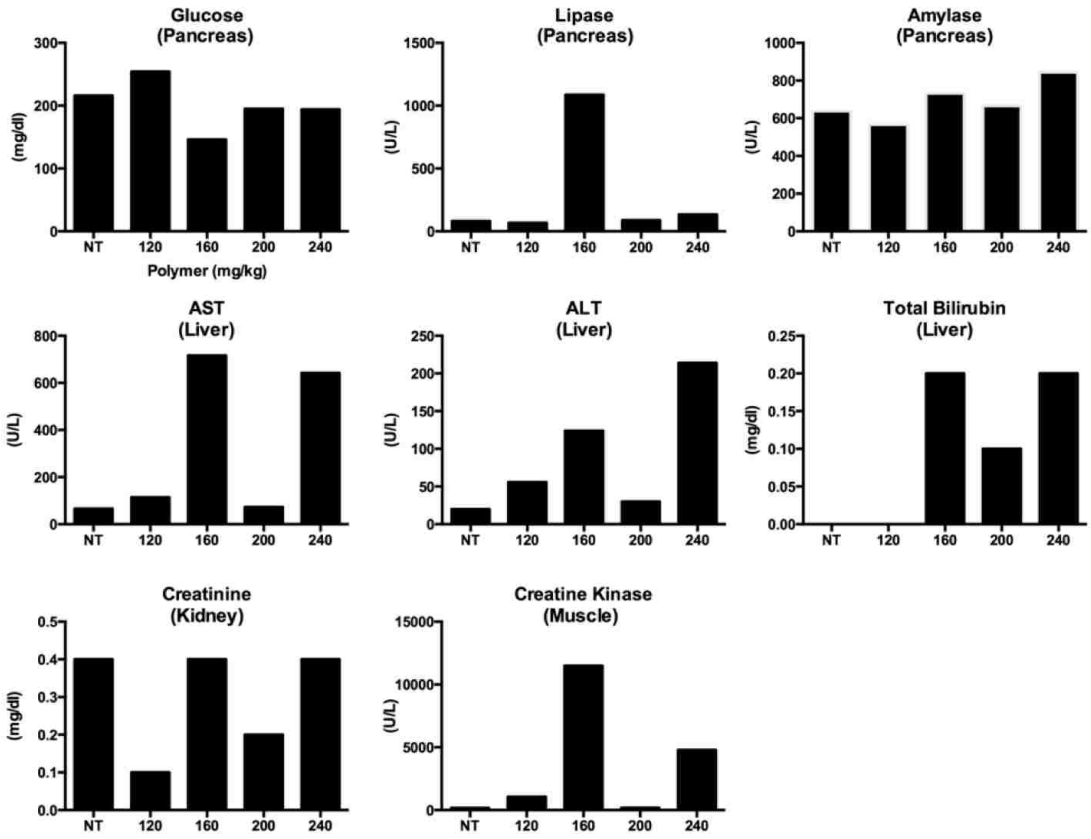

Figure 5.14: To determine the maximum tolerated dose of the O950 polymer, 5 concentrations of polymer were prepared and administered via tail vein injection at 120, 160, 200, and 240 mg/kg (n = 1). Blood samples were collected after 1, 3, and 5 days, processed to measure enzyme levels for toxicity in pancreas, liver, kidney and muscle.

5.3.12 Tumor activity measured by cleaved caspase 3

The activity of the O950-BIM conjugates was evaluated in athymic nude mice using Ramos cell tumor-xenografts. In the following study, O950-BIM was formulated with two different lymphoma targeting antibody conjugates, anti-CD22/SA and anti-CD19/SA. CD19 has been measured to have 222,000 receptor sites per Ramos cell, while CD22 has 35,000[37], however a number of studies have shown that CD22 receptors are more readily endocytosed than CD19 upon antigen binding. Mice bearing tumor xenografts were treated with a combination of low dose chemotherapy to elicit synergistic activity in the tumor cells. Cyclophosphamide at 35 mg/kg was selected as the chemotherapeutic which had been previously used in combination with Bcl-2 antisense oligonucleotides[38]. Three days following dual administration, mice were sacrificed and blood was collected for systemic toxicity; lung, liver, kidneys and tumors for histology and immunohistochemistry.

Three days after treatment, 400 μL of blood was drawn via heart stick. Plasma was processed and submitted to Phoenix Laboratory for analysis. Serum glucose, lipase, and amylase were analyzed for pancrease, AST, ALT, and total bilirubin were measured for liver, creatinine for kidney, and creatine kinase for muscle (Figure 5.15). No elevated enzyme activity levels were measured in any of the treatment groups. These results indicate that the conjugates are non toxic up to three days following administration.

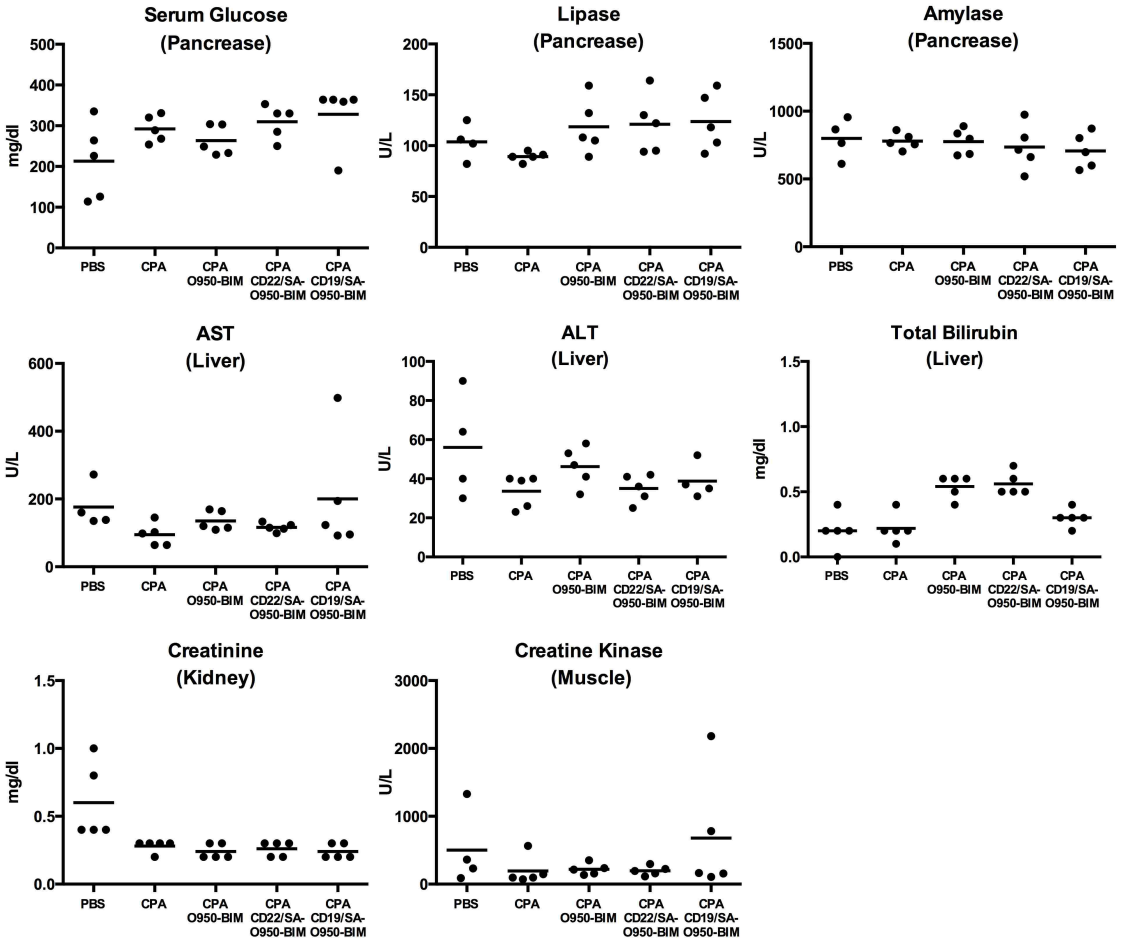

Figure 5.15: Three days after administration of conjugates, blood was collected by heart sticks, processed and submitted to Phoenix Laboratories. Blood enzymes including serum glucose, lipase, and amylase (for pancreas), AST, ALT, and total bilirubin (for liver), creatinine (for kidney), and creatine kinase (for muscle) were analyzed. Plots include all five mice per treatment group and their mean.

In a single blind sampling of histological samples stained by hematoxylin and eosin staining, the pathologist noted no marked effects or toxicity in the lungs, liver or kidneys for any treatment. Initially, these results were surprising given the high dosage of polymer and peptide administered to each mouse. Coupled with the blood enzyme activity levels, these results suggest that the complete conjugates exhibit good in vivo biocompatibility with a potentially high therapeutic index window.

Body weights for all mice was measured on day 0 and day 3 and averaged for each treatment group (Figure 5.16A). No significant changes were observed for any treatment group. After harvesting organs, tumor masses were weighed on a scale Figure 5.16B. While no significant differences were observed, analysis by histology found that many of the tumors from the CD22-Pol-BIM treatment group contained a large portion of mammary fat pads which would have added to the measured mass.

Following formalin fixation for each organ, tumors were bisected and embedded in paraffin, then sectioned for histology, Ki67, and cleaved caspase 3 staining. The Ki67 staining was inconclusive because of the background signal from rabbit anti-asialo injected during cell inoculation. Cleaved caspase 3 (CC3) however, successfully stained all apoptotic cells. Bisected tumors stained with CC3 were imaged on a slide imager at 10X magnification and analyzed using HistoQuest software. The algorithm applied to each tissue section was able to identify all cells by the nuclear stain (blue), and the percent of those cells which were also CC3 positive (brown). The percent of CC3 positive cells for two sections of each tumor were averaged and plotted on the dot plot in Figure 5.16C. No distinguishable differences were observed between any group except the CD22-O950-BIM. CD22-O950-BIM was significantly greater than PBS alone according to a Bartletts test ($P < 0.05$) which measures deviation from the normal distribution.

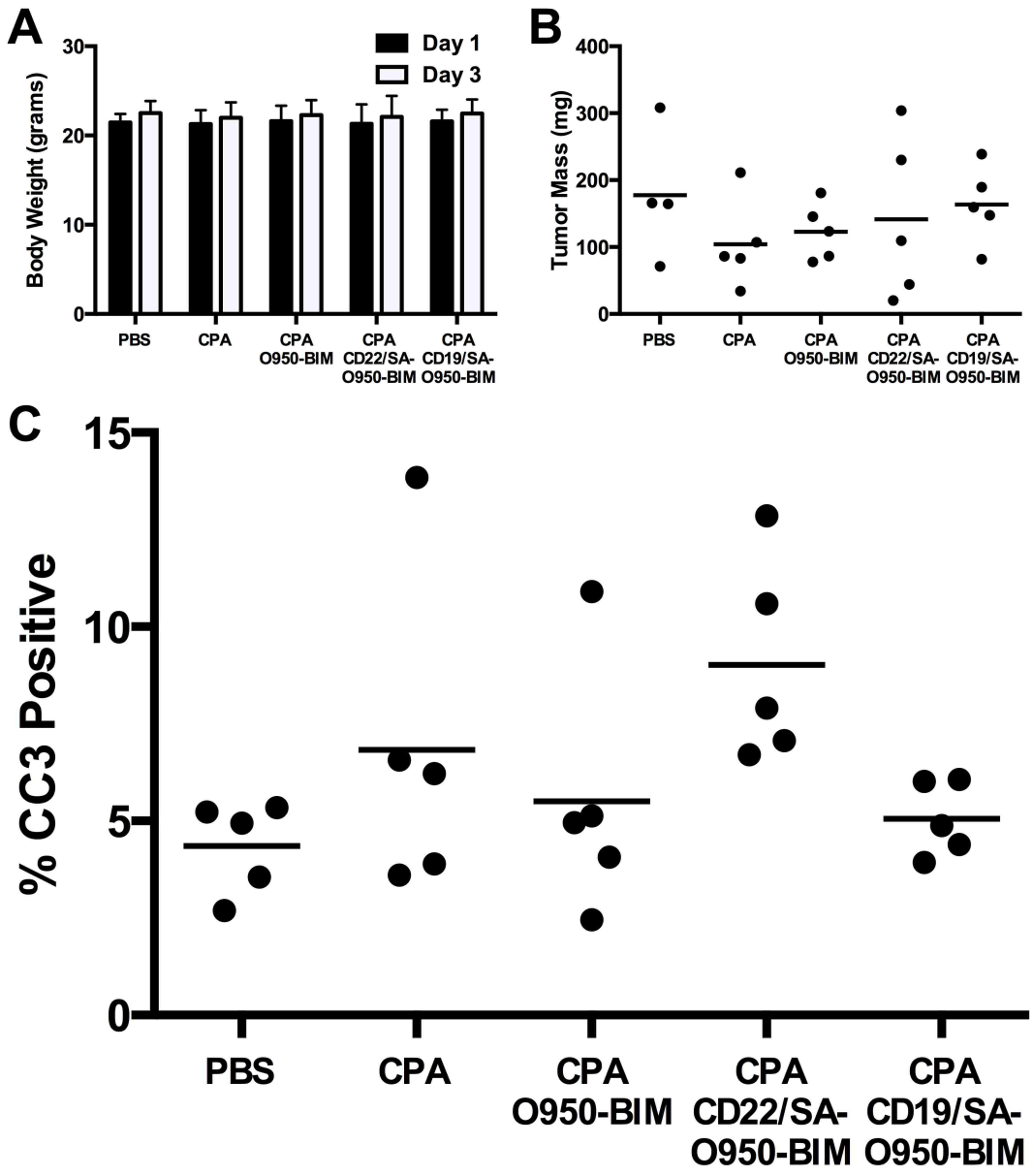

Figure 5.16: The body weight of each mouse in the study was monitored on day 1 and day 3 following administration(A). Following tissue harvesting on day three, tumors were also weighed(B). Tumors were harvested and bisected, then fixed, sectioned, and IHC stained for cleaved caspase 3 activity then analyzed by microscopy and image analysis. The percentage of brown nuclei (CC3+) versus blue nuclei (CC3-) stained cells was plotted for each tumor.

After analyzing tumors by CC3 activity we looked at all the tumors by hematoxylin and eosin staining. We observed by CC3 staining that there were fewer cells per area within the tumors treated with CD22-O950-BIM treated tumors. At first it appeared to be empty or void space between many of the cells. A deeper look by Hemotoxylin and Eosin staining revealed that the void space was likely polymer material stuck within the tumors. These findings were only observed in the CD22-O950-BIM treated mice. The pathologist said the only other time she had seen such artifacts was when mice were given collagen or some other polymer scaffolds. These non biological artifacts could therefore be attributed to the injected polymers. It is not clear however, whether the polymer had precipitated due to the low pH environment of the tumor or because of the hydrophobic nature of the peptides conjugated to the cells.

To characterize the results seen in the tissue sections we plotted the cell density (cells/mm^2) of each tumor bisection against the tumor area measured (Figure 5.17). Using the Pearsons Correlation calculation we found that only in CD22-Pol-BIM treatment, the number of cells per area correlated with tumor size, such that the smaller the tumor, the lower the density of the cells inside of it. These results may suggest that the CD22-targeted conjugates exhibited better penetration into the tumors. The propensity to penetrate the tumors however was also related to the size of the tumors, with smaller tumors resulting in better penetration.

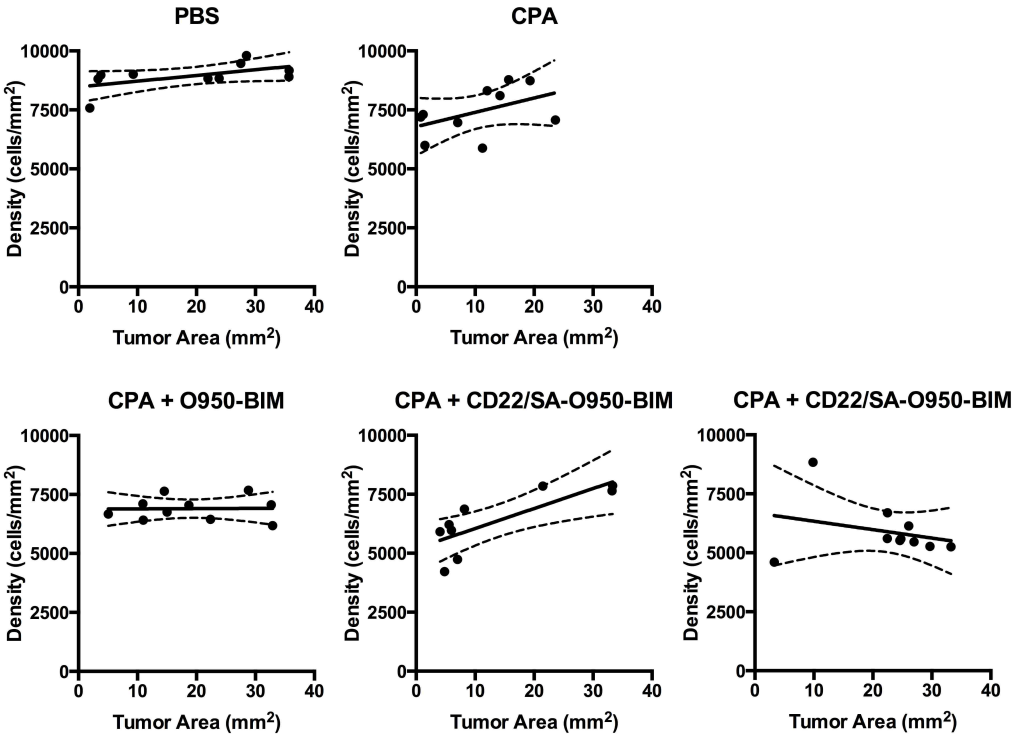

Figure 5.17: A Pearson correlation function was applied to each tumor image from the cleaved caspase 3 analysis. The tumor size from each tumor bisection was plotted against cell density (cell/mm^2). A Pearson correlation equation was applied to each data set to determine if there was a correlation between tumor area and cell density. A linear fit (solid line) and 95% confidence interval (dotted line) was applied to the data set. The only group that showed a significant correlation was CPA + CD22/SA-O950-BIM.

Conclusions from cleaved caspase study: In the cleaved caspase study we delivered a low dose of chemotherapy in combination with antibody-polymer-peptide conjugates in tumor xenograft-bearing mice. No toxic effects from the polymer conjugates was observed by blood enzyme analysis or Hematoxylin and Eosin staining after three days following administration. Cleaved caspase 3 activity, a marker for apoptosis was measured by immunohistochemistry. Elevated levels were observed in tumors treated with CD22 antibody conjugated to the polymer-peptide system however these levels were only statistically significant compared to PBS treatment using a Bartletts test.

5.3.13 In vitro comparison of two BIM peptides on O950 polymer

While the BIM peptide synthesized and characterized in this chapter did not exhibit any activity on O950, we tested a second BIM peptide described in the previous chapters and found high activity on the O950 polymer. Note: the activity data for this new peptide will be included in an updated version of this thesis document.

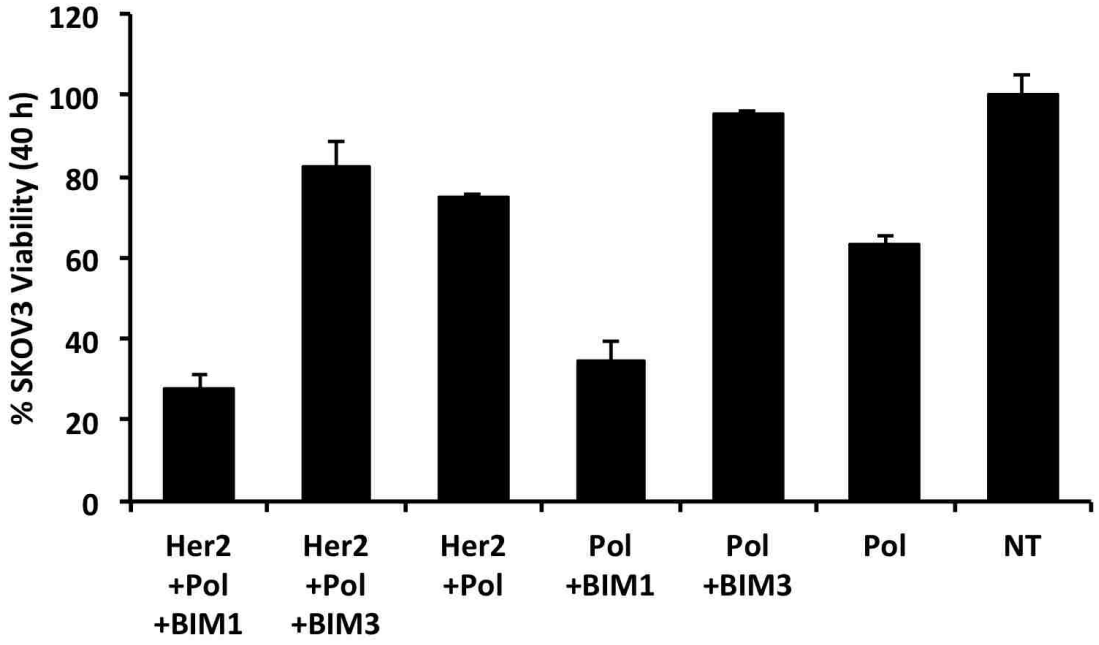

Figure 5.18: The in vitro activity of two BIM peptides was evaluated with the O950 polymer using MTS to measure cell viability.

5.4 References

[1] Nathan Susnow, Liyun Zeng, Daciana Margineantu, and David M Hockenbery. Bcl-2 family proteins as regulators of oxidative stress. *Seminars in Cancer Biology*, 19(1):42–49, February 2009.

[2] N N Danial. BCL-2 Family Proteins: Critical Checkpoints of Apoptotic Cell Death. *Clinical Cancer Research*, 13(24):7254–7263, December 2007.

[3] Guillaume Lessene, Peter E Czabotar, and Peter M Colman. BCL-2 family antagonists for cancer therapy. *Nature Reviews Drug Discovery*, 7(12):989–1000, December 2008.

[4] T N Chonghaile, K A Sarosiek, T T Vo, J A Ryan, A Tammareddi, V D G Moore, J Deng, K C Anderson, P Richardson, Y T Tai, C S Mitsiades, U A Matulonis, R Drapkin, R Stone, D J DeAngelo, D J McConkey, S E Sallan, L Silverman, M S Hirsch, D R Carrasco, and A Letai. Pretreatment Mitochondrial Priming Correlates with Clinical Response to Cytotoxic Chemotherapy. *Science*, 334(6059):1129–1133, November 2011.

[5] Shibu Thomas, Bridget A Quinn, Swadesh K Das, Rupesh Dash, Luni Emdad, Santanu Dasgupta, Xiang-Yang Wang, Paul Dent, John C Reed, Maurizio Pellecchia, Devanand Sarkar, and Paul B Fisher. Targeting the Bcl-2 family for cancer therapy. *Expert Opinion on Therapeutic Targets*, 17(1):61–75, January 2013.

[6] D Yecies, N E Carlson, J Deng, and A Letai. Acquired resistance to ABT-737 in lymphoma cells that up-regulate MCL-1 and BFL-1. *Blood*, 115(16):3304–3313, April 2010.

[7] Kylie D Mason, Cassandra J Vandenberg, Clare L Scott, Andrew H Wei, Suzanne Cory, David CS Huang, and Andrew W Roberts. In vivo efficacy of the Bcl-2 antagonist ABT-737 against aggressive Myc-driven lymphomas. *Proceedings of the National Academy of Sciences*, 105(46):17961–17966, 2008.

[8] C Zhang, T y Cai, H Zhu, L q Yang, H Jiang, X w Dong, Y z Hu, N m Lin, Q j He, and B Yang. Synergistic Antitumor Activity of Gemcitabine and ABT-737 In Vitro and In Vivo through Disrupting the Interaction of USP9X and Mcl-1. *Molecular Cancer Therapeutics*, 10(7):1264–1275, July 2011.

[9] A Letai, M C Bassik, L D Walensky, M D Sorcinelli, S Weiler, and S J Korsmeyer. Distinct BH3 domains either sensitize or activate mitochondrial apoptosis, serving as prototype cancer therapeutics. *Cancer Cell*, 2(3):183–192, 2002.

[10] Michael Certo, Victoria Del Gaizo Moore, Mari Nishino, Guo Wei, Stanley Korsmeyer, Scott A Armstrong, and Anthony Letai. Mitochondria primed by death signals determine cellular addiction to antiapoptotic BCL-2 family members. *Cancer Cell*, 9(5):351–365, May 2006.

[11] Hiroyuki Kashiwagi, Jonathan E McDunn, Peter S Goedegebuure, Mary C Gaffney, Katherine Chang, Kathryn Trinkaus, David Piwnica-Worms, Richard S Hotchkiss, and William G Hawkins. TAT-Bim Induces Extensive Apoptosis in Cancer Cells. *Annals of Surgical Oncology*, 14(5):1763–1771, January 2007.

[12] James L LaBelle, Samuel G Katz, Gregory H Bird, Evripidis Gavathiotis, Michelle L Stewart, Chelsea Lawrence, Jill K Fisher, Marina Godes, Kenneth Pitter, Andrew L Kung, and Loren D Walensky. A stapled BIM peptide overcomes apoptotic resistance in hematologic cancers. *Journal of Clinical Investigation*, 122(6):2018–2031, June 2012.

[13] Loren D Walensky, Kenneth Pitter, Joel Morash, Kyoung Joon Oh, Scott Barbuto, Jill Fisher, Eric Smith, Gregory L Verdine, and Stanley J Korsmeyer. A Stapled BID BH3 Helix Directly Binds and Activates BAX. *Molecular Cell*, 24(2):199–210, October 2006.

[14] A G Polson, J Calemine-Fenaux, P Chan, W Chang, E Christensen, S Clark, F J de Sauvage, D Eaton, K Elkins, J M Elliott, G Frantz, R N Fuji, A Gray, K Harden, G S Ingle, N M Kljavin, H Koeppen, C Nelson, S Prabhu, H Raab, S Ross, D S Slaga, J-P Stephan, S J Scales, S D Spencer, R Vandlen, B Wranik, S-F Yu, B Zheng, and A Ebens. Antibody-Drug Conjugates for the Treatment of Non-Hodgkin's Lymphoma: Target and Linker-Drug Selection. *Cancer Research*, 69(6):2358–2364, March 2009.

[15] Peter D Senter. Potent antibody drug conjugates for cancer therapy. *Current Opinion in Chemical Biology*, 13(3):235–244, June 2009.

[16] David Schrama, Ralph A Reisfeld, and Jürgen C Becker. Antibody targeted drugs as cancer therapeutics. *Nature Reviews Drug Discovery*, 5(2):147–159, January 2006.

[17] Anna M Wu and Peter D Senter. Arming antibodies: prospects and challenges for immunoconjugates. *Nature Biotechnology*, 23(9):1137–1146, September 2005.

[18] B A Teicher. Antibody-drug conjugate targets. *Current cancer drug targets*, 9(8):982–1004, 2009.

[19] V Bulmus. A new pH-responsive and glutathione-reactive, endosomal membrane-disruptive polymeric carrier for intracellular delivery of biomolecular drugs. *Journal of Controlled Release*, 93(2):105–120, December 2003.

[20] Suzanne Flanary, Allan S Hoffman, and Patrick S Stayton. Antigen Delivery with Poly(Propylacrylic Acid) Conjugation Enhances MHC-1 Presentation and T-Cell Activation. *Bioconjugate Chemistry*, 20(2):241–248, February 2009.

[21] Steven R Little and Daniel S Kohane. Polymers for intracellular delivery of nucleic acids. *Journal of Materials Chemistry*, 18(8):832, 2008.

[22] Daniel W Pack, Allan S Hoffman, Suzie Pun, and Patrick S Stayton. Design and development of polymers for gene delivery. *Nature Reviews Drug Discovery*, 4(7):581–593, July 2005.

[23] Matthew J Manganiello, Connie Cheng, Anthony J Convertine, James D Bryers, and Patrick S Stayton. Diblock copolymers with tunable pH transitions for gene delivery. *Biomaterials*, 33(7):2301–2309, March 2012.

[24] Shinji Takeoka, Katsura Mori, Haruki Ohkawa, Keitaro Sou, and Eishun Tsuchida. Synthesis and Assembly of Poly(ethylene glycol)Lipids with Mono-, Di-, and Tetraacyl Chains and a Poly(ethylene glycol) Chain of Various Molecular Weights. *Journal of the American Chemical Society*, 122(33):7927–7935, August 2000.

[25] Konstantinos Avgoustakis. Pegylated Poly(Lactide) and Poly(Lactide-Co-Glycolide) Nanoparticles: Preparation, Properties and Possible Applications in Drug Delivery. *Current Drug Delivery*, 1(4):321–333, October 2004.

[26] Hidenori Otsuka, Yukio Nagasaki, and Kazunori Kataoka. PEGylated nanoparticles for biological and pharmaceutical applications. *Advanced Drug Delivery Reviews*, 64:246–255, December 2012.

[27] Frank Alexis, Eric Pridgen, Linda K Molnar, and Omid C Farokhzad. Factors Affecting the Clearance and Biodistribution of Polymeric Nanoparticles. *Molecular Pharmaceutics*, 5(4):505–515, August 2008.

[28] Kumiko Ueda, Yuriko Kawaguchi, and Seigo Iwakawa. Effect of oxyethylene numbers on the pharmacokinetics of menatetrenone incorporated in oil-in-water lipid emulsions prepared with polyoxyethylene-polyoxypropylene block copolymers and soybean oil in rats. *Biological and Pharmaceutical Bulletin*, 31(12):2283–2287, 2008.

[29] Zhiliang Cheng, Drew R Elias, Neha P Kamat, Eric D Johnston, Andrei Poloukhtine, Vladimir Popik, Daniel A Hammer, and Andrew Tsourkas. Improved Tumor Targeting of Polymer-Based Nanovesicles Using Polymer–Lipid Blends. *Bioconjugate Chemistry*, 22(10):2021–2029, October 2011.

[30] Connie Cheng, Anthony J Convertine, Patrick S Stayton, and James D Bryers. Multifunctional triblock copolymers for intracellular messenger RNA delivery. *Biomaterials*, 33(28):6868–6876, October 2012.

[31] Craig L Duvall, Anthony J Convertine, Danielle S W Benoit, Allan S Hoffman, and Patrick S Stayton. Intracellular Delivery of a Proapoptotic Peptide via Conjugation to a RAFT Synthesized Endosomolytic Polymer. *Molecular Pharmaceutics*, 7(2):468–476, April 2010.

[32] Maria C Palanca-Wessels, Anthony J Convertine, Richelle Cutler-Strom, Garrett C Booth, Fan Lee, Geoffrey Y Berguig, Patrick S Stayton, and Oliver W Press. Anti-CD22 Antibody Targeting of pH-responsive Micelles Enhances Small Interfering RNA Delivery and Gene Silencing in Lymphoma Cells. *Molecular Therapy*, 19(8):1529–1537, May 2011.

[33] John T Wilson, Salka Keller, Matthew J Manganiello, Connie Cheng, Chen-Chang Lee, Chinonso Opara, Anthony Convertine, and Patrick S Stayton. pH-Responsive Nanoparticle Vaccines for Dual-Delivery of Antigens and Immunostimulatory Oligonucleotides. *ACS Nano*, page 130506085827001, April 2013.

[34] Cyrille Boyer, Volga Bulmus, Thomas P Davis, Vincent Ladmiral, Jingquan Liu, and Sébastien Perrier. Bioapplications of RAFT Polymerization. *Chemical Reviews*, 109(11):5402–5436, November 2009.

[35] Brittany B Lundy, Anthony Convertine, Martina Miteva, and Patrick S Stayton. Neutral Polymeric Micelles for RNA Delivery. *Bioconjugate Chemistry*, 24(3):398–407, March 2013.

[36] Geoffrey Y Berguig, Anthony J Convertine, Julie Shi, Maria Corinna Palanca-Wessels, Craig L Duvall, Suzie H Pun, Oliver W Press, and Patrick S Stayton. Intracellular Delivery and Trafficking Dynamics of a Lymphoma-Targeting Antibody–Polymer Conjugate. *Molecular Pharmaceutics*, 9(12):3506–3514, 2012.

[37] X Du, R Beers, D J FitzGerald, and I Pastan. Differential Cellular Internalization of Anti-CD19 and -CD22 Immunotoxins Results in Different Cytotoxic Activity. *Cancer Research*, 68(15):6300–6305, August 2008.

[38] Richard J Klasa, Marcel B Bally, Rebecca Ng, James H Goldie, Randy D Gascoyne, and Frances MP Wong. Eradication of human non-Hodgkin's lymphoma in SCID mice by BCL-2 antisense oligonucleotides combined with low-dose cyclophosphamide. *Clinical Cancer Research*, 6(6):2492–2500, 2000.